Swansea University
Prifysgol Abertawe

National Oceanography Centre

Blue Carbon in an Exposed Temperate Island Nation: Organic Carbon Variability in Coastal and Shelf Sediments in the Isle of Man

by

Hannah Catherine Muir

MSc, MChem

A thesis submitted in fulfilment of the requirements

for the degree of Doctor of Philosophy

Swansea University

April 2025

Abstract

Blue carbon ecosystems remove and store atmospheric CO_2 for centuries to millennia, offering a scalable and cost-effective solution for climate change mitigation. Their integration into national climate strategies is hindered by limited regional data on their spatial extent and long-term organic carbon (OC) storage, especially in temperate and human-impacted regions such as trawled seabed. In this thesis, I address these gaps to inform blue carbon management on the Isle of Man. Through empirical sedimentary analyses and habitat mapping, I quantify OC stocks, accumulation, and burial rates across a range of blue carbon ecosystems, in the island's saltmarshes, seagrass meadows, and trawled muddy shelf sea sediments in the Western Irish Sea Mud Belt (WISMB). The WISMB was found to be a major long-term OC reservoir due to its OC density and vast extent (49,212.30 ha), exceeding saltmarshes and seagrass meadows. The average long-term (≥100 years) OC burial rate for the WISMB is estimated as 23 gC m^{-2} yr^{-1}, with an OC burial efficiency of 74% compared to an average short-term (≤30 years) OC accumulation rate of 31 gC m^{-2} yr^{-1}. The disparity between the average OCAR and OCBR in the WISMB likely reflects the degradation of OC over the first 100 years, from 1.06 ± 0.27 % OC and 10.37 ± 1.62 gC cm^{-3} in the top 10 cm of sediments to 0.70 ± 0.20 % OC and 7.72 ± 1.51 gC cm^{-3} below 30 cm sediment depth. However, areas where modern trawling pressure was highest in the WISMB were associated with the lowest measured OC stocks in subsurface sediments. Trawling pressure was significantly associated with sedimentary OC depletion in sediments deposited around 1960–1990 (10–20 cm), while gear penetration into deeper sediments from 1860–1960 (≥20 cm) had less effect, and sediment mixing by competing environmental factors potentially masked trawling effects in surface sediments deposited around 1990–2022 (≤10 cm). Saltmarsh had the highest OC density of 94.14 ± 62.51 MgC ha^{-1} and accumulation rate of 1.08 ± 0.76 MgC ha^{-1} yr^{-1} (107.96 ± 75.83 gC m^{-2} yr^{-1}), amounting to 694.78 ± 461.34 MgC and 7.97 ± 5.60 MgC yr^{-1} over their full extent of 7.38 ha, which were comparable with other temperate regions. The seagrass meadow OC density of 1.33 ± 0.25 MgC ha^{-1}, amounting to 261.10 ± 49.08 MgC in the top 10 cm over their full extent of 195.88 ha, was among the lowest values reported and comparable only with exposed temperate meadows. In all three ecosystems, OC content declined with sediment depth, which were found to vary within and between saltmarshes. These findings highlight the importance of quantifying sediment depth and age alongside OC content to estimate long-term OC storage for accurate blue carbon assessments. This study demonstrates the potential for temperate blue carbon ecosystems to contribute to climate change mitigation, and provides vital insights for informing robust, evidence-based national and international blue carbon strategies.

Declarations

I, Hannah C. Muir, declare that this thesis and the work presented herein are my own, and have been generated by me as the result of my own original research.

I confirm that:

- This work has not previously been accepted in substance for any degree and is not being concurrently submitted in candidature for any degree.
- This thesis is the result of my own investigations, except where otherwise stated. Other sources are acknowledged by footnotes giving explicit references. A bibliography (references list) is appended.
- I hereby give consent for my thesis, if accepted, to be available for electronic sharing.
- The University's ethical procedures have been followed and, where appropriate, that ethical approval has been granted.

Hannah C. Muir

April 2025

Acknowledgements

I would like to thank everyone who has supported me throughout this PhD.

Firstly, Claire, thank you for believing in me from day one, for trusting me with this project, and for supporting me enthusiastically through every challenge. Here's to many more! James, from your mapping wizardry to patiently explaining stats and GIS to me, you've helped me more than you know, thank you. Richard, thank you for challenging me to think like a scientist and for teaching me to trust my intuition, I am a better researcher for it. A massive thank you to everyone I have worked with at the National Oceanography Centre (NOC), GAU-Radioanalytical, British Ocean Sediment Core Research Facility (BOSCORF), and the University of Southampton, working alongside you all has been a pleasure.

The Manx Blue Carbon Project team (incl. Bangor University, Manx Wildlife Trust, and Barrule skipper and crew) and everyone on the Island, thank you for welcoming me and for letting me explore your coastal waters. Your kindness, curiosity, and support have made this one of the most enjoyable and memorable experiences. Rowan and Jacqui, I feel incredibly lucky to have had colleagues so passionate, entertaining, and supportive as you, thank you. A huge thank you to the Isle of Man Government for sponsorship, without which none of this would have been possible.

My Southampton "familia", thank you for showing me that a PhD is about more than just research. Living between two cities wasn't easy, but through climbing, beers, and bike rides, you made it feel like home (with more sunshine!). To my life-long friends in Edinburgh, thank you for always being there to come home to. You are the best respite from academia and know exactly how to keep me sane. My wonderful family, thank you for your unwavering support and for always believing in me. I guess I'm more like my parents than I thought! And finally, Nathan, you've had the toughest job of all. Thank you for being there for me through it all, and for encouraging me to chase my dreams, even if I ignored your advice: "don't do a PhD!"

Contents

List of Figures

List of Tables

Abbreviations

BCE – Blue carbon ecosystem

BOSCORF – British Ocean Sediment Core Research Facility

CF–CS – Constant flux–constant sedimentation model

DBD – Sediment dry bulk density (g cm^{-3})

DD – Drop-down video camera

DEFA – Department of Environment, Food and Agriculture, Isle of Man Government

DRB – Boat dredge

EA – Elemental analyser

ECZ – Eelgrass Conservation Zone

GHG – Greenhouse gas

HPGe detector – High Purity Germanium well-type gamma spectrometer

IC – Inorganic carbon

IPCC – Intergovernmental Panel on Climate Change

IRMS – Isotope ratio mass spectrometer

MNR – Marine Nature Reserve

NDC – Nationally Determined Contribution

OC – Organic carbon

OCAR – Organic carbon accumulation rate (gC m^{-2} yr^{-1})

OCBE – Organic carbon burial efficiency (%)

OCBR – Organic carbon burial rate (gC m^{-2} yr^{-1})

OTB – Bottom otter trawl

OTT – Multi-rig otter trawl

PSA – Particle size analysis

PTB – Bottom pair trawl

RPD – Root penetration depth (cm)

SAR – Swept area ratio (yr^{-1})

SCD – Sediment organic carbon density ($gC\ cm^{-3}$)

SML – Surface sediment mixed layer

SSS – Side scan sonar

TB – Beam trawl

TBB – Beam trawl

TBN – Beam trawl

TUV – Towed underwater video camera

VIF – Variance inflation factor

VMS – Vessel monitoring system

WISMB – Western Irish Sea Mud Belt

Glossary

Allochthonous carbon – Carbon produced in one location and deposited in another location.

Autochthonous carbon – Carbon produced and deposited in the same location.

Blue carbon ecosystem (BCE) – Marine and coastal ecosystems that can accumulate and store organic carbon for centuries to millennia, which can be enhanced through management measures.

Carbon sequestration – The process of directly capturing atmospheric CO_2 and storing it within a temporary or permanent reservoir.

Labile organic carbon – Carbon compounds that readily undergo chemical change and are considered relatively unstable. These are usually decomposed or respired first by microbes or chemical oxidation.

Long-term organic carbon burial – Organic carbon stored within sediments for greater than 100 years (herein ≥30 cm).

Organic carbon accumulation rate (OCAR) – The rate that organic carbon is stored within sediments for less than 30 years ("short term"), estimated using the sediment organic carbon density at a depth representing sediments ≤30 years old (herein 0–10 cm) multiplied by the sedimentation rate.

Organic carbon burial efficiency (OCBE) – The organic carbon density within sediments stored for greater than 100 years (herein ≥30 cm) as a percentage of the organic carbon density within sediments stored for less than 30 years (herein 0–10 cm).

Organic carbon burial rate (OCBR) – The rate that organic carbon is stored within sediments for over 100 years ("long-term"), estimated using the sediment organic carbon density at a depth representing sediments ≥100 years old (herein ≥30 cm) multiplied by the sedimentation rate.

Recalcitrant organic carbon – Carbon compounds that cannot be decomposed and are considered stable.

Refractory organic carbon – Carbon compounds that are resistant to decomposition and are considered relatively stable.

Short-term organic carbon accumulation – Organic carbon stored within sediments for less than 30 years (herein 0–10 cm).

Publications

Chapter 2 is related to a paper that is currently under review by a peer-review journal and has been published in *ESS Open Archive* as a preprint research article.

Muir, H. C., Reading, D. G., Warwick, P. E., Strong, J. A., Peel, K., Henthorn, R., Keenan, J., Duncan, P. F., Hiddink, J. G., Skov, M. W., Unsworth, R. K. F. & Evans, C. (2025). Organic Carbon Burial Rates in Muddy Temperate Shelf Sea Sediments [Preprint]. *ESS Open Archive*. https://doi.org/10.22541/essoar.174293123.38519064/v1.

Author contributions:

H. C. Muir: Conceptualisation, Methodology, Sample Collection, Data Analysis, Data Visualisation, Investigation, Data Curation, Writing (Original Draft), Writing (Review and Editing), Funding Acquisition

D. G. Reading: Data Analysis (Radionuclides), Writing (Review and Editing)

P. E. Warwick: Data Analysis (Radionuclides), Writing (Review and Editing)

J. A. Strong: Sample Collection, Writing (Review and Editing), Supervision

K. Peel: Data Analysis (Elemental Analysis)

R. Henthorn: Sample Collection, Writing (Review and Editing), Funding Acquisition

J. Keenan: Sample Collection, Funding Acquisition

P. F. Duncan: Writing (Review and Editing)

J. G. Hiddink: Writing (Review and Editing)

M. W. Skov: Writing (Review and Editing)

R. K. F. Unsworth: Conceptualisation, Writing (Review and Editing), Supervision

C. Evans: Conceptualisation, Methodology, Sample Collection, Writing (Review and Editing), Funding Acquisition, Supervision

Chapter 3 is related to a paper that is currently under review by a peer-review journal and is pending publication in a preprint research article.

Muir, H. C., Strong, J. A., Hiddink, J. G., Reading, D. G., Warwick, P. E., Henthorn, R., Keenan, J., Unsworth, R. K. F. & Evans, C. (2025). Stratigraphic Evidence of Organic Carbon Depletion in an Intensely Trawled Muddy Seabed [In review].

Author contributions:

H. C. Muir: Conceptualisation, Methodology, Sample Collection, Data Analysis, Data Visualisation, Investigation, Data Curation, Writing (Original Draft), Writing (Review and Editing), Funding Acquisition

J. A. Strong: Conceptualisation, Methodology, Sample Collection, Data Analysis and Visualisation (VMS data), Investigation, Writing (Review and Editing), Supervision

J. G. Hiddink: Methodology (Statistics), Data Analysis and Visualisation (Statistics), Investigation, Writing (Review and Editing)

D. G. Reading: Data Analysis (Radionuclides)

P. E. Warwick: Data Analysis (Radionuclides)

R. Henthorn: Sample Collection, Funding Acquisition

J. Keenan: Sample Collection, Funding Acquisition

R. K. F. Unsworth: Conceptualisation, Supervision

C. Evans: Conceptualisation, Methodology, Sample Collection, Writing (Review and Editing), Funding Acquisition, Supervision

This thesis provides scientific evidence for the Manx Blue Carbon Project Report that is currently in preparation by the Department of Environment, Food & Agriculture (DEFA), Isle of Man Government.

Henthorn, R., **Muir, H. C.**, Kennington, K., Keenan, J., Gell, F., Emmerson, J., Duncan, P. F., Strong, J. A., Jenkins, S., Hiddink, J. G., Skov, M. W., Evans, C. (In preparation). Manx Blue Carbon Project Report. Isle of Man Government.

Author contribution, H. C. Muir: Data Analysis, Data Visualisation, Investigation, Data Curation, Writing (Review and Editing)

Chapter 1

Introduction

To limit global warming increase to 1.5 °C above pre-industrial levels and to prevent catastrophic breakdown of the climate, immediate reduction and removal of atmospheric greenhouse gas (GHG) emissions is essential (United Nations, 2015). While rapid development of infrastructure such as renewable energy and carbon capture technologies is required to achieve this at scale, the conservation and restoration of natural ecosystems offers cost-effective and scalable atmospheric carbon removal, while preserving existing organic carbon (OC) stores and supporting natural ecosystem processes (Macreadie et al., 2021; Seddon et al., 2020; Smith et al., 2016). Historically, natural climate solutions have been almost exclusively terrestrial, but since 2009, coastal and oceanic "blue carbon" ecosystems (BCEs) have gained recognition for their carbon sequestration potential (Griscom et al., 2017; Macreadie et al., 2021; Nellemann et al., 2009). Like terrestrial ecosystems such as forests, BCEs draw down significant quantities of atmospheric CO_2, which can be preserved within sediments for centuries to millennia, removing it from the active global carbon cycle, provided these ecosystems are protected (de Haas et al., 2002; Macreadie et al., 2021; Nellemann, 2009).

Despite significant progress in understanding OC accumulation and storage in BCEs, substantial data gaps remain, particularly in temperate regions that are less well-studied than tropical regions and in regions impacted by anthropogenic activities. Spatial and temporal variability of OC within and between ecosystems further complicates efforts to integrate BCEs into national climate change mitigation and adaptation strategies. To address these challenges, this thesis investigates sedimentary OC accumulation and storage in temperate BCEs in the Isle of Man, to inform the island's national Blue Carbon Strategy (Figure 1.1). Specifically, this research examines three key BCEs—saltmarshes, seagrass meadows, and shelf sea sediments in the Western Irish Sea Mud Belt (WISMB)—which are predicted to contain substantial OC reserves (Burrows et al., 2024; Legge et al., 2020). By

characterising their spatial and temporal variability, high-resolution estimates are generated that can inform coastal and marine spatial planning for the island.

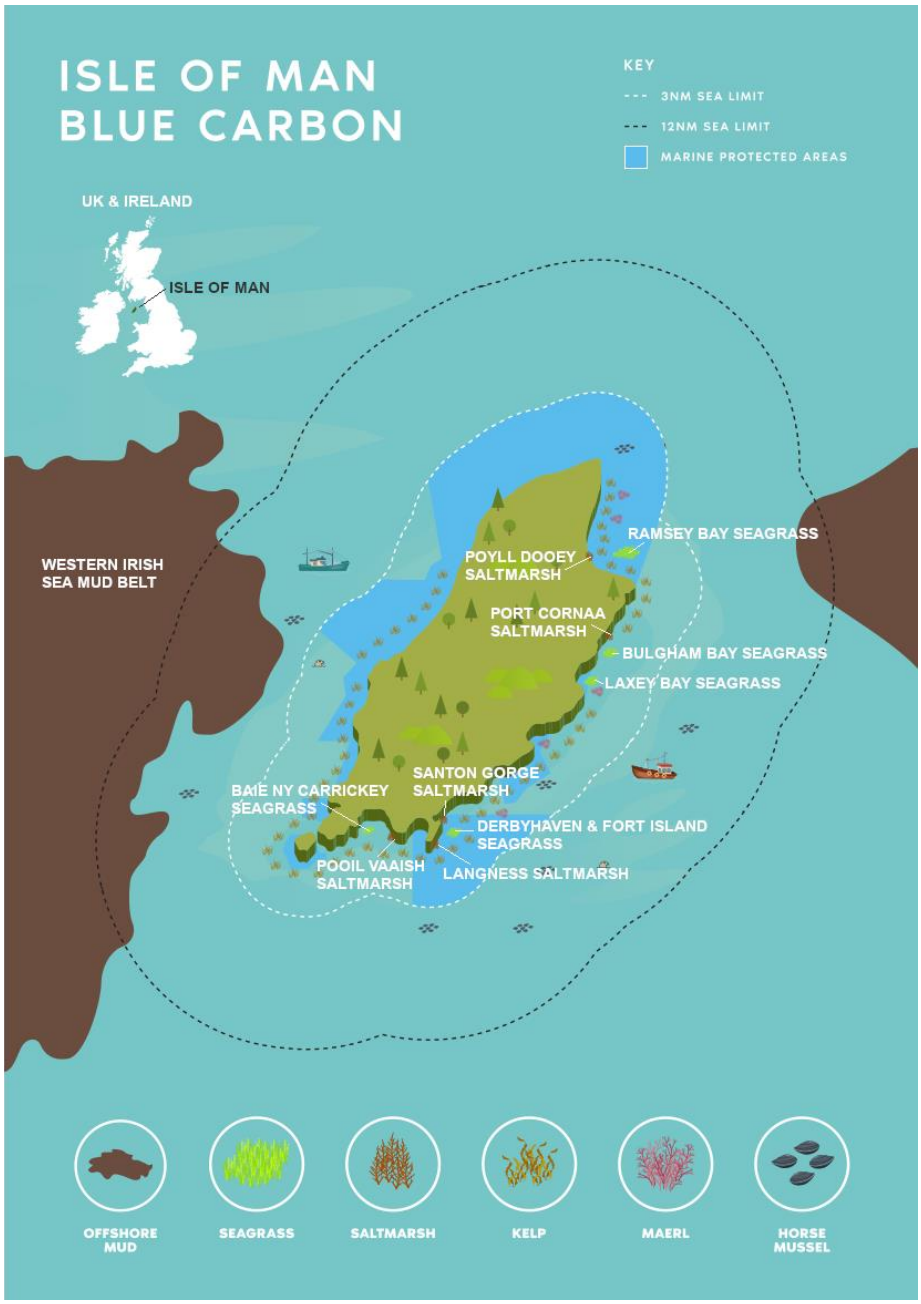

Figure 1.1 Infographic map of the Isle of Man, relative to the United Kingdom, showing the 3 nm boundary (white dashed line), the 12 nm boundary (black dashed line), and Marine Nature Reserves (MNRs, shaded blue). Blue carbon ecosystems include seagrass meadows, saltmarshes, kelp forests, maerl beds, horse mussel reefs, and offshore mud. The ecosystems investigated in this thesis—Western Irish Sea Mud Belt, seagrass meadows, and saltmarshes—are labelled. Adapted from the Isle of Man Blue Carbon Strategy (Isle of Man Government, 2025).

1.1 Blue Carbon Ecosystems

Traditionally, only vegetated coastal wetlands—saltmarshes, seagrass meadows, and mangrove forests—have been considered as BCEs, for their ability to sequester and store organic carbon. This is considered ‘autochthonous carbon’, whereby carbon is produced and deposited in the same area (Howard et al., 2014). Despite covering only 0.2% of the seabed, vegetated coastal wetlands generate up to 10% of the global marine net primary production, contributing to over 50% of marine OC burial in their underlying sediments, and exporting OC to other ecosystems (Duarte, 2017). As a result, vegetated coastal wetlands store sediment OC equivalent to more than half of terrestrial ecosystems (Duarte et al., 2005), sequestering as much as four times more OC per hectare over significantly shorter time scales than terrestrial forests (Davis et al., 2023). Unlike terrestrial ecosystems, where most carbon is stored in plant biomass, 50–90% of OC in BCEs resides in sediments, which continues to accumulate over time (Duarte et al., 2005; Mcleod et al., 2011; Prentice et al., 2020).

The capacity of these coastal wetlands to sequester and store significant quantities of OC in-situ long term, as well as their ability to be effectively managed for enhancing long-term OC storage and monitored for GHG emissions or removals, enables quantification of their capacity for reducing atmospheric GHGs, allowing their inclusion in GHG accounting frameworks and in Nationally Determined Contributions (NDCs) to the Paris Agreement (Hamilton et al., 2023). Furthermore, these BCEs provide services such as coastal protection, biodiversity enhancement, and fisheries support, aligning with multiple United Nations Sustainable Development Goals, providing more co-benefits than carbon capture technologies (Macreadie et al., 2021). Their role in mitigating climate change while improving coastal resilience and livelihoods makes these “actionable” BCEs valuable for climate adaptation strategies.

The definition of BCEs has evolved since 2009 to include “emerging” BCEs, such as donor ecosystems like macroalgae/kelp, which fix carbon via photosynthesis and export it to marine sediments, and acceptor ecosystems like benthic sediments that accumulate organic carbon (Crooks et al., 2018; James et al., 2024). This is considered ‘allochthonous carbon’, whereby carbon is produced and deposited in different areas (Howard et al., 2014). Continental shelf sediments are one example of

these emerging BCEs as critical long-term oceanic carbon reservoirs (Atwood et al., 2020; Legge et al., 2020). Despite covering less than 10% of the ocean, continental shelf sediments have been estimated to contribute up to 30% of global marine primary productivity and bury around 80% of sedimentary OC (Bauer et al., 2013; Harris et al., 2014). Carbon inputs come from air–sea and pelagic–benthic fluxes (e.g. assimilation by photoautotrophic marine organisms), coastal and riverine inputs, and sediment burial, including kelp-derived carbon (Legge et al., 2020; Mathis et al., 2024).

The broader perspective of BCEs considers ecosystems where carbon stores and fluxes can be quantified, and where management measures could be used to enhance carbon storage, for example, by mitigating negative trawling impacts (Crooks et al., 2018; Hamilton et al., 2023; Intergovernmental Panel on Climate Change, 2023). The definition of BCEs in this thesis therefore considers marine and coastal ecosystems that promote net accumulation and long-term storage of OC on climate-relevant timescales (centuries to millennia), which can be enhanced through management measures (Figure 1.2). While emerging BCEs are excluded from blue carbon inventories and Intergovernmental Panel on Climate Change (IPCC) GHG accounting guidelines, improved scientific understanding could enable their inclusion in future (Crooks et al., 2018; Hamilton et al., 2023; Intergovernmental Panel on Climate Change, 2023).

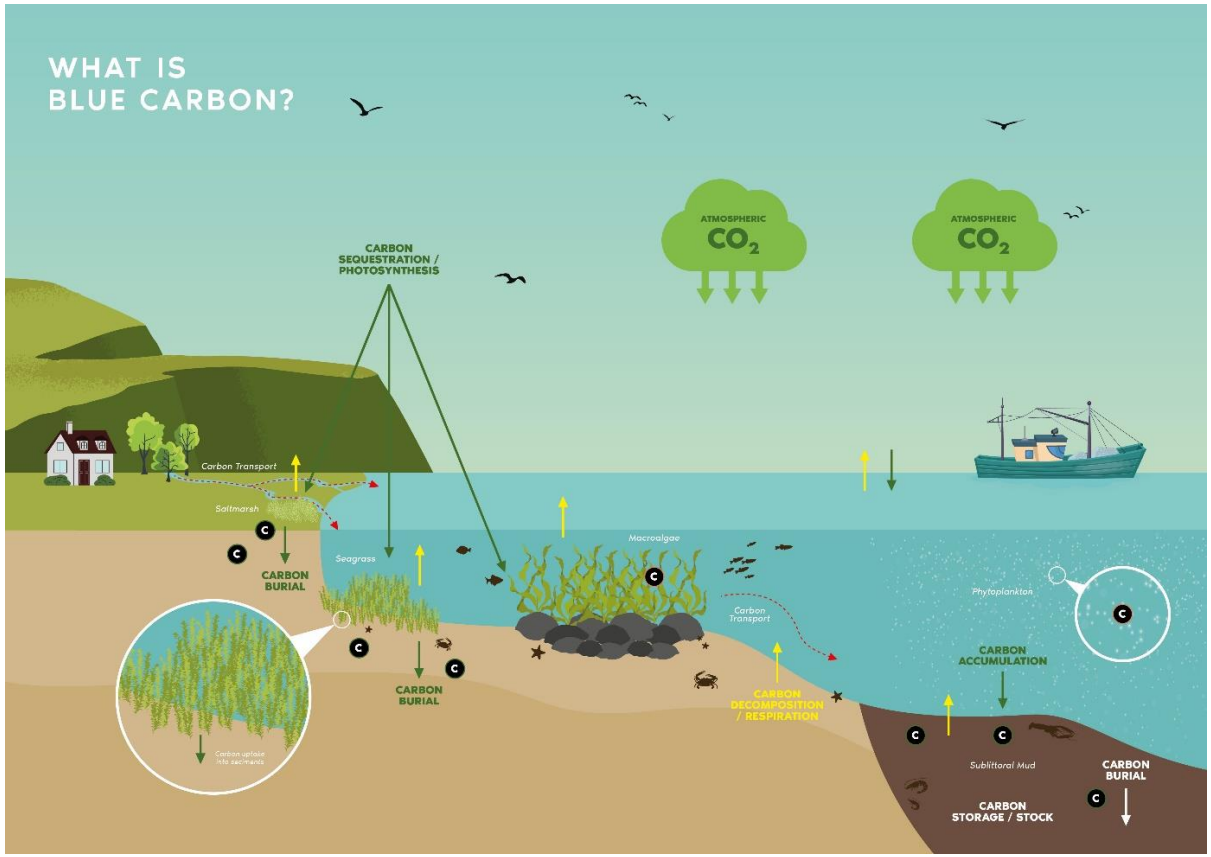

Figure 1.2 Infographic of blue carbon flows in the Isle of Man. Atmospheric CO_2 is sequestered through photosynthesis by photoautotrophs, including terrestrial plants, saltmarsh, seagrass, macroalgae, and phytoplankton. Carbon is transported from land to sea by rivers and currents. Carbon accumulates in the sediment where it can be remineralised/decomposed by respiration or becomes buried. Reproduced from the Isle of Man Blue Carbon Strategy (Isle of Man Government, 2025).

1.2 Sedimentary Organic Carbon Variability

Despite their benefits, estimating long-term carbon storage within coastal and offshore BCEs is challenging due to the spatial and temporal variability within and between ecosystems, on local and global scales, which can be compounded by anthropogenic disturbances such as land use changes and trawling. Current blue carbon management often relies on unrepresentative datasets with high uncertainties that risk over- or underestimating the OC storage, accumulation, and burial capacity of BCEs. Addressing these knowledge gaps is essential to accurately quantify and maximise atmospheric GHG reductions by BCEs, and for ensuring their effective inclusion in national and global climate strategies.

A key challenge in resolving OC storage capacities in BCEs are uncertainties in OC preservation and degradation in sediments. Only a fraction of OC reaching the seabed is buried due to its reactivity and the influence of biological, geochemical, and physical factors (LaRowe et al., 2020). The majority (>95%) of sedimentary OC that reaches the seabed undergoes remineralisation through aerobic and anaerobic pathways (Burdige, 2007; Chen et al., 2022; de Haas et al., 2002), while the remaining <5% becomes buried longer term, enabling net CO_2 removal from the active carbon cycle (Figure 1.3) (Burdige, 2007).

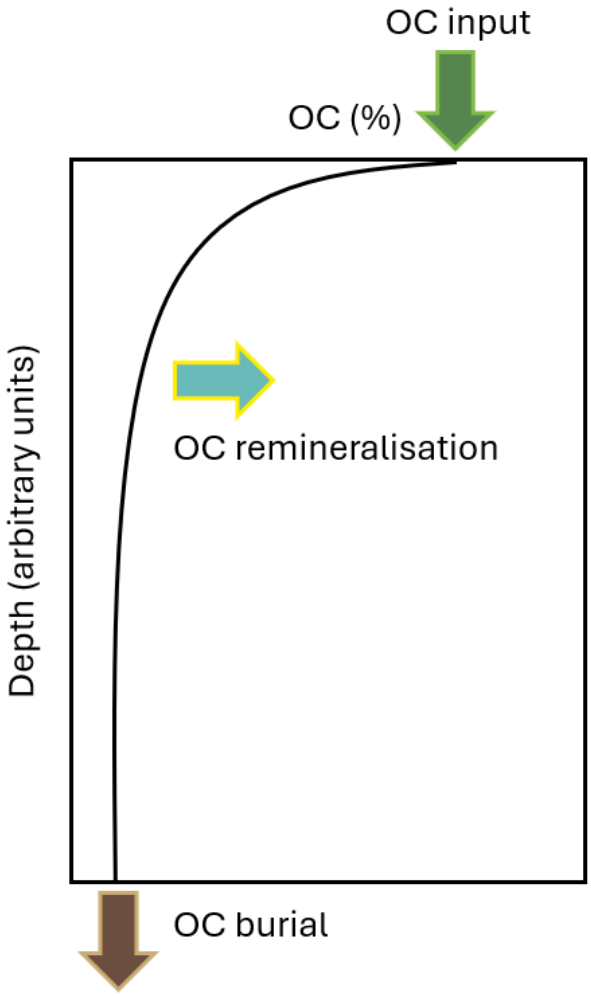

Figure 1.3 A simplified conceptual model of a hypothetical organic carbon (OC) depth profile in marine sediments illustrating the relationship between OC input to the sediment surface, OC remineralisation with sediment depth, and OC burial, which may eventually become preserved over geological timescales. Figure adapted from Burdige (2007).

A lack of standardised methods and limited data availability reduces the accuracy of short-term OC accumulation and long-term OC burial estimates, and restricts comparability between studies (Middelburg, 2019; Smeaton et al., 2021). Blue carbon assessments often rely on OC stocks measured within the top 10 cm of sediments due to sampling limitations, which may overestimate long-term burial if OC remineralisation is ongoing (Burdige, 2007; Diesing et al., 2021). Estimating OC burial efficiencies (OCBEs) based on empirical measurements can improve understanding of long-term OC burial (Bradley et al., 2022).

Furthermore, anthropogenic impacts such as bottom trawling can modify sedimentation rates and OC stocks on continental shelves, increasing uncertainty in OC accumulation and burial estimates (Epstein et al., 2022; Legge et al., 2020; Paradis et al., 2019; Wilkinson et al., 2018). Trawling disturbs sediments through resuspension, mixing, and erosion, exposing OC to successive oxic and anoxic conditions, and microbial degradation, which can accelerate OC remineralisation (Coughlan et al., 2015; Hiddink et al., 2017; Martín et al., 2014a,c; Paradis et al., 2020; Sala et al., 2021). Environmental variables like hydrodynamics and biological activity influence OC storage and reactivity by changing sediment composition, deposition, and oxygen penetration, further complicating trawling impact assessments (Sciberras et al., 2016; Tiano et al., 2019). Most studies examining trawling effects focus only on shallow surface sediments (<10 cm), with limited data on deeper layers, despite mobile trawl gears penetrating up to 40 cm in soft sediments and evidence of trawling impacts within sub-surface sediments (>10 cm) (Epstein et al., 2021; Martín et al., 2014b; Paradis et al., 2019, 2021). These data gaps limit understanding of trawling's long-term impact on OC storage, which could be resolved by empirical research and used to inform fisheries management strategies for blue carbon conservation.

Coastal vegetated ecosystems also face increasing anthropogenic pressures. Global loss of ~50% of seagrass and saltmarsh habitats, the key actionable vegetated coastal BCEs in temperate regions (mangroves are restricted to warmer climates), has reduced their capacity to draw down and store carbon (Grech et al., 2012; Jones and Unsworth, 2016; Macreadie et al., 2021). To date, saltmarshes are estimated to span ~52,880 km² across 120 countries in temperate and Arctic regions (Worthington et al., 2024), while seagrass meadows are estimated to cover 160,387 km² to 266,562 km² across 103–136 nations globally (McKenzie et al., 2020). However, incomplete mapping has led to high estimate uncertainties and hinders targeted ecosystem conservation (Macreadie et al., 2019; Unsworth et al., 2019). Accurate spatial data is therefore needed for effective conservation and management (Strachan et al., 2022).

Sedimentary OC stocks also vary within and among coastal vegetated ecosystems, complicating efforts to extrapolate data across broad geographical scales (Dahl et al., 2016; Greiner et al., 2013, 2016; Prentice et al., 2020; Röhr et al., 2016, 2018). For example, global OC stock estimates for seagrass meadows range from 139.7 to 329.5

± 55.9 MgC ha^{-1} (Fourqurean et al., 2012), while saltmarshes store an estimated 231 ± 134 MgC ha^{-1} in the top meter of tidal marsh soils worldwide (Maxwell et al., 2023). This variability reflects a range of factors influencing OC accumulation and storage rates, including vegetation structure, hydrodynamics, sediment type, sedimentation rates, seasonal variations, and anthropogenic impacts (Dahl et al., 2020; Davidson et al., 2017; Oreska et al., 2017; Smeaton et al., 2023). For instance, the seagrass species *Posidonia oceanica*, endemic to the Mediterranean, accumulates and stores significantly more OC than temperate seagrasses like *Zostera marina* due to the long lifespan of the mats formed by *P. oceanica* (up to 12,500 years), its high primary production rate, and structural adaptations that enhance sediment and particle trapping (Fourqurean et al., 2012; Röhr et al., 2018). Such species-specific differences highlight how OC sequestration estimates from well-studied tropical BCEs can overestimate storage in temperate regions, underscoring the need for region-specific data (Röhr et al., 2018; Smeaton et al., 2024). While progress has been made in quantifying long-term OC storage in BCEs, significant challenges remain for improving accuracy, particularly at local and regional scales (Needelman et al., 2018; Prentice et al., 2020; Sutton-Grier & Moore, 2016). Localised assessments are essential for informing national climate policies and conservation efforts, ensuring effective implementation of blue carbon management strategies.

1.3 Blue Carbon as a Climate Solution

In recent years, coastal nations have started to include BCEs in their national climate action plans as NDCs under the Paris Agreement, and have developed regional blue carbon strategies to help reduce atmospheric GHGs and to adapt to climate change impacts (Bertram et al., 2021; Giritharan et al., 2024; Sun et al., 2024). The UK has acknowledged BCEs (saltmarshes and seagrass meadows) in their NDCs for their climate change mitigation and adaptation measures (Giritharan et al., 2024). As a British Crown Dependency, the Isle of Man aligns with UK ambitions to include coastal BCEs in national emissions reporting, and to achieving Net Zero emissions by 2050 and a 68% emissions reduction on 1990 levels by 2030 (Burden and Clilverd, 2021; UK Climate Change Committee, 2022).

1.4 Blue Carbon in the Isle of Man

In 2019, the chief minister of the Isle of Man recognised the global climate emergency, leading to unanimous approval of the Phase 1 Climate Action Plan in parliament (High Court of Tynwald) (Isle of Man Government, 2021). This Plan committed to developing "a comprehensive blue carbon management plan to maximise carbon sequestration and maintain and restore biodiversity and wider ecosystem services" (Isle of Man Government, 2022a,b). Enhancing natural carbon capture by conservation, restoration, and research of BCEs was identified as a potential strategy for achieving net zero emissions (Curran, 2019). The Manx Blue Carbon Project, which was committed to in the Isle of Man Climate Change Plan 2022–2027, was established to develop a Blue Carbon Strategy informed by comprehensive mapping and quantification of sedimentary OC stocks and accumulation in the island's key BCEs.

The Isle of Man, situated in the Irish Sea, has a 160 km coastline, where most of the population (85,000 people) live, and a 4,000 km² territorial sea, equating to 85% of the total jurisdiction. Marine Nature Reserves (MNRs) cover 10% of the territorial sea (0–12 nm) and over 50% of the inshore area (0–3 nm), with restrictions on mobile fishing gear, except within the Ramsey Bay Marine Reserve, which permits controlled fishing activities (including trawling, dredging, and scallop diving). The seabed and most of its resources (excl. fisheries) are owned by the Isle of Man Government, where the seabed and non-living resources are managed by the Department of Infrastructure, and living resources are managed by the Department of Environment, Food and Agriculture (DEFA). Working together with Government therefore provides an opportunity for evidence-informed policy development and blue carbon management.

Previous research has identified the main BCEs on the Isle of Man as seagrass (*Z. marina*) meadows, saltmarshes, kelp, maerl beds, horse mussel (*Modiolus modiolus*) reefs, and fine-grained (mud or fine sand) sediments (Burrows et al., 2024; Towle, 2018). By extrapolating values from other temperate blue carbon studies to the Isle of Man, these are estimated to store 10.64 Mt within the top 10 cm of sediments and to have a sequestration capacity of 200,000 MgC yr^{-1} (Towle, 2018).

1.4.1 Actionable Blue Carbon Ecosystems

Seagrass meadows, of which *Z. marina* is the sole species in the Isle of Man, and saltmarshes are the only actionable BCEs on the island that could be included within the island's GHG emissions accounting and UK's NDCs (Towle, 2018).

1.4.1.1 Seagrass Meadows

Seagrass forms intertidal and subtidal meadows, with OC storage estimates of 0.0007 MtC yr^{-1} for the Isle of Man (Burrows et al., 2024). Seagrass has been recorded at five sites prior to this study, with the largest known patch located within the Eelgrass Conservation Zone (ECZ) in Ramsey Bay MNR (seagrass is referred to as "eelgrass" within the Isle of Man and its Wildlife Act, but is herein referred to as seagrass or *Z. marina*) (Howe, 2018; Tmmink, 1994). However, the full extent of seagrass meadows remains uncertain, highlighting the need for further research. Nevertheless, *Z. marina* seagrass meadows are protected under the Wildlife Act 1990 and the associated byelaws of the MNRs (Manx Marine Nature Reserves Byelaws 2018, SD2018/0186) (Isle of Man Government, 2018).

1.4.1.2 Saltmarshes

Saltmarshes are estimated to store 0.003 MtC yr^{-1} on the Isle of Man (Burrows et al., 2024). Their areas are well documented, having a total extent of 7.38 ha across five locations, including Poyll Dooey saltmarsh (Sulby River), Port Cornaa, St Michael's Isle (Fort Island), Pooil Vaaish, and Langness (Sayle, 1995; Spencer, 2005). Sedimentation rates have been estimated at three saltmarshes (Poyll Dooey, Langness, and Port Cornaa) using radionuclide-based dating techniques (Croudace et al., 2019; Spencer, 2005). However, like seagrass meadows, the carbon storage capacities of saltmarshes remain largely unknown, necessitating further research. Saltmarshes are not designated as protected habitats in the Isle of Man, although certain plant species found within them are protected under the Wildlife Act 1990. The saltmarshes at Langness, St Michael's Isle, and Pooil Vaaish are afforded land-based protection as designated features within Areas of Special Scientific Interest.

1.4.2 Emerging Blue Carbon Ecosystems

1.4.2.1 Shelf Sediments

Most blue carbon stored around the Isle of Man is estimated within fine-grained (mud or fine sand) sublittoral sediments, particularly in the WISMB (Burrows et al., 2024; Towle, 2018), which is considered a major store of OC in the Northeast Atlantic continental shelf (Burrows et al., 2024; Smeaton et al., 2021a). Low tidal currents and bed stress, coupled with a seasonal gyre, enhance sediment retention and contribute to significant OC deposition in the WISMB, with mud deposits up to 40 meters thick (Belderson, 1964; Coughlan et al., 2015, 2021; Hill et al., 1997; Kershaw, 1986; Williams et al., 2019). Cyclonic tidal currents generate a narrow tidal benthic boundary layer with low overlying water turbulence, which promotes deposition of fine-grained sediment and limits the movement of resuspended sediment (Williams et al., 2019). A seasonal baroclinic gyre over the WISMB driven by seasonal solar heating of the Irish Sea in spring and summer also promotes sediment deposition and enables sediment retention (Hill et al., 1997; Williams et al., 2019). While these fine-grained subtidal sediments have been identified as significant stores of OC in the Isle of Man territorial sea (Towle et al., 2018), limited scientific understanding limits their inclusion within Net Zero plans, necessitating further research.

Modern sedimentation rates in the Irish Sea are well constrained through the use of natural and anthropogenic radionuclides. The naturally occurring radionuclide ^{210}Pb (22.3-year half-life) is deposited from the atmosphere at a relatively constant rate, decaying with depth in marine sediments and serving as a robust chronological marker (Appleby and Oldfield, 1978; Graves et al., 2022). Meanwhile, anthropogenic radionuclides such as ^{137}Cs (30-year half-life) and ^{241}Am (432.6-year half-life; Marouli et al., 2020) have been released into the Irish Sea primarily from the Sellafield nuclear facility, serving as distinct time markers that are useful for impulse dating of sediments (Gray et al., 1995). The Sellafield nuclear facility was the dominant source of ^{137}Cs from 1952 to 1998, with a significant discharge event in 1975, surpassing other major inputs such as the 1986 Chernobyl accident (6,000 TBq), discharges from the Cap de la Hague facility in France (1,000 TBq), and global fallout from nuclear weapons testing in the 1950s–1960s (12,000 TBq)

(Coughlan et al., 2015; Gray et al., 1995; Povinec et al., 2003; Maderich et al., 2021). These radionuclides have since been redistributed across the Irish Sea through hydrodynamic processes, including tidal current rotation and sedimentary circulation patterns, and incorporated into sediments (Coughlan et al., 2015; Gray et al., 1995; Kershaw et al., 1986; Povinec et al., 2003). When used in conjunction with ^{210}Pb profiles, these anthropogenic radionuclides offer a reliable means of estimating sedimentation rates (Coughlan et al., 2015), which can be used to improve assessments of carbon accumulation potential in the region.

Phytoplankton, primarily comprising diatoms, dinoflagellates, and green algae, is the dominant source of OC to the WISMB, contributing approximately 0.35 MtC yr^{-1} (Burrows et al., 2024). Primary production exhibits strong seasonal variability, driven by light availability and surface mixing, with peak production occurring in spring and summer when light penetration and thermal stratification are at their highest (Hill, 2007). Conversely, zooplankton grazing, particularly by copepods, serves as a key pathway for OC mineralisation (Hill, 2007). In addition to autochthonous production, allochthonous OC inputs originate from water masses circulating in the Irish Sea, with contributions from the Celtic Sea (66%), Irish waters (14%), and English waters (20%) (Bowers et al., 2013). The distribution and fate of OC from phytoplankton and zooplankton are influenced by distinct hydrographic regimes, including deep-channel flow along the Western Irish Sea (Ramster and Hill, 1969; Williams et al., 2019) and surface and near-seabed currents around the Isle of Man (Legge et al., 2020; Ramster and Hill, 1969). Seasonal hydrographic zonation, particularly within the summer gyre, further modulates OC transport and deposition (O'Reilly et al., 2014). Phytoplankton biomass is significantly higher in well-mixed waters than in stratified regions, and copepod grazing plays a critical role in organic matter remineralisation, especially during seasonal phytoplankton blooms (O'Reilly et al., 2014). Additional sources of sedimentary OC include kelp beds, salt marshes, intertidal macroalgae, and seagrass beds (Burrows et al., 2024), while rivers along the Irish coastline supply substantial terrestrial recalcitrant OC, which is widely distributed in Irish Sea sediments (O'Reilly et al., 2014).

Kelp forests, as well as maerl beds (coralline algae) and horse mussel beds, have also been identified as emerging BCEs in the Isle of Man (Figure 1.1) (Burrows et al.,

2024; Towle et al., 2018). These ecosystems are important for the biological carbon cycle as they store carbon through processes including photosynthesis and dissolution, and release carbon through processes including remineralisation, respiration, and calcification (Howard et al., 2023; James et al., 2024). However, currently there is insufficient evidence of the net OC sequestration capacity of these ecosystems and uncertainty around whether management measures could increase their contribution to long-term OC stocks. Considering these significant scientific and management uncertainties, quantifying the OC stocks, accumulation, and burial rates of kelp forests (and other macroalgae), maerl beds, and horse mussel beds is outside the scope of this PhD thesis.

1.5 Thesis Overview

This thesis investigates the spatial and temporal variability of sedimentary OC in temperate actionable BCEs (saltmarshes and seagrass meadows) and emerging BCEs (shelf sediments/WISMB) in the Isle of Man. The findings aim to inform blue carbon management and policy, aligned with the Isle of Man Government's ambition to develop a Blue Carbon Strategy to enhance carbon sequestration.

Three research questions guide this study:

1. What are the OC stocks, accumulation, and burial rates in the WISMB sediments? (Chapter 2)
2. How does bottom trawling impact sedimentary OC stocks in the WISMB? (Chapter 3)
3. What are the OC stocks and accumulation rates in saltmarshes and seagrass meadows (coastal vegetated BCEs) in the Isle of Man? (Chapter 4)

1.5.1 Hypothesis

For each research question, the following hypotheses were developed:

Chapter 2:

- Impulse dating of radionuclide discharges from the Sellafield nuclear facility, combined with OC depth profiles, will enable quantification of age- and depth-resolved OC accumulation and burial rates.
- OC stocks will decrease with depth due to degradation over time.

Chapter 3:

- Chronic bottom trawling (repeated, long-term, and intensive trawling in the same area over time) will negatively impact OC stocks in the WISMB.
- Mixing effects in surface sediments will obscure trawling impacts on OC stocks.

Chapter 4:

- Saltmarshes will have higher OC stocks than seagrass meadows.
- Seagrass meadows will have higher OC stocks than adjacent unvegetated sediments.
- Seagrass meadows will have greater spatial extent than saltmarshes.

1.5.2 Thesis Summary

These hypotheses were tested in the following data chapters:

Chapter 2 examines OC accumulation and burial in the WISMB using impulse dating of radionuclide discharges from Sellafield nuclear facility and high-resolution OC depth profiles. The findings indicate that 74% of OC accumulated annually in surface sediments (younger than 30 years) becomes buried for over 100 years. These findings highlight that OC stocks in the top 10 cm of sediments do not reliably reflect long-term OC storage, due to OC degradation over time within sediments.

Chapter 3 investigates the impact of modern *Nephrops norvegicus* fisheries in the WISMB on OC stocks, by examining different sediment depth horizons. The findings reveal that OC is depleted in sub-surface sediments deposited in 1960–1990 (10–20 cm), while gear penetration into deeper sediments from 1860–1960 (≥20 cm)

has less effect, and sediment mixing by competing environmental factors potentially masks trawling effects in surface sediments deposited in 1990–2022 (≤10 cm).

Chapter 4 presents the first estimates of OC storage in saltmarshes and *Z. marina* seagrass meadows in the Isle of Man. Using side-scan sonar and in-situ surveys, 195.88 ha of seagrass were mapped, in addition to 7.38 ha of saltmarshes. Sediment thickness and OC density are greater in saltmarshes, whereas total OC stock was 35% greater in seagrass meadows (top 10 cm) due to their larger extent. Seagrass sediments store 43% more OC than unvegetated sediments in the top 10 cm, though this difference diminished with depth.

The results of this thesis underscore the significance of the WISMB as a long-term OC reservoir, surpassing conventional vegetated BCEs in storage capacity, despite the negative impact of trawling on this region. These findings also highlight the need to integrate sediment depth and age assessments alongside OC stock data to refine blue carbon assessments and to inform policy development.

Chapter 2

Organic Carbon Burial Rates in Muddy Temperate Shelf Sea Sediments

Abstract

Continental shelves are globally significant sinks for atmospheric CO_2, thereby mitigating climate change. Evaluating their contribution to climate regulation requires quantification of long-term organic carbon (OC) burial rates into the seabed. However, this understanding is hindered by a scarcity of age-resolved sedimentary OC data resulting from methodological challenges, primarily in obtaining sedimentation rates and quantifying OC degradation, as well as challenges associated with sampling offshore sediments. Herein, sedimentation rates were estimated for the Western Irish Sea Mud Belt (WISMB) by dating sediments using natural and anthropogenic radionuclides from authorised radionuclide discharges from the Sellafield nuclear facility. In combination with empirical high-resolution OC depth profiles, the average long-term (>100 years) OC burial rate for the WISMB is estimated as 23 gC m^{-2} yr^{-1}, with an OC burial efficiency of 74% compared to an average short-term (<30 years) OC accumulation rate of 31 gC m^{-2} yr^{-1}. These results highlight that OC burial rates in the WISMB are comparable with other global depositional zones, including coastal fjords and glacial troughs. This study shows that empirical age-resolved sediment depths and OC degradation profiles can improve assessments of long-term OC burial in depositional shelf seas, helping to resolve the significant role of shelf seas in climate regulation.

2.1 Introduction

Continental shelf sediments play a crucial role in climate change mitigation as a significant sink for CO_2 absorbed by the ocean (Atwood et al., 2020). This is particularly notable in net-depositional zones, such as coastal mud belts and glacial troughs (Diesing et al., 2021; Smeaton et al., 2021a). Photosynthetic plants and algae can assimilate CO_2 from the atmosphere or water column, converting inorganic carbon (IC) to organic carbon (OC). This OC is naturally reactive, and most becomes remineralised (LaRowe et al., 2020), while the remainder can be transported to and settle on the seabed (Mathis et al., 2024; Nellemann et al., 2009). More than 95% of this settled OC undergoes remineralisation through various aerobic and anaerobic pathways before it can become buried (Burdige, 2007; Chen et al., 2022; de Haas et al., 2002; LaRowe et al., 2020). As sedimentary OC becomes buried, reactive labile OC is degraded, leaving behind less reactive refractory OC. This OC degradation can be enhanced by repeated exposure to oxic and anoxic conditions caused by sediment resuspension and mixing, such as from hydrodynamics (waves, tides, storm events), bioturbation, and bottom trawling, which are prevalent across shelf seas (Burdige, 2007; de Haas et al., 2002; Song et al., 2022).

OC accumulation rates (OCARs) and OC burial rates (OCBRs) are primary metrics for quantifying the capacity of coastal and marine sediments to uptake atmospheric greenhouse gases (GHGs) and store OC over short-term (accumulation) and long-term (burial) periods (Wilkinson et al., 2018). Distinguishing between OCARs and OCBRs is essential to avoid overestimating the long-term climate change mitigation capacity of these sediments and for developing effective conservation management and greenhouse gas accounting (Wilkinson et al., 2018; Williamson and Gattuso, 2022). However, inconsistent definitions of OC accumulation and burial, and a lack of standardised methodologies for estimating these has led to misleading conclusions, making these estimates uncertain and limiting comparability across studies (Bradley et al., 2022; Wilkinson et al., 2018). Terms such as OC fluxes, accumulation, sequestration, and burial have been used interchangeably to describe both short-term accumulation and long-term burial within sediments, further complicating comparisons (Hu et al., 2016; Wilkinson et al., 2018). Clearly defining and differentiating between OCARs and OCBRs is therefore crucial for a better

understanding of long-term ocean carbon cycling and estimating the role of coastal and marine sediments in climate change mitigation.

A fundamental challenge in this context is that OC significantly degrades at the sediment surface, particularly near the sediment-water interface, before it eventually stabilises at greater sediment depths (Burdige, 2007). Despite this, OC burial and storage is often estimated from surface sediments or undefined sediment depths, without knowing sediment age or OC stability (Hu et al., 2016; LaRowe et al., 2020; Sanders et al., 2010). This can potentially overestimate the long-term CO_2 mitigation capacity of marine sediments. Use of surface sediments is often due to a scarcity of OC concentration data at deeper sediment depths compared to an abundance of surface sediment data obtained from grab samples and short sediment cores, often more conveniently obtained during routine monitoring programs (Dubosq et al., 2021; Graves et al., 2022; Wilkinson et al., 2018). Furthermore, rates of OC degradation vary depending on depositional settings, sedimentation rates, and sediment mineralogy, making it difficult to constrain these processes (Bradley et al., 2022; LaRowe et al., 2020).

To quantify how OC degradation with sediment depth can impact OC burial compared to OC accumulation, estimates of OC burial or transfer efficiencies (OCBEs) based on empirical measurements can more accurately describe long-term OC storage as the proportion of OC deposited on the seafloor that becomes buried long term, on centennial to millennial timescales (Bradley et al., 2022; de Haas et al., 2002; Nellemann et al., 2009). This approach acknowledges that OC continues to degrade within deeper sediment layers, moving through sediment depth horizons over time (Bradley et al., 2022). But, as degradation rate slows past a certain depth, i.e. OC concentration changes approach zero, long-term OC burial can be estimated. Estimating OCBEs requires an understanding of sediment depth and age, along with associated OC concentrations. However, comparability of OCARs and OCBRs is often hindered by insufficient information on sediment ages, which can result in comparisons between sediment layers of notably different ages, leading to misleading conclusions about OC degradation and burial (Wilkinson et al., 2018). Moreover, sediment disturbance from bioturbation, hydrodynamics, and anthropogenic activities (e.g. chronic bottom trawling) can alter sedimentation rates, composition, and OC concentrations, increasing variability and uncertainty in OCAR

and OCBR estimates (Dubosq et al., 2021; Paradis et al., 2019; Wilkinson et al., 2018).

Various studies have estimated long-term OCBEs based on modelled sedimentary age and OC concentrations (Bradley et al., 2020; LaRowe et al., 2020; Wilkinson et al., 2018), but empirical measurements remain limited. Herein, high-resolution analysis of OC concentration depth profiles combined with sediment dating, provides the first estimates of OCARs, OCBRs, and OCBEs for the Western Irish Sea Mud Belt (WISMB), a muddy depositional zone in the Irish Sea. Analysis of natural radionuclides (^{210}Pb, ^{210}Po) and anthropogenic radionuclides (^{137}Cs, ^{241}Am) from the Sellafield nuclear facility (Gray et al., 1995)—the main source of anthropogenic radionuclides to Irish Sea sediments over the past 100 years (1952 to 1998), which have been widely used to estimate sedimentation rates in the Irish Sea (Coughlan et al., 2015; Gray et al., 1995; Kershaw et al., 1986; Povinec et al., 2003)—facilitates accurate sediment dating herein.

Based on the results of this study, the term OCAR is defined as the rate that OC is stored within sediments for less than 30 years ("short term"), estimated using the sediment OC density at a depth representing sediments ≤30 years old multiplied by the sedimentation rate. Meanwhile, the term OCBR is defined as the rate that OC is stored within sediments for over 100 years ("long-term"), estimated using the sediment OC density at a depth representing sediments ≥100 years old multiplied by the sedimentation rate. The term OCBE is defined as the OC density within sediments stored for greater than 100 years as a percentage of the OC density within sediments stored for less than 30 years.

This study offers high-resolution data on OC burial over a century (de Haas et al., 2002; Nellemann et al., 2009) and provides empirical evidence of OC degradation over time, supporting conceptual models and modelled estimates for shelf seas (Bradley et al., 2020; Burdige, 2007; LaRowe et al., 2020; Wilkinson et al., 2018). Acknowledging the potentially degraded state of the WISMB caused by chronic bottom trawling and extensive bioturbation, the impacts of sediment mixing on OC accumulation and burial are also discussed, which are often omitted from global OCBE models (LaRowe et al., 2020). This study enhances our understanding of the

long-term climate change mitigation potential of the WISMB and depositional zones across global shelf seas.

2.2 Materials and Methods

2.2.1 Sampling Site Selection

Sediments were sampled from the northeastern corner of the WISMB where permits were provided by the Isle of Man Government within their territorial sea. Sampling stations were distributed across muddy sediments within the study region to ensure sediment samples were representative of the WISMB and to account for spatial variability in sediment type and water depth at the edge of the WISMB. Sediment textural classifications informed the selection of muddy sediment sites (Figure 2.1; British Geological Survey, 2024; Folk, 1954). GEBCO Gridded Bathymetry Data informed the selection of sites distributed across water depths of approximately 60–130 m (Figure 2.2; GEBCO Compilation Group, 2024), to account for changes in tidal and current energy away from the edge of the WISMB.

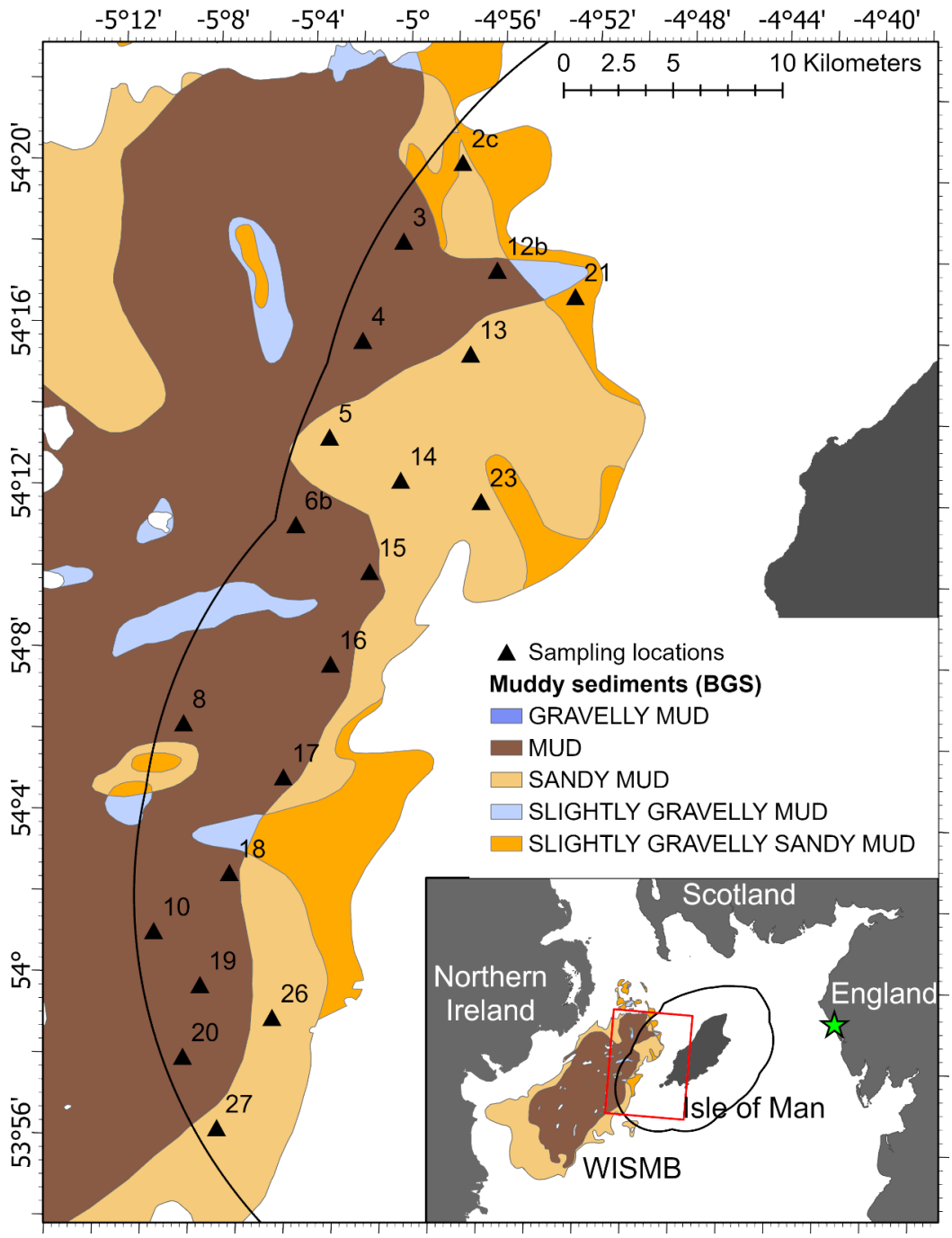

Figure 2.1 Map of the Western Irish Sea Mud Belt (WISMB) and sampling site locations labelled with sediment core identification codes. Muddy sediment classifications by the British Geological Survey Seabed sediments 250K dataset (mud (M), sandy mud (sM), gravelly mud and slightly gravelly mud ((g)M), and slightly gravelly sandy mud ((g)sM)) are shown (British Geological Survey, 2024). The inset map shows the WISMB in the Irish Sea relative to neighbouring countries. The sampling region is highlighted by a red box. The Sellafield nuclear facility is marked with a green star on the west coast of England.

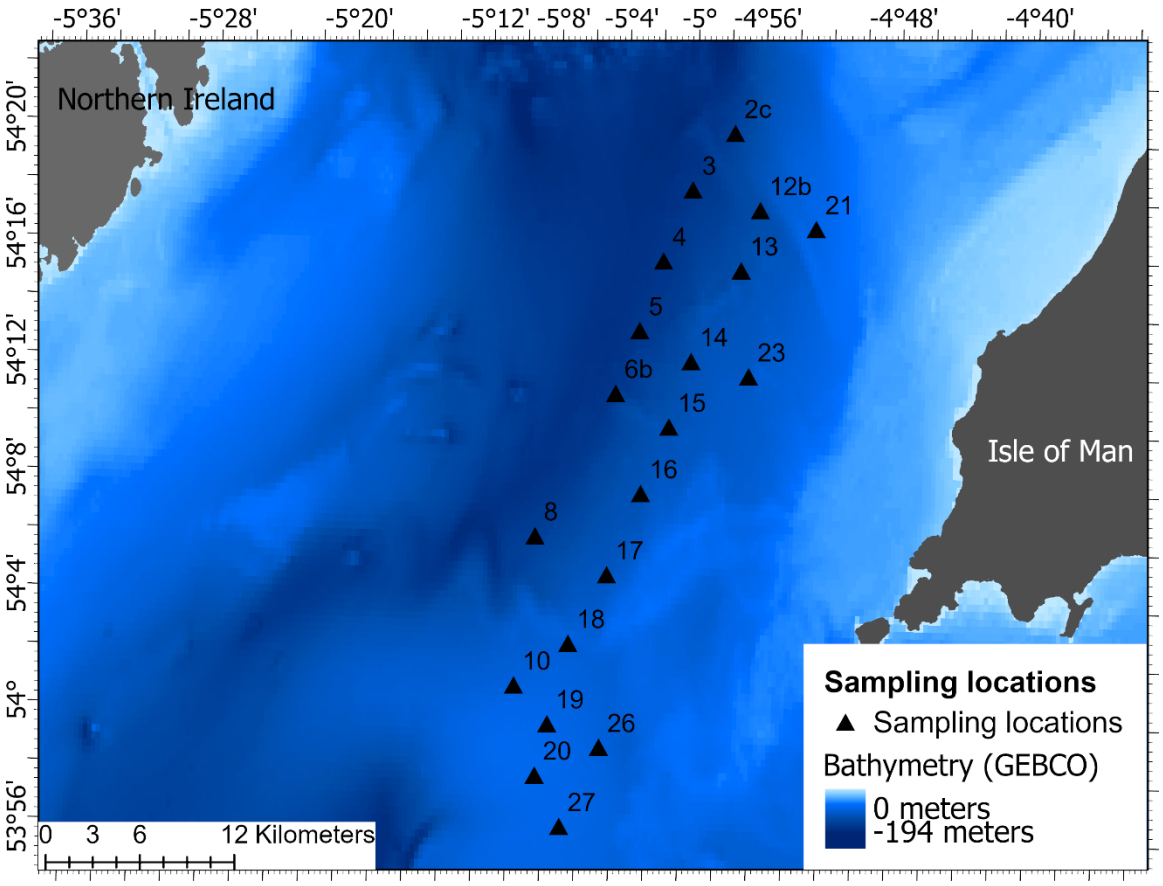

Figure 2.2 Map of the Western Irish Sea bathymetry (meters) and sampling site locations labelled with sediment core identification codes. Bathymetry sourced from GEBCO Gridded Bathymetry Data (GEBCO Compilation Group, 2024).

2.2.2 Sediment Sampling

A total of 20 sediment cores of ≥50 cm length was collected from the fisheries enforcement vessel 'Barrule' across a benthic fishing pressure gradient in the WISMB in June 2022. Sediment cores were collected at each site using a UWITEC gravity corer (height = 120 cm; internal diameter = 9 cm) deployed from the Barrule, which free-fell through the water column and was retrieved onboard the vessel using a winch (Figure 2.3). Water depth at each site was recorded using the research vessel depth sounder during corer deployment when the corer reached the seabed, as indicated by slack rope. Depths were later corrected for tidal state by adding the tidal elevation (+ or -) at the time/date and position that each core was collected using tide charts. The corer was held upright and after the resuspended sediment settled at the

sediment surface in the corer, the overlying water was drained by drilling a hole in the PVC core liner approximately 3–5 cm above the sediment surface, to limit sediment–water mixing during transport. The whole cores were stored upright in a commercial fridge at temperatures below 5°C on the Isle of Man to preserve their integrity. The cores were transported upright in a chilled container to the British Ocean Sediment Core Research Facility (BOSCORF) at the National Oceanography Centre, Southampton, where all subsequent laboratory analyses were performed. The sediment cores collected during this survey were the same cores that were used in Chapter 3 of this thesis.

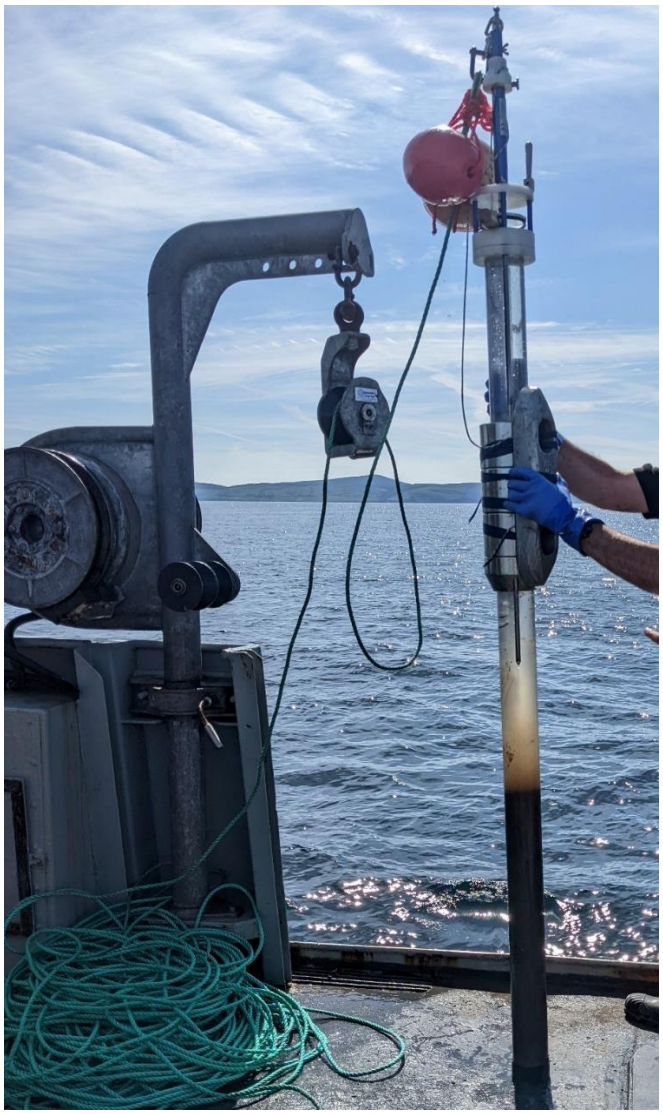

Figure 2.3 Photograph of a UWITEC sediment corer stood upright attached to a winch on the fisheries enforcement vessel ‘Barrule’ after sediment core retrieval from the Western Irish Sea Mud Belt in June 2022.

2.2.3 Sediment Core Processing

Sediment cores were split lengthwise using a Geotek core splitter at BOSCORF. High-resolution images of the smoothed sediment surfaces were captured using a Geotek Core Imaging System (MSCL-CIS) with a Geoscan V camera (1,000 pixels cm^{-1}). X-ray radiography images were collected for all sediment cores (except Sites 4, 8, 13, 14, 20, 2c, due to equipment failure) using a ScoutXcan Multi-Angle Digital 2D X-Ray System.

Sediment samples were taken from the centre of each core to minimise disturbance effects from coring. A U-channel of known volume was used to extract samples at depth intervals: every 2 cm for the top 20 cm of the sediment core, every 5 cm between 20–50 cm, and every 10 cm beyond 50 cm. Sampling resolution increased towards the sediment surface to account for more significant changes expected in sediment properties at shallower sediment depths (Howard et al., 2014). Samples were freeze-dried and homogenised, and both wet and dry weights were recorded before analysis. It was not possible to estimate the degree of sediment compaction that could have occurred during sediment sampling due to the inaccessible deep-water sampling environment, therefore sediment compaction correction factors have not been estimated to correct for compaction in these sediment cores.

2.2.4 Sediment Dry Bulk Density

Sediment dry bulk densities (DBDs) were estimated using Equation 2.1 (Howard et al., 2014).

Equation 2.1 Sediment dry bulk density (DBD) calculation.

$$DBD\ (g\ cm^{-3}) = \frac{Mass\ of\ dry\ sediment\ (g)}{Original\ volume\ sampled\ (cm^3)}$$

2.2.5 Sediment Organic Carbon Content

The OC and total carbon concentrations were measured using a Flash 2000 Elemental Analyser (EA). Triplicate measurements were taken for a few samples every run, to ensure sub-samples were representative of the bulk sample, and to ensure measurement accuracy and precision. The IC was removed using 50% HCl and dried on a hot plate before analysis.

Sediment organic carbon density (SCD) was estimated using Equation 2.2 (Howard et al., 2014).

Equation 2.2 Sediment organic carbon density (SCD) calculation.

$$SCD\ (gC\ cm^{-3}) = \frac{OC\ concentration\ (\%)}{100\%} * DBD\ (g\ cm^{-3})$$

2.2.6 Sediment Particle Size

Particle size distributions were determined using a Malvern Mastersizer 3000 laser microgranulometer, following the NE Atlantic Marine Biological AQC Best Practice Guidance for Particle Size Analysis (PSA) (Mason, 2022). Every other sample depth was analysed down to 40–45 cm (e.g. 0–2 cm, 4–6 cm, etc.), due to resource limitations. Samples were dispersed in a 1% Calgon solution (sodium hexametaphosphate) and sonicated for 10 minutes prior to analysis. Samples with particle diameters >2000 µm were sieved using a 1000 µm mesh prior to analysis, and the results from laser diffraction (volumetric) were scaled to the overall sample (mass) by assuming constant sediment density. Particle size classes were grouped as: clay (<3.9 µm), silt (3.9–62.5 µm), mud (<62.5 µm), and sand (62.5–2000 µm) based on Udden (1914) and Wentworth (1922). The Folk (1954) classification scheme was used for sediment classification.

2.2.7 Sediment Accumulation Rate

Radionuclide analysis was carried out on freeze-dried sediments sampled at 1 cm resolution from the top 40 cm of 7 sediment cores (Sites 4, 8, 14, 15, 20, 21, 27) that

represented the main environmental and anthropogenic gradients in the study region. Sediments were measured for ^{210}Pb, ^{137}Cs, and ^{241}Am using Mirion (Canberra) Canberra High Purity Germanium (HPGe) well-type gamma spectrometers (GAU-Radioanalytical, University of Southampton) under their accreditation to ISO/IEC17025. Data acquisition was performed using Genie-2000 (Mirion Canberra) and spectral analysis was performed using Fitzpeaks 32 deconvolution software. The HPGe detectors were efficiency calibrated using a certified, mixed gamma radionuclide standard (National Physical Laboratory, UK), which was homogenised into a near-identical sample matrix to that of the test sample. Samples were counted for at least 8 hours to achieve low limits of detection. Alpha spectrometry (Ortec Octete) was conducted to measure the grand-daughter radionuclide, ^{210}Po, which would be in equilibrium with ^{210}Pb, for 3 sediment cores (Sites 4, 8, and 20), to cross-validate the ^{210}Pb activities, which were close to the instrumental limit of detection and had higher uncertainty. To prepare samples for alpha spectrometry, an aliquot of sample was spiked with ^{209}Po as a chemical yield monitor and then digested using *aqua regia*. A clean silver disc was then placed in the resultant digest for ^{210}Po autodeposition. Average linear sedimentation rates were estimated from ^{210}Pb and ^{210}Po using the constant flux constant sedimentation (CF–CS) model (Appleby and Oldfield, 1978), which were validated using ^{137}Cs activity (impulse) peaks corresponding to the 1975 discharge maximum from the Sellafield nuclear facility relative to the core surface representing the year 2022, and the onset of cumulative ^{241}Am activities corresponding to ^{241}Am discharge records from the Sellafield nuclear facility (Gray et al., 1995). The ^{241}Am radionuclide was used as an onset marker due to its association with fine-grained sediments in the vicinity of Sellafield nuclear reprocessing facility, which provide a continuous supply of ^{241}Am to the WISMB after discharges ceased (Ray et al., 2020). A degree of uncertainty was accepted to account for a lag time between ^{241}Am discharge and its deposition in the sediment record. Meanwhile, the ^{137}Cs radionuclide was used as an impulse marker due to its widespread dispersal throughout the Irish Sea as a Cs^{+} cation in seawater and weaker sediment association, such that instantaneous deposition in the WISMB was therefore assumed (Ray et al., 2020). Average linear sedimentation rates were estimated from ^{210}Pb, ^{210}Po, and ^{137}Cs activity profiles, where reliable data were available, and used to estimate sediment age for the top 50 cm.

2.2.8 Organic Carbon Accumulation and Burial Rates and Efficiencies

The OC concentrations and sedimentation rates were used to define depths representing short-term OC accumulation and long-term OC burial. Short-term OC accumulation was based on average sediment properties for the top 10 cm of sediments to minimise the influence of surface mixing at the sediment–water interface and to enable comparison with other studies (Diesing et al., 2021). Long-term OC burial was based on average sediment properties for 30–50 cm of sediments to ensure a comparable number of data points were used (n = 4) compared to the top 10 cm (n = 5).

OCARs were estimated using Equation 2.3, OCBRs were estimated using Equation 2.4, and OCBEs were estimated using Equation 2.5.

Equation 2.3 Organic carbon accumulation rate (OCAR) calculation.

$$\text{OCAR (gC } m^{-2}\ yr^{-1}) = \text{ Sediment organic carbon density}_{0-10\text{ cm}}(\text{gC } cm^{-3}) * \text{sedimentation rate (cm } yr^{-1}) * 10000$$

Equation 2.4 Organic carbon burial rate (OCBR) calculation.

$$\text{OCBR (gC } m^{-2}\ yr^{-1}) = \text{ Sediment organic carbon density}_{30-50\text{ cm}}(\text{gC } cm^{-3}) * \text{sedimentation rate (cm } yr^{-1}) * 10000$$

Equation 2.5 Organic carbon burial efficiency (OCBE) calculation.

$$\text{OCBE (\%)} = \frac{\text{Organic carbon burial rate (gC } m^{-2}\ yr^{-1})}{\text{Organic carbon accumulation rate (gC } m^{-2}\ yr^{-1})} * 100\%$$

Sediment cores that had anomalous sediment properties or which exhibited characteristics of freshly deposited sediments were excluded from the dataset to ensure estimates represented short-term and long-term OC burial across the study region. As such, the average values for OC concentration, DBD, and SCD were based on results from 18 sediment cores and excluded data from two anomalous sediment cores (Sites 14 and 6b). Data were excluded from Site 14, as this had OC concentrations and radionuclide activities comparable with surface sediment deposits at 0–40 cm sediment depth, likely reflecting rapid deposition (short-term accumulation) of modern sediment, but not OC burial. Data were excluded from Site 6b, as this reflected an anomalous depositional environment, whereby sediment type varied with depth from a red-coloured layer at 0–10 cm overlying a coarse gravel layer at 10–20 cm with significantly lower OC concentrations that increased with sediment depth below 20 cm.

2.3 Results

2.3.1 Sediment Core Samples

Sediment cores were collected from 20 sites across the study area at water depths ranging from 66 m to 132 m, with core lengths of 50 cm to 88 cm (Table 2.1). Analytical data (DBD, OC content, SCD, and particle sizes) were successfully collected from all samples up to 50 cm, except for Site 2c due to a dense shell layer at 48–50 cm. Average datasets used for sediment depth 45–50 cm therefore excluded data for Site 2c. Sediment depth profiles were produced for all data analysed in this study, with an example for Site 20 in Figure 2.4 and all other cores in Appendix Figures A.1–A.19.

Table 2.1 Sampling site IDs, latitude, longitude, water depth (m, tidal state corrected), and sediment core lengths (cm).

Site ID	Latitude	Longitude	Water depth (m)	Core length (cm)
2c	54.3368	-4.9623	108	50
3	54.3038	-5.0022	132	74
4	54.2626	-5.0290	119	88
5	54.2225	-5.0503	120	64
6b	54.1862	-5.0721	110	52
8	54.1035	-5.1465	116	83
10	54.0178	-5.1629	72	73
12b	54.2930	-4.9360	98	58
13	54.2583	-4.9531	103	61
14	54.2056	-4.9996	100	69
15	54.1678	-5.0194	98	73
16	54.1294	-5.0451	96	67
17	54.0825	-5.0758	90	74
18	54.0426	-5.1114	77	68
19	53.9963	-5.1296	68	73
20	53.9667	-5.1403	66	83
21	54.2830	-4.8808	68	77
23	54.1978	-4.9430	86	62
26	53.9837	-5.0788	73	59
27	53.9377	-5.1150	68	76

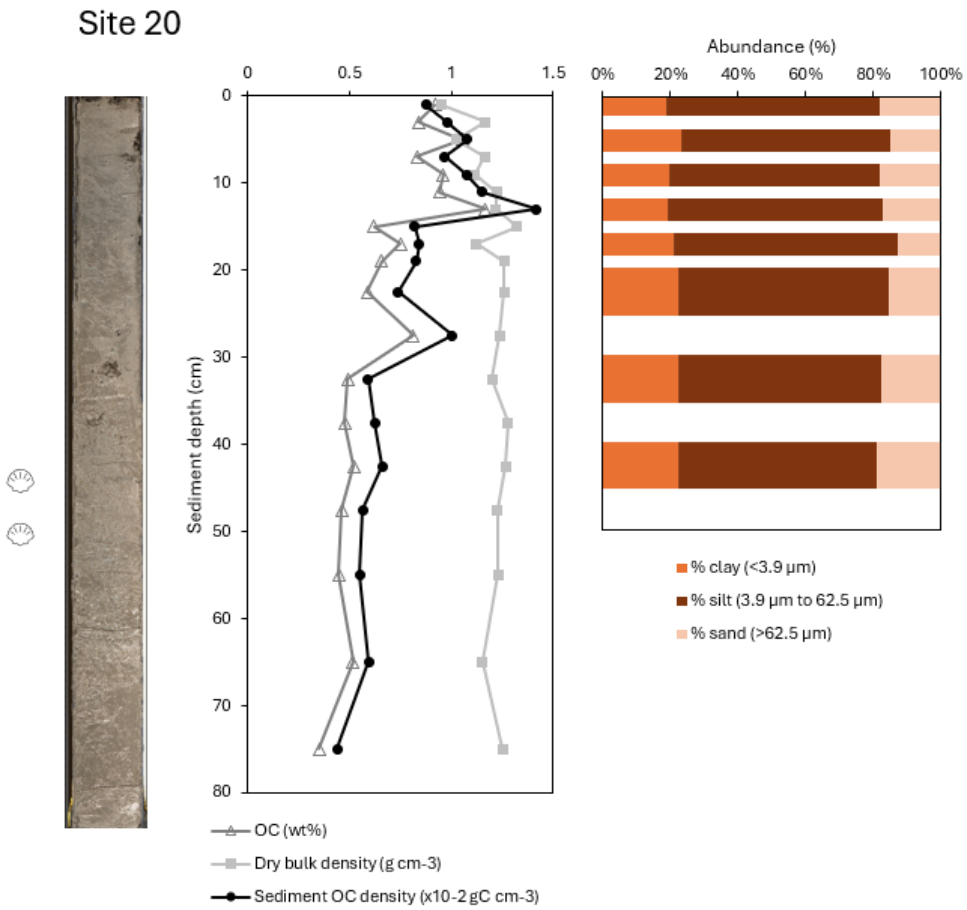

Figure 2.4 Sediment depth profiles for Site 20. Left to right: High-resolution colour image; organic carbon (OC) concentration (wt%), dry bulk density (g cm^{-3}), and sediment OC density (x10^{-2} gC cm^{-3}); and particle size distributions (% clay, % silt, % sand). Shell symbols (left) indicate depths where whole shells or shell fragments were found (44 cm, and 52 cm).

2.3.2 Sediment Classification

Overall, sediments were classified as mud and sandy mud, with average mud content ranging from 76.96% to 96.13% within the upper 50 cm of the seabed (Appendix Table A.1). Site 6b and Site 2c were exceptions, exhibiting lower average mud contents of 71.25% and 74.83%, respectively, and having a coarse (sieved) sediment fraction >1000 µm constituting 0.63% to 32.41% and 0.05% to 0.67% of the total sample mass, respectively.

2.3.3 Sediment Properties

The OC concentrations and SCDs were highest in the top 10 cm and stabilised below 30 cm, where their change between 30–40 cm and 40–50 cm was significantly lower compared to preceding depths, at just -0.03% and +0.01 gC cm^{-3}, respectively (Table 2.2; Figure 2.5). The SCD below 30 cm ($7.72 \times 10^{-3} \pm 1.51 \times 10^{-3}$ gC cm^{-3}) was approximately 26% lower than SCD in the top 10 cm ($10.37 \times 10^{-3} \pm 1.62 \times 10^{-3}$ gC cm^{-3}), while OC concentration below 30 cm (0.70 ± 0.20%) was at least 34% lower than OC concentration in the top 10 cm (1.06 ± 0.27%). The change in SCDs with depth was lower than OC concentration because of the counter effect of DBD, which was approximately 13% higher below 30 cm (1.13 ± 0.16 g cm^{-3}) compared to the top 10 cm (1.00 ± 0.12 g cm^{-3}).

Table 2.2 The average organic carbon (OC) concentration (%), sediment dry bulk density (DBD, g cm^{-3}), and sediment organic carbon density (SCD, $x10^{-3}$ gC cm^{-3}) for sediment depths of 0–10 cm, 10–20 cm, 20–30 cm, 30–40 cm, 40–50 cm derived from 18 sediment cores in the Western Irish Sea Mud Belt (WISMB). The change (Δ) in each parameter compared to the previous sediment depth are provided.

Sediment depth (cm)	OC (%)	Δ OC (%)	DBD (g cm^{-3})	Δ DBD (g cm^{-3})	SCD ($x10^{-3}$ gC cm^{-3})	Δ SCD (gC cm^{-3})
0–10	1.06 ± 0.27	-	1.00 ± 0.12	-	10.37 ± 1.62	-
10–20	0.95 ± 0.25	-0.11	1.06 ± 0.19	+0.06	9.70 ± 1.62	-0.67
20–30	0.80 ± 0.25	-0.15	1.11 ± 0.22	+0.05	8.46 ± 1.67	-1.24
30–40	0.70 ± 0.20	-0.10	1.13 ± 0.16	+0.02	7.72 ± 1.51	-0.74
40–50	0.67 ± 0.20	-0.03	1.16 ± 0.15	+0.03	7.73 ± 1.57	+0.01

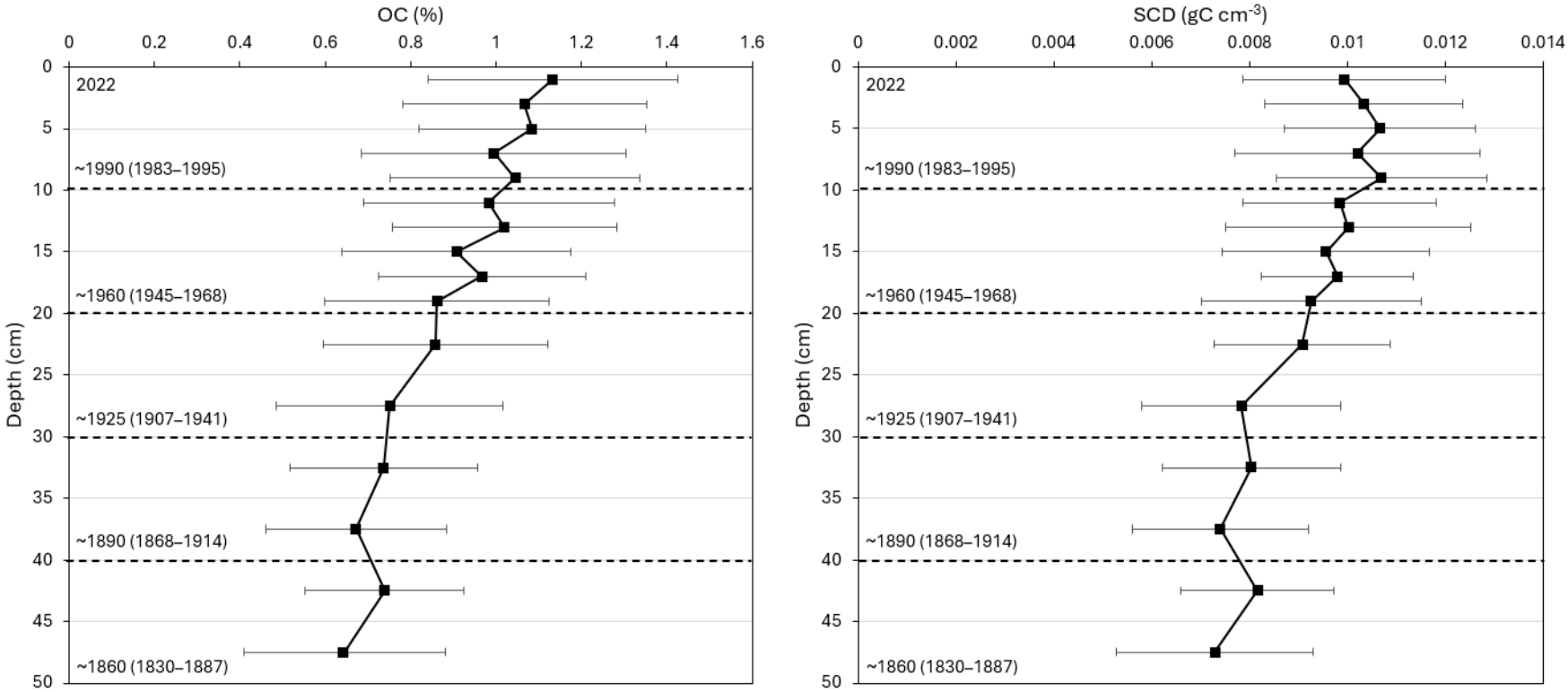

Figure 2.5 Average sediment organic carbon concentration (OC, %) (left) and average sediment carbon density (SCD, gC cm^{-3}) (right) versus sediment depth (cm) for 18 sediment cores. Errors bars represent standard deviations. Dates indicate the sediment deposition year (average (range)) at 10 cm depth intervals quantified by radionuclide analysis.

2.3.4 Sedimentation Rates

The estimated average sedimentation rate for the study region was 0.29 cm yr^{-1}, ranging from 0.26 cm yr^{-1} to 0.37 cm yr^{-1}, based on the analysis of radionuclides in five sediment cores spatially distributed across the study region (Table 2.3; Table 2.4; Appendix Figures A.20–A.25; Appendix Table A.2). An example of the radionuclide (^{210}Pb, ^{210}Po, ^{137}Cs, ^{241}Am) profiles for Site 20 is shown in Figure 2.6 and the profiles for the other sites are in Appendix A (Figures A.20–A.25). Sedimentation rates for Site 4 and Site 20 were estimated using ^{210}Po due to its higher sensitivity and lower measurement uncertainty compared to ^{210}Pb, while Site 8 rates were estimated using ^{210}Pb due to there being insufficient ^{210}Po data points (n=3) for regression analysis of the exponential decay curve. Sedimentation rates could not be estimated for Sites 14 and 21, as these had mixed radionuclide activity profiles.

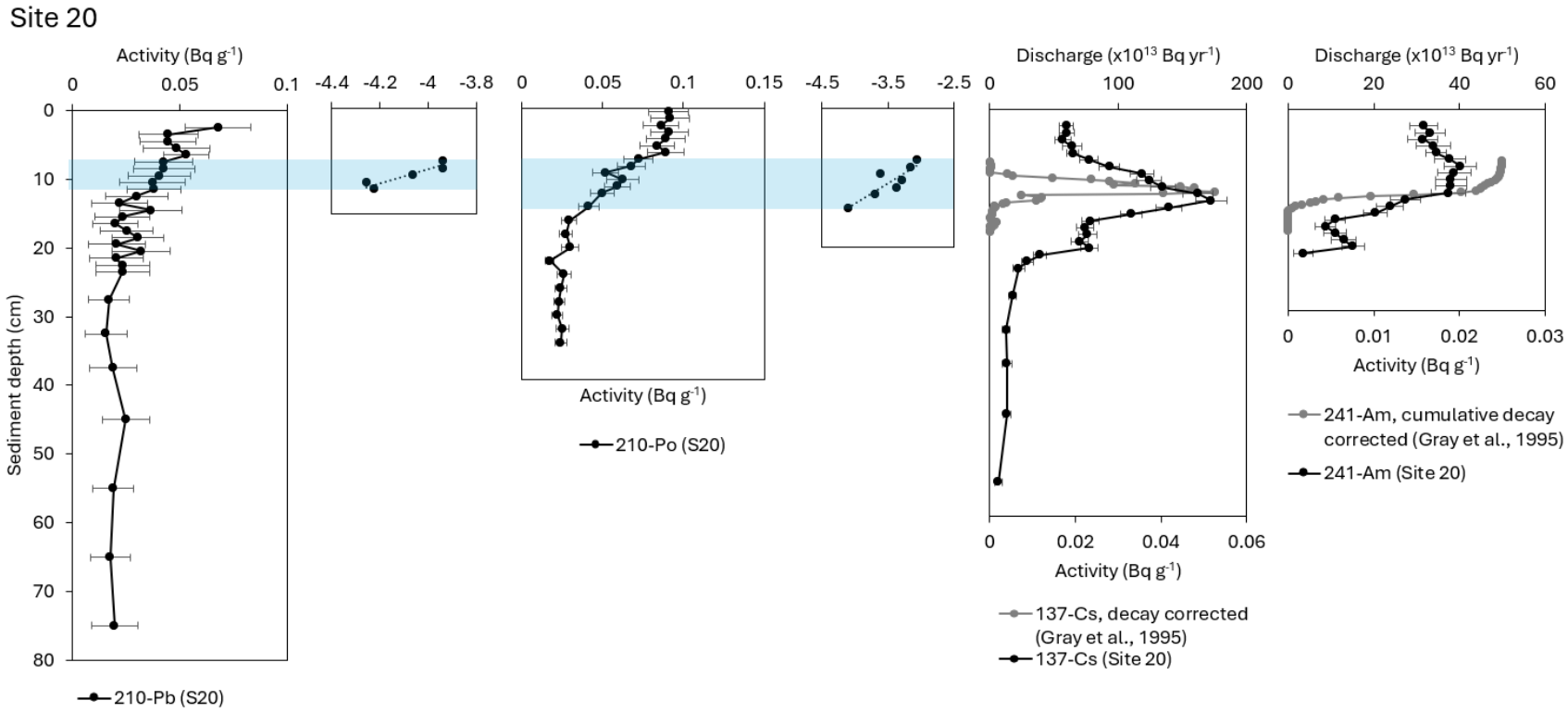

Figure 2.6 Radionuclide profiles for Site 20. Left to right: ^{210}Pb activities; natural logarithm of excess ^{210}Pb activities; ^{210}Po activities; natural logarithm of excess ^{210}Po activities; ^{137}Cs activities (black, lower axis) and ^{137}Cs discharge profile from Sellafield nuclear facility (grey, upper axis) with 0.26 cm yr^{-1} sedimentation rate applied; ^{241}Am activities (black, lower axis) and cumulative ^{241}Am discharge profile from Sellafield nuclear facility (grey, upper axis) with 0.26 cm yr^{-1} sedimentation rate applied. Blue bands indicate the regions of data used for estimating sedimentation rates for ^{210}Po and ^{210}Pb.

Table 2.3 Average sedimentation rates estimated from ^{210}Pb, ^{210}Po, and ^{137}Cs radioisotope data. Sedimentation rates in parenthesis were not included in the average sedimentation rate calculated due to their high measurement uncertainty (Sites 20 and 4) and insufficient data points for regression analysis (Site 8).

Site	Mean rate, 210-Pb (cm yr^{-1})	Mean rate, 210-Po (cm yr^{-1})	Mean rate, 137-Cs (cm yr^{-1})	Average rate (cm yr^{-1})
4	(0.12)	0.32	0.31	0.31 ± 0.01
8	0.37	(0.26)	0.37	0.37 ± 0.00
15	0.23	-	0.29	0.26 ± 0.03
20	(0.35)	0.23	0.29	0.26 ± 0.04
27	0.24	-	0.29	0.26 ± 0.03
Average	-	-	-	0.29 ± 0.02

Table 2.4 The average number of years since sediments were sampled in 2022 and the corresponding sediment deposition date relating to sediment depths (0 cm (surface), 10 cm, 20 cm, 30 cm, 40 cm, 50 cm) based on the average linear sedimentation rate of 0.29 ± 0.02 cm yr^{-1} and linear sedimentation rates of 0.26–0.37 cm yr^{-1} from 5 sediment cores (ranges are in parenthesis).

Sediment depth (cm)	Years since 2022	Estimated deposition date
0	0	2022
10	33 (27–39)	~1990 (1983–1995)
20	66 (54–77)	~1960 (1945–1968)
30	98 (81–115)	~1925 (1907–1941)
40	131 (108–154)	~1890 (1868–1914)
50	164 (135–192)	~1860 (1830–1887)

2.3.5 Sediment Mixing

Radionuclide activities were constant within the upper 3.5 cm to 11 cm, followed by ^{137}Cs peaks from the discharge maximum in 1975 from Sellafield nuclear facility, indicating surface sediment mixed layers (SMLs) over preserved sediments at Sites 4, 8, 15, 20, and 27. Sites 21 and 14 exhibited highly mixed sediments overlying older layers, with radionuclide activities constant up to 19 cm and 40 cm, respectively, but that fell below the limit of detection below these depths. These results were corroborated by the X-ray radiographs and high-resolution images, which showed contrasting light and dark features, and air pockets, respectively above 40 cm, below which sediments were more consolidated. DBDs were also lower in the top 2 cm, suggesting mixing at the sediment–water interface.

2.3.6 Organic Carbon Accumulation and Burial Rates and Efficiencies

The average OCAR (<30 years) was 30.55 ± 0.32 gC m^{-2} yr^{-1}, ranging from 17.42 ± 0.47 gC m^{-2} yr^{-1} to 51.57 ± 0.03 gC m^{-2} yr^{-1} (Table 2.5). The average OCBR (>100 years) was 22.73 ± 0.22 gC m^{-2} yr^{-1}, ranging from 14.06 ± 0.32 gC m^{-2} yr^{-1} to 38.54 ± 0.01 gC m^{-2} yr^{-1}. Consequently, the average OCBE was 74.41%, with values ranging from 74.73% to 80.68%. Based on average OCARs and OCBRs, the WISMB (380,779 ha; British Geological Survey, 2024) is estimated to accumulate 116,316 ±

1,231 MgC yr^{-1} and bury 86,556 ± 835 MgC yr^{-1}. Based on the five sites where sedimentation rates were estimated using radionuclide analysis, the sites situated in the deepest water and with the highest mud content (Sites 4 and 8) had the highest OCARs and OCBRs, while the sites situated in the shallowest water and with the lowest mud content (Sites 15, 20, and 27) had the lowest OCARs and OCBRs (Table 2.5).

Table 2.5 Sedimentation rate (cm yr^{-1}), average OC concentration (%) in the top 10 cm and 30–50 cm, organic carbon accumulation rate (OCARs, gC m^{-2} yr^{-1}), organic carbon burial rate (OCBRs, gC m^{-2} yr^{-1}), organic carbon burial efficiency (%), water depth (m, corrected for tidal state), and average mud content (%) in the top 10 cm of sediments. Average, minimum, and maximum values are presented for the Western Irish Sea Mud Belt (WISMB) study region, and for selected sites where sedimentation rates were estimated using radionuclide analysis.

	Sedimentation rate (cm yr^{-1})	**OC (%), 0–10 cm**	**OC (%), 30–50 cm**	**OCAR (gC m^{-2} yr^{-1})**	**OCBR (gC m^{-2} yr^{-1})**	**OCBE (%)**	**Water depth (m)**	**Mud (%), 0–10 cm**
Average	0.29 ± 0.02	1.06 ± 0.27	0.70 ± 0.20	30.55 ± 0.32	22.73 ± 0.22	74.41	93 ± 20	85.13 ± 7.55
Minimum	0.26 ± 0.03	0.62	0.43	17.42 ± 0.47	14.06 ± 0.32	80.68	66	68.12
Maximum	0.37 ± 0.00	1.59	1.03	51.57 ± 0.03	38.54 ± 0.01	74.73	132	95.93
Site 4	0.31 ± 0.01	1.41	0.90	38.19 ± 0.04	26.53 ± 0.02	69.48	119	95.57
Site 8	0.37 ± 0.00	1.59	1.00	51.57 ± 0.03	32.91 ± 0.00	63.83	116	94.61
Site 15	0.26 ± 0.03	0.89	0.52	23.55 ± 1.00	14.68 ± 0.24	62.35	98	85.70
Site 20	0.26 ± 0.04	0.92	0.49	25.90 ± 0.32	15.91 ± 0.16	61.43	66	82.97
Site 27	0.26 ± 0.03	0.78	0.48	22.15 ± 0.42	14.32 ± 0.37	64.66	68	78.33

2.4 Discussion

The average long-term (>100 years) OCBR for the WISMB is estimated as 23 gC m^{-2} yr^{-1}, with an OCBE of 74% compared to an average short-term (<30 years) OCAR of 31 gC m^{-2} yr^{-1}. These results indicate that, on average, 74% of OC stored within the top 10 cm of sediments becomes buried for at least a century. On a site-specific basis, OCBEs were even lower, ranging from 61% to 70%. The disparity between the average OCAR and OCBR in the WISMB reflects significant degradation of OC over the first 100 years within surface sediments (1.06 ± 0.27 % and 10.37 ± 1.62 gC cm^{-3}) before reaching a relatively steady state at around 100 years, at approximately 30 cm depth (0.70 ± 0.20 % and 7.72 ± 1.51 gC cm^{-3}). This finding emphasises the importance of age-resolved OC stocks for differentiating between short-term OC accumulation and long-term OC burial, which can be used to refine estimates of the long-term climate change mitigation potential of marine sediments.

These results support simplified conceptual models of OC remineralisation and burial (Arndt et al., 2013; Burdige, 2007; LaRowe et al., 2022), showing enhanced degradation of labile OC in surface sediments and near-steady-state recalcitrant OC with depth (Burdige, 2007; Chen et al., 2022; de Haas et al., 2002). While it is acknowledged that microbial degradation of OC can persist deep within sediments (Bradley et al., 2022; LaRowe et al., 2020), potentially overestimating OCBRs over centuries to millennia, the OC degradation rate in the WISMB notably decreases below 30 cm, reaching relatively constant OC concentrations and SCDs that likely comprise a higher fraction of refractory or recalcitrant OC. While ongoing degradation of OC is observed within the sediments sampled in this study, it is partially offset by increased DBD, which may be due to sediment compaction, leading to constant SCDs below 30 cm (Figure 2.5, Table 2.1). Thus, OC stocks below 30 cm in the WISMB could be considered stable over climate-relevant timescales. This steady-state depth horizon at 30 cm is deeper than those determined in other studies at 10–15 cm (Bakker and Helder, 1993; Hartnett et al., 1998). While the depth where OC stocks stabilise can vary regionally, this study shows that determining age-resolved OC stocks is essential for assessing long-term OC storage, which studies without these data could overestimate.

The OCARs and OCBRs estimated for the five sediment cores that were dated herein were highest in deeper water (Table 2.4), where sedimentation rates were greatest, reflecting lower hydrodynamic energy and entrainment by the gyre (Belderson, 1964; Coughlan et al., 2021; Williams et al., 2019), and where OC concentrations were higher, reflecting the affinity between finer sediment grain sizes (higher mud content) and OC adsorption (Burdige, 2007). Moreover, sedimentation rates estimated herein (0.26–0.37 cm yr^{-1}) were lower than previously reported for the southwest WISMB (modern rates of 0.8–1.0 cm yr^{-1} and historic rates of 2.1–2.7 cm yr^{-1}) (Coughlan et al., 2015), potentially reflecting spatial variability across the region.

The OCARs for the WISMB (17–52 gC m^{-2} yr^{-1}) are within the range of those for other temperate shelf seas based on the top 10 cm of sediment, including the North Sea and Skagerrak (0.02–66.18 gC m^{-2} yr^{-1}) (Diesing et al., 2021) and the Baltic Sea (18 ± 10 to 35 ± 5 gC m^{-2} yr^{-1}) (Winogradow and Pempkowiak, 2014). In these regions, OC accumulation is concentrated in net deposition zones, including the glacial Norwegian Trough (19.4 gC m^{-2} yr^{-1}, 4–66 gC m^{-2} yr^{-1}) (Diesing et al., 2021), which is attributed to having the highest regional sedimentation rates and OC concentrations, comparable with the WISMB. OCARs at the deepest sites in the WISMB study region are also comparable with average OCARs in Scottish fjords (57.1 ± 10.9 gC m^{-2} yr^{-1}, which ranged from 35.5–110.9 gC m^{-2} yr^{-1}) (Smeaton et al., 2021b), which had higher average OC concentration but lower average sedimentation rate relative to the WISMB. Additionally, the OCBEs in the WISMB (75% to 81%) were comparable with Scottish fjords which were 77% ± 20%, ranging from 35%–98%, using similar calculation methods (Smeaton et al., 2021b). The OCBRs for the WISMB (14–39 gC m^{-2} yr^{-1}) are also comparable with depositional shelf sea zones, including the West Gironde Mud Patch (WGMP) in the Bay of Biscay (28–45 gC m^{-2} yr^{-1}) (Dubosq et al., 2021), which had similar OC concentrations throughout the sediment and comparable sedimentation rates. However, OCBRs in the WGMP were estimated over decades (<65 years) (Dubosq et al., 2021), and so do not strictly constitute “long-term” OC burial for greater than a century, as in this present study. While the relatively smaller area of the WISMB (380,779 ha) compared to other shelf sea regions (e.g. North Sea: 52,600,000 ha (Diesing et al., 2021); UK Exclusive Economic Zone: 74,395,900 ha (Smeaton et al., 2021a) limits its global significance

for OC accumulation (116,316 ± 1,231 MgC yr^{-1}) and burial (86,556 ± 835 MgC yr^{-1}), the results of this study highlight the regional significance of the WISMB, comparable with OC burial in other depositional coastal zones, such as Scottish fjords (84,000 MgC yr^{-1} over 260,800 ha; Smeaton et al., 2021b) and surpassing the WGMP (11,760–18,900 MgC yr^{-1} over 42,000 ha; Dubosq et al., 2021).

2.4.1 Future Outlook

Compared with modelled approaches that estimate OCBEs based on OC fluxes at the sediment–water interface, this study and others that use empirical datasets could overestimate OCBEs by underestimating OCARs at the undisturbed sediment surface (Dubosq et al., 2021; Smeaton et al., 2021b). Degradation of surficial sedimentary OC prior to sampling could explain why OC concentrations in the top 10 cm were lower than might be expected compared to the exponential decay curve presented in the conceptual model of OC degradation (Burdige, 2007). Over 95% of OC that settles on the seabed is remineralised before it can become buried, for example by consumption of labile phytoplankton by bacteria and benthic invertebrates (Burdige, 2007; Chen et al., 2022; de Haas et al., 2002; LaRowe et al., 2020). As a result, the model compares OC rain rate to the sediment surface, prior to degradation within the sediment, with OC burial below the zone of early diagenesis (Burdige, 2007). Future work is needed to quantify OC fluxes to the WISMB seabed and to investigate OC reactivity, to further constrain OC accumulation and long-term OC storage.

Furthermore, post-depositional sediment reworking by tidal currents, bioturbation (e.g., by *N. norvegicus*) (Coughlan et al., 2015; Hughes et al., 1996; Kershaw et al., 1986; Lundy et al., 2019), and bottom trawling (Epstein et al., 2021; Hiddink et al., 2023; Lundy et al., 2019; Paradis et al., 2019; Williams et al., 2019;), can accelerate OC remineralisation in surface sediments, further degrading OC within the top 10 cm prior to sampling. Surface mixing effects in the top 10 cm were observed in this study by constant levels of excess ^{210}Pb and ^{137}Cs activities, and lower than expected OC concentrations compared to conceptual models (Burdige, 2007). Similar mixing effects have also been observed in other mud patches (Dubosq et al., 2021) and trawled regions (Paradis et al., 2019), reflecting the disturbed nature of the global

seabed. Future work could investigate the impacts of sediment mixing processes (hydrodynamics, bioturbation, and chronic trawling) on sedimentary OC stocks.

2.5 Conclusions

This study enhances our understanding of long-term sedimentary OC storage in muddy temperate continental shelf sediments, by using high-resolution age-resolved OC datasets to estimate OC accumulation and burial. Significant OC degradation within sediments in the first 100 years since deposition was followed by steady OC stocks in older sediments. These findings highlight a need for age-resolved sedimentary OC analysis to prevent overestimating long-term OC storage from temporary OC stocks. The results herein found that the WISMB has comparable OCARs and OCBRs with other temperate depositional shelf regions, including coastal fjords and glacial troughs. The depositional context of the WISMB is unusual within the Northwest European Shelf (NWES), where the majority of shelf sediment are permeable and dominated by advective flow (Legge et al., 2020), which highlights the complexity of OC accumulation and burial on continental shelves, and underscores the importance of capturing variability through empirical studies. Recognising the potentially degraded state of surface sediments, future research could refine OCBE estimates by investigating the effect of environmental, biological, and anthropogenic factors on OC reactivity and storage in the WIMSB. Overall, this study provides empirical evidence of OC degradation within surface sediments and OC burial over 100 years in the WISMB, enhancing understanding and improving estimates of the contribution of muddy shelf sea regions to long-term climate regulation.

Chapter 3

Stratigraphic Evidence of Organic Carbon Depletion in an Intensely Trawled Muddy Seabed

Abstract

Understanding the long-term effects of bottom trawling on sedimentary organic carbon (OC) is crucial for determining its impact on OC cycling and the climate. Yet current evidence is inconclusive, with most studies focusing on recently deposited surface sediments (≤10 cm) prone to multiple sources of mixing. Herein, the influence of intense chronic bottom trawling by commercial *Nephrops norvegicus* fisheries on OC concentrations was investigated at 20 sites in the Western Irish Sea Mud Belt (WISMB) across stratigraphic horizons in the top 50 cm of sediments, representing the years 1860 to 2022. Trawling pressure was significantly associated with sedimentary OC depletion in sediments deposited around 1960–1990 (10–20 cm), while gear penetration into deeper sediments from 1860–1960 (≥20 cm) had less effect, and sediment mixing by competing environmental factors potentially masked trawling effects in surface sediments deposited around 1990–2022 (≤10 cm). OC concentrations were significantly higher in siltier sediments at all sediment depths, while bioturbation by *N. norvegicus* was not significantly related to sediment OC concentration. This investigation is one of the highest resolution empirical stratigraphic analyses of OC depletion in intensely trawled muddy shelf-sea sediments to date and highlights the challenges of resolving trawling impacts in shallow surface sediments.

3.1 Introduction

Chronic and widespread disturbance of the seabed could limit the ocean's capacity to sequester atmospheric CO_2 into seafloor ecosystems and regulate the climate (Epstein et al., 2021; Hiddink et al., 2023). Bottom trawl gears scour the seafloor for benthic and demersal species, causing sediment resuspension, mixing, and erosion (Coughlan et al., 2015; Martín et al., 2014a,c; Paradis et al., 2021). Resultant resuspended sediments can become more vulnerable to organic carbon (OC) degradation and remineralisation due to enhanced oxygen exposure and microbial activity, particularly under repeated, chronic trawling (Hiddink et al., 2017; Martín et al., 2014a; Sala et al., 2021). This activity could result in net greenhouse gas emissions from seabed sediments into the water column, which may eventually be emitted back into the atmosphere (Epstein et al., 2021; Sala et al., 2021).

There remains significant uncertainty regarding the effects of bottom trawling on sedimentary OC concentrations in shelf seas (Epstein et al., 2022; Legge et al., 2020). Most studies report no significant impact of trawling, while other studies indicate a reduction or enhancement of OC concentrations (Epstein et al., 2022). Environmental and biological factors, such as hydrodynamics and infauna, that affect sediment composition, sediment deposition rates, and oxygen penetration depths can vary the effects of trawling on OC reactivity and storage (Sciberras et al., 2016; Tiano et al., 2019). Trawling is thought to have stronger negative effects on OC remineralisation in cohesive muddy sediments found in lower energy regions, which typically store more OC due to their naturally lower permeability and oxygen penetration (Burdige, 2007). Trawl gears are estimated to penetrate from a few centimetres up to 35–40 cm in soft, muddy sediments (Eigaard et al., 2016), for example, ranging from 6 cm for beam trawls to 40 cm deep for dredges (Martín et al., 2014b). In comparison, trawling effects are often negligible or inconclusive in sandier naturally disturbed seabed (Epstein et al., 2022; Sciberras et al., 2016), for example in regions impacted by waves or high-energy tidal currents, which can mimic or exceed trawling impacts by resuspending sediments and enhancing oxygen penetration (Diesing et al., 2013; Palanques et al., 2014; Pusceddu et al., 2005; Sciberras et al., 2016). Trawling can also alter microbial biomass and benthic fauna (e.g. bioturbation and burrow density), which in turn affects carbon biogeochemistry

by slowing remineralisation and modifying sedimentary redox structure; however, these effects can vary depending on trawling intensity (Queirós et al., 2006; Sciberras et al., 2016; Watling et al., 2001).

Added to these uncertainties are limitations in the available data. Most studies that reported no significant effect of fishing pressure on sediment OC only examined surface sediment layers (≤10 cm) (Epstein et al., 2021), yet the effects of trawling on fresh sediment deposits and older buried sediments can vary (Paradis et al., 2021). Sediment OC concentration can be enhanced in surface layers due to accumulation of modern OC-rich sediments, elevating OC concentrations for trawled and untrawled regions, while chronic disturbance of sediments by trawling can lead to OC depletion within deeper sediments (Paradis et al., 2021). In a review by Epstein et al. (2021), only three published studies investigated fishing impacts on sedimentary OC down to 30 cm (Palanques et al., 2014; Paradis et al., 2019; van de Velde et al., 2018), and only one published study examined effects down to 50 cm, which was limited to two sediment cores (Martín et al., 2014a). These low spatial resolution and stratigraphic limitations restrict insights into the impacts of trawling on long-term OC storage in soft, muddy sediments where trawl gears can penetrate up to 40 cm (Martín et al., 2014b).

Another key challenge to investigating the impact of trawling on sedimentary OC is identifying regions where trawling pressure varies significantly, either with and without trawling or across a notable gradient of trawling intensity, whilst other influences on sedimentary OC concentration are constant. The Western Irish Sea Mud Belt (WISMB) has one of the most heavily trawled seabeds globally (Amoroso et al., 2018; Eigaard et al., 2017), offering the potential for investigating chronic trawling effects on sedimentary OC concentration. An active *Nephrops norvegicus* fishery targeting one of the densest *N. norvegicus* populations worldwide, averaging one burrow per square meter (Lundy et al., 2019), was established in the 1950s and intensified from the 1960s to the 1990s (Coughlan et al., 2015; ICES, 2020). Furthermore, the WISMB contains significant sedimentary OC concentrations compared to other shelf sea regions (Black et al., 2022; Burrows et al., 2024; Legge et al., 2020; Muir et al., 2025 (Preprint)), due to substantial muddy sediment accumulation below the Western Irish Sea gyre (Belderson, 1964; Coughlan et al., 2015, 2021; Kershaw, 1986). Predicted OC losses from trawling make this region

one of the most vulnerable to trawling around the British Isles (Black et al., 2022; Epstein and Roberts, 2022). The WISMB therefore provides a potential test bed into which an improved understanding of trawling impacts on sedimentary OC can be developed, enhanced by a comprehensive understanding of modern commercial fishing activity and gear types used, which are estimated to penetrate to an average depth of 30 cm in muddy sediments (Coughlan et al., 2015). Furthermore, anthropogenic radionuclide discharges from the Sellafield nuclear facility to Irish Sea sediments over the past 100 years (1952 to 1998) have been widely used to estimate sedimentation rates in the Irish Sea (Coughlan et al., 2015; Gray et al., 1995; Kershaw et al., 1986; Muir et al., 2025 (Preprint); Povinec et al., 2003), enabling accurate sediment dating.

Through stratigraphic analysis of sedimentary OC concentrations within the top 50 cm of sediments, and natural (^{210}Pb, ^{210}Po) and anthropogenic (^{137}Cs, ^{241}Am) radionuclides in the WISMB, coupled with modern *N. norvegicus* fisheries datasets for the Irish Sea, this study investigates the impact of intense, chronic bottom trawling in the WISMB on sedimentary OC stocks. This study aims to provide one of the highest resolution age-resolved analyses of modern trawling impacts on sedimentary OC to date, adding to a handful of studies that have investigated bottom trawling impact on sedimentary OC concentrations within sub-surface sediments.

3.2 Materials and Methods

3.2.1 Sampling Site Selection

The sediment cores used in Chapter 3 are the same cores that were collected in Chapter 2 of this thesis.

A total of 20 sediment cores of ≥50 cm length were collected from the fisheries enforcement vessel ‘Barrule’ across a benthic fishing pressure gradient (described in more detail below) in the WISMB in June 2022 to examine the relationship between chronic (the repeated and sustained use of) bottom trawling (swept area ratio (SAR), yr^{-1}) and sedimentary OC concentration (Figure 3.1; Table 3.1). To resolve this relationship, environmental variables that could influence sediment OC

concentrations (e.g. sediment type, *N. norvegicus* burrow densities, and water depth) were controlled for, where possible. British Geological Survey sediment textural classifications informed the selection of muddy sediment sites (British Geological Survey, 2024; Folk, 1954) to control for sediment grain sizes, as increased mud content was expected to relate to increased OC concentration (Figure 2.1; Muir et al., 2025 (Preprint)). Kriged density estimates of *N. norvegicus* burrow densities for the Functional Unit 15 (FU15, Irish Sea, West) for years 2013 to 2022 (Agri-Food and Biosciences Institute, 2023) were interpolated to a heat map in ArcGIS Pro (Figure 3.2), to control for the main source of bioturbation, as increased *N. norvegicus* burrow density was expected to relate to decreased OC concentration. These data were collected during the annual Western Irish Sea *N. norvegicus* Grounds Underwater towed video (UWTV) Surveys in August by the Agri-Food and Biosciences Institute, which are conducted to estimate *N. norvegicus* burrow distribution and abundance. These UWTV surveys follow protocols agreed by the International Council for the Exploration of the Sea (ICES) (Dobby et al., 2021) and detailed methods can be found in the annual UWTV Survey Reports (e.g. Lundy et al., 2019). Briefly, a high-definition camera mounted to a sledge was towed across a randomised fixed isometric survey grid of 100 UWTV stations with 4.5 nautical mile (nm) spacing for 10 minutes at 0.8 knots (approx. 200 m), then burrows were identified and their densities estimated using geo-statistical methods. GEBCO Gridded Bathymetry Data informed the selection of sites distributed across water depths of approximately 60–130 m, as deeper water was expected to relate to increased mud content, and therefore increased OC concentrations (Figure 2.2; GEBCO Compilation Group, 2024). For analyses, water depths recorded on site and corrected for tidal state were used (Table 3.1). A high sample number was taken to minimise water depth effects, which were unavoidable in the study region at the edge of the WISMB. Tidal and wave bed-stress are negligible in the WISMB, so did not need to be controlled for within the study region (Coughlan et al., 2021; Williams et al., 2019).

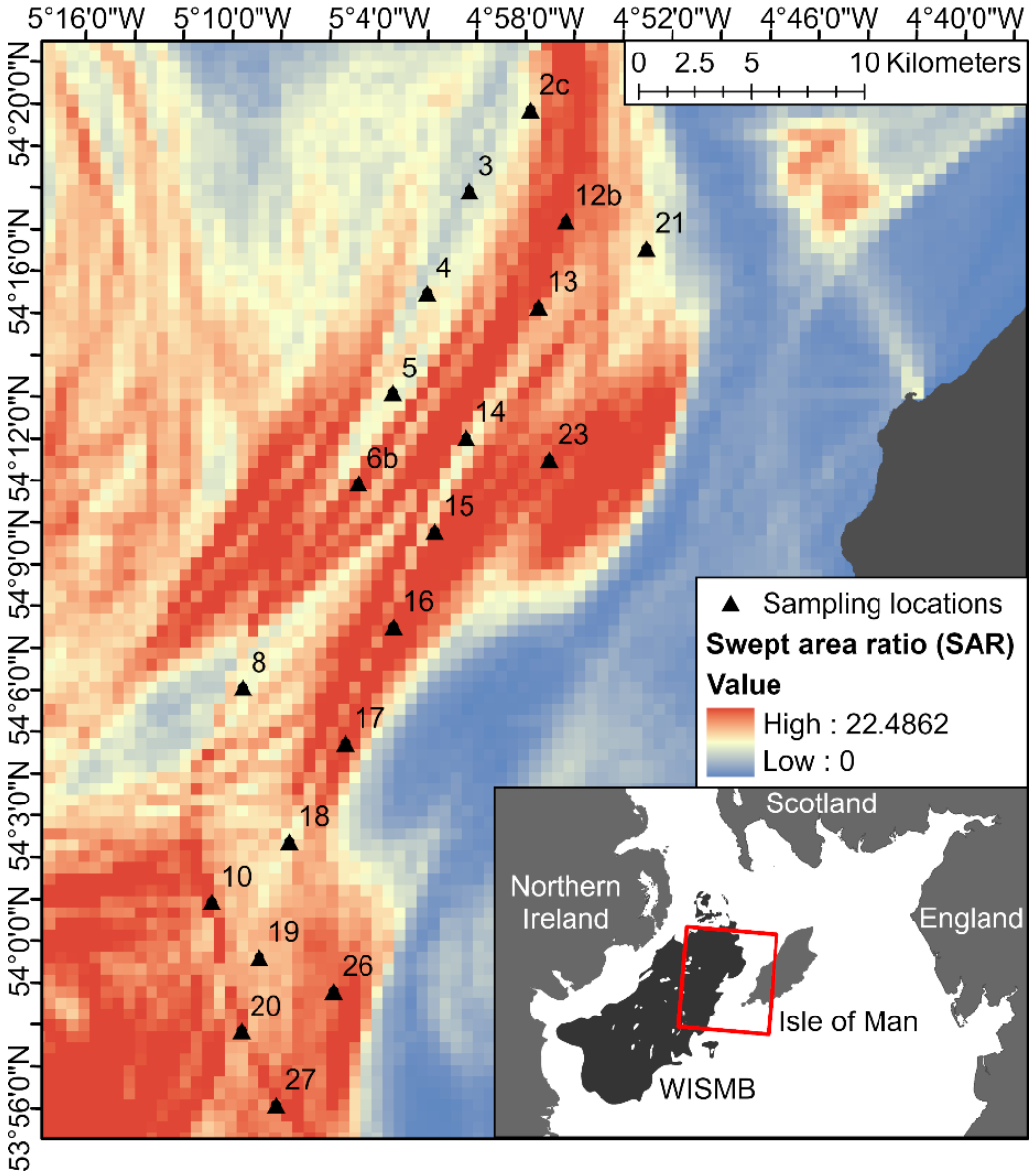

Figure 3.1 Map of surface swept area ratio (SAR, yr^{-1}) for the period 2016–2021 in the Western Irish Sea Mud Belt (WISMB) reconstructed using anonymised vessel monitoring system (VMS) data provided by the Marine Management Organisation, and sampling site locations labelled with sediment core identification codes. The inset map shows the WISMB (based on muddy sediments classified by the British Geological Survey Seabed sediments 250K dataset (British Geological Survey, 2024)) in the Irish Sea relative to neighbouring countries. The study region is highlighted by a red box.

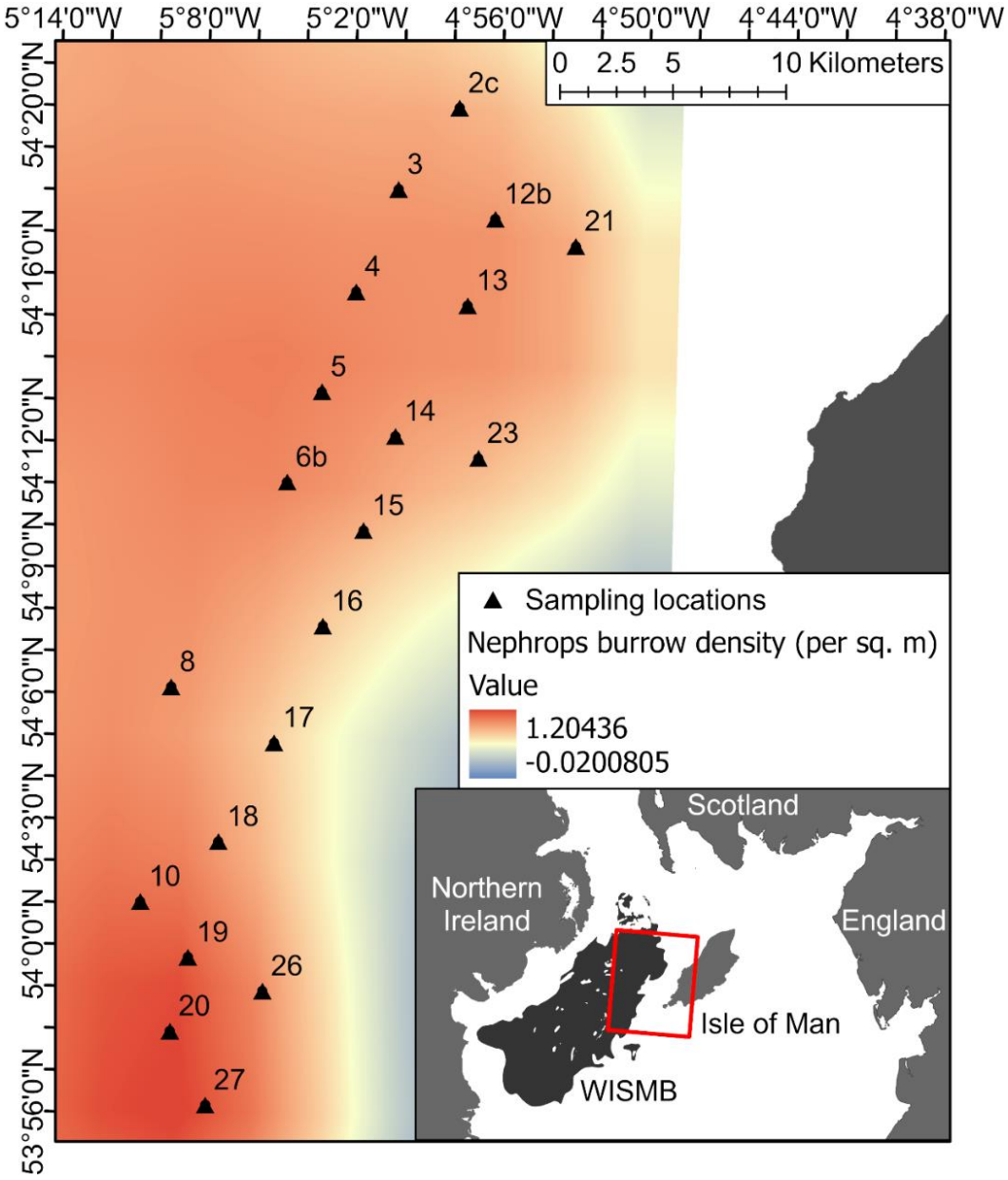

Figure 3.2 Map of sampling site locations labelled with sediment core identification codes and a heat map of kriged *Nephrops norvegicus* burrow densities (m^{-2}) for the Functional Unit 15 (FU15, Irish Sea, West) for years 2013 to 2022 (Agri-Food and Biosciences Institute, 2023) in the Western Irish Sea Mud Belt (WISMB). The inset map shows the WISMB in the Irish Sea relative to neighbouring countries. The sampling region is highlighted by a red box.

Table 3.1 Sampling site IDs, latitude, longitude, water depth (m) corrected for tidal state, sediment core length (cm), *Nephrops norvegicus* burrow density (m^{-2}) and swept area ratio (SAR, yr^{-1}) estimated in this study.

Site ID	Latitude	Longitude	Water depth (m)	Core length (cm)	*N. norvegicus* burrow density (m^{-2})	SAR (yr^{-1})
2c	54.3368	-4.9623	108	50	0.86	5.50
3	54.3038	-5.0022	132	74	0.94	2.34
4	54.2626	-5.0290	119	88	0.94	3.05
5	54.2225	-5.0503	120	64	0.98	4.62
6b	54.1862	-5.0721	110	52	0.98	8.92
8	54.1035	-5.1465	116	83	0.90	3.95
10	54.0178	-5.1629	72	73	1.02	10.14
12b	54.2930	-4.9360	98	58	0.93	8.47
13	54.2583	-4.9531	103	61	0.93	8.64
14	54.2056	-4.9996	100	69	0.84	4.09
15	54.1678	-5.0194	98	73	0.93	7.00
16	54.1294	-5.0451	96	67	0.74	9.40
17	54.0825	-5.0758	90	74	0.77	9.54
18	54.0426	-5.1114	77	68	0.99	3.54
19	53.9963	-5.1296	68	73	1.14	5.96
20	53.9667	-5.1403	66	83	1.14	8.52
21	54.2830	-4.8808	68	77	0.86	4.92
23	54.1978	-4.9430	86	62	0.77	8.55
26	53.9837	-5.0788	73	59	0.98	7.75
27	53.9377	-5.1150	68	76	1.18	8.11

3.2.2 Fishing Pressure Estimates

3.2.2.1 Data Source

Fishing pressure was estimated by calculating the mean annual SAR from bottom-contact fishing gears for fishing vessels over 12 meters from 2016 to 2021 (6 years) using satellite-based vessel monitoring system (VMS) data provided by the Marine Management Organisation for the Isle of Man and Northern Irish territorial waters. Data coverage for vessels over 12 m in length is near complete, as VMS are mandatory for enforcement purposes in European waters, while data coverage for vessels under 12 metres may be unrepresented, as these vessels were not legally required to have VMS installed during 2016–2021 (Gerritsen, 2023).

3.2.2.2 Data Preparation

Data were filtered prior to calculating SARs to include towed benthic fishing gears and to exclude static benthic fishing gears, pelagic gears, and vessels carrying only "unknown" gear codes (Appendix Table B.1). Towed benthic fishing gears included boat dredge (DRB), bottom otter trawl (OTB), multi-rig otter trawl (OTM), bottom pair trawl (PTB), and beam trawls (TB, TBB, TBN). Scottish seine (fly dragging) was excluded as these were not widespread within the study region (e.g. activity only recorded in 2016, 2017, and 2018, with only 15 records in 2018). The proportion of unknown gear codes for the years 2016–2019 were typically less than 0.01%; however, this proportion increased to nearly 10% in 2021. Most vessels carrying "unknown" gear codes travelled at speeds outside the 1–6 knots fishing threshold (see below). For example, only 1.6% of vessels within this fishing speed envelope in 2021 carried "unknown" gears.

These data were filtered to exclude stationary (<1 knots) or steaming (>6 knots) vessels, based on histograms of vessel speed, which were used to determine the fishing speed thresholds (Appendix Figure B.1). The data were filtered to remove "NULL" or "blank" values from the speed column and to include only towed benthic fishing gear codes (DRB, OTB, OTT, PTB, TB, TBB, TBN). Histograms for years 2016–2021 had a broad peak at 1–5 knots, which was expected to represent fishing activity. Meanwhile, a spike at <1 knot was expected to represent stationary/turning vessels and a broad peak at >6 knots was expected to represent steaming vessels. To capture all potential fishing vessels and in agreement with Lee et al. (2010), the speed rule was determined as 1–6 knots. This fishing threshold was aligned with the Joint Nature Conservation Committee (JNCC) and previous studies, who outlined that fishing occurred when a vessel carrying mobile demersal fishing gear is travelling between 1 and 6 knots (Church et al., 2016; Lee et al., 2010).

3.2.2.3 Swept Area Ratio (SAR)

This Section 3.2.2.3 was supported by Dr. James Strong at the National Oceanography Centre Southampton. In ArcGIS Pro, swept area (SA) was calculated by connecting consecutive VMS pings to generate daily polylines based on date/time and vessel ID, which were clipped to grids of equal size (500 m x 500 m, UTM

30N). This method ensured that duplicate VMS pings (same date/time and vessel ID, but different gear codes) did not alter line formation or double count/overestimate fishing effort, and ensured erroneous joins between fishing sessions for individual vessels were excluded. The length of polylines in each grid cell was summed and their lengths multiplied by surface gear widths (DRB = 12 m, OTB = 60 m, OTT = 100 m, PTB = 250 m, TB/TBB/TBN = 18 m), which were advised by the JNCC (Appendix Table B.2) (Church et al., 2016). SA was divided by the area of the grid cell and number of years to give SAR.

The commercial trawling pressure gradient in the WISMB study region appeared to be influenced by the presence of wrecks, pipelines, and distance to port, but independent of environmental variables that could influence sediment OC concentration (water depth, sediment type, *N. norvegicus* burrow densities).

3.2.3 Sediment Sampling and Processing

Please see sections 2.2.2 and 2.2.3 for the detailed methods used for sediment sampling and processing. A summary of these methods is provided in this section. Data for the top 50 cm are compared herein to investigate modern trawling impacts.

Briefly, sediment cores were collected at each site using a UWITEC gravity corer (height = 120 cm; internal diameter = 9 cm) in June 2022. Water depth at each site was recorded using the research vessel depth sounder during corer deployment, then corrected for tidal state. Sediment cores were split and sampled lengthwise at the British Ocean Sediment Core Research Facility (BOSCORF), and samples were freeze-dried and homogenised before analysis.

3.2.4 Sediment Analysis

3.2.4.1 Sediment Organic Carbon Content

Please see sections 2.2.4 and 2.2.5 for the detailed methods used for estimating sediment dry bulk density and sediment OC content. Biogeochemical analyses were carried out on the top 50 cm of sediments at depths of every 2 cm in the top 20 cm

and every 5 cm in the top 20–50 cm, to account for more significant changes expected in sediment properties at shallower sediment depths (Howard et al., 2014). The sediment dry bulk densities (DBDs) were estimated by dividing the mass of dry sediment by the original volume sampled using Equation 2.1. The OC concentration (OC, %) was determined from acidified samples (IC removed) using a Flash 2000 Elemental Analyser (EA) (Thermo Fisher Scientific). Sediment organic carbon density (SCD, gC cm^{-3}) was estimated by multiplying the OC concentration by the DBD using Equation 2.2.

3.2.4.2 Sediment Particle Size

Please see sections 2.2.6 for the detailed methods used for sediment particle size analysis. Particle size distributions were determined for samples dispersed in a 1% Calgon solution (sodium hexametaphosphate) using a Malvern Mastersizer 3000 laser microgranulometer, for every other sample depth down to 40–45 cm (e.g. 0–2 cm, 4–6 cm, etc.), due to resource limitations. Samples with particle diameters >2000 µm were dry sieved using a 1000 µm mesh prior to analysis, and the results from laser diffraction (volumetric) were scaled to the overall sample (mass) by assuming constant sediment density. Particle size classes were grouped as: clay (<3.9 µm), silt (3.9–62.5 µm), mud (<62.5 µm), and sand (62.5–2000 µm) based on Udden (1914) and Wentworth (1922). The Folk (1954) classification scheme was used for sediment classification.

3.2.4.3 Sediment Accumulation Rate

Please see sections 2.2.7 for the detailed methods used for estimating sediment accumulation rate. Radionuclide analysis was carried out on freeze-dried sediments sampled at 1 cm resolution from the top 40 cm of 7 sediment cores (Sites 4, 8, 14, 15, 20, 21, 27), which reflected samples from the range of sediment type, water depth, *N. norvegicus* burrow density, and SAR in the study region. Sediments were measured for ^{210}Pb, ^{137}Cs, and ^{241}Am using Mirion (Canberra) Canberra High Purity Germanium (HPGe) well-type gamma spectrometers (GAU-Radioanalytical, University of Southampton) under their accreditation to ISO/IEC17025. Alpha

spectrometry (Ortec Octete) was also conducted to measure the grand-daughter radionuclide, ^{210}Po, which would be in equilibrium with ^{210}Pb, for 3 sediment cores (Sites 4, 8, and 20) to cross-validate the ^{210}Pb activities, which were close to the instrumental limit of detection and had higher uncertainty.

Average linear sedimentation rates were estimated from ^{210}Pb and ^{210}Po using the constant flux constant sedimentation (CF–CS) model (Appleby and Oldfield, 1978), which were validated using ^{137}Cs activity (impulse) peaks corresponding to the 1975 discharge maximum from the Sellafield nuclear facility relative to the core surface representing the year 2022, and the onset of cumulative ^{241}Am activities corresponding to ^{241}Am discharge records from the Sellafield nuclear facility (Gray et al., 1995). Average linear sedimentation rates were estimated from ^{210}Pb, ^{210}Po, and ^{137}Cs activity profiles, where reliable data were available, and used to estimate sediment age for the top 50 cm.

3.2.5 Statistical Analysis

Sediment sites were attributed with water depth (tidal corrected), OC content, particle sizes, and fishing effort (SAR) (Table 3.1; Appendix Table B.3). The dataset used for statistical analyses included 18 study sites comprising sediments with a minimum of 77% mud content and minimum of 56% silt content. Sites 2c and 6b were excluded from the dataset used for statistical analyses, as these sites were less representative of muddy sediments, having coarser sediments that required different particle size analysis methods.

3.2.5.1 General Linear Model Selection

Pearson's correlation coefficients were estimated to assess the relative strength of association between environmental parameters (water depth, *N. norvegicus* burrow density, SAR) and sediment properties (OC concentration, SCD, DBD, clay content, silt content, mud content, and sand content), to control for collinearity. The relative significance of the Pearson's coefficients (correlations) was used to determine the set of predictor variables to include in the GLMs, by excluding highly or very highly

correlated terms from the model. Variables were broadly considered uncorrelated ($0 \leq r \leq 0.1$), weaky correlated ($0.1 \leq r \leq 0.39$), moderately correlated ($0.4 \leq r \leq 0.69$), highly correlated ($0.7 \leq r \leq 0.89$), and very highly correlated ($0.9 \leq r \leq 1$), whilst acknowledging the limitations of these boundaries (Schober et al., 2018). These correlations were visualised in correlation matrices for all sediment depths (Appendix Figure B.2).

Water depth and DBD were excluded from the model due to collinearity with sediment type, which is considered a driver of sediment OC concentration (Burdige, 2007). Sand content was omitted from the model due to having a very high inverse correlation with mud content, while silt and clay content were selected for the model over mud content as they provide a more resolved picture of the associations between mud (silt + clay) and OC concentration, and were not strongly correlated to each other. As a result, clay content (%), silt content (%), *N. norvegicus* burrow density (m^{-2}, 2013–2022), and SAR (yr^{-1}, 2016–2021) were selected as independent variables for the GLMs. OC concentration was selected over SCD as the dependent variable, as SCD is the product of OC concentration and DBD, so is related to sediment type predictor variables in the model. Clay and silt content were expected to have a positive relationship with OC concentration (Burdige, 2007), while the expected relationship between *N. norvegicus* burrow density and SAR with OC concentration was uncertain (Epstein et al., 2021).

3.2.5.2 General Linear Models

The effect of fishing pressure on OC concentration was examined using GLMs for sediment depths 0–10 cm, 10–20 cm, 20–30 cm, 30–40 cm, and 40–50 cm (Muir et al., 2025 (Preprint)).

GLMs used log-transformed OC concentration as the dependent variable, as the standardised residuals (sresids) for the depth 20–30 cm had a non-normal distribution. Log-transformation was applied to the dependent variable for all sediment depths for comparability between models. GLMs initially included each of the predictor variables and their interaction terms, then the highest order insignificant terms ($p > 0.05$) were iteratively removed from the model until the highest-order

term in the model was significant. This approach ensured interactions between variables were considered prior to omission.

Variance inflation factors (VIFs) were calculated to check for collinearity between variables, whereby VIF < 3 was used to indicate that there was no concerning collinearity in the dataset (Kock and Lynn, 2012). The slope (effect size) and significance of the effect for each predictor variable on the dependent variable were evaluated using the *t*-statistic and *p*-value of the model. Model validation was performed to check that the assumptions of normality and homoscedasticity for the selected model were met.

3.3 Results

A total of 20 sediment cores were collected from the study region, which ranged from 50 cm to 88 cm in length (Table 3.1). SAR values based on the high-resolution (0.25 km² grid) fishing pressure map ranged from 2.34 yr^{-1} to 10.14 yr^{-1} across the study region, which were within the low to mid-range estimated for the broader region of 0 yr^{-1} to 22.49 yr^{-1} (Figure 3.1). Fishing pressure gradients were observed at the edge of the WISMB and around seabed infrastructure (e.g., cables and pipelines). *N. norvegicus* burrow densities ranged from 0.74 m^{-2} to 1.18 m^{-2}, which were within the upper range estimated for the broader region of 0 m^{-2} to 1.2 m^{-2} (Figure 3.2). Water depths recorded on site and corrected for tidal state ranged from 66 m to 132 m.

Data for sediment depths 0–10 cm, 10–20 cm, 20–30 cm, 30–40 cm, and 40–50 cm assessed herein are summarised in Appendix Table B.3, which includes sampling site ID, sediment DBD (g cm^{-3}), OC concentrations (%), SCD (gC cm^{-3}), and the average proportion (%) of mud (clay + silt, <3.9 µm to 62.5 µm), clay (<3.9 µm), silt (3.9 µm to 62.5 µm), and sand (62.5 µm to 2000 µm).

All sampling sites were classified as mud or sandy mud. Mud content was relatively constant with sediment depth, whilst clay content increased with sediment depth and silt content decreased with sediment depth. Average mud and silt content (within the mud) in the top 50 cm of sediment were 87% ± 6% (minimum: ≥77%) and 63% ± 3% (minimum: ≥56%), respectively, for all sites excluding Sites 2c and 6b, which

had lower mud contents of 71.77% and 68.55%, respectively, and lower silt contents of 50.24% and 43.66%, respectively. Sites 2c and 6b also comprised coarser sediments that could not be quantified using laser diffraction (due to methodological limitations), so these sites were excluded from the dataset used for statistical analysis.

The linear sedimentation rate estimated for the study region based on radionuclide profiles from five sediment cores was 0.29 ± 0.02 cm yr^{-1}, ranging from 0.26 cm yr^{-1} to 0.37 cm yr^{-1} (Muir et al., 2025 (Preprint)), which corresponds to approximately 33 years (27 to 39 years) for every 10 cm of sediment (Figure 3.3). The lowest sedimentation rate of 0.26 cm yr^{-1} was estimated for Sites 15, 20, and 27, which had the lowest OC concentrations and were situated in shallower water (66–98 m) with higher *N. norvegicus* burrow densities on average (0.93–1.18 m^{-2}) and the greatest fishing pressure (7.01–8.82 yr^{-1}) (Table 3.2; Figure 3.4). Sites 4 and 8 had the highest sedimentation rates of 0.31 cm yr^{-1} and 0.37 cm yr^{-1}, respectively, and among the highest OC concentrations, which were situated in deeper water (116–119 m) with lower *N. norvegicus* burrow densities on average (0.90–0.94 m^{-2}) and lower fishing pressure (3.05–3.95 yr^{-1}) (Table 3.2; Figure 3.4). Radionuclide profiles showed no notable differences in surface sediment mixing depths between these five sites. Sediments were significantly more mixed at Sites 14 and 21, which prevented sedimentation rate estimates for these sites, despite having among the lowest *N. norvegicus* burrow densities (0.84–0.86 m^{-2}) and SARs (4.09–4.92 yr^{-1}), and water depths comparable with other sites (68–100 m) (Table 3.2; Figure 3.4; Appendix Figure A.20–A.25).

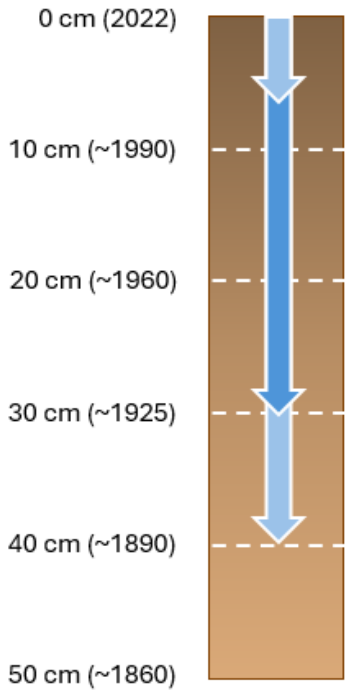

Figure 3.3 Schematic representing the top 50 cm of sediment in the Western Irish Sea Mud Belt (WISMB) divided into 10 cm segments (white dashed lines) and labelled with average sediment deposition dates based on the average linear sedimentation rate of 0.29 ± 0.02 cm yr^{-1} estimated from 5 sediment cores (Muir et al., 2025 (Preprint)). Trawl penetration is represented by blue arrows from the sediment surface to 6 cm for beam trawls and up to 40 cm deep for dredges (light blue arrows; Martín et al., 2014), with an average of 30 cm (dark blue arrow; Coughlan et al., 2015).

Table 3.2 Average sedimentation rate ± standard deviation (cm yr^{-1}) estimated from ^{210}Pb, ^{210}Po, and ^{137}Cs radionuclide analysis for sediment cores from Sites 4, 8, 14, 15, 20, 21, and 27 (Muir et al., 2025 (Preprint)), and their corresponding water depth (m, corrected for tidal state), *Nephrops norvegicus* burrow density (m^{-2}), swept area ratio (SAR, yr^{-1}), organic carbon (OC) concentration (%) at 0–10 cm, 10–20 cm, 20–30 cm, 30–40 cm, and 40–50 cm sediment depths, and surface sediment mixing depth (cm) estimated from radionuclide activity.

					Organic carbon concentration (%)					
Site ID	**Sedimentation rate (cm yr^{-1})**	**Water depth (m)**	***N. norvegicus* burrow density (m^{-2})**	**SAR (yr^{-1})**	**0–10 cm**	**10–20 cm**	**20–30 cm**	**30–40 cm**	**40–50 cm**	**Surface mixing depth (cm)**
4	0.31 ± 0.01	119	0.94	3.05	1.41	1.32	1.14	0.93	0.86	0–6
8	0.37 ± 0.00	116	0.90	3.95	1.59	1.35	1.11	1.01	0.99	0–11
14	N/A	100	0.84	4.09	1.32	1.36	1.38	1.32	1.22	0–40
15	0.26 ± 0.03	98	0.93	7.01	0.89	0.75	0.74	0.53	0.50	0–8
20	0.26 ± 0.04	66	1.14	8.52	0.92	0.83	0.70	0.48	0.49	0–7
21	N/A	68	0.86	4.92	0.77	0.73	0.62	0.69	0.75	0–19
27	0.26 ± 0.03	68	1.18	8.12	0.78	0.60	0.49	0.49	0.47	0–4
Avg.	0.29 ± 0.02	-	-	-	-	-	-	-	-	-

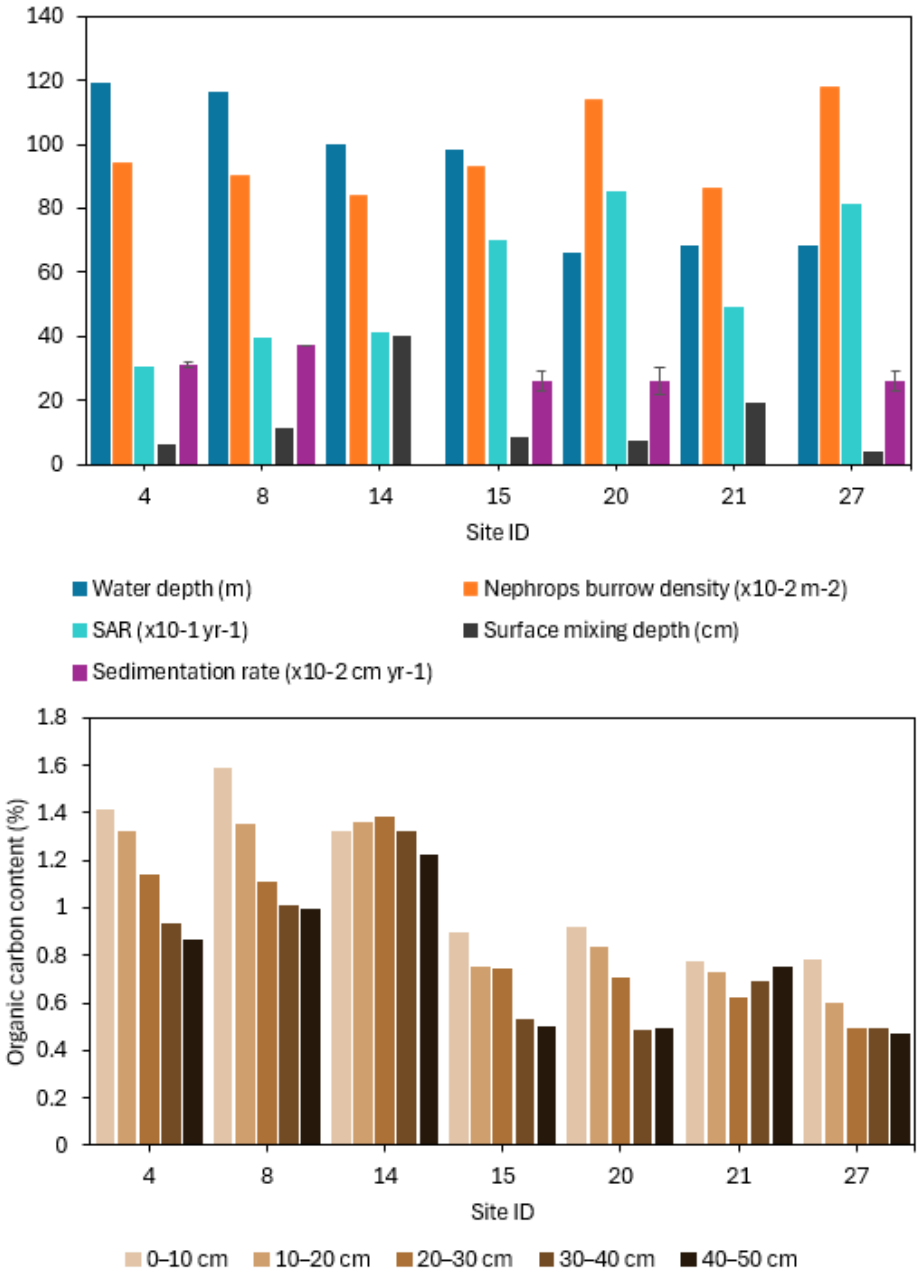

Figure 3.4. Top: Graphs of water depth (m, corrected for tidal state), swept area ratio (SAR, $x10^{-1}$ yr^{-1}), sedimentation rate (± standard deviation, $x10^{-2}$ cm yr^{-1}), *Nephrops norvegicus* burrow density ($x10^{-2}$ m^{-2}), and surface mixing depth (cm) for sediment cores from Sites 4, 8, 14, 15, 20, 21, and 27. Unit have been scaled for comparability on the y-axis. Bottom: Organic carbon concentration (%) for sediment depths of 0–10 cm, 10–20 cm, 20–30 cm, 30–40 cm, and 40–50 cm.

3.3.1 Statistical Analysis

3.3.1.1 Model Development and Selection

The outputs of the GLMs are summarised in Table 3.3. All interaction terms were insignificant in the models and removed from the final model after model selection. The predictor variables explained 59% to 87% of the variance (adjusted R^2) in OC concentration for depths down to 40 cm and 43% of the variance in OC concentration for 40–50 cm depth. The assumptions of normality and homoscedasticity were met for models at all sediment depths, excluding at 40–50 cm, where observation 7 (Site 21) was highly influential (Appendix Figures B.4–B.9; Appendix Tables B.5 and B.6). Site 21 is situated at the edge of the WISMB with relatively lower silt content (50.99%) (Figure 3.1; Appendix Table B.3), representing a rare but valid condition in the dataset (average silt content = 61.29% ± 4.06%). When data for Site 21 were removed from the dataset for sediment depth 40–50 cm the predictor variables explained 69% of the variance in OC concentration and the assumption of homoscedasticity was met. The VIFs were <3 for all predictor variables, indicating that there was no concerning collinearity between SAR, *N. norvegicus* burrow densities, clay content, and silt content in the datasets (Appendix Table B.4).

Fishing pressure (SAR) had a highly significant ($p < 0.01$) negative influence on OC concentration at 10–20 cm, and no significant ($p > 0.05$) effect at any other depth (Table 3.3). At 10–20 cm, the slope for SAR is -0.50 (standard error (SE) = 0.01), which is also statistically significant ($p = 0.0020$), suggesting that higher SAR values are associated with a significant decrease in OC concentration, with an estimated effect size of -0.50 per unit increase. The slope for SAR is comparable in deeper sediments but smaller (-0.002 (SE = 0.01)) in the top 10 cm, and its effect on OC concentration is insignificant.

Clay content and silt content had a highly significant ($p < 0.05$) positive relationship with OC concentration in the top 10 cm of sediment, while only silt content had a significant ($p < 0.05$) positive influence on OC concentration in deeper sediment (Table 3.3). In the top 10 cm, the slope for clay (3.06, SE = 0.77, $p = 0.0015$) and silt (3.60, SE = 0.94, $p = 0.0021$), suggest that higher clay and silt content are associated with a significant increase in OC concentration of 3.06 and 3.60 units for every unit

increase of clay and silt content, respectively. In deeper sediment, the slopes and SEs for clay and silt content decrease to magnitudes comparable to SAR, having a weaker effect on OC concentration with sediment depth.

N. norvegicus burrow densities had no significant ($p \geq 0.05$) influence on OC concentration at any sediment depth (Table 3.3). Nevertheless, the slope for *N. norvegicus* burrow densities is approximately -0.3 (SE = 0.17–0.38) at all depths, excl. at 20–30 cm (where slope = -0.05, SE = 0.42), suggesting that higher *N. norvegicus* burrow densities are associated with a decrease in OC concentration of approximately 0.3 units for every unit increase of *N. norvegicus* burrow densities, but the statistical significance of this relationship is weak.

Table 3.3 Summary of the statistical outputs of general linear models (slope, standard error (SE), t-statistic, p-value, and adjusted r^2) for the relationship between sedimentary organic carbon concentration (%) and *Nephrops norvegicus* burrow densities (m^{-2}), swept area ratio (SAR, yr^{-1}), clay content (%), and silt content (%). $p < 0.05$ denotes significance at 95% confidence level (significant values in bold font).

Sediment depth (cm)	Sediment deposition date	Parameter	Slope	Standard error (SE)	t-statistic	p-value	adj-r^2
0–10	1990–2022	*Nephrops*	-0.30	0.17	-1.80	0.095	0.87
		SAR	-0.002	0.01	-0.25	0.809	
		Clay	3.06	0.77	3.99	**0.002**	
		Silt	3.60	0.94	3.82	**0.002**	
10–20	1960–1990	*Nephrops*	-0.39	0.23	-1.67	0.119	0.80
		SAR	-0.05	0.01	-3.87	**0.002**	
		Clay	0.02	0.01	1.79	0.097	
		Silt	0.05	0.01	4.88	**0.000**	
20–30	1925–1960	*Nephrops*	-0.05	0.42	-0.12	0.910	0.59
		SAR	-0.05	0.02	-2.14	**0.052**	
		Clay	0.02	0.02	1.14	0.275	
		Silt	0.05	0.02	2.84	**0.014**	
30–40	1890–1925	*Nephrops*	-0.34	0.36	-0.94	0.363	0.65
		SAR	-0.04	0.02	-1.73	0.108	
		Clay	0.01	0.01	0.67	0.514	
		Silt	0.06	0.02	3.78	**0.002**	
40–50	1860–1890	*Nephrops*	-0.27	0.46	-0.57	0.577	0.43
		SAR	-0.05	0.02	-2.12	**0.054**	
		Clay	0.53	1.44	0.37	0.719	
		Silt	3.44	1.55	2.23	**0.044**	

40–50 (excl. Site 21)	1860–1890	*Nephrops*	0.05	0.38	0.14	0.892	0.67
		SAR	-0.01	0.02	-0.46	0.651	
		Clay	0.01	0.01	0.81	0.434	
		Silt	0.08	0.02	4.12	**0.001**	

3.4 Discussion

This study shows that intense chronic bottom trawling has a long-term negative impact on sedimentary OC in the WISMB. The OC stored in sediments deposited between 1960 to 1990 is significantly depleted in areas of higher modern trawling activity. Modern fishing gears targeting *N. norvegicus* have been estimated to penetrate 15–30 cm into soft, muddy seabed (Coughlan et al., 2015; Eigaard et al., 2016), which could resuspend and remobilise OC within the sediments at 10–20 cm, accelerating OC mineralisation and degradation, and reducing long-term OC storage (Palanques et al., 2014). Sedimentation rates were lower at the most intensely trawled sites, which could be attributed to resuspension and export of finer sediments by trawling, leading to the coarser sediments observed in these areas. However, these sites are also situated in shallower water, which may experience elevated hydrodynamic resuspension similar to the effects of trawling. The sediments at 10–20 cm also correspond to the intensification of *N. norvegicus* trawling activities in the WISMB during the 1960s to 1990s (Coughlan et al., 2015; Davie and Lordan, 2011), so OC depletion could have resulted from historic fishing pressure. However, accurate historic fishing pressure could not be reconstructed due to a paucity of data, so further work would be needed to assess if spatial patterns of modern fishing pressure (2016–2021) reflect historic fishing pressure (1960–2022).

Conversely, OC concentrations in sediments deposited before 1960 (below 20 cm) were not significantly depleted in more intensely trawled regions. Modern trawling impacts may be reduced in these deeper sediments as the footprint and subsurface abrasion of demersal gears can be significantly smaller in subsurface sediments compared to surface sediments (Church et al., 2016; Coughlan et al., 2015; Martín et al., 2014b). Gear penetration can vary with vessel speed, gear operation, and use of add-ons (e.g. rakes, groundropes, rockhoppers, tickler chains), with some estimates ranging from 6 cm (beam trawls) up to 40 cm (dredges) (Martín et al., 2014b). Furthermore, the effect of modern trawling may be weaker in deeper sediments in the WISMB where sedimentary OC is depleted due to ongoing degradation of labile OC and retention of recalcitrant or refractory OC, that is more resistant to remineralisation (Burdige, 2007; Muir et al., 2025 (Preprint)). While the GLMs explained most of the variance in OC concentration at all sediment depths (59%–

87%), their predictive power generally decreased with sediment depth, indicating that other unmeasured variables could also influence OC concentration in deeper sediments while predictors like fishing pressure have weaker explanatory power.

Despite this, sediment composition was significantly related to OC concentrations at all sediment depths, with more silty sediments having higher OC concentrations, reflecting the affinity of finer sediments for OC adsorption (Burdige, 2007). This relationship was particularly strong in the upper 10 cm of sediment where OC concentrations are highest. Here, OC concentrations in sediments deposited since the 1990s (upper 10 cm) were not significantly related to trawling pressure. Modern trawling impacts may be masked by other surface processes that can enhance OC remineralisation by increasing oxygen exposure through sediment mixing, remobilisation, and redeposition, similar to the effects of trawling (Coughlan et al., 2021; Martín et al., 2014b; Paradis et al., 2019; Song et al., 2022; Williams et al., 2019). Such processes could include environmental and biological processes, such as tidal currents and bioturbation; lateral transport of sediments that have been resuspended by trawling and their re-deposition adjacent to trawling grounds (Thompson et al., 2017); or deposition of fresh OC-rich sediments (Paradis et al., 2019).

Widespread surface sediment mixing was observed in the radionuclide profiles and OC concentrations within the upper 3.5–11 cm of all seven sediment cores analysed for radionuclides, independent of fishing pressure (Muir et al., 2025 (Preprint)). Whilst seabed mobility induced by natural hydrodynamic forces, mainly tides and waves, is low in the WISMB relative to the Irish Sea (Belderson, 1964; Coughlan et al., 2021; Williams et al., 2019), temporary erosive near-bottom currents induced by seasonal cyclonic gyres during spring and summer could mix and redeposit the sediments, potentially masking the effects of trawling (Coughlan et al., 2021). Furthermore, *N. norvegicus* are a major bioturbator in the WISMB and have relatively large complex burrows that can penetrate up to 30 cm into the sediment (Coughlan et al., 2015; Rice and Chapman, 1971), comparable with trawling penetration depths (Agri-Food and Biosciences Institute, 2023). Upward movement of sediments by burrowing *N. norvegicus* could cause these surface mixed sediments. While previous research suggests bioturbation has a limited influence on OC concentration (Lindeboom and de Groot, 1998; Sciberras et al., 2016), *N. norvegicus*

burrow densities were more strongly associated with OC concentrations than SAR or clay and silt content, despite the weak statistical significance of this relationship.

These sediment mixing processes, particularly chronic trawling, have previously been shown to enhance seabed erosion and sediment deposition (Arias-Ortiz et al., 2018; Coughlan et al., 2015; Paradis et al., 2019), as observed by altered excess ^{210}Pb activities in marine sediments (Barsanti et al., 2020). However, agreement between linear sedimentation rates estimated from excess ^{210}Pb and ^{137}Cs radionuclide activity profiles herein confirmed net sedimentation in the study region. This indicates that trawling does not significantly erode the seabed, rather sediments are retained, which could be facilitated by the thin benthic boundary layer formed by cyclonic currents and low bed shear stress in the WISMB (Williams et al., 2019).

The findings herein are comparable with other studies that have investigated the stratigraphic impacts of modern trawling on sedimentary OC concentrations. Paradis et al. (2019) found that OC concentration in surface sediments and sediments below 30 cm were unaffected by otter trawling in a deep-water (550 m) muddy continental slope in the Gulf of Castellammare (Southwestern Mediterranean), while sediment OC concentrations were approximately 20% lower overall between 2 cm to 20 cm in trawled regions compared with an untrawled regions. Martín et al. (2014c) also found that sedimentary OC was impoverished down to 30 cm in otter trawled regions compared with an untrawled region in deep-water (453–591 m) mud-rich flanks of La Fonera submarine canyon (Northwestern Mediterranean). As a result, our study adds to the growing body of evidence of the negative effects of bottom trawling on sedimentary OC concentrations within sub-surface sediments, potentially limiting their long-term ability to regulate climate. The low sedimentation rates and repeated trawling could hinder the recovery of OC in the WISMB, prolonging the impacts of trawling on OC storage (Smeaton and Austin, 2022). Future research would be needed to assess sediment OC recovery in the absence of trawling, which could include implementing fishery management measures, such as gear restrictions and closure zones, accompanied by empirical research to investigate changes in OC content and predictor variables such as sediment properties and biological communities.

3.5 Conclusions

Overall, this study reveals the long-term negative impact of intense chronic bottom trawling on sedimentary OC in the WISMB. Through stratigraphic analysis of sedimentary OC concentrations and radionuclides within the top 50 cm of sediments in the WISMB, this study provides one of the highest resolution, age-resolved analyses of modern trawling impacts on sedimentary OC to date. While the effects of trawling pressure on sedimentary OC concentrations were unresolved in sediments deposited since the 1990s (upper 10 cm) due to significant sediment mixing, the OC stored in sediments deposited between 1960 to 1990 (10–20 cm) was significantly depleted in areas of higher modern trawling activity. These findings support other studies that show trawling negatively impacts sub-surface sedimentary OC, highlighting the potentially depleted state of trawled shelf sea OC stocks. These findings emphasise the need for fisheries management strategies that consider biogeochemical characteristics of sediments, which could be crucial for protecting and enhancing OC storage on coastal and shelf seas, and mitigating anthropogenic climate change.

Chapter 4

Organic Carbon Storage and Accumulation in Saltmarshes and Seagrass Meadows along an Exposed Temperate Coastline

Abstract

Seagrass meadows and saltmarshes are regarded as vital blue carbon ecosystems, accumulating and storing organic carbon (OC) within their sediments. Estimates of their OC storage and accumulation are increasingly required for natural capital assessments and proposed carbon credit mechanisms. These estimates are restricted by a paucity of ecosystem extent data and depth-/age-resolved OC data, as well as their spatial variability. This study provides a novel case study of sedimentary OC storage and accumulation in seagrass meadows and saltmarshes in the Isle of Man, Irish Sea. Using side-scan sonar and in-situ surveys, 195.88 ha of seagrass meadows were mapped, in addition to 7.38 ha of saltmarsh based on existing data. Saltmarsh sediments store 94.14 ± 62.51 MgC ha^{-1} (694.78 ± 461.34 MgC) and accumulate 7.97 ± 5.60 MgC yr^{-1} at a rate of 107.96 ± 75.83 gC m^{-2} yr^{-1} (1.08 ± 0.76 MgC ha^{-1} yr^{-1}). Seagrass sediments store 1.33 ± 0.25 MgC ha^{-1} (261.10 ± 49.08 MgC) in the top 10 cm, which is 43% greater than unvegetated sediments (0.93 ± 0.86 MgC ha^{-1}), but the mixed seagrass meadow sediments prevented OC accumulation rate estimates. Spatial variability in saltmarsh OC stocks and accumulation rates was mainly attributed to differences in estuarine location, tidal inundation, and land use. Meanwhile, seagrass meadow properties such as canopy cover, plant density, leaf length, connectivity, and sediment type varied around the island, reflecting site exposure, which may influence OC storage. These findings underscore the role of saltmarshes and seagrass meadows in climate regulation, and highlight the need for their conservation to protect existing OC stocks and to support future OC sequestration.

4.1 Introduction

Temperate vegetated coastal ecosystems, such as seagrass meadows and saltmarshes, serve as significant sinks for atmospheric CO_2, comparable to terrestrial ecosystems (Lovelock and Duarte, 2019; McLeod et al., 2011). This recognition has led to the development of blue carbon strategies aimed at mitigating climate change through ecosystem conservation and restoration (Giritharan, 2024; Macreadie et al., 2021). These ecosystems can store organic carbon (OC) within their sediments over centuries to millennia, making them essential nature-based solutions for carbon sequestration (Macreadie et al., 2021). However, ongoing degradation threatens their role as carbon sinks, leading to OC loss and reduced future accumulation (Campbell et al., 2022; Dunic et al., 2021; Goldberg et al., 2020). Despite growing interest in their climate regulation function, limited regional data on their sedimentary OC stocks and accumulation, and their extents pose challenges for effective coastal ecosystem management (Macreadie et al., 2019; Unsworth et al., 2019).

Accurate assessment of OC storage requires understanding of the extent and spatial variability of these ecosystems. Global estimates indicate that saltmarshes cover approximately 52,880 km² across 120 countries predominantly in temperate and Arctic regions (Worthington et al., 2024), while seagrass meadows occupy between 160,387 km² and 266,562 km² across 103 to 136 countries, respectively (McKenzie et al., 2020). However, large knowledge gaps in the spatial extent and variability persist due to incomplete mapping, particularly for seagrass meadows (Macreadie et al., 2019). Mapping methods for saltmarshes typically rely on satellite and aerial imagery, while seagrass mapping presents challenges due to their subtidal location, water turbidity, and patchy distribution (McKenzie et al., 2020). Remote sensing, coupled with ground truthing techniques such as video surveys and acoustic imaging (e.g., side-scan sonar, multi-beam echosounder), has improved mapping accuracy of subtidal meadows, particularly in energetic environments (Greene et al., 2018; Lefebvre et al., 2009; Strong et al., 2023). Yet, many of the world's seagrass meadows remain unmapped.

Furthermore, high spatial and temporal variability of sedimentary OC stocks and accumulation limits the applicability of global estimates to inform local blue carbon ecosystems (BCE) management (Green et al., 2018; Penk and Perrin, 2022; Prentice

et al., 2020; Oreska et al., 2017). Global estimates of saltmarsh OC stocks in the top meter of sediment are 231 ± 134 MgC ha^{-1}, varying by vegetation type, sediment characteristics, and land use (Davidson et al., 2017; Maxwell et al., 2023; Smeaton et al., 2023), yet saltmarsh sediment thickness varies, complicating OC stock projections (Ladd et al., 2022; Miller et al., 2023). Meanwhile, estimates of global seagrass sediment OC stocks in the top meter of sediment are 139.7 to 329.5 ± 55.9 MgC ha^{-1} (Fourqurean et al., 2012), varying by species, hydrodynamics, sedimentation, and seasonal influences (Dahl et al., 2020a,b; Oreska et al., 2017). Furthermore, assessments comparing OC stocks between vegetated and unvegetated sites remain limited (Dahl et al., 2016; Potouroglou et al., 2021; Prentice et al., 2020).

To accurately quantify the OC storage capacity of temperate coastal vegetated BCEs, high-resolution mapping and depth-/age-resolved OC data are needed. This study combines remote sensing (side-scan sonar) and in situ methods (video surveys, diver surveys) with publicly available and unpublished datasets to produce a comprehensive saltmarsh and seagrass meadow extent map for the Isle of Man. The ecosystem extents derived from these maps were combined with age-resolved sedimentary OC density data to provide island-wide sedimentary OC stock and accumulation estimates for these BCEs.

4.2 Materials and Methods

4.2.1 Ecosystem Extent Estimates

Extent data for saltmarshes was extracted from polygon shapefiles in ArcGIS Pro, based on habitat survey data from 1991–1994 (Figure 4.1; Sayle et al., 1995).

Seagrass meadows were mapped using remote sensing by side-scan sonar (SSS) surveys and towed underwater video camera (TUV) surveys, and ground truthed by drop-down (DD) video camera and diver surveys. Extents were estimated from these combined datasets in ArcGIS Pro software (Figure 4.1).

Remote sensing surveys were conducted from fisheries protection vessel Glashtyn in August 2023. Acoustic images were collected at Ramsey Bay and Laxey Bay using

methods described by Strong et al. (2023). A Blueprint 452F Starfish SSS system operating at 450 kHz generating a 200 m ensonified swathe (beam angles 0.8° horizontal and 60° vertical) was connected to a processing box and a laptop running Scanline acquisition software. Acoustic data were processed using SonarWiz software, which enabled tracking of the seabed, application of layback offsets, empirical gain normalisation to all tracks, and a de-stripe filter to remove heavy weather artifacts, as well as exporting of the data to a 10 cm GeoTIFF of the survey area, in line with methods used by Strong et al. (2023). Subsequent analysis of the outputs was undertaken in ArcGIS Pro software. The DD video footage (live stream) was collected at Ramsey Bay, Laxey Bay, and Bulgham Bay using a battery powered DeepTrekker 4 Remotely Operated Vehicle (ROV). The ROV was navigated to the seabed with a steep descent angle and facing the prevailing current, to obtain optimal georeferencing with the GPS locator on board the survey vessel. The ROV was held on the seabed for approximately 20 seconds where it completed a slow, controlled 360-degree turn, to assess the seagrass meadow and environmental properties.

The TUV surveys were conducted off the fisheries protection vessel Barrule using a HD camera at Ramsey Bay (July 2019), Bulgham Bay (November 2021), and Laxey Bay (November 2022). Video tows were performed along transects and points were plotted on the vessel's chart system when seagrass was located. These surveys were conducted prior to this PhD research (2022–2025) and the unpublished datasets were provided by the Isle of Man Government for use in this research. Point datasets were converted to seagrass presence and absence data points in ArcGIS Pro software.

Various diver surveys were conducted by the Manx Wildlife Trust and Seasearch volunteers at Bulgham Bay (June 2021 and May 2024), Derbyhaven and Langness (Fort Island Gully) (May–July, September, and November 2022), Ramsey Bay (December 2023 and May 2024), and at Baie Ny Carrickey (February and March 2024) to locate seagrass. Most of these surveys were conducted prior to this PhD research (2022–2025) and the unpublished datasets were provided by the Isle of Man Government and Manx Wildlife Trust (MWT) for use in this research. Observations of surface sediments, seagrass canopy cover, leaf blade length, biodiversity, and other details recorded in diver survey reports (unpublished) and during DD video surveys (this study) were summarised herein. All point datasets were converted to

seagrass presence and absence data points in ArcGIS Pro software, which were used to generate extent (polygon) estimates.

Seagrass meadow extents were estimated directly from polygon datasets provided by Manx Wildlife Trust for Baie Ny Carrickey, Derbyhaven, and Langness (Fort Island Gully). These polygons were generated by connecting point datasets based on diver surveys around the periphery of seagrass meadows. Seagrass meadow extents for Bulgham Bay were estimated from Thiessen polygons generated using point data from diver surveys, TUV surveys, and DD video surveys denoting seagrass presence and absence, which were constrained within absence data generated using aerial images of the rocky coastline and bathymetry data. Seagrass meadow extents for Laxey Bay and Ramsey Bay were estimated from SSS surveys, which were validated by TUV surveys, DD video surveys, and diver surveys. Thiessen polygons were also generated for Ramsey Bay to validate these results.

Details of the approaches used to estimate each seagrass meadow extent are provided in Appendix C (Appendix Figures C.1–C.5).

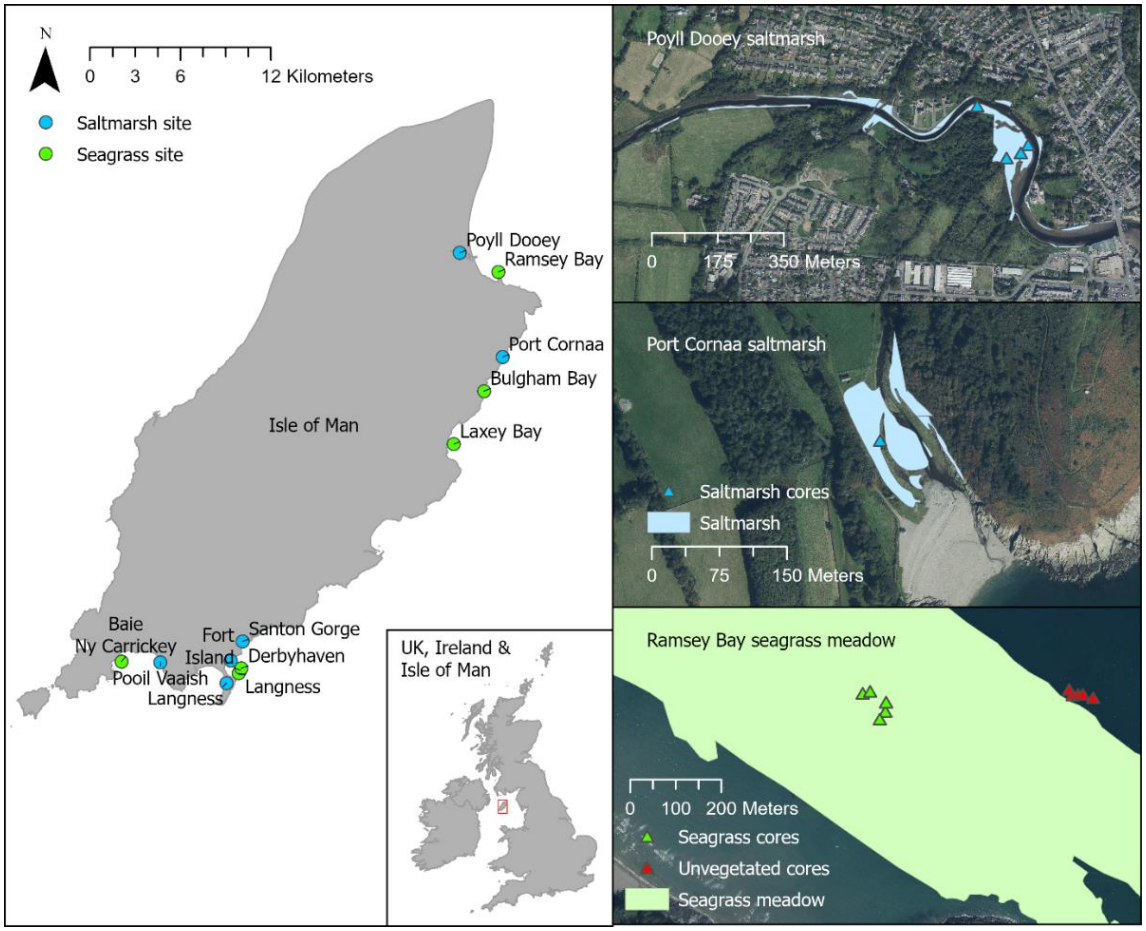

Figure 4.1 Left: Map of the Isle of Man with saltmarsh (blue dots) and seagrass meadow (green dots) locations. Inset of the Isle of Man in the Irish Sea. Right: Sampling location maps of Poyll Dooey and Port Cornaa saltmarshes (blue shade) and saltmarsh sediment core sites (blue triangles), and of and Ramsey Bay seagrass meadow (green shade) and seagrass sediment core sites (green triangles).

4.2.2 Sampling Site Selection

Saltmarsh sampling stations were selected in two distinct saltmarsh environments, estuarine Poyll Dooey and lagoonal Port Cornaa, representing approximately half of the Isle of Man's saltmarsh ecosystem (3.34 ha, 45.18%) (Figure 4.1). A single sediment core was collected from Port Cornaa saltmarsh on 26th April 2022 and from Poyll Dooey saltmarsh on 29th April 2022, with a further three sediment cores collected from Poyll Dooey saltmarsh on 8th August 2023. Sediment cores were taken from areas comprising the most prolific saltmarsh species on the island: pioneer marsh (SM8 (*Salicornia europea*)), low-mid marsh (SM13 (*Puccinellia*

maritima)), and high marsh (SM16 (*Juncus maritimusi*)) (Spencer, 2005). These communities were characterised in a previous report by Spencer (2005), based on a vegetation survey completed in July 2003 following the British National Vegetation Classification (NVC) scheme (Pigott, 2000).

Seagrass sampling stations were in the island's largest *Zostera marina* seagrass meadow, Ramsey Bay, which represents approximately two-thirds of the island's seagrass cover (125.27 ha, 63.95%). Five sediment cores were collected from the centre of Ramsey Bay seagrass meadow and a further five from an adjacent area of unvegetated sediment in August 2023 using SCUBA dives (Figure 4.1).

4.2.3 Sediment Sampling

Sediment cores were extracted at low tide using a PVC corer (saltmarsh: h = 100 cm/$ø_{internal}$ = 11 cm; seagrass: h = 70 cm/$ø_{internal}$ = 9 cm) with a serrated edge and internal drain test cap, which was pushed by hand into the sediment until the point of refusal. Seagrass meadow cores were extracted by SCUBA dives conducted at low tide by divers at the Isle of Man Government. A mallet was used to assist sediment penetration in saltmarshes. Coordinates of coring sites were recorded using a GPS navigation unit. For SCUBA dives, an inReach Explorer®+ handheld satellite communicator was also used and water depth was recorded using a depth sounder on the diver support vessel. A 0.25 m^2 quadrat was photographed at each core using a Google Pixel phone camera for saltmarshes, and a Novasub SSC-1VL GVR D3 camera for seagrasses. The sediment surface depth was marked on the outside of the corer indicating the uncompacted core length. End caps were applied to the corer and cores were labelled with unique identification codes. Overlying water was drained from the seagrass cores, to limit sediment–water mixing during transport. The cores were stored at temperatures below 5°C to preserve their integrity and transported upright to the National Oceanography Centre, Southampton, where all subsequent laboratory analyses were performed.

4.2.4 Sediment Core Processing

Sediment cores were split lengthwise using a Geotek core splitter at the British Ocean Sediment Core Research Facility (BOSCORF). High-resolution images of the smoothed sediment surfaces were captured using a Geotek Core Imaging System with a Geoscan V camera (1,000 pixels cm^{-1}). X-ray radiography images were obtained using a ScoutXcan Multi-Angle Digital 2D X-Ray System. Sediment core profiles were described for details of sediment uniformity, depth horizons, root penetration depths (RPDs), and other notable features. Saltmarsh sediment layers were identified using the methods described by Miller et al. (2023) and Smeaton et al. (2023), which are based on the Troels-Smith classification scheme (Troels-Smith, 1955), to describe and classify unconsolidated sediments based on their composition (sediment type) and physical properties (e.g. colour, stratification, OC content, presence of plant biomass).

4.2.5 Sediment Compaction Correction

Linear compaction correction factors were calculated using Equation 4.1, to account for sediment compaction during coring. Where the sediment core surface was sloped, the mid-point on the sediment surface was recorded as the top of the sediment core.

Equation 4.1 Sediment compaction correction factor calculation.

$$Compaction\ correction\ factor\ = \frac{Length\ of\ sample\ recovered\ (cm)}{Length\ of\ core\ penetration\ (cm)}$$

The compaction-corrected depth of each sediment subsample was calculated by dividing the subsampling depth interval by the compaction correction factor using Equation 4.2.

Equation 4.2 Compaction-corrected depth measurement.

$$Compaction\ corrected\ depth\ (cm)\ = \frac{Subsample\ measured\ depth\ (cm)}{Compaction\ correction\ factor}$$

4.2.6 Sediment Sub-sampling

Sediment samples were taken from the centre of each core to minimise disturbance effects from coring. A U-channel of known volume was used to extract samples at depth intervals: every 2 cm for the top 20 cm of the sediment core, every 5 cm between 20–50 cm, and every 10 cm beyond 50 cm. Sampling resolution increased towards the sediment surface to account for more significant changes expected in sediment properties at shallower sediment depths (Howard et al., 2014). Samples were freeze-dried and large pieces of vegetation (roots, rhizomes, and leaves) were removed using tweezers before the samples were homogenised. Wet and dry sediment weights were recorded before analysis.

4.2.7 Sediment Dry Bulk Density

Sediment dry bulk densities (DBDs), which were corrected for sediment compaction using the compaction correction factor, were estimated using Equation 4.1.

Equation 4.1 Sediment dry bulk density (DBD) calculation.

$$DBD\ (g\ cm^{-3}) = \left(\frac{Mass\ of\ dry\ sediment\ (g)}{Original\ volume\ sampled\ (cm^3)}\right) * Compaction\ correction\ factor$$

4.2.8 Sediment Organic Carbon Content

The OC and total carbon concentrations, along with stable carbon isotope ratios ($\delta^{13}C$), were measured using a Flash 2000 Elemental Analyser (EA) coupled with a Delta V Advantage isotope ratio mass spectrometer (IRMS). The inorganic carbon (IC) was removed via acid fumigation before OC analysis. Isotope data were reported in delta notation relative to the Vienna Pee Dee Belemnite (VPDB) standard. Sediment organic carbon density (SCD) was estimated using Equation 2.2 (reproduced from Chapter 2).

Equation 2.2 Sediment organic carbon density (SCD) calculation.

$$SCD\ (gC\ cm^{-3}) = \frac{OC\ concentration\ (\%)}{100\%} * DBD\ (g\ cm^{-3})$$

4.2.9 Sediment Particle Size

Particle size distributions were determined using a Malvern Mastersizer 3000 laser micrograngulometer, following the NE Atlantic Marine Biological AQC Best Practice Guidance for Particle Size Analysis (PSA) (Mason, 2022). Every other sample depth was analysed down to 40–45 cm (e.g. 0–2 cm, 4–6 cm, etc.), due to resource limitations. Freeze-dried samples were dispersed in a 1% Calgon solution (sodium hexametaphosphate) and sonicated for 10 minutes prior to analysis. Samples with particle diameters >2000 μm were sieved using a 1000 μm mesh prior to analysis, and the results from laser diffraction (volumetric) were scaled to the overall sample (mass) by assuming constant sediment density. Particle size classes were grouped as: clay (<3.9 μm), silt (3.9–62.5 μm), mud (<62.5 μm), and sand (62.5–2000 μm) based on Udden (1914) and Wentworth (1922). The Folk (1954) classification scheme was used for sediment classification for sediment depths with >99% of sediment <1000 μm (i.e. trace coarse sand/gravel). Sediment classifications were not attributed to sediment depths having <99% of sediment <1000 μm, as the proportion of sediment >1000 μm that was coarse sand/gravel was unknown.

4.2.10 Sediment Accumulation Rate

Radionuclide analysis was carried out on freeze-dried sediments sampled at 1 cm resolution from the top 40 cm of 3 seagrass sediment cores (Sites V2, V4, and V5) and 5 saltmarsh cores (Sites SM8, SM13, SM16, S7C1, and S2C5). Sediments were sieved and weighed prior to analysis, to separate vegetation and coarse sediments (>1000 μm) from fine sediments. Sediments of the 3 seagrass sediment cores and 2 saltmarsh sediment cores (Sites SM8 and S2C5) were measured for ^{210}Pb, ^{137}Cs, and ^{241}Am using Mirion (Canberra) High Purity Germanium (HPGe) well-type gamma spectrometers (GAU-Radioanalytical, University of Southampton) under their

accreditation to ISO/IEC17025. Additionally, sediments of all 5 saltmarsh cores were measured for ^{137}Cs and ^{241}Am using Hidex AMG gamma counters, based on methods by Reading et al. (2025, in preparation). Data acquisition was performed using Genie-2000 (Mirion Canberra) and spectral analysis was performed using Fitzpeaks 32 deconvolution software. The HPGe detectors were efficiency calibrated using a certified, mixed gamma radionuclide standard (National Physical Laboratory, UK), which was homogenised into a near-identical sample matrix to that of the test sample. Samples were counted for 8 hours to achieve low limits of detection.

Average linear sedimentation rates were estimated from ^{137}Cs activity (impulse) peaks corresponding to the 1975 discharge maximum from the Sellafield nuclear facility relative to the core surface representing the year 2022 or 2023, and the onset of cumulative ^{241}Am activities corresponding to ^{241}Am discharge records from the Sellafield nuclear facility (Gray et al., 1995). The ^{241}Am radionuclide was used as an onset marker due to its association with fine-grained sediments in the vicinity of Sellafield nuclear facility, which provide a continuous supply of ^{241}Am to the Irish Sea after discharges ceased (Ray et al., 2020). A degree of uncertainty was accepted to account for a lag time between ^{241}Am discharge and its deposition in the sediment record. Meanwhile, the ^{137}Cs radionuclide was used as an impulse marker due to its widespread dispersal throughout the Irish Sea as a Cs^{+} cation in seawater and weaker sediment association, such that instantaneous deposition in the Irish Sea was therefore assumed (Ray et al., 2020). Average linear sedimentation rates were not estimated from excess ^{210}Pb using the constant flux constant sedimentation (CF–CS) model (Appleby and Oldfield, 1978), as the supported ^{210}Pb activities were undetermined. All sedimentation rates were corrected for compaction.

4.2.11 Organic Carbon Accumulation and Burial Rates and Efficiencies

The OC concentrations and sedimentation rates were used to date saltmarsh and pre-saltmarsh sediment layers, and to determine saltmarsh OC accumulation rates (OCARs). OCARs were not determined for seagrass meadows, as their mixed sediments inhibited sedimentation rate estimates. OCARs were estimated using Equation 2.3 (reproduced from Chapter 2, independent of sediment depth).

Equation 2.3 Organic carbon accumulation rate (OCAR) calculation.

$$\text{OCAR (gC } m^{-2}\ yr^{-1}) = \text{ SCD (gC } cm^{-3}) * \text{sedimentation rate (cm } yr^{-1}) * 10000$$

OCARs were assigned for each sediment depth based on sedimentation rates and SCDs for each core, where data were available, then the average value for each core was calculated for the saltmarsh sediments. The average OCAR value for saltmarsh sediments for the Isle of Man was estimated by upscaling the average of the Port Cornaa and Poyll Dooey saltmarsh cores to the total saltmarsh area.

OC burial efficiencies (OCBEs) were estimated for seagrass meadows based on the proportion of OC (%) stored at 20–30 cm depth where OC concentrations reached a relatively steady state compared to OC concentrations in the top 10 cm.

4.2.12 Photoquadrat Analysis

Saltmarsh photoquadrats from each sampling site were analysed to assess the broad vegetation type (e.g. grasses or succulents), but vegetation classification was outside the scope of this study. Seagrass meadow photoquadrats from each sampling site were analysed for surface sediment type and seagrass canopy cover. Seagrass canopy cover was assessed by estimating the proportion (%) of quadrat covered by leaves, according to standard methodologies (Duarte and Kirkman, 2001). The average of three estimates was reported with their standard deviations, to reflect estimate precision.

4.3 Results

4.3.1 Habitat Extents and Descriptions

4.3.1.1 Saltmarshes

Saltmarshes cover a total extent of 7.38 ha on the Isle of Man and are formed naturally (not restored), amounting to 0.01% of the landmass (57,200 ha), based on

polygons provided by the Isle of Man Government (Figure 4.2). Langness (2.74 ha), Poyll Dooey (2.64 ha), Pooil Vaaish (1.14 ha), and Port Cornaa (0.7 ha) saltmarshes account for approximately 98% of the total saltmarsh area on the Isle of Man, while Fort Island (Saint Michael's Isle) (0.1 ha), Derbyhaven (0.06 ha), and Santon Gorge (0.004 ha) make up the remaining 2% (Sayle et al., 1995; Spencer, 2005).

4.3.1.2 Seagrass Meadows

Seagrass meadows cover a total extent of 195.88 ha around the Isle of Man (Figure 4.2), equivalent to 0.05% of the territorial sea area (400,000 ha), and are all formed naturally (not restored). Ramsey Bay (125.27 ha) and Laxey Bay (60.63 ha) seagrass meadows account for 95% of the total area on the Isle of Man, while Bulgham Bay (9.87 ha) accounts for 5% of the remaining area, and Langness (Fort Island Gully) (0.1 ha), Derbyhaven (0.01 ha), and Baie Ny Carrickey (0.003 ha) account for <1%. All seagrass meadows except Bulgham Bay are situated within Marine Nature Reserves (MNRs). Only 39% of seagrass meadows are inside Eelgrass Conservation Zones (ECZs), including 9% of Ramsey Bay seagrass meadow, 40% of Laxey Bay seagrass meadow, and 100% of Langness (Fort Island Gully) seagrass meadow. Ramsey Bay seagrass meadow is also situated in the Rocky Shore Zone (32%) and in the Conservation Zone and Fisheries Management Zone (59%). All other seagrass meadows (Bulgham Bay, Derbyhaven, and Baie Ny Carrickey) are situated outside of ECZs. Detailed results of the seagrass meadow maps are in Appendix C (Appendix Figures C.1–C.5).

Based on diver and DD video surveys, the seagrass meadow canopy cover and leaf length varied within and between the seagrass meadows, from a few plants (<5%) to dense meadow (100%), and from a few cm to >60 cm in length (Table 4.1; Appendix Table C.1; Appendix Figures C.6–C.10). Surface sediments were generally gravellier (coarser) in the smaller southern meadows (Derbyhaven, Langness, and Baie Ny Carrickey) compared to the larger north-eastern meadows (Ramsey Bay and Laxey Bay), which had muddier (finer) sediments, but these were not empirically analysed using PSA. Occasional worm casts were observed, indicating infaunal bioturbation. Drift/unattached macroalgae, including *Saccharina latissima* and red, green, and brown algae, and occasional rocky outcrops with attached kelp and mixed seaweeds,

were observed in some seagrass meadows, highlighting potential allochthonous OC sources. A variety of other species were also recorded in the seagrass meadows, including snakelocks anemones, grooved topshell, spider and hermit crabs, and juvenile fish, highlighting their ecosystem function. Note that these data were recorded from diver surveys and DD video surveys available at the time of this study and may not represent the entire meadow at each site or during all seasons.

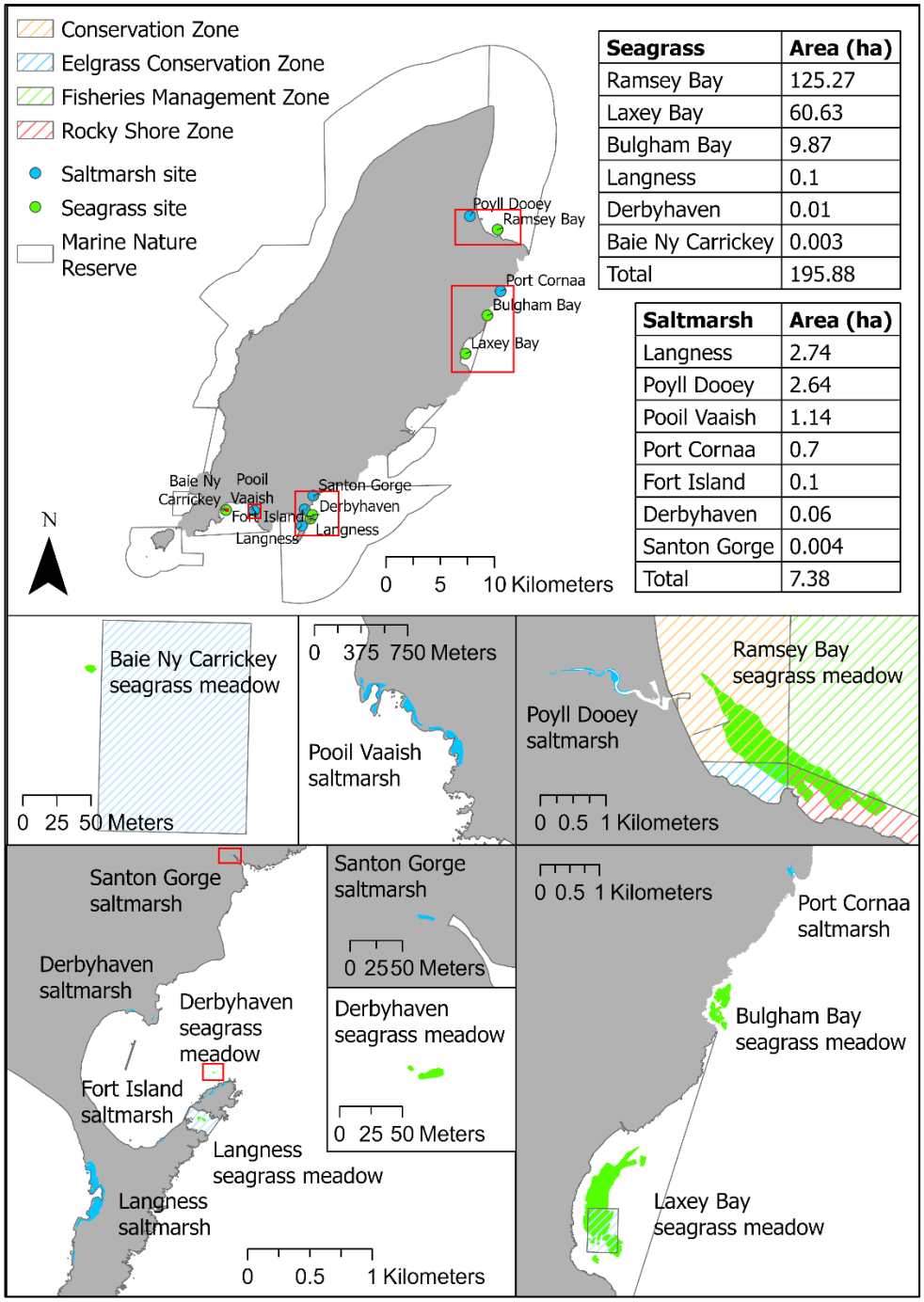

Seagrass	Area (ha)
Ramsey Bay	125.27
Laxey Bay	60.63
Bulgham Bay	9.87
Langness	0.1
Derbyhaven	0.01
Baie Ny Carrickey	0.003
Total	195.88

Saltmarsh	Area (ha)
Langness	2.74
Poyll Dooey	2.64
Pooil Vaaish	1.14
Port Cornaa	0.7
Fort Island	0.1
Derbyhaven	0.06
Santon Gorge	0.004
Total	7.38

Figure 4.2 Map of saltmarshes (blue dots and shade) and seagrass meadows (green dots and shade) around the Isle of Man (grey). Inset maps are highlighted by extent indicators (red) on the main map and for the smallest sites in the bottom left inset map. Tables of the saltmarsh and seagrass meadow extents (hectares) are included. Marine Nature Reserves (black outline) and Eelgrass Conservation Zones (hatched blue), as well as Ramsey Bay Conservation Zone (hatched orange), Fisheries Management Zone (hatched green), and Rocky Shore Zone (hatched red) are also shown.

Table 4.1 Seagrass meadow descriptions of surface sediments, seagrass canopy (cover and leaf length), and other observations, based on diver surveys by Manx Wildlife Trust (MWT) and Seasearch (unpublished), and drop-down (DD) video surveys (this study).

Seagrass meadow	Location	Surface sediment	Seagrass canopy	Observations	Source
Ramsey Bay	Whole meadow	Muddy sand, sand, and gravel, with occasional worm casts and ripples	<5% to 100%, a few cm to 30 cm	Occasional drift/unattached *Saccharina latissima* and kelp, brown leaf marks	This study (DD, 2023), MWT divers (unpublished, 2023 and 2024)
	Ramsey Pier	Not recorded	Canopy cover unknown, 25 cm to 60 cm	Seeds on leaves (common on smaller plants), drift/unattached red algae	MWT/Seasearch divers (2x unpublished, 2022)
Laxey Bay	South	Muddy sand and sandy mud, with occasional worm casts	<5% to 25%, length unknown	Dead shells	This study (DD, 2023)
Bulgham Bay	South	Muddy sand and sand	<5% to 50%, approx. 30 cm	Occasional rocky outcrop and gravel patches, developing seeds on some leaves	This study (DD, 2023), MWT divers (unpublished, 2021 and 2024)
Langness	Fort Island Gully	Mixed (sand and gravel with pebbles)	Canopy cover unknown, 35 cm to 40 cm	Occasional boulder with mixed seaweeds (incl. harpoon weed) and sea lace	MWT/Seasearch divers (2x unpublished, 2022)
Derbyhaven	Whole meadow	Sand and gravel, occasional worm casts	Canopy cover unknown, >60 cm	Rocky reef nearby, calcium deposit on older leaves, dead shells	MWT/Seasearch divers (7x unpublished, 2022)
Baie Ny Carrickey	Whole meadow	Sandy, gravelly, pebbly	"Patchy and sparse", <14 cm to 20 cm	Short and thin seagrass blades, clean, "little signs of blackening leaves", raised sediment under meadows, bedrock and kelp habitat on seaward site, exposed rhizomes	MWT divers (unpublished, 2024)

4.3.2 Sediment Properties

4.3.2.1 Saltmarshes

Sampling site locations for sediment coring are shown in Figure 4.3. Saltmarsh sediment core lengths ranged from 54 cm to 84 cm (Table 4.2) and saltmarsh sediment thickness ranged from 18 cm to ≥60 cm, with an average thickness of 39.6 cm (assuming a maximum of 60 cm) (Table 4.3). The plant communities varied from grasses (Sites S2C5, S7C1, SM13, SM16) to succulents (Site SM8) (Table 4.2; Appendix Figures C.11 and C.12). Classifying the saltmarsh vegetation species was outside the scope of this thesis, so reference to saltmarsh species and zones is based on vegetation classifications by Spencer (2005).

Four distinct sediment units were identified from sediment images and biogeochemical profiles for each core associated with saltmarsh and pre-saltmarsh intertidal mudflat or sandflat environments (Appendix Figures C.13–C.16). An example of the sediment core properties and radionuclide activities for Site SM8 are given in Figures 4.4 and 4.5, while figures for all other cores are given in Appendix C. The saltmarsh sediment layers included a fibrous peat layer in the uppermost sediment characterised by high OC content, dark colour, and fibrous texture with a high proportion of living roots; a humified peat layer below the surface characterised by generally declining OC content, lighter coloured sediment, and decomposing organic matter; and a transitional layer below characterised by lower OC content, lighter coloured sediment sometimes with iron staining, and minimal vegetation. These layers are collectively referred to as saltmarsh in this study and are used for OC stock calculations. The basal pre-saltmarsh intertidal layer was characterised by low OC content relative to the overlaying saltmarsh, generally lighter coloured sediment, more marine character (more positive $\delta^{13}C$), and minimal or no vegetation.

The $\delta^{13}C_{org}$ values increased with sediment depth, ranging from approximately -28 ‰ to -29 ‰ in the saltmarsh layers (excluding an outlier at 50–60 cm at Site S7C1, which had a value of -32.04 ‰), compared to approximately -27 ‰ in the basal layers (Table 4.3; Appendix Figures C.13–C.16). The $\delta^{13}C_{org}$ values were more negative in Port Cornaa saltmarsh sediments than in Poyll Dooey.

Sediments were classified as muddy sand and sandy mud throughout Port Cornaa saltmarsh layers, with all sediments ≤1000 μm (Table 4.3; Appendix Table C.2). The top 2 cm of sediments had a notably higher proportion of sand (>80%) than deeper sediments (44–56%). Sediments were also classified as muddy sand and sandy mud throughout the Poyll Dooey saltmarsh layers at Sites S7C1 and SM8. The sandy mud sediments corresponded to the thickest saltmarsh sediments situated in the low–mid marsh (Site S7C1), high marsh (Site S2C5), and pioneer marsh (Site SM8) zones (Figure 4.3). Meanwhile, saltmarsh sediments were only classified as muddy sand for Sites SM13 and SM16, corresponding with the shallowest saltmarsh cores situated in the low-mid marsh (Site SM13) and a narrow band of high marsh (Site SM16). The top of the basal sediments was classified as muddy sand for the low-mid marsh (Site SM13) and the narrow band of high marsh (Site SM16), with bands of unclassified coarser sediments. Unclassified sediments had >1% of particles >1000 μm, amounting to around 4% for Sites S7C1, SM8, and SM13, and 6%–64% for Site SM16.

The DBDs increased with sediment depth, despite the constant sediment type in Port Cornaa saltmarsh and finer sediments with depth into Poyll Dooey saltmarsh, reflecting sediment compaction (Table 4.3; Figure 4.4; Appendix Figures C.13–C.16). DBDs were higher for sediments sampled from Poyll Dooey compared to Port Cornaa. In Poyll Dooey saltmarsh, DBDs were highest for low–mid marsh (Site SM13) sediments, followed by high marsh (Site SM16) sediments, and lowest for pioneer marsh (Site SM8) sediments at Poyll Dooey sampled in August 2023 (Figure 4.3). DBDs were higher for high marsh (Site SM16) sediments from Poyll Dooey compared to Port Cornaa.

Despite having the highest OC concentrations in the fibrous peat layer, high marsh (Site S2C5) and low–mid marsh (Site S7C1) communities had among the lowest SCDs due to their low DBDs (Table 4.3; Appendix Figures C.13–C.16). Meanwhile, low–mid marsh (Site SM13) and pioneer marsh (Site SM8), as well as the narrow band of high marsh (Site SM16) had among the highest SCDs in the fibrous peat layers, despite having the lowest OC concentrations (Figure 4.3). As DBD increased below the fibrous peat layers, the high marsh (Sites S2C5) and low–mid marsh (Site S7C1), with the lowest DBDs and highest OC concentrations had the highest SCDs, while the low–mid marsh (Site SM13) and pioneer marsh (Site SM8), as well as the

narrow band of high marsh (Site SM16) had the lowest SCDs. Overall, SCD was highest in the core sampled from Port Cornaa saltmarsh compared to all cores sampled from Poyll Dooey saltmarsh. Negative SCD values for deeper sediment at Site SM13 were caused by OC concentrations at the limit of detection for the elemental analyser, which are effectively zero.

The average OC stock estimated in Isle of Man saltmarsh sediments (fibrous peat, humified peat, and transitional, ranging from 18 cm to ≥60 cm thick) was 94.14 ± 62.51 MgC ha^{-1}, ranging from 26.16 MgC ha^{-1} to 161.25 MgC ha^{-1} (Table 4.3). This equates to 694.78 ± 461.38 MgC, ranging from 193.10 MgC to 1190.04 MgC for the full extent of Isle of Man saltmarshes (7.38 ha). The average OC stock estimated in the top 10 cm of Isle of Man saltmarsh sediments, corresponding to peat layers, was 22.96 ± 4.62 MgC ha^{-1} over the 5 sediment cores, ranging from 15.93 MgC ha^{-1} in Port Cornaa (Site S2C5) to 27.58 MgC ha^{-1} in Poyll Dooey (Site S7C1) (Table 4.3). This equates to 169.47 ± 34.09 MgC, ranging from 117.53 MgC to 203.57 MgC for the full extent of Isle of Man saltmarshes (7.38 ha).

The average sedimentation rates estimated for Port Cornaa and Poyll Dooey saltmarshes were 0.82 ± 0.02 cm yr^{-1} and 0.31 ± 0.03 cm yr^{-1}, respectively (Table 4.4; Figure 4.5; Appendix Figures C.17–C.19). Data were unavailable for Site SM13. Port Cornaa saltmarsh was thus established pre-1946, but initial colonisation is undetermined as basal layers were not reached (Table 4.3). Meanwhile, the broad section of Poyll Dooey saltmarsh was estimated to have been established in the 1800's, with the inner section (Site S7C1) being dated older dated from 1814 compared to the sediment nearer the riverbank (Site SM8) dated from 1887. The narrow band of low marsh (Site SM16) was significantly younger as it was estimated to have been established in 1950. Unfortunately, the high marsh zone (Site SM13) could not be dated. The average OCAR for Isle of Man saltmarshes was 107.96 ± 75.83 gC m^{-2} yr^{-1} (1.08 ± 0.76 MgC ha^{-1} yr^{-1}), based on four sediment cores (excl. Site SM13) (Table 4.3).

Table 4.2 Port Cornaa saltmarsh (Site S2C5) and Poyll Dooey saltmarsh (Sites S7C1, SM8, SM13, SM16) sampling site locations (latitude and longitude), sediment core length (cm), compaction correction factor, broad plant type, and vegetation community identified by Spencer (2005).

Site ID	Latitude	Longitude	Core length (cm)	Compaction correction factor	Broad plant type	Vegetation community
S2C5	54.2646	-4.3474	54	0.8267	Grass	*Juncetum (Juncus) maritimus* (SM16)
S7C1	54.3262	-4.3922	84	0.8162	Grass (and unvegetated mud)	*Puccinellia maratima* (SM13)
SM8	54.3264	-4.3920	67	0.9465	Succulent	*Salicornia europea* (SM8)
SM13	54.3261	-4.3928	65	0.9155	Grass (occasional flowers)	*Puccinellia maratima* (SM13)
SM16	54.3273	-4.3941	65	0.8540	Grass (occasional flowers)	*Junecitum (Juncus) maritimusi* (SM16)

Table 4.3 Saltmarsh sediment layer, sediment thickness (cm), $\delta^{13}C_{vPDB}$ (‰), sediment dry bulk density (DBD, g cm^{-3}), organic carbon (OC) concentration (%), sediment organic carbon density (SCD, gC cm^{-3}), OC stock (MgC ha^{-1}), OC accumulation rate (gC m^{-2} yr^{-1}), OC accumulation capacity (OCAC, MgC yr^{-1}), sediment date range, and Folk (1954) classification for sediment cores from Port Cornaa saltmarsh and Poyll Dooey saltmarsh as sandy mud (SM) and muddy sand (MS). All values have been corrected for compaction.

Site	Layer	Depth (cm)	$\delta^{13}C_{vPDB}$ (‰)	DBD (g cm^{-3})	OC (%)	SCD (gC cm^{-3})	OC (MgC ha^{-1})	OCAR (gC m^{-2} yr^{-1})	OCAC (MgC yr^{-1})	Date	Folk class
Port Cornaa (S2C5)	Top 10 cm	0–10	-29.93	0.11	15.16	0.02	15.93	129.99	9.59	2010–2022	SM–MS
	Saltmarsh	0–55	-29.30	0.33	11.88	0.03	161.25	218.82	16.15	≤1946–2022	SM–MS
	Peat (fibrous)	0–16	-29.73	0.16	13.90	0.02	32.02	163.35	12.06	2000–2022	SM–MS
	Peat (humified)	16–30	-29.68	0.35	10.50	0.04	50.45	286.58	21.15	1981–2000	SM–MS
	Transitional	30–55	-28.32	0.59	5.52	0.03	78.79	257.24	18.98	≤1946–1981	SM
Poyll Dooey (S7C1)	Top 10 cm	0–10	-28.42	0.26	10.97	0.03	27.58	82.92	6.12	1989–2022	SM–MS
	Saltmarsh	0–60	-28.14	0.53	7.64	0.03	143.46	77.59	5.73	1814–2022	SM–MS
	Peat (fibrous)	0–14	-28.21	0.24	12.50	0.03	40.35	86.63	6.39	1973–2022	SM–MS
	Peat (humified)	14–30	-27.81	0.44	6.39	0.03	42.87	81.45	6.01	1918–1973	SM (incl. >1000 μm)
	Transitional	30–60	-28.37	1.02	2.08	0.02	60.25	61.06	4.51	1814–1918	SM
	Basal	60–80	-27.34	1.40	0.53	0.01	14.94	22.46	1.66	1745–1814	N/A
Poyll Dooey (SM8)	Top 10 cm	0–10	N/A	0.62	4.00	0.02	24.21	83.86	6.19	1993–2022	SM–MS
	Saltmarsh	0–45	N/A	0.71	4.01	0.03	108.01	87.67	6.47	1887–2023	SM–MS
	Peat (fibrous)	0–10	N/A	0.62	4.00	0.02	24.21	83.86	6.19	1993–2023	SM–MS
	Peat (humified)	10–25	N/A	0.60	5.15	0.03	41.75	100.73	7.43	1947–1993	SM
	Transitional	25–45	N/A	0.98	2.31	0.02	42.05	72.84	5.38	1887–1947	SM (incl. >1000 μm)

	Basal	45–60	N/A	1.42	0.24	0.00	5.25	11.93	0.88	1842 – 1887	N/A
Poyll Dooey (SM13)	Top 10 cm	0–10	N/A	0.57	4.87	0.02	21.08	N/A	N/A	N/A	MS (incl. >1000 µm)
	Saltmarsh	0–20	N/A	0.79	2.71	0.01	26.17	N/A	N/A	N/A	MS (incl. >1000 µm)
	Peat (fibrous)	0–6	N/A	0.37	6.85	0.02	14.25	N/A	N/A	N/A	MS (incl. >1000 µm)
	Peat (humified)	6–12	N/A	0.90	1.74	0.02	9.45	N/A	N/A	N/A	MS
	Transitional	12–20	N/A	1.02	0.34	0.00	2.47	N/A	N/A	N/A	MS
	Basal	20–60	N/A	1.27	-0.12	-0.00	-5.98	N/A	N/A	N/A	SM–MS (incl. >1000 µm)
Poyll Dooey (SM16)	Top 10 cm	0–10	-28.67	0.47	6.00	0.03	26.02	70.25	5.18	1985–2022	MS (incl. >1000 µm)
	Saltmarsh	0–18	-28.17	0.69	3.68	0.02	31.84	47.76	3.52	1950–2023	MS (incl. >1000 µm)
	Peat (fibrous)	0–2	-29.13	0.40	10.68	0.04	8.61	116.21	8.58	2015–2023	MS
	Peat (humified)	2–10	-28.55	0.49	4.83	0.02	17.41	58.77	4.33	1983–2015	MS (incl. >1000 µm)
	Transitional	10–18	-27.56	0.96	0.78	0.01	5.82	19.63	1.45	1950–1983	MS
	Basal	18–45	-27.53	1.18	0.65	0.01	21.06	19.88	1.47	1841–1950	MS (incl. >1000 µm)
All	Top 10 cm	0–10	-29.01 ± 0.81	0.41 ± 0.22	8.20 ± 4.74	0.02 ± 0.01	22.96 ± 4.62	91.76 ± 13.42	6.77 ± 1.94	N/A	N/A
	Saltmarsh	0–18 to 0–≥60	-28.54 ± 0.66	0.61 ± 0.18	5.98 ± 3.79	0.02 ± 0.01	94.14 ± 62.51	107.96 ± 75.83	7.97 ± 5.60	N/A	N/A

Table 4.4 Average sedimentation rate ± standard deviation, estimated from ^{137}Cs radioisotope data, attributed to Chernobyl and Sellafield discharges.

Location	Site ID	Chernobyl sedimentation rate (cm yr^{-1})	Sellafield sedimentation rate (cm yr^{-1})	Average sedimentation rate (cm yr^{-1})
Port Cornaa	S2C5	0.83	0.80	0.82 ± 0.02
Poyll Dooey	S7C1	0.30	0.30	0.30 ± 0.00
Poyll Dooey	SM8	0.37	0.33	0.35 ± 0.03
Poyll Dooey	SM16	0.23	0.31	0.27 ± 0.06
Average Poyll Dooey		0.30	0.31	0.31 ± 0.03

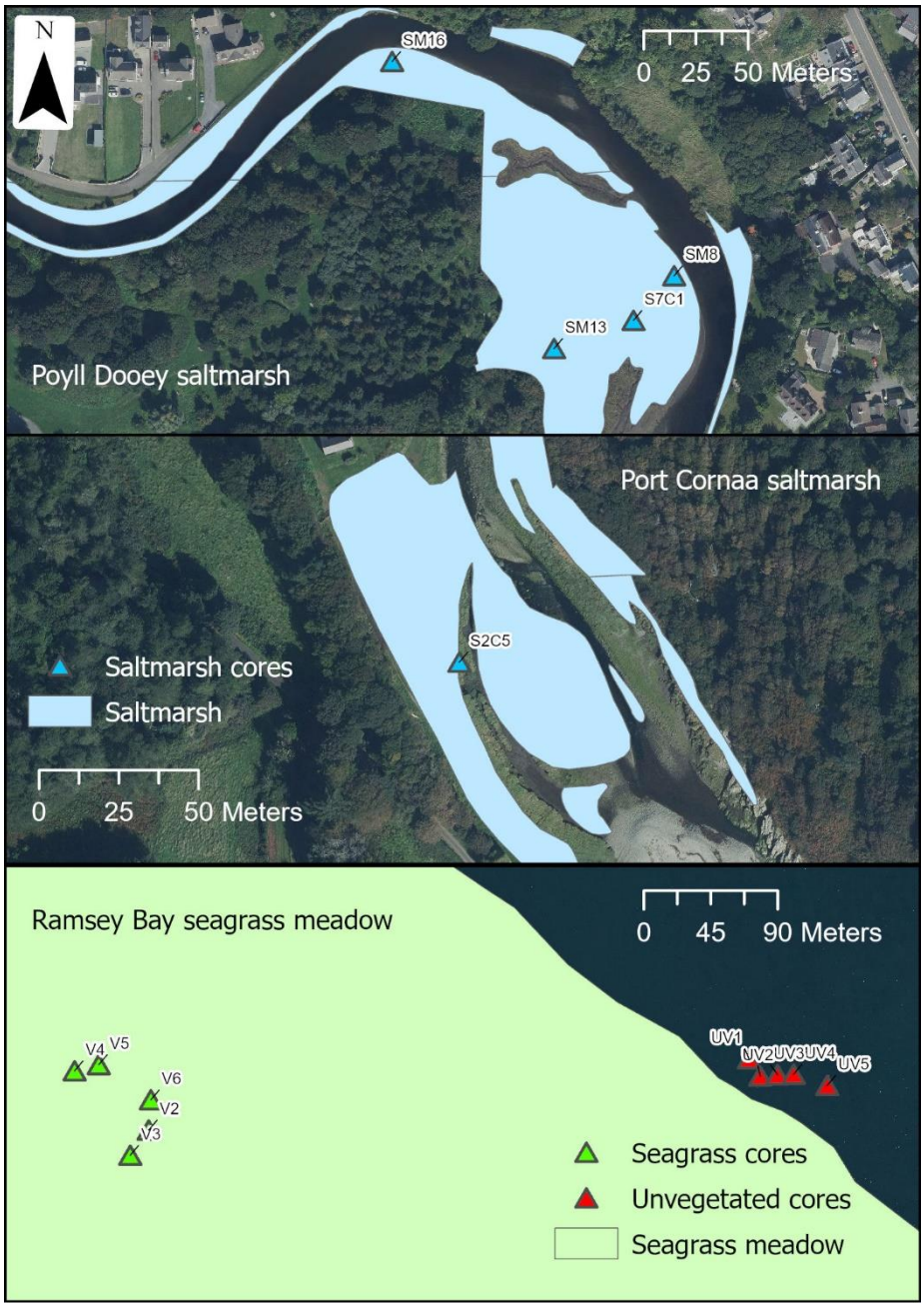

Figure 4.3 Sediment coring locations in Poyll Dooey saltmarsh, Port Cornaa saltmarsh, and Ramsey Bay seagrass meadow and unvegetated sediments.

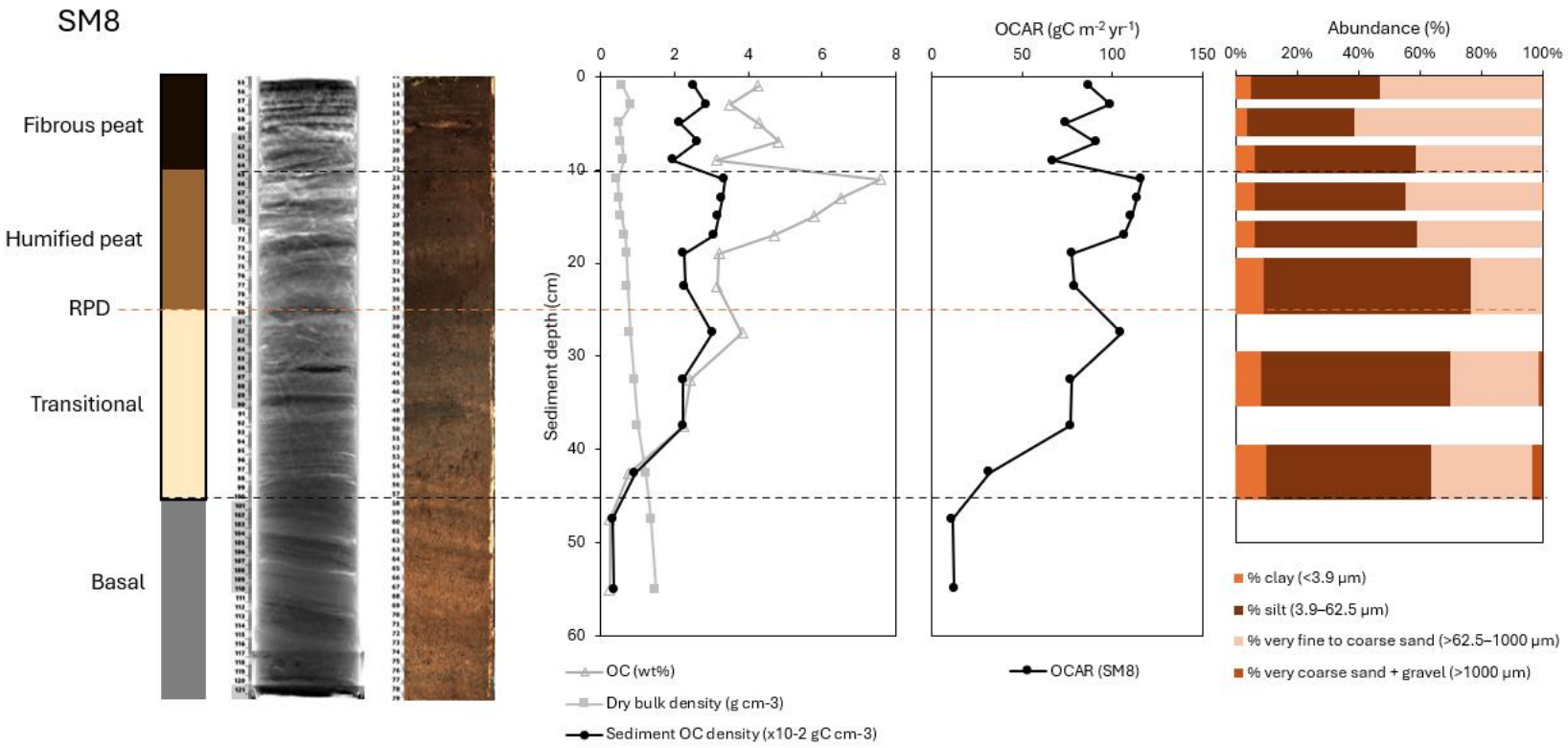

Figure 4.4 Sediment core depth profiles for saltmarsh Site SM8. Left to right: Sediment layer graphic based on data, X-ray radiograph image, high-resolution surface image, root penetration depth (RPD, dashed orange line), organic carbon (OC) concentration (%), sediment dry bulk density (DBD, g cm^{-3}), sediment organic carbon density (SCD, gC cm^{-3}), OC accumulation rate (OCAR, gC m^{-2} yr^{-1}), and sediment grain size fractions.

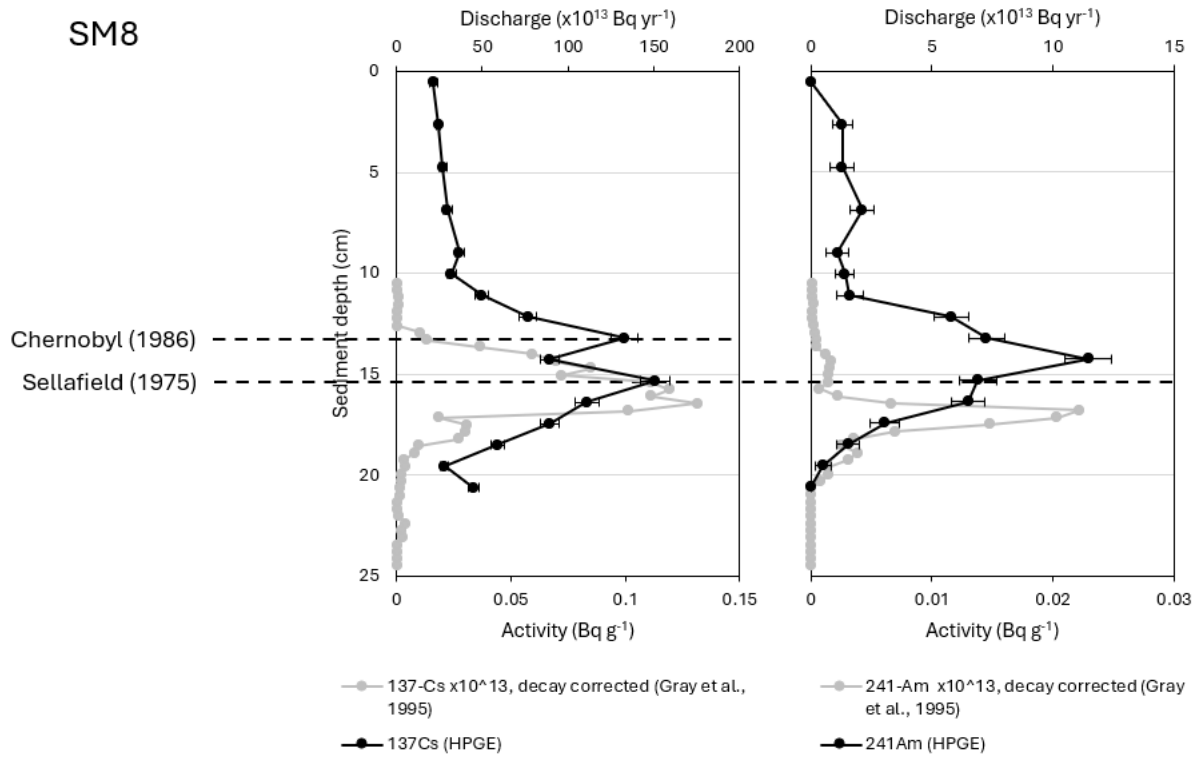

Figure 4.5 Radionuclide profiles for saltmarsh Site SM8. Left to right: ^{137}Cs activities (black, lower axis) and ^{137}Cs discharge profile from Sellafield nuclear facility (grey, upper axis) with the average sedimentation rate applied; ^{241}Am activities (black, lower axis) and ^{241}Am discharge profile from Sellafield nuclear facility (grey, upper axis) with the average sedimentation rate applied.

4.3.2.2 Ramsey Bay Seagrass Meadow

Sampling site locations for sediment coring are shown in Figure 4.3. Sediment cores from Ramsey Bay seagrass meadow varied in length from 37 cm to 49 cm, while unvegetated sediment cores varied from 10 cm to 33 cm (Table 4.5). In the seagrass meadow, *Z. marina* cover was patchy and medium to dense on sandy substrate (Table 4.5; Figure 4.6). Meanwhile, seagrass was not observed in the unvegetated region (Appendix Figure C.20).

Seagrass sediments were classified as sand at all sediment depths, with very fine to coarse sand content ≥99% and mud content ≤5% for most cores (Appendix Table C.3). This excluded sediment layers which were unclassified due to having >1 % of particles >1000 μm, ranging from 1.83% in a slightly coarser layer in Site V3 to 46.14% in a gravel layer at Site V6. Very coarse sand or gravel layers with particles ≥1000 μm were present in all sediment cores at around 15–20 cm sediment depth. Unvegetated sediments were mostly unclassified due to having >1 % of particles >1000 μm, ranging from 1.40% to 62.84% due to the presence of gravel layers (Appendix Table C.4).

Seagrass sediments were bioturbated in the top 5–15 cm, as observed by high-contrast burrow features in the X-ray radiograph images and as darker sediments in the high-resolution images. An example of the sediment core properties and radionuclide activities for Site V5 is given in Figure 4.7, while figures for all other sites are given in Appendix C (Figures C.21–C.24). These areas were considered the surface sediment mixed layer (SML) and corresponded with root penetration depths (RPDs) of 12–16 cm. Rhizomes were also present within the upper 5 cm of the southeast-most sites (Sites V2, V3, V6) (Figure 4.3). Unvegetated sediments were less bioturbated than seagrass meadows in approximately the top 10 cm (Appendix Figures C.25–C.28).

Seagrass sediment DBDs were comparable for most sites and fluctuated with sediment depth (Table 4.6; Figure 4.7; Appendix Figures C.21–C.24). However, Site V3 had notably lower DBD overall, with dark sediments and dense razor shells at 10–25 cm, followed by laminated sediment layers below 25 cm, corresponding to a change in sedimentary environment. DBD was anomalously low at 18–20 cm for Site V4 as a complete sediment sample could not be excavated due to the presence of a

stone that had a larger diameter than the width of the U-channel used for subsampling. Unvegetated sediment DBDs were relatively stable with sediment depth, excluding in the coarse sediment layer of Site UV3, but varied between sediment cores, whereby Sites UV2 and UV3 were notably denser than Sites UV1, UV4, and UV5 (Table 4.6). An example of the sediment core properties and radionuclide activities for Site UV3 is given in Figure 4.8, while figures for all other cores are given in Appendix C (Figures C.25–C.28).

Seagrass sediment OC content and SCD was highest in the SML, with slightly lower values in the paler surface sediments at <4 cm compared with darker sediments at 4–10 cm (Table 4.6; Appendix Figures C.21–C.24). OC content decreased through the SML and stabilised below the RPD. The $\delta^{13}C_{org}$ values fluctuated around –22 ‰ to –23 ‰ in the SML and were more negative at around –23 ‰ to –25 ‰ below the RPD, indicating a change in sedimentary environment and potentially more marine character. In contrast, OC content and SCDs increased with sediment depth (excluding in gravel layers) in unvegetated sediments, while $\delta^{13}C_{org}$ values fluctuated around –20 ‰ to –24 ‰ (Table 4.6; Appendix Figures C.25–C.28).

The average OC stock in the top 10 cm of seagrass sediments was 1.33 ± 0.25 MgC ha^{-1}, ranging from 1.13 MgC ha^{-1} to 1.74 MgC ha^{-1} over the 5 sediment cores (Table 4.6). This corresponds to 261.10 ± 49.08 MgC, ranging from 222.22 MgC to 340.99 MgC for the full extent of Isle of Man seagrass meadows (195.88 ha). Meanwhile, the average OC stock at a sediment depth of 20–30 cm, below the SMLs and RPDs, was 0.56 ± 0.28 MgC ha^{-1}, ranging from 0.17 MgC ha^{-1} to 0.95 MgC ha^{-1} over the 5 sediment cores (Table 4.6). This equated to 109.94 ± 54.18 MgC, ranging from 34.03 MgC to 186.18 MgC for the full extent of Isle of Man seagrass meadows. Based on these results, the OCBE of the seagrass meadow is estimated to be 44.08% ± 21.47%, ranging from 15.03% to 74.42%. Furthermore, the average OC stock in the top 30 cm of seagrass sediments was 2.67 ± 0.83 MgC ha^{-1}, ranging from 1.93 MgC ha^{-1} to 3.65 MgC ha^{-1}. This equated to 523.00 ± 162.58 MgC, ranging from 378.05 MgC to 714.96 MgC for the full extent of Isle of Man seagrass meadows (195.88 ha). Comparably, the average OC stock in the top 10 cm of unvegetated sediments was 0.93 ± 0.86 MgC ha^{-1}, ranging from 0.20 MgC ha^{-1} to 2.34 MgC ha^{-1}(Table 4.6).

Sedimentation rates and therefore OC accumulation rates could not be estimated for the seagrass meadow, as radionuclide activities did not have notable peaks in the ^{137}Cs or ^{241}Am activity depth profiles, or significant decay of the excess ^{210}Pb activities (Appendix Figures C.21–C.24). The fluctuation in radionuclide activity observed with sediment depth in the seagrass meadows likely corresponds with changes in sediment composition, particularly changes in the finer particle fractions which have a higher affinity for radionuclides, rather than changes in Sellafield nuclear facility discharges over time.

Table 4.5 Ramsey Bay seagrass sampling site location (latitude and longitude), sediment core length (cm), compaction correction factor, and root penetration depth (RPD, cm), surface substrate recorded during diver surveys, and seagrass canopy cover estimated from photoquadrat analysis.

Study site ID	Latitude	Longitude	Core length (cm)	Compaction correction factor	RPD (cm)	Surface substrate	Canopy cover (%)
V2	54.3156	-4.3546	46	0.9492	16	Sand	81.88 ± 1.25
V3	54.3155	-4.3548	37	0.7979	12	Sand	95.83 ± 0.95
V4	54.3160	-4.3554	45	1.0000	12	Sand, Shingle	100 ± 0.00
V5	54.3160	-4.3551	46	1.0000	16	N/A	62.92 ± 3.21
V6	54.3158	-4.3546	49	0.9643	16	Sand, Gravel	97.19 ± 0.63
UV1	54.3161	-4.3484	14	0.4141	N/A	Pebbles, rock, sand	N/A
UV2	54.3160	-4.3483	33	0.9167	N/A	Sand	N/A
UV3	54.3160	-4.3481	28	0.9474	N/A	Sand, clay	N/A
UV4	54.3160	-4.3479	10	0.2487	N/A	Sand	N/A
UV5	54.3160	-4.3476	18	0.3067	N/A	Silty sand	N/A

Table 4.6 Ramsey Bay seagrass meadow and adjacent unvegetated sediment properties, including sediment depth (cm), $\delta^{13}C_{vPDB}$ (‰), sediment dry bulk density (DBD, g cm^{-3}), organic carbon (OC) concentration (%), sediment organic carbon density (SCD, gC cm^{-3}), OC stock (MgC ha^{-1}), and OC burial efficiency (%). Values have been corrected for sediment compaction.

Site ID	Depth (cm)	$\delta^{13}C_{vPDB}$ (‰)	DBD (g cm^{-3})	OC (%)	SCD (x10^{-3} gC cm^{-3})	OC stock (MgC ha^{-1})	OCBE (%)
V2	0–10	-22.88	1.62	0.11	1.74	1.74	39.42
	20–30	N/A	1.42	0.04	0.61	0.61	
	0–30	N/A	1.59	0.08	1.30	3.49	
V3	0–10	-22.40	1.32	0.09	1.15	1.15	15.03
	20–30	-24.21	1.31	0.01	0.17	0.17	
	0–30	-23.23	1.31	0.06	0.76	1.93	
V4	0–10	-22.86	1.77	0.07	1.24	1.24	40.68
	20–30	-23.67	1.85	0.03	0.54	0.54	
	0–30	-23.41	1.73	0.05	0.80	2.24	
V5	0–10	N/A	1.80	0.06	1.13	1.14	50.88
	20–30	N/A	1.64	0.03	0.53	0.53	
	0–30	N/A	1.74	0.04	0.71	2.03	
V6	0–10	-22.41	1.70	0.08	1.40	1.40	74.42
	20–30	-23.69	1.53	0.06	0.95	0.95	
	0–30	-23.15	1.61	0.08	1.28	3.65	
Average	0–10	-22.64 ± 0.27	1.64 ± 0.19	0.08 ± 0.02	1.33 ± 0.25	1.33 ± 0.25	44.08 ± 21.47
	20–30	-23.86 ± 0.31	1.55 ± 0.21	0.04 ± 0.02	0.56 ± 0.28	0.56 ± 0.28	
	0–30	-23.16 ± 0.23	1.59 ± 0.17	0.06 ± 0.02	0.97 ± 0.29	2.67 ± 0.83	
UV1	0–10	N/A	0.72	0.08	0.60	0.60	N/A
UV2	0–10	-23.68	1.61	0.07	1.12	1.12	N/A
UV3	0–10	-23.31	1.89	0.12	2.34	2.34	N/A
UV4	0–10	-23.11	0.44	0.06	0.26	0.20	N/A

UV5	0–10	-23.44	0.56	0.07	0.40	0.40	N/A
Average	0–10	-23.38 ± 0.24	1.04 ± 0.66	0.08 ± 0.02	0.94 ± 0.85	0.93 ± 0.86	N/A

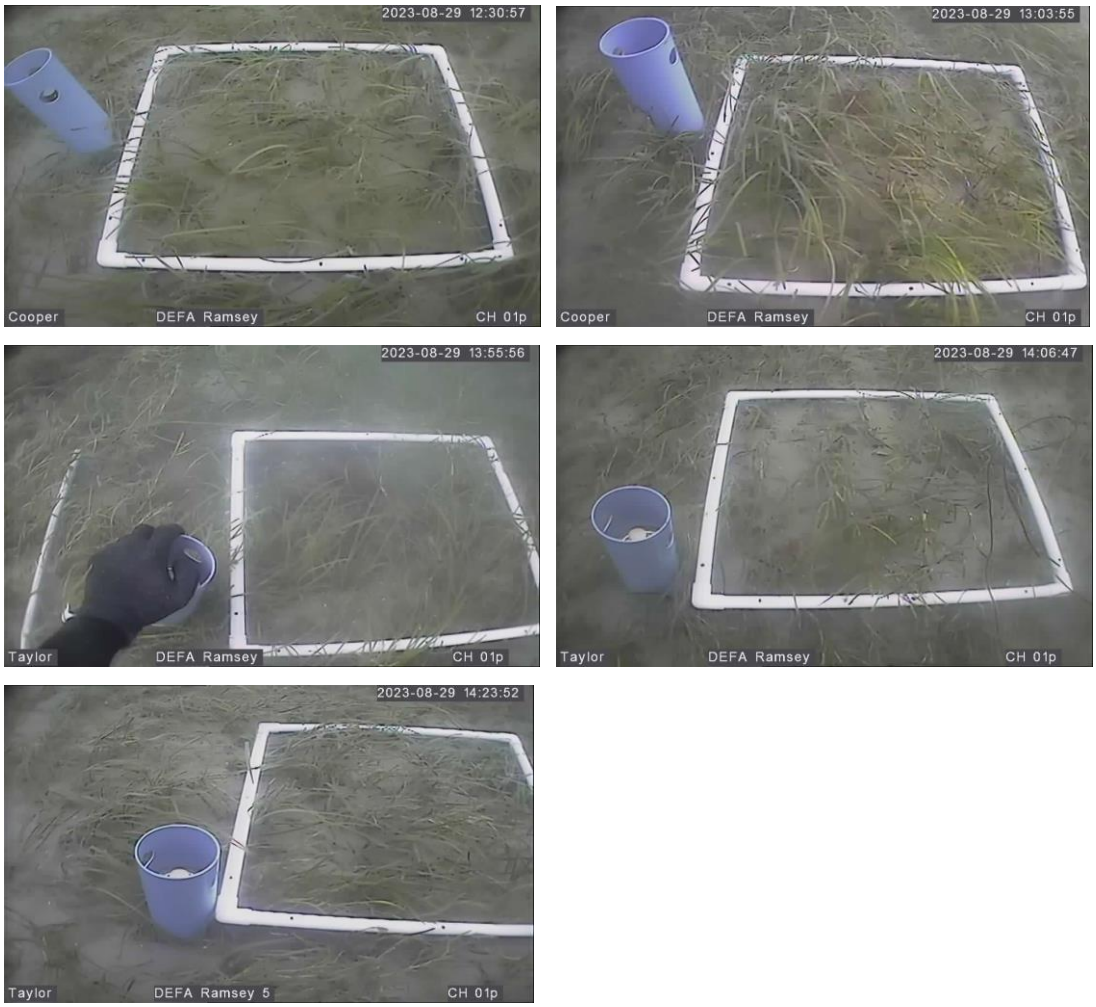

Figure 4.6 Core 1 (V2) (top left), Core 2 (V3) (top right), Core 3 (V4) (centre left), Core 4 (V5) (centre right), Core 5 (V6) (bottom left). Photo credit: Isle of Man Government Divers.

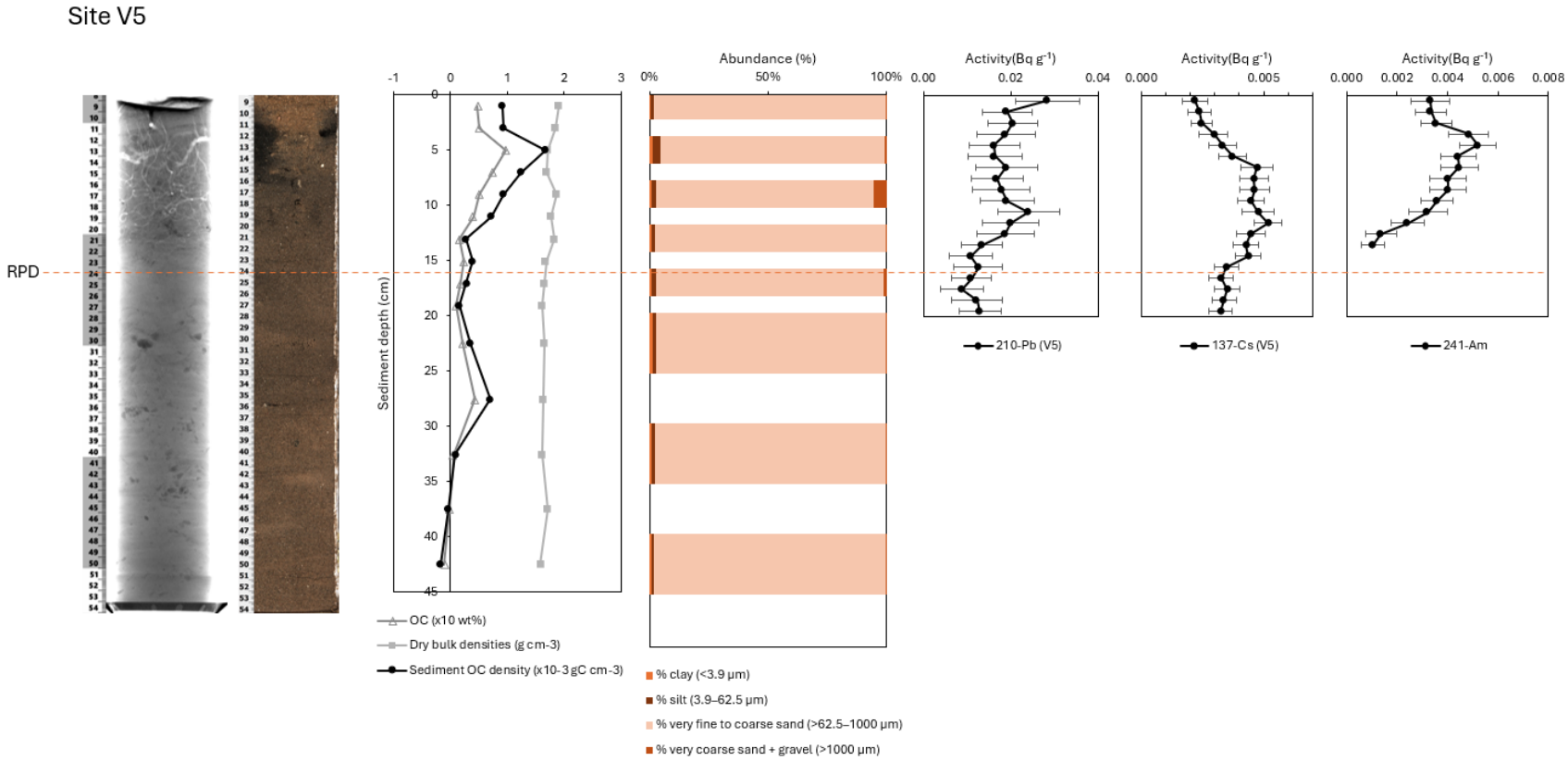

Figure 4.7 Sediment core depth profiles for seagrass meadow sediments from Site V5. Left to right: X-ray radiograph image, high-resolution surface image, root penetration depth (RPD, dashed orange line), organic carbon (OC) concentration (%), sediment dry bulk density (DBD, g cm^{-3}), sediment organic carbon density (SCD, gC cm^{-3}), sediment grain size fractions, and radionuclide profiles for ^{210}Pb, ^{137}Cs, and ^{241}Am.

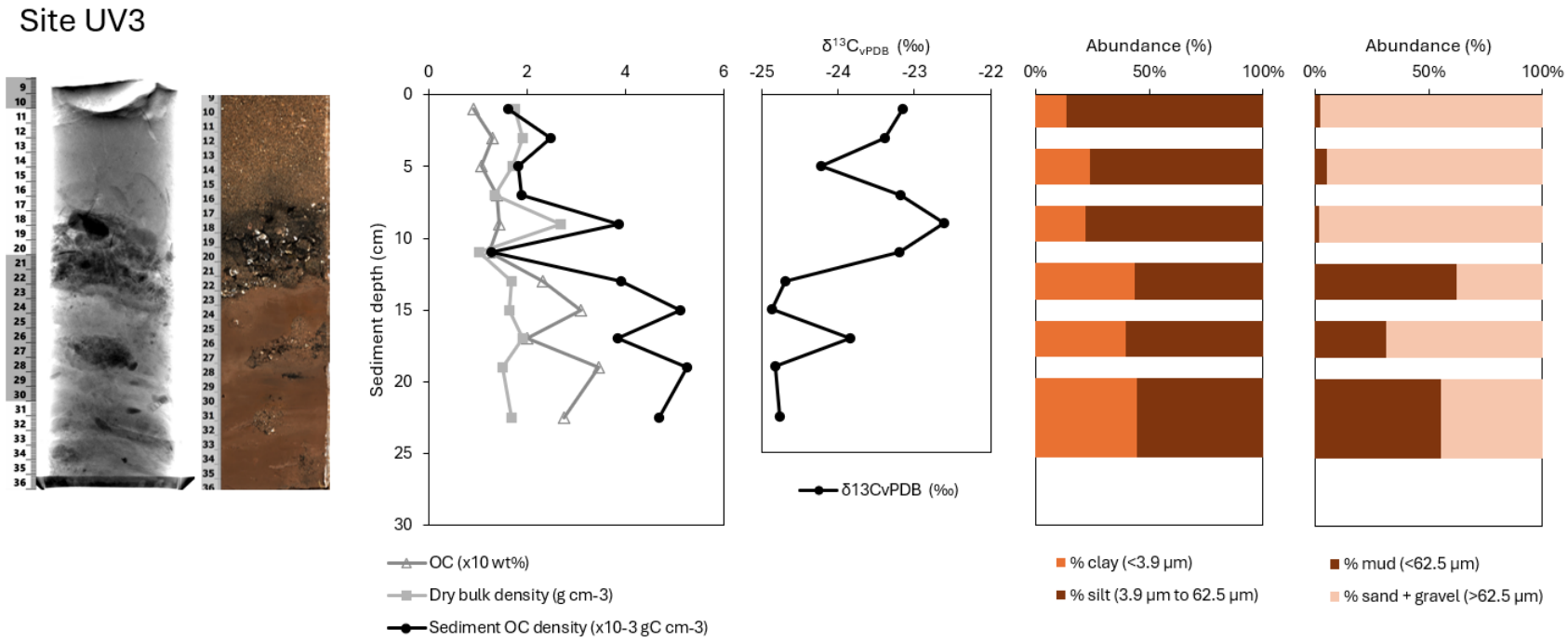

Figure 4.8 Sediment core depth profiles for unvegetated sediments adjacent to the seagrass meadow from Site UV3. Left to right: X-ray radiograph image, high-resolution surface image, organic carbon (OC) concentration (%), sediment dry bulk density (DBD, g cm^{-3}), sediment organic carbon density (SCD, gC cm^{-3}), $\delta^{13}C_{vPDB}$ (‰), and sediment grain size fractions.

4.4 Discussion

4.4.1 Saltmarshes

Upscaling OC stocks and accumulation from Poyll Dooey and Port Cornaa saltmarshes estimates that Isle of Man saltmarshes (7.38 ha) store 694.78 ± 461.34 MgC (94.14 ± 62.51 MgC ha^{-1}) and accumulate 7.97 ± 5.60 MgC annually at a rate of 107.96 ± 75.83 gC m^{-2} yr^{-1}, over an average sediment thickness of 39.6 cm. These OC stocks align with recent estimates for global saltmarshes (79.2 ± 38.1 MgC ha^{-1} in the top 30 cm) (Maxwell et al., 2023) and OC accumulation rates align with Northern European saltmarshes, including in Great Britain (110.88 ± 43.12 gC m^{-2} yr^{-1}) (Smeaton et al., 2024), Denmark (31.5 gC m^{-2} yr^{-1}, and 58 MgC ha^{-1} to 71 MgC ha^{-1} in the top 30 to 50 cm) (Leiva-Dueñas et al., 2024), and Germany (112–149 gC m^{-2} yr^{-1}) (Mueller et al., 2019).

The OCARs and OC stocks exhibited temporal variability within the sediment cores, whereby higher values in younger peat layers declined towards a steady state in older basal sediments. These findings likely reflect greater OC accumulation in vegetated saltmarshes compared to pre-saltmarsh tidal flats, and post-depositional OC degradation and remineralisation (Gore et al., 2024; Mueller et al., 2019). However, uncertainty in OCAR and OC stock estimates could vary with sediment depth in stratigraphically complex sediments such as the saltmarsh sediments in this study, as hammer coring can compress sediment layers differently, which can affect sedimentation rate estimates and sediment DBDs (Smeaton et al., 2020). Therefore, while the comparison of OCARs and OC stocks in different sediment layers is useful for understanding temporal changes in these saltmarshes, the variability between OCARs and OC stocks in different layers may be larger or smaller than estimated herein, due to this uncertainty.

Spatial variations in OCARs (47.76 gC m^{-2} yr^{-1} to 218.82 gC m^{-2} yr^{-1}) and OC stocks (26.16 MgC ha^{-1} to 161.25 MgC ha^{-1}) reflect changes in sediment accumulation and OC preservation between and within saltmarshes (Ladd et al., 2019). In Poyll Dooey saltmarsh, the older, finer, thicker sediment deposits are situated in salt-tolerant pioneer and low-mid marsh zones with higher OC stocks, reflecting prolonged OC accumulation and enhanced OC preservation associated

with minerogenic binding and limited oxygen exposure (Kelleway et al., 2016). Saltmarsh channels in this region absorb tidal energy and enable flooding and drainage of the marsh (Cornacchia et al., 2024; Puppin et al., 2024; Spencer, 2005), which facilitates sediment transport and settling under lower hydrodynamic energy (Smeaton et al., 2024). Conversely, younger, coarser, thinner sediments are situated in low-mid and high marsh zones with lower OC stocks, reflecting limited fine sediment deposition along the inner bend of the Sulby River, which likely experiences higher hydrodynamic energy and limited tidal inundation with distance from the riverbank (Puppin et al., 2024). A gravel layer at approximately 40 cm depth in high marsh sediments (Site SM16) potentially reflects an irregular high-energy event.

Hydrodynamic energy appears to have a notable influence on OC storage, as sedimentation rates are higher and sediments are finer at the centre of Port Cornaa (0.82 ± 0.02 cm yr^{-1} (this study)) compared to at the edges (0.46 cm yr^{-1} (0–25 cm, ≤44 years) and 0.32 cm yr^{-1} (25–70 cm, 44–≥141 years) (Croudace et al., 2019)). In the broad saltmarsh section, tidal velocities are likely reduced by the saltmarsh vegetation, which can facilitate fine particle settling, whereas at the saltmarsh edge, higher river velocity likely increases sediment erosion (Puppin et al., 2024). Increasing sedimentation rates observed over time by Croudace et al. (2019) may be linked to riverbank stabilisation that was carried out using rock and soil layers to preserve the saltmarsh and promote recolonisation, and cessation of livestock grazing in the 1960s, which could have reduced sediment compaction at the marsh edge (Spencer, 2005).

Sediment supply and geomorphology can significantly impact OC stocks and accumulation (Smeaton, 2024). Port Cornaa exhibited higher OC concentrations and OCARs than Poyll Dooey, which could be attributed to its location as a lagoonal saltmarsh behind a semi-protective shingle bank. This may slow tidal flow and reduce wave erosion, enhancing fine particle settling and leading to higher sedimentation rates (0.82 ± 0.02 cm yr^{-1}) compared to Poyll Dooey (0.31 ± 0.03 cm yr^{-1}), which is situated along river meanders. Frequent tidal inundation in Port Cornaa could facilitate sediment trapping and OC accumulation, leading to enhanced OC preservation. Increased sedimentation in recent decades in Port Cornaa saltmarsh could also result from agricultural expansion upstream, which can mobilise sediment

(Croudace et al., 2019). Historic alterations like landfill conversion and building of a stone wall upstream may have also impacted sedimentation dynamics and OC sequestration over time in Poyll Dooey saltmarsh.

Sediment accretion of approximately 5–7 cm based on sediment accumulation rates 0.27–0.35 cm yr^{-1} over 20 years, combined with land-use changes (e.g. agriculture, grazing on saltmarshes, building walls, etc.), could have changed the plant communities identified by Spencer (2005) around 20 years ago. Changes in plant communities are likely to have influenced sediment OC stocks, through changes in autochthonous OC (saltmarsh plant biomass) and trapping of allochthonous OC (Miller et al., 2023; Penk and Perrin, 2022). Future work could re-classify saltmarsh vegetation to improve understanding of the influence of plant communities on sedimentary OC stocks, which have previously been shown to have a significant effect (Ford et al., 2019).

Enhanced OC stocks in Port Cornaa saltmarsh could also be due to greater allochthonous inputs from upstream broadleaf woodland (Spencer, 2005) and autochthonous marine inputs like macroalgae (Miller et al., 2023). Whereas Poyll Dooey, located further inland, may receive more terrestrial OC inputs from agricultural lands and lower marine contributions. However, minor differences in $\delta^{13}C$ values between Poyll Dooey (-28.1 ‰) and Port Cornaa (-29.3 ‰) indicate a similar balance of terrestrial and marine OC inputs. Meanwhile, depleted $\delta^{13}C$ with sediment depth suggests a greater marine influence at both sites in the pre-saltmarsh tidal flats.

4.4.2 Seagrass Meadows

Seagrass OC stocks in Ramsey Bay (2.67 ± 0.83 MgC ha^{-1}, 0–30 cm) are among the lowest recorded for *Z. marina* meadows in northern temperate regions. These low OC stocks are comparable to other exposed seagrass meadows in the Baltic Sea (5.78 MgC ha^{-1}, 0–25 cm) (Röhr et al., 2018), but lower than other temperate seagrass meadows in the Eastern Atlantic (13.84 MgC ha^{-1}, 0–25 cm) (Röhr et al., 2018), Southwest of England (41.54 MgC ha^{-1}, 0–30 cm) (Green et al., 2018), and in the sheltered Skagerrak and Swedish west coast (10.54–39.65 MgC ha^{-1}, 0–30 cm)

(Dahl et al., 2020a,b). Despite this, seagrass meadows in the Isle of Man store approximately 35% more OC (261.10 ± 49.08 MgC) in surface (top 10 cm) sediments compared to saltmarshes (169.47 ± 34.09 MgC), due to their significantly larger area (195.88 ha vs. 7.38 ha).

The relatively low OC densities in Ramsey Bay could be attributed to the high hydrodynamic energy in the Irish Sea, which is reflected in the sandy sediments and low mud content in the seagrass meadow, potentially limiting OC preservation (Dahl et al., 2016; Röhr et al., 2018). The exposed Manx coastline causes high sediment mixing, which was observed in radionuclide profiles, which can lead to sediment resuspension, and enhanced OC degradation and export (Röhr et al., 2018). Furthermore, the Ramsey Bay seagrass meadow is fragmented and patchy with varying biomass cover, from a few plants (<5%) to dense meadow (100%), which could reduce sediment trapping compared to continuous dense meadows (Potouroglou et al., 2021; Oreska et al., 2017). The variable seagrass meadow canopy cover and leaf lengths, from a few cm to >60 cm in length, could also limit autochthonous OC inputs from seagrass biomass, compared to dense, highly productive meadows (Potouroglou et al., 2021). The variability of seagrass meadows around the Isle of Man, from the larger meadows in the north-east with sandy/muddy sediments, to the smaller exposed southern meadows with gravelly sediments and boulders (e.g. Baie Ny Carrickey), suggest that the OC storage may also vary spatially around the island. Proximity to OC sources (e.g. rivers, macroalgae forests, etc.) and anthropogenic inputs (sewage outflow, etc.) could also influence OC stocks within seagrass meadows (Potouroglou et al., 2021). Future work would be needed to assess OC stocks within all the islands seagrass meadows.

Nevertheless, the Ramsey Bay seagrass meadows store 43% more OC (1.33 MgC ha^{-1}) in the top 10 cm than nearby unvegetated sediments (0.93 MgC ha^{-1}), which aligns with findings from other temperate regions (Jankowska et al., 2016; Potouroglou et al., 2021). Although OC concentrations are similar in seagrass and unvegetated sediments (0.08% ± 0.02%), the denser sediments in seagrass meadows result in their higher OC stocks, which could reflect enhanced sediment stabilisation by seagrass meadow vegetation (Potouroglou et al., 2017, 2021). Furthermore, the comparable $\delta^{13}C$ values coupled with similar OC concentrations could indicate that these environments alternate between vegetated and unvegetated states, which is

plausible due to the proximity of the unvegetated sampling sites to the seagrass meadow edge. However, a lack of age-resolved data and historical monitoring of seagrass meadows limits this understanding. Further work to quantify OC stocks in unvegetated sediments situated further from the seagrass meadow edge and from different locations within the seagrass meadows could help resolve this.

Despite this, only 44% of OC accumulated in the top 10 cm of seagrass meadows is retained at depths of 20–30 cm (0.56 ± 0.28 MgC ha^{-1}), where it declines to levels comparable to the top 10 cm of unvegetated sediments. This suggests that seagrass may not have been established in the sampled region when deeper sediments were laid down or that OC degradation may reduce OC stocks over time. Hydrodynamic mixing and bioturbation, which were observed in the top 5–15 cm of sediments in both seagrass and unvegetated sediments, can accelerate microbial degradation and remineralisation of OC (O'Neill et al., 2024; Thomson et al., 2019). These results highlight challenges in quantifying long-term OC accumulation, particularly in the highly dynamic North Atlantic, as surface OC stocks may overestimate the long-term sequestration potential of seagrass meadows. Low radionuclide activities in reworked sediments inhibited sediment dating and the quantification of OC accumulation herein. The low sediment accumulation rates estimated elsewhere suggest that seagrass meadow loss and subsequent sediment resuspension could lead to loss of centuries of sediment and associated OC sequestration with limited scope for quick recovery (Dahl et al., 2023).

4.4.3 Implications for Blue Carbon Estimates

Spatial and temporal variations in sediment OC stocks in saltmarshes and seagrass meadows present challenges for extrapolating values for comparison with other studies. While the Intergovernmental Panel on Climate Change (IPCC) (Hamilton et al., 2023) recommends standardising OC stocks over 1 m for cross-study comparisons, our findings, along with others (Ladd et al., 2022; Miller et al., 2023), highlight the risks associated with this approach. Extrapolating shallow core data may overestimate long-term OC stocks, while retrieving full 1 m cores can include sediments laid down before saltmarsh or seagrass meadow colonisation, which do not reflect OC storage by BCEs. Considering these issues, OC stocks herein were

reported to the true depth of saltmarsh sediments, though values could be extrapolated for international reporting if necessary. Similarly, seagrass OC stocks were reported for the top 10 cm and top 30 cm of sediments, for comparison between BCEs and with other studies, and were not extrapolated to 1 m. Doing so could misrepresent long-term storage, especially considering the observed sediment variability with depth, including gravel and shell layers, which indicate past environmental changes.

4.4.4 Future Actions

While the overall extent of saltmarshes (7.38 ha) and seagrass meadows (195.88 ha) are equivalent to only 0.01% of the Isle of Man landmass (57,200 ha) and 0.05% of the Isle of Man territorial sea (400,000 ha), respectively, limiting their capacity for OC storage, these ecosystems are globally recognised for their additional benefits to society, nature, and the economy. Therefore, expanding protection of existing OC stores and mitigating anthropogenic pressures on these rare and unique ecosystems should be prioritised, not only to provide climate benefits through avoided emissions, but to protect the range of broader ecosystem services they provide, including biodiversity support for the species observed within the existing meadows (including snakelocks anemones, grooved topshell, spider and hermit crabs, and juvenile fish), coastal protection, and fisheries habitat. This could include expansion of ECZs around the Isle of Man to protect the 61% of seagrass meadows that are currently outside of these zones, and creation of a MNR for Bulgham Bay. Ongoing monitoring would improve understanding of the dynamic nature of these environments, including their spatial and seasonal variability, which could influence OC stocks and accumulation. Additional sampling for sedimentary OC in the other saltmarshes and seagrass meadows around the Isle of Man, which were not sampled herein due to resource limitations, and sampling of adjacent unvegetated sediments further from the seagrass meadow would also improve estimates and understanding of spatial variability in these ecosystems.

4.5 Conclusions

This study provides a novel case study of sedimentary OC storage and accumulation in exposed temperate seagrass meadows and saltmarshes in the Isle of Man. The findings highlight the comparable OC storage capacity of Isle of Man saltmarshes with other temperate regions, but the lower OC storage capacity of the island's *Z. marina* meadows per hectare, comparable only to exposed temperate coastlines. Saltmarsh sediments store 94.14 ± 62.51 MgC ha^{-1}, amounting to 694.78 ± 461.34 MgC over 7.38 ha, and accumulate 7.97 ± 5.60 MgC yr^{-1} at a rate of 1.08 ± 0.76 MgC ha^{-1} yr^{-1}, aligning with values reported for northern European saltmarshes. Seagrass sediments store 1.33 ± 0.25 MgC ha^{-1}, amounting to 261.10 ± 49.08 MgC over 195.88 ha, in the top 10 cm, which is 43% greater than unvegetated sediments (0.93 ± 0.86 MgC ha^{-1}). Seagrass meadow OC density decreases with depth to levels comparable to unvegetated sediments, indicating that surface values may overestimate the long-term OC storage potential of seagrass meadows. This study highlights the potential influence of hydrodynamic conditions, land use changes, and sedimentation dynamics in shaping OC storage in vegetated BCEs, emphasising the vulnerability of these ecosystems to environmental change and anthropogenic pressures. Given their importance for climate regulation, biodiversity, and coastal protection, conservation measures should be expanded. Future research should aim to quantify long-term sedimentary OC burial, to inform conservation strategies for protecting existing OC stocks and to support future OC sequestration in these ecosystems.

Chapter 5

Conclusion

5.1 Summary and Key Results

This PhD research aimed to quantify organic carbon (OC) stocks, accumulation, and burial rates within three key blue carbon ecosystems (BCEs) in the Isle of Man—saltmarshes, seagrass meadows, and the Western Irish Sea Mud Belt (WISMB)—to inform the island's Blue Carbon Strategy. This study was driven by the growing recognition that, alongside reducing greenhouse gas (GHG) emissions and utilising carbon capture technologies, BCEs provide a natural solution for atmospheric CO_2 removal and long-term storage (Macreadie et al., 2021; Seddon et al., 2020). These ecosystems could play a critical role in achieving international climate goals of limiting global warming to below 1.5°C above pre-industrial levels (Smith et al., 2016; United Nations, 2015), while offering a range of other ecosystem services that benefit society.

For the Isle of Man to maximise OC storage in BCEs for climate regulation, it first required a comprehensive assessment of existing OC stocks (a measure of the vulnerability potential), OC accumulation and burial rates (a measure of the mitigation potential), and an understanding of the factors that influence them. A significant barrier to integrating BCEs into climate change mitigation and adaptation strategies is the lack of accurate spatial extent data and an understanding of the spatial and temporal variability of sedimentary OC, particularly in understudied temperate regions and human-impacted areas such as trawled seabed. This thesis addresses these gaps by providing high-resolution empirical analyses of sedimentary OC stocks and, where possible, OC accumulation and burial rates in three of the Isle of Man's key BCEs, along with habitat extent mapping. As a result, this research has produced spatially explicit maps of sedimentary OC stocks in the Isle of Man's BCEs, while assessing the environmental and anthropogenic factors influencing their distribution, with particular attention to the impacts of bottom trawling on the WISMB. These findings provide critical insights to inform both national and

international blue carbon strategies, while contributing to the broader field of blue carbon research.

5.2 Addressing the Research Aims

Overall, the WISMB was found to be a major long-term OC reservoir due to its OC density and vast extent, exceeding saltmarshes and seagrass meadows. However, modern intense, chronic trawling was associated with depleted OC stocks in the WISMB. Saltmarsh had the highest OC density and accumulation rate, which were comparable with other temperate regions, while seagrass meadow OC density was among the lowest values reported and comparable with exposed temperate coastlines.

Chapter 2 examined the temporal variability of sedimentary OC in the WISMB using radionuclide dating from Sellafield discharges and high-resolution OC depth profiles to assess OC stocks and burial efficiencies. The findings indicate that up to 74% of OC accumulated in surface sediments (≤30 years old) remains buried for over a century. These findings revealed that surface sediments (≤10 cm) do not reliably represent long-term OC storage on climate-relevant timescales and that age-resolved OC concentration depth profiles are required to assess their climate mitigation potential.

Building on these insights, Chapter 3 investigated the effects of intense chronic bottom trawling by *Nephrops norvegicus* fisheries on OC stocks in the WISMB. The study found that OC stocks in sediments laid down in 1960–1990 (10–20 cm) were depleted in regions with more intense modern bottom trawling, likely caused by resuspension and mixing by penetrating gears. Meanwhile, the impacts of modern trawling on younger sediments laid down since 1990 (≤10 cm) were unresolved, potentially due to competing environmental mixing processes that mask the effects of trawling. The OC concentrations within sediment deposited before 1960 (≥20 cm) were not significantly associated with trawling, suggesting that the effects of penetrating gears are limited to the upper 20 cm in the WISMB. These findings highlighted the negative sub-surface impact of modern trawling on sedimentary OC, providing a more resolved picture compared to most previous studies that only assessed trawling impacts in surface sediments.

Chapter 4 assessed the OC storage potential of temperate saltmarshes and seagrass meadows. While saltmarsh sediments were found to have the highest OC densities, seagrass meadows store 35% more OC in the top 10 cm due to their larger spatial extent (195.88 ha), which was mapped for the first time in this study. However, degradation of OC in seagrass meadows to levels comparable to unvegetated sediments limits understanding of their long-term storage potential. In contrast, saltmarsh sediments exhibit enhanced OC accumulation compared to pre-saltmarsh sediments, demonstrating their role as long-term carbon reservoirs.

Overall, this thesis highlights the substantial spatial and temporal variability in BCE sedimentary OC stocks in the Isle of Man and provides high-resolution datasets to support the Isle of Man Government's Blue Carbon Strategy. These findings have important implications for BCE management in the Isle of Man and globally, which will be discussed throughout this concluding chapter.

5.3 Discussion

5.3.1 Blue Carbon in the Isle of Man

This thesis presents the first comprehensive empirical analysis of sedimentary OC in the Isle of Man, providing essential data to support the island's Blue Carbon Strategy. The results of these studies, which quantify BCE extents and sedimentary OC stocks and accumulation/burial rates, also provide a baseline for future monitoring efforts on the Isle of Man, including monitoring changes related to ecosystem management and land/seabed use. Furthermore, these results contribute valuable broader insights for informing the inclusion of BCEs in GHG inventories and can be used to inform blue carbon research in other exposed temperate island nations.

By empirically measuring BCEs on the Isle of Man, this study enhances the accuracy of OC storage estimates compared to previous assessments that have relied on extrapolated UK datasets (Burrows et al., 2024; Smeaton et al., 2024; Towle, 2018). The OC stocks in the top 10 cm of the Isle of Man's saltmarshes (169.47 ± 34.09 MgC) and seagrass meadows (261.10 ± 49.08 MgC), measured herein, revealed that prior estimates substantially overestimated OC storage in saltmarshes (323.16 MgC)

and seagrass meadows (5,951.10 MgC) (Burrows et al., 2024). This overestimation stemmed from the higher average OC stocks reported for the top 10 cm of UK saltmarshes (43.67 MgC ha^{-1}) and seagrass meadows (23.90 MgC ha^{-1}) compared to the values measured in this study (22.96 ± 4.62 MgC ha^{-1} and 1.33 ± 0.25 MgC ha^{-1}, respectively). While saltmarsh extent estimates remained consistent across studies (7.4 ha; Sayle, 1995), the seagrass extent estimated herein (195.88 ha) was both 27% lower than (249 ha; Burrows et al., 2024) and over twice as large as (78.50 ha; Towle, 2018) previous estimates used to generate OC stocks. These findings emphasise the need for precisely mapping BCEs for accurate OC stock assessments. The OC stocks measured herein for the in WISMB sediments (10.37 ± 1.62 MgC ha^{-1}), and in muddy saltmarsh sediments, were also considerably lower than prior estimates for mud and fine sand sediments in the Isle of Man (39–208 MgC ha^{-1}; Towle, 2018). This demonstrates the risks of extrapolating from external datasets and highlights the importance of local data collection to improve the precision of OC stock estimates, ensuring a robust scientific foundation for BCE management and policy development.

5.3.2 Relative Significance of Blue Carbon Ecosystems

Traditionally, only actionable BCEs such as saltmarshes and seagrass meadows in northern temperate regions have been considered for inclusion in Intergovernmental Panel on Climate Change (IPCC) GHG accounting guidelines and Nationally Determined Contributions (NDCs) under the Paris Agreement (Hamilton et al., 2023). These ecosystems are deemed actionable due to their significant, long-term OC sequestration capacity and their potential for effective management and measurement of GHG fluxes. However, this thesis highlights the critical role of the WISMB as an emerging BCE and the dominant OC store in the Isle of Man, surpassing coastal vegetated BCEs in its OC storage potential (Figure 5.1).

Although saltmarshes have the highest OC density (22.96 MgC ha^{-1}), followed by the WISMB (10.37 MgC ha^{-1}) and seagrass meadows (1.33 MgC ha^{-1}), ecosystem extent plays a crucial role in total OC storage. The WISMB (49,212.30 ha) accounts for over 99.9% of total OC storage (510,198.96 MgC) in the top 10 cm of sediments, whereas saltmarshes and seagrass meadows contribute only 0.1% (169.47 MgC and

261.1 MgC, respectively). These results underscore the importance of considering ecosystem extent when assessing BCE contributions to OC storage. Despite its substantial OC storage capacity, shelf sediments remain excluded from blue carbon inventories and GHG accounting frameworks (Crooks et al., 2018; Hamilton et al., 2023; Intergovernmental Panel on Climate Change, 2023) due to scientific uncertainties in their location, extent, permanence, and factors driving OC storage variability (Hamilton et al., 2023). By addressing some of these uncertainties, this thesis provides empirical evidence supporting the future inclusion of muddy shelf sea sediments in blue carbon strategies and management.

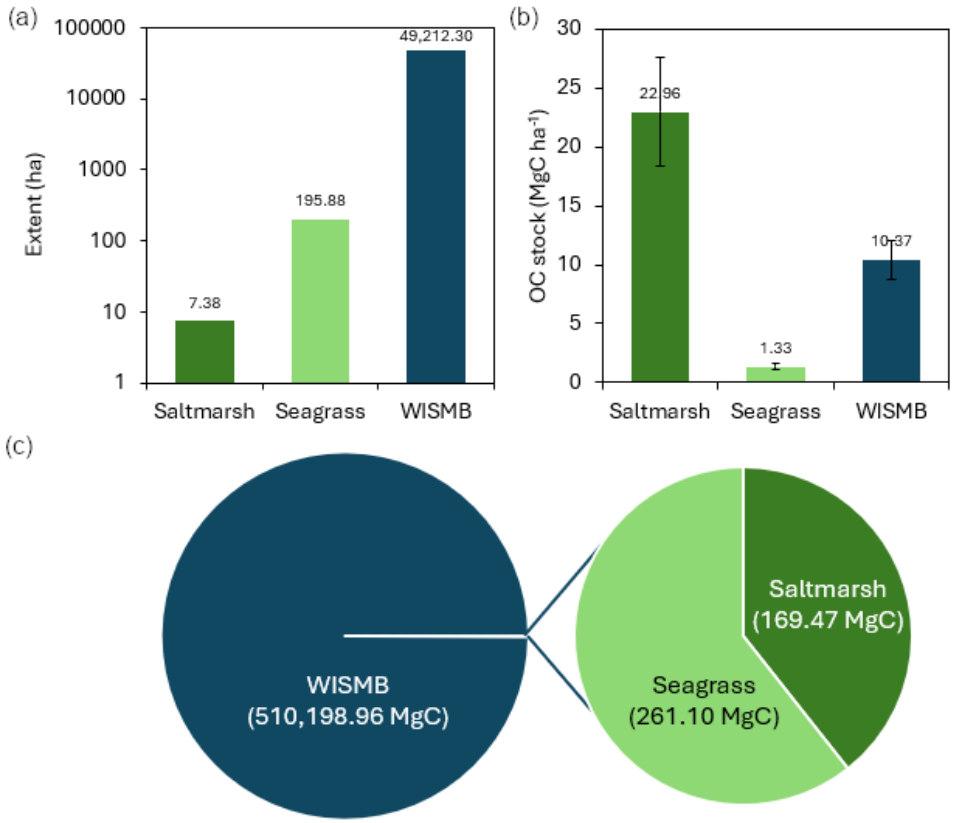

Figure 5.1 A comparison of: (a) ecosystem extent (ha); (b) organic carbon density (MgC ha^{-1}); and (c) organic carbon stock (MgC), in the top 10 cm of saltmarshes, seagrass meadows, and the Western Irish Sea Mud Belt (WISMB) sediments in the Isle of Man.

5.3.3 Resolving Sedimentary Organic Carbon Variability

One of the main challenges in resolving long-term sedimentary OC storage is the uncertainty associated with OC preservation and degradation. Only a fraction of OC reaching the seabed is ultimately buried due to varying reactivities and the influence of biological, geochemical, and physical factors (LaRowe et al., 2020). Limited empirical data typically constrain accurate estimates of long-term OC burial rates (OCBRs) (Middelburg, 2019) and OC burial efficiencies (OCBEs) (Bradley et al., 2022), leading to blue carbon assessments that rely on reactive surface sediment OC stocks (Diesing et al., 2021), which may overestimate long-term burial. Using high-resolution OC depth profiles and radionuclide dating linked to Sellafield discharges, Chapter 2 resolved OCBEs in the WISMB and proved the hypotheses set out in this thesis: that impulse dating of radionuclide discharges from the Sellafield nuclear facility, combined with OC depth profiles, will enable quantification of age- and depth-resolved OC accumulation rates (OCARs) and OCBRs; and that OC stocks will decrease with depth due to degradation over time. By comparing short-term OCARs in sediments ≤30 years old with long-term OCBRs in sediments ≥100 years old, this study determined an average OCBE of 74%, with an OCBR of 23 gC m^{-2} yr^{-1} and an OCAR of 31 gC m^{-2} yr^{-1}. These findings indicate that the most significant OC degradation occurs within the first 100 years of sediment accumulation, supporting conceptual models of OC degradation (Bradley et al., 2022; Burdige, 2007) and emphasising the necessity of age-resolved OC stock assessments and OCBEs for accurate climate regulation estimates for BCEs.

Furthermore, bottom trawling has previously been shown to modify sedimentation rates and OC stocks on continental shelves (Epstein et al., 2022; Legge et al., 2020; Paradis et al., 2019; Wilkinson et al., 2018). However, data are generally inconclusive in studies that are restricted to surface sediments where environmental variables like hydrodynamics and biological activity can also influence OC storage and reactivity (Sciberras et al., 2016; Tiano et al., 2019). Chapter 3 investigated the influence of bottom trawling and natural disturbances on sedimentary OC stocks in the WISMB, and proved the hypotheses set out in this thesis: that chronic bottom trawling negatively impacts OC stocks in WISMB; and that mixing effects in surface sediments obscure trawling impacts on OC. Using vessel monitoring system (VMS)

data and kriged density estimates of *N. norvegicus* burrows from towed underwater video camera (TUV) surveys, trawling pressure and bioturbation were reconstructed, and their impacts alongside sediment properties on OC stocks were assessed by general linear models (GLMs). The findings revealed that trawling pressure was significantly associated with sedimentary OC depletion in sediments from 1960–1990 (10–20 cm), while gear penetration into deeper sediments from 1860–1960 (≥20 cm) had less effect, and sediment mixing by competing environmental factors potentially masked trawling effects in surface sediments from 1990–2022 (≤10 cm). These results highlight the need for subsurface sediment analysis to accurately assess trawling impacts on long-term OC stocks, which could inform future studies globally. From a local perspective, these results provide empirical evidence supporting sustainable fisheries management in the WISMB, which could include placing spatial restrictions on areas for bottom trawling, limiting bottom fishing to static gears, or implementing gear modifications to reduce seabed impact from trawls. Fisheries management policies that consider sedimentary OC stocks could therefore help to protect existing and future long-term OC storage, based on the results of this thesis. Domestic regulations concerning conservation and sustainable use of the seabed could become increasingly important if the UK extends the 'High Seas Treaty' (UN Agreement on Biodiversity Beyond National Jurisdiction (BBNJ)), which it signed in 2023, to the Isle of Man for consent. The results of this research also make way for further studies to assess the potential for seabed recovery by alleviating trawling pressure.

Coastal vegetated ecosystems also face increasing anthropogenic pressures, yet incomplete mapping limits knowledge of their distributions and extents, hindering targeted conservation efforts (Macreadie et al., 2019; Unsworth et al., 2018). The variability of sedimentary OC stocks and sediment thickness within and among these ecosystems also complicates data extrapolation between regions (Dahl et al., 2016; Greiner et al., 2016; Prentice et al., 2020; Röhr et al., 2018). To address these challenges, Chapter 4 quantified sedimentary OC storage in *Z. marina* seagrass meadows and saltmarshes on the Isle of Man, as well as saltmarsh OC accumulation rates, proving the hypotheses set out in this thesis: that saltmarshes have higher OC densities; that seagrass meadows have a greater spatial extent than saltmarshes; and that seagrass meadows store more OC than adjacent unvegetated sediments. This

study utilised side-scan sonar, in-situ diver, and video surveys to map 195.88 ha of seagrass meadows for the first time, alongside 7.38 ha of saltmarsh based on existing datasets. OC densities were higher in saltmarsh sediments, yet total OC stocks in the top 10 cm were 35% greater in seagrass meadows due to their larger spatial extent. Seagrass sediments contained 43% more OC than unvegetated sediments in the top 10 cm, though this difference diminished with sediment depth. Spatial variability in saltmarsh OC stocks and accumulation rates was attributed to differences in estuarine location, tidal inundation, and land use, while seagrass meadow morphology varied with site exposure, likely influencing OC accumulation and storage. These findings underscore the additional OC accumulation and storage provided by temperate saltmarshes and seagrass meadows, reinforcing the need for their ongoing protection to preserve OC stocks and future sequestration, alongside their broader ecosystem service benefits. However, the relatively low OC stocks quantified in the Isle of Man's seagrass meadows highlight the challenges of extrapolating values between regions, as this can lead to overestimations of an ecosystem's OC storage capacity. These results suggest that sedimentary OC stocks in seagrass meadows in other exposed temperate island nations could be lower than global values, providing valuable insights to inform and encourage empirical blue carbon research in other exposed regions. From an international perspective, these results reveal a key limitation in current approaches for reporting the climate change mitigation potential of saltmarshes and seagrass meadows within IPCC GHG accounting frameworks, which require OC stock reporting over a 1-meter depth. Chapter 4 demonstrated that saltmarsh and seagrass meadow sediments can be significantly shallower than 1 m, so applying this methodology may substantially overestimate their OC storage capacity. This study therefore provides a high-resolution and more transparent approach to informing local BCE management.

Overall, while OC stocks in the top 10 cm of sediments reflect recent OC accumulation, the results of Chapters 2 and 4 reveals significant temporal variability in OC storage, with concentrations decreasing with sediment depth across all BCEs. These findings emphasise the necessity of age-resolved OC stock assessments to accurately evaluate BCEs' long-term climate change mitigation potential. Current methodologies, such as IPCC GHG accounting frameworks (Hamilton et al., 2023), that rely on extrapolating surface OC data or assuming uniform concentrations over

the top 1 m of sediments risk overestimating long-term OC burial. Such overestimations may misguide national carbon accounting strategies and inflate expectations of BCEs' contributions to Net Zero targets. This study thus underscores the need to integrate sediment depth and age assessments alongside OC stock data to refine blue carbon assessments and to inform policy development.

5.3.4 Recommendations

5.3.4.1 Conserving Coastal Blue Carbon Ecosystems

The primary recommendation from this thesis is for the protection and conservation of saltmarshes, seagrass meadows, and the WISMB in the Isle of Man, to safeguard existing OC stocks and to enable future OC accumulation and burial. Preventing their degradation can reduce carbon emissions, reinforcing their role in climate change mitigation, while safeguarding crucial climate adaptation benefits, including coastal protection, flood mitigation, and resilience against sea level rise and extreme weather events.

Whilst there is mounting interest globally for establishing carbon markets based on carbon credits to offset emissions by BCE conservation and restoration, there is limited scope for this on the Isle of Man. Seagrass meadows and some saltmarsh plants are already protected under the Wildlife Act 1990, which is in part enforced through the designation of conservation zones in these regions (e.g. Areas of Special Scientific Interest (saltmarshes) and Marine Nature Reserves (MNRs) (seagrass meadows)). This means that additional protection would not necessarily lead to additional carbon storage through mitigated impacts. Additionally, there is limited scope for expansion of these ecosystems by restoration, due to physical natural and anthropogenic constraints in-land for saltmarshes, and high associated costs with restoration of degraded sites. Habitat suitability modelling would likely be needed to determine suitable sites for seagrass meadow restoration, as historic understanding of seagrass meadow extents is limited. Nevertheless, additional carbon accumulation and burial through BCE restoration is uncertain and would not be guaranteed immediately, as previous studies have shown carbon stocks can take decades to recover to natural ecosystem levels (McMahon et al., 2023; Rahayu et al., 2023).

Considering these challenges for restoration on the Isle of Man, the most plausible action for saltmarshes and seagrass meadows is their protection by government for their holistic ecosystem service benefits. For example, expanding the Eelgrass Conservation Zones (ECZs), which currently cover only 39% of the mapped seagrass meadow extent, and implementing a MNR at Bulgham Bay could help mitigate damage from boat moorings, pot fishing, and other anthropogenic activities.

5.3.4.2 Reducing Pressures on Blue Carbon Ecosystems

Reducing pressures on vegetated BCEs would help these to thrive, which could help conserve existing OC stocks and enable future OC accumulation and burial. Major threats to saltmarshes that could be managed include land use change (e.g. coastal development), pollution, and invasive species, all of which can degrade these ecosystems and reduce their capacity for OC accumulation and storage (Hansen and Reiss, 2015). In the temperate North Atlantic, key threats to seagrasses that could be managed include agricultural and urban runoff, dredging, and inshore trawling (Grech et al., 2012). Policy development, planning, and stakeholder consultation have been identified as preferred approaches for seagrass management over prescriptive enforcement or reactive restoration efforts (Grech et al., 2012), thus incorporating seagrass meadows into national blue carbon policies could enhance their protection and contribute to broader climate mitigation strategies.

5.3.4.3 Sustainable Fisheries Management for Blue Carbon in the WISMB

Fisheries management could be used to enhance OC storage in shelf sediments, particularly within the WISMB, which holds significant OC stocks despite being depleted by chronic disturbance from bottom trawling. The findings demonstrate that trawling-induced sediment disturbance could lead to long-term reductions in OC storage, aligning with broader evidence of bottom trawling's detrimental effects on OC retention in muddy seabeds. Implementing fisheries management policies that limit bottom trawling impacts, such as spatial restrictions or gear modifications, could play a crucial role in preserving and enhancing OC storage within the Isle of Man's territorial waters.

5.3.5 Study Limitations and Future Perspectives

This thesis contributes to global blue carbon knowledge through high-resolution empirical analyses of depth- and age-resolved sedimentary OC accumulation and burial within key BCEs, which can be used to inform local management in the Isle of Man. However, several limitations exist, which are outlined below, alongside recommendations for future research.

5.3.5.1 Long-term Organic Carbon Stability (Chapter 2)

While Chapter 2 provided an age-resolved understanding of OC burial in the WISMB, OC degradation continued more slowly past 100 years, and longer-term trends could not be assessed due to limited sediment core lengths. The average core length was 69.2 ± 10.2 cm, ranging from 50 cm to 88 cm, and sedimentary analyses in this study were limited to the shortest sediment core length of 50 cm to enable comparison between sites. Future research could analyse deeper sediments using different coring methods (e.g. piston corer) to overcome the relatively shallow sediment depths obtained using the gravity corer, to evaluate OC stability over centuries to millennia. This could further support the results of this chapter, emphasising how OC burial efficiencies reported alongside accumulation estimates could avoid overestimating long-term storage potential. Furthermore, analysing OC reactivity could refine estimates of the long-term OC storage potential, complimentary to OCBEs estimated herein (Graves et al., 2022). Analysing OC sources within the WISMB could also inform actions to protect not only the WISMB as an OC sink, but also OC sources, potentially helping to facilitate inclusion of the WISMB and other emerging BCEs in national GHG inventories (Graves et al., 2022).

5.3.5.2 Reducing Fishing Pressure on Organic Carbon Stocks (Chapter 3)

Chapter 3 demonstrated the negative impact of bottom trawling on sedimentary OC stocks, though all sites experienced relatively high fishing pressures. Future studies could explore effects across a broader fishing pressure gradient, including the lowest

and highest-pressure areas. Furthermore, working closely with the Isle of Man Government could facilitate investigations into OC stock recovery in closed fishing areas. This could determine whether fisheries management can support additional OC accumulation and burial compared to the current situation, helping to inform blue carbon management strategies for climate mitigation (Graves et al., 2022). Additionally, while a negative relationship between fishing pressure and OC stocks was found, the magnitude of OC remineralisation after trawling and the fate of OC released from sediments remains unknown. Future research could assess empirically whether this OC is remineralised into the atmosphere or sequestered elsewhere, to further refine disturbance risk assessments. Addressing these topics would help to clarify some of the key uncertainties around the fate of disturbed OC and magnitude of trawl-induced CO_2 release, which has been a controversial topic that has gained widespread coverage over the past ~4 years (Atwood et al., 2024; Epstein et al., 2021; Hiddink et al., 2023; Sala et al., 2021).

5.3.5.3 Coastal Vegetated Blue Carbon Ecosystems (Chapter 4)

Chapter 4 quantified OC stocks in saltmarsh and seagrass meadows; however, the long-term stability of these stocks remains unresolved. Since sediment thickness varies spatially, future studies could refine sediment thickness estimates to improve OC stock assessments. Estimating OC accumulation rates (OCARs) and OC burial efficiencies (OCBEs) in the mixed seagrass meadow sediments was prohibited by mixing of the excess ^{210}Pb decay profile and the ^{137}Cs Chernobyl fallout and Sellafield discharge peaks. However, understanding OC burial rates is essential for GHG inventories, so future work should aim to resolve sedimentation rates within seagrass meadows.

5.3.5.4 Beyond Saltmarshes, Seagrass Meadows, and the WISMB

This thesis focused on saltmarshes, seagrass meadows, and the WISMB, but other emerging BCEs such as kelp forests, maerl beds, and horse mussel reefs were excluded (Burrows et al., 2024; Towle, 2018). Expanding future research to these

additional BCEs would contribute to a comprehensive blue carbon audit for the Isle of Man.

5.3.5.5 Collaborative Research for Informed Ecosystem Management

The Manx Blue Carbon Project, co-designed by researchers and government, demonstrates how integrating environmental research with policy can facilitate real-world impact. It is hoped that this PhD research will actively inform the Isle of Man's Blue Carbon Strategy, while advancing the global blue carbon research field. Building on the success of this research program, future research should continue fostering collaborative projects between scientists, policymakers, and local communities to ensure actionable science is delivered on policy-relevant timescales.

5.4 Conclusion

Overall, this thesis makes a novel contribution to the field of blue carbon research, both locally in the Isle of Man and globally. This study provides the first empirical assessment of sedimentary OC stocks, accumulation, and burial within three key temperate BCEs—saltmarshes, seagrass meadows, and the WISMB—in the Isle of Man. Additionally, it advances understanding of the temporal and spatial variability of sedimentary OC within these BCEs, by challenging conventional methods for quantifying OC stocks and their accumulation and burial using high-resolution empirical datasets. This research offers valuable insights for international blue carbon policies and coastal management, including the Isle of Man Government's Blue Carbon Strategy.

The findings successfully support the initial hypotheses and address the main aims of this research, outlined in Chapter 1:

- Quantification of OC accumulation and burial rates in WISMB sediments demonstrated that OC stocks decrease with sediment depth (Chapter 2).

- Assessment of the effects of bottom trawling, bioturbation, and sediment type on OC stocks revealed that OC stocks are significantly depleted in more intensely trawled regions (Chapter 3).
- Evaluation of OC stocks and accumulation in saltmarshes and seagrass meadows showed variability within and between BCEs, and highlighted their additional OC accumulation benefits (Chapter 4).

From an Isle of Man perspective, this research underscores the following:

- The significance of the WISMB as a long-term OC reservoir, reinforcing its importance as an emerging BCE.
- The vulnerability of the WISMB sedimentary OC stocks to bottom trawling, highlighting a need for evidence-informed fisheries management.
- The high OC densities of saltmarshes and their limited extent, emphasising a need for their legal protection.
- The enhanced OC densities and ecological value of seagrass meadows compared to unvegetated regions, highlighting the importance of conservation zoning.
- The risks of overestimating OC storage in BCEs based on extrapolated datasets due to spatial and temporal OC variability, underscoring the necessity for local empirical data collection for accurate BCE assessments.

These findings contribute to the growing body of evidence advocating for the protection and restoration of BCEs and their effective integration into national climate policies and climate change mitigation strategies. On a local scale, it is hoped that this research informs sustainable blue carbon management in the Isle of Man, ensuring that BCE protection is informed by robust scientific evidence.

Appendix A

Organic Carbon Burial Rates in Muddy Temperate Shelf Sea Sediments

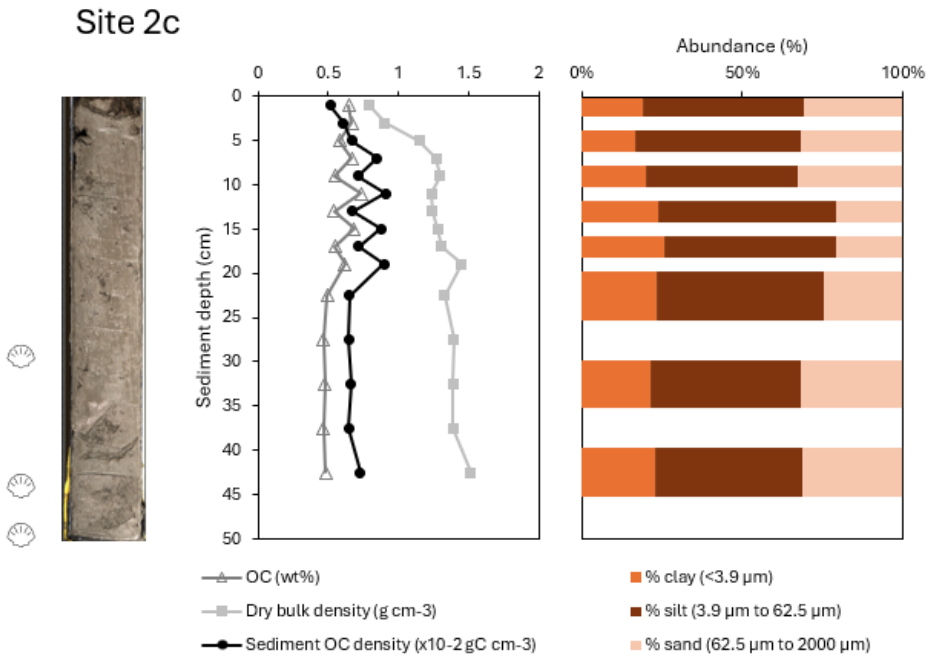

Figure A.1 Sediment depth profiles for Site 2c. Left to right: High-resolution colour image; organic carbon (OC) concentration (wt%), dry bulk density (g cm^{-3}), and sediment OC density (x10^{-2} gC cm^{-3}); and particle size distributions (% clay, % silt, % sand). Shell symbols (left) indicate depths where whole shells or shell fragments were found (29 cm, 43–46 cm, and 49 cm).

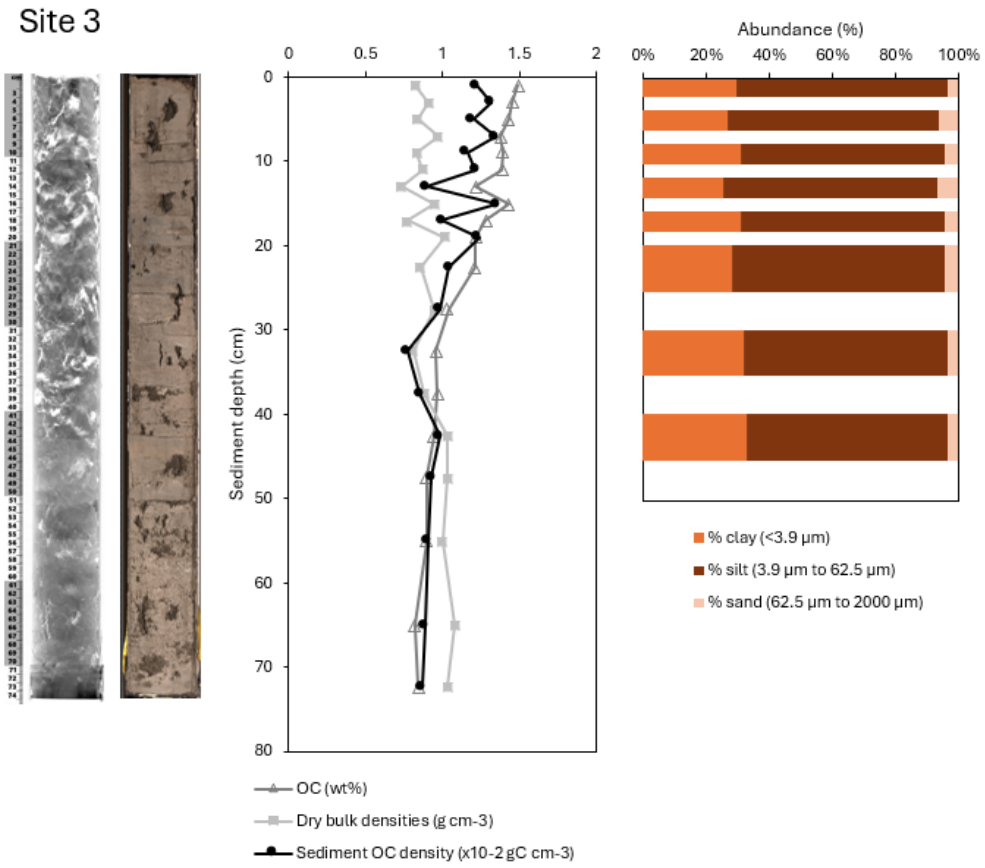

Figure A.2 Sediment depth profiles for Site 3. Left to right: X-ray radiograph; high-resolution colour image; organic carbon (OC) concentration (wt%), dry bulk density (g cm^{-3}), and sediment OC density (x10^{-2} gC cm^{-3}); and particle size distributions (% clay, % silt, % sand).

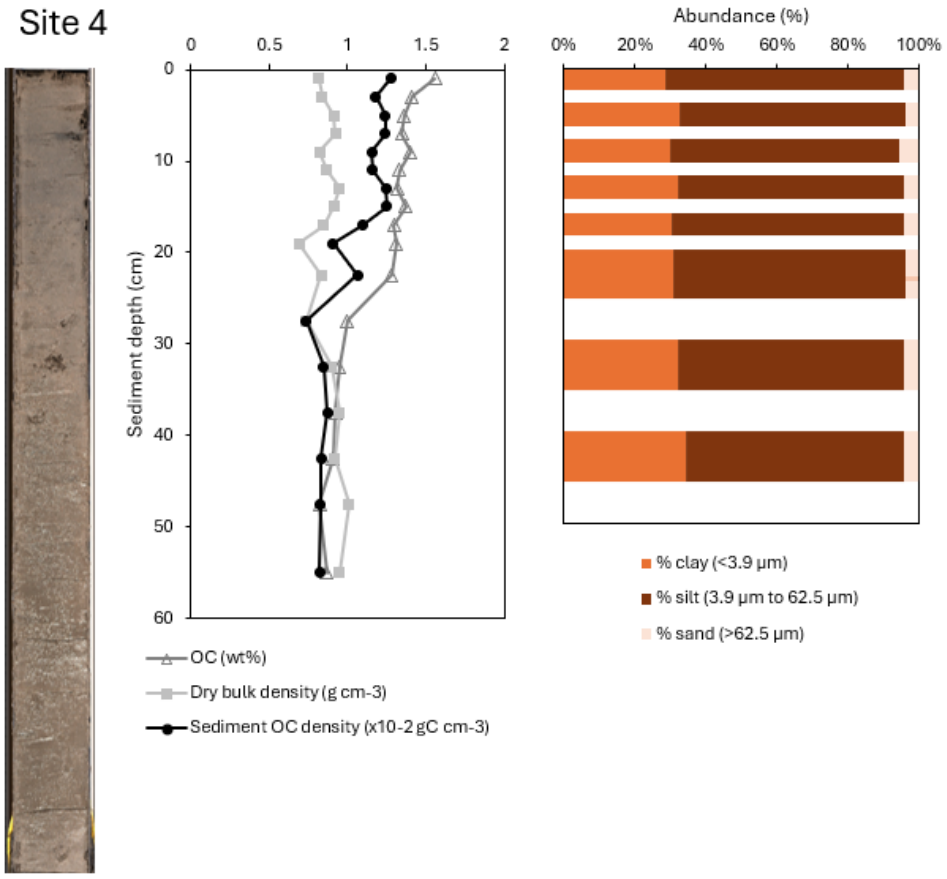

Figure A.3 Sediment depth profiles for Site 4. Left to right: High-resolution colour image; organic carbon (OC) concentration (wt%), dry bulk density (g cm^{-3}), and sediment OC density (x10^{-2} gC cm^{-3}); and particle size distributions (% clay, % silt, % sand).

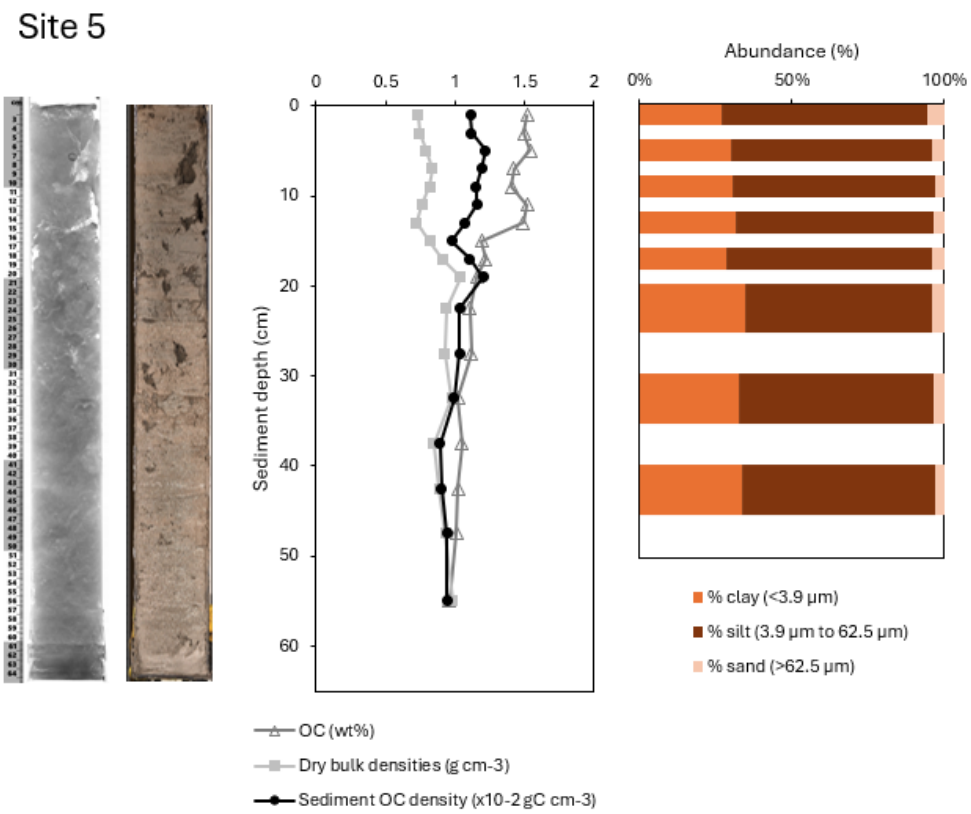

Figure A.4 Sediment depth profiles for Site 5. Left to right: X-ray radiograph; high-resolution colour image; organic carbon (OC) concentration (wt%), dry bulk density (g cm^{-3}), and sediment OC density (x10^{-2} gC cm^{-3}); and particle size distributions (% clay, % silt, % sand).

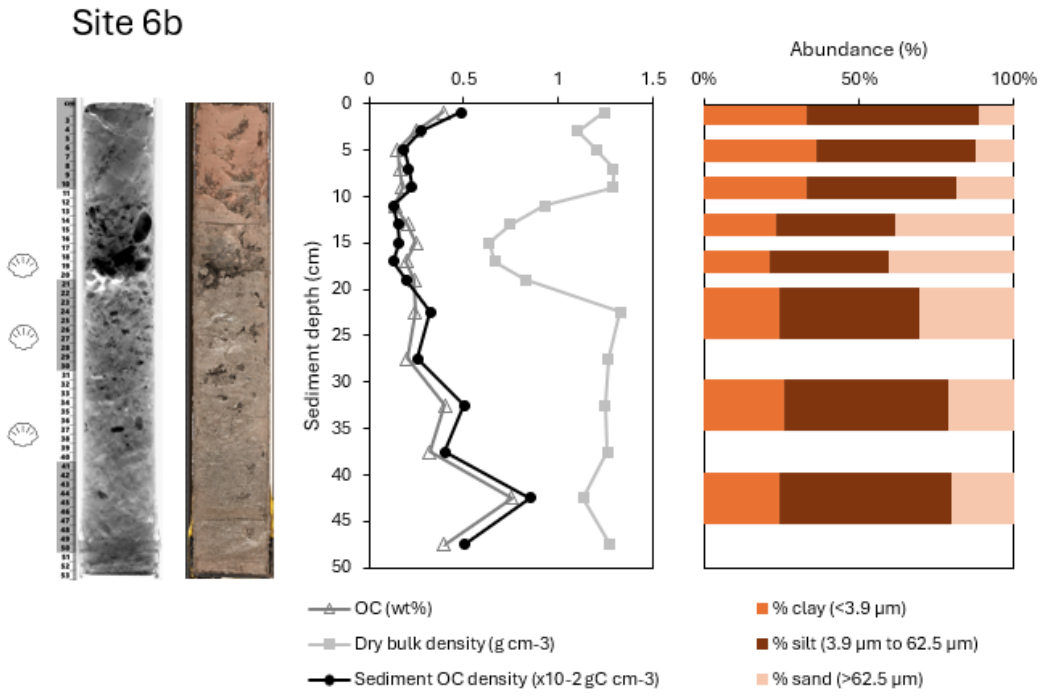

Figure A.5 Sediment depth profiles for Site 6b. Left to right: X-ray radiograph; high-resolution colour image; organic carbon (OC) concentration (wt%), dry bulk density (g cm^{-3}), and sediment OC density (x10^{-2} gC cm^{-3}); and particle size distributions (% clay, % silt, % sand). Shell symbols (left) indicate depths where whole shells or shell fragments were found (15–20 cm, 26 cm, and 36 cm).

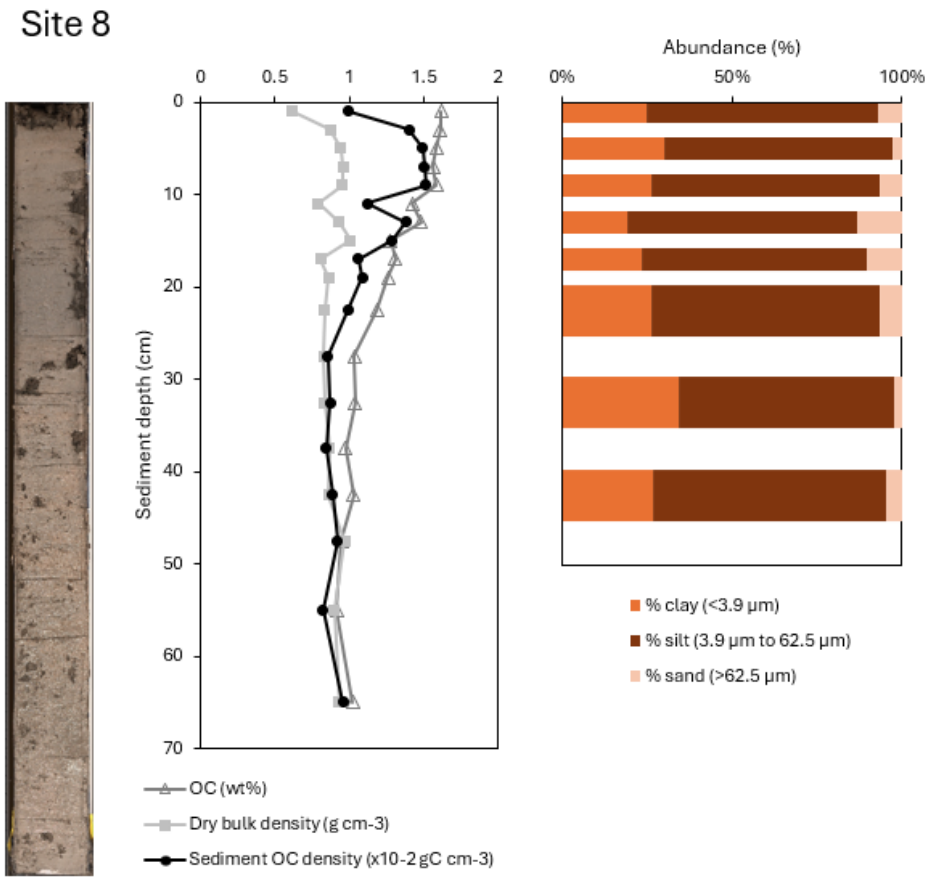

Figure A.6 Sediment depth profiles for Site 8. Left to right: High-resolution colour image; organic carbon (OC) concentration (wt%), dry bulk density (g cm^{-3}), and sediment OC density (x10^{-2} gC cm^{-3}); and particle size distributions (% clay, % silt, % sand).

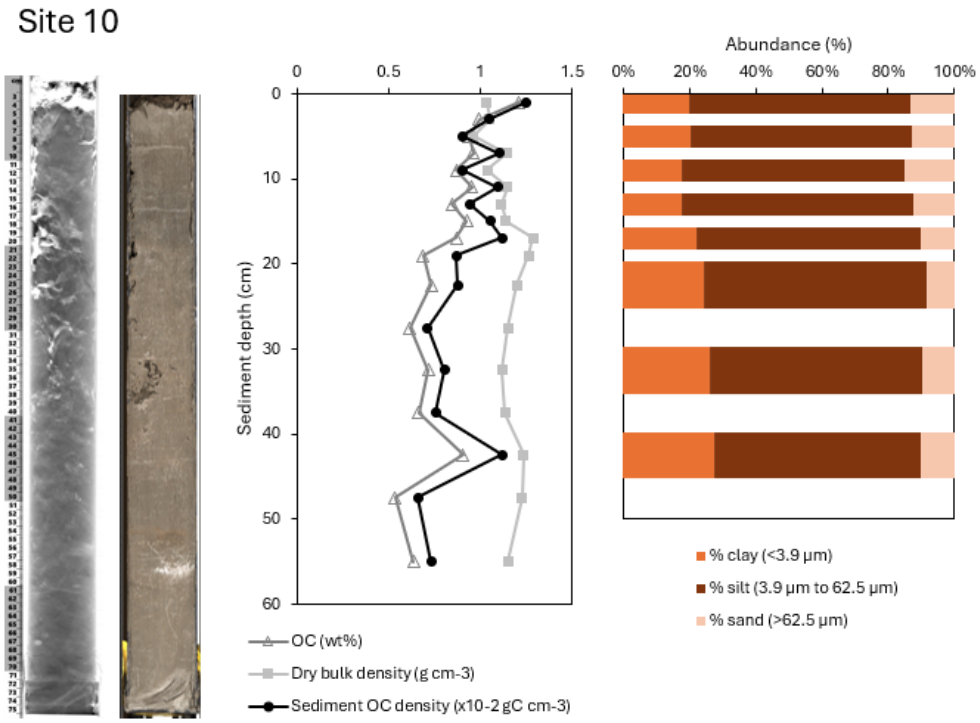

Figure A.7 Sediment depth profiles for Site 10. Left to right: X-ray radiograph; high-resolution colour image; organic carbon (OC) concentration (wt%), dry bulk density (g cm^{-3}), and sediment OC density (x10^{-2} gC cm^{-3}); and particle size distributions (% clay, % silt, % sand).

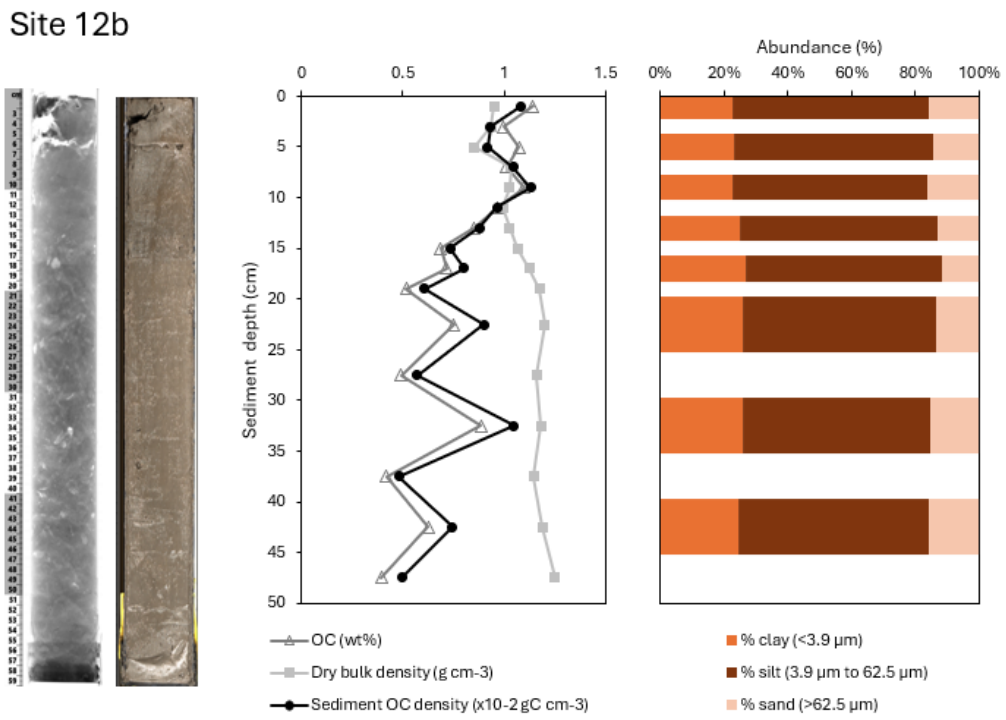

Figure A.8 Sediment depth profiles for Site 12b. Left to right: X-ray radiograph; high-resolution colour image; organic carbon (OC) concentration (wt%), dry bulk density (g cm^{-3}), and sediment OC density (x10^{-2} gC cm^{-3}); and particle size distributions (% clay, % silt, % sand).

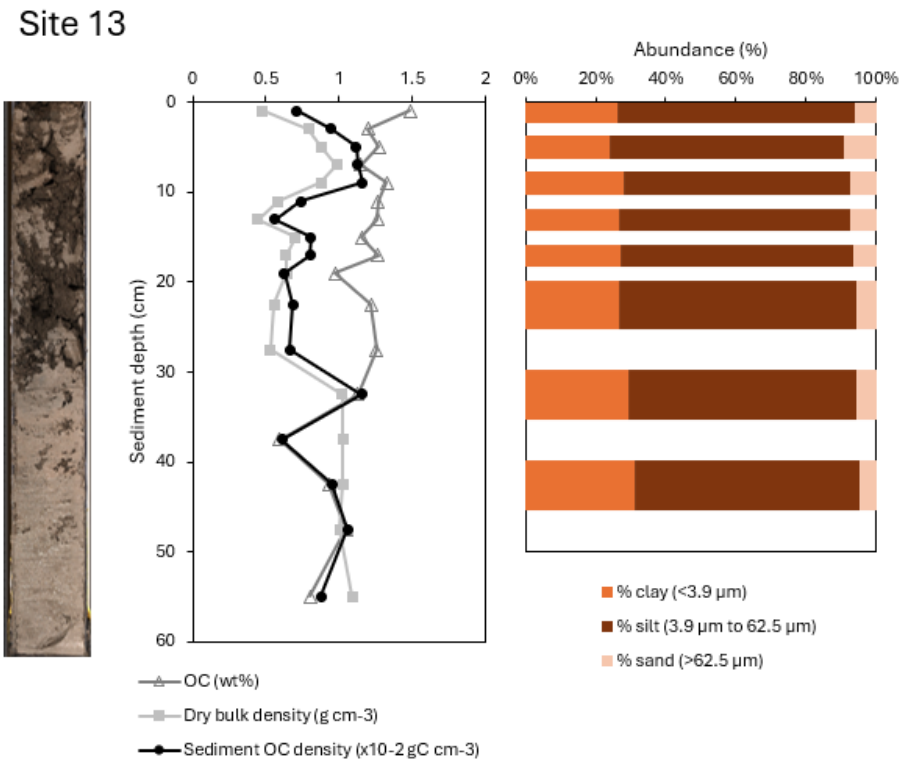

Figure A.9 Sediment depth profiles for Site 13. Left to right: High-resolution colour image; organic carbon (OC) concentration (wt%), dry bulk density (g cm^{-3}), and sediment OC density (x10^{-2} gC cm^{-3}); and particle size distributions (% clay, % silt, % sand).

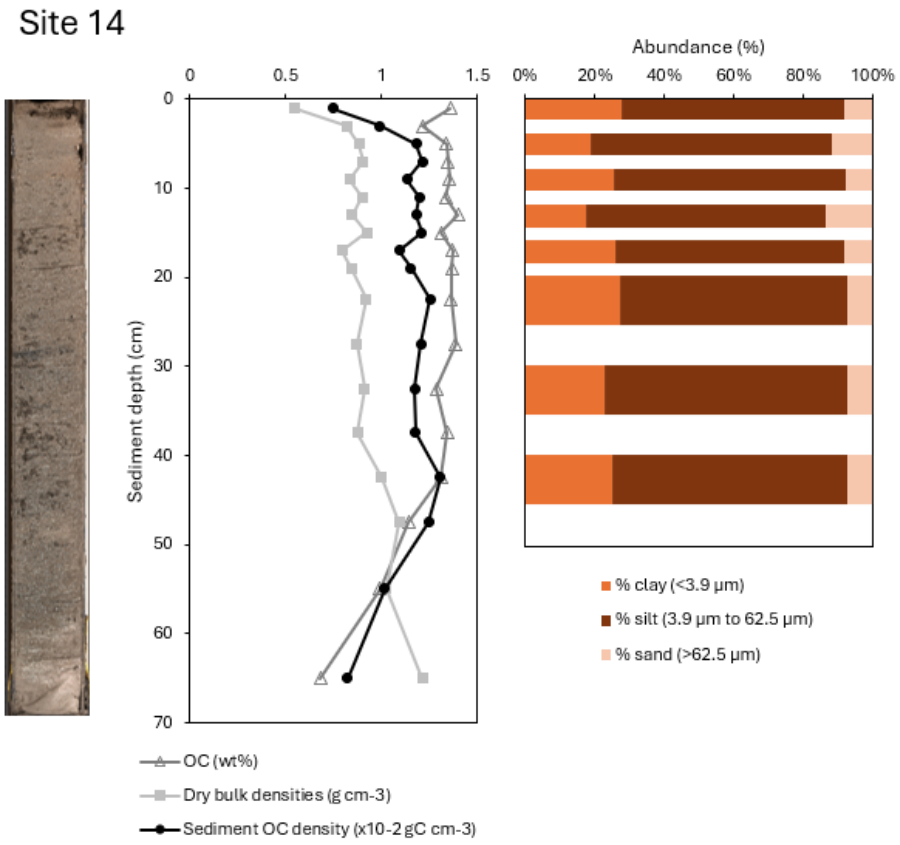

Figure A.10 Sediment depth profiles for Site 14. Left to right: High-resolution colour image; organic carbon (OC) concentration (wt%), dry bulk density (g cm^{-3}), and sediment OC density (x10^{-2} gC cm^{-3}); and particle size distributions (% clay, % silt, % sand).

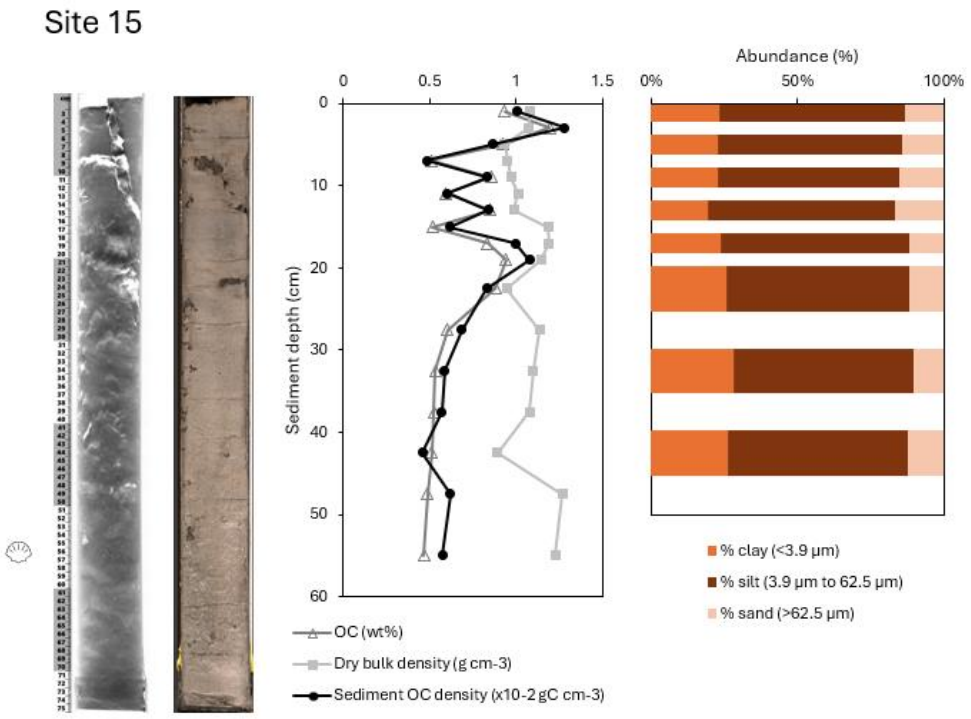

Figure A.11 Sediment depth profiles for Site 15. Left to right: X-ray radiograph; high-resolution colour image; organic carbon (OC) concentration (wt%), dry bulk density (g cm^{-3}), and sediment OC density (x10^{-2} gC cm^{-3}); and particle size distributions (% clay, % silt, % sand). Shell symbol (left) indicates depth where whole shells or shell fragments were found (55 cm).

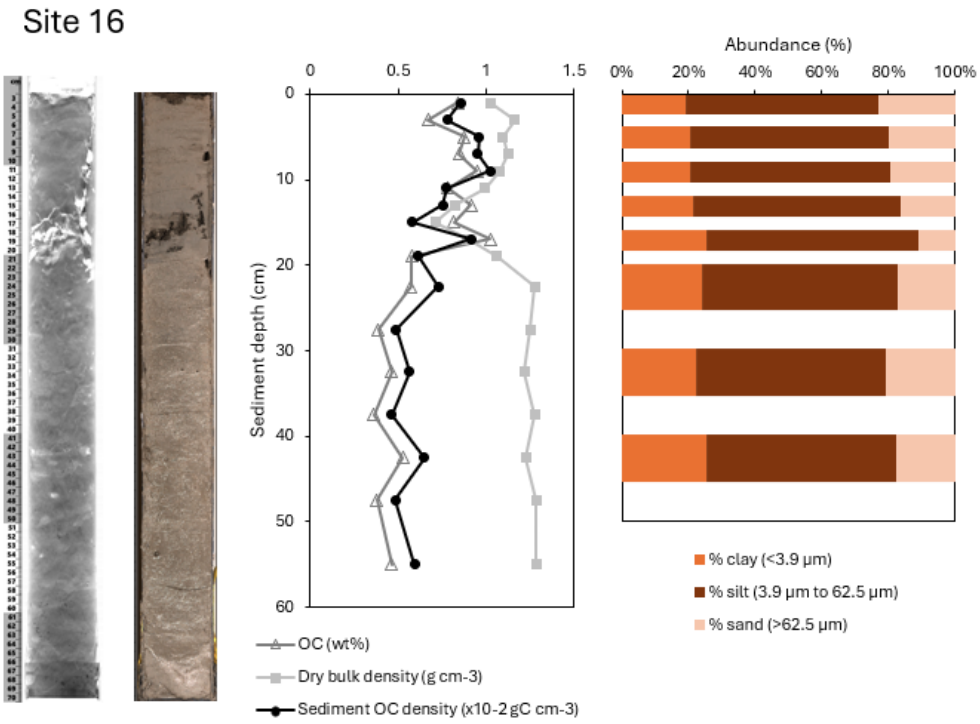

Figure A.12 Sediment depth profiles for Site 16. Left to right: X-ray radiograph; high-resolution colour image; organic carbon (OC) concentration (wt%), dry bulk density (g cm^{-3}), and sediment OC density (x10^{-2} gC cm^{-3}); and particle size distributions (% clay, % silt, % sand).

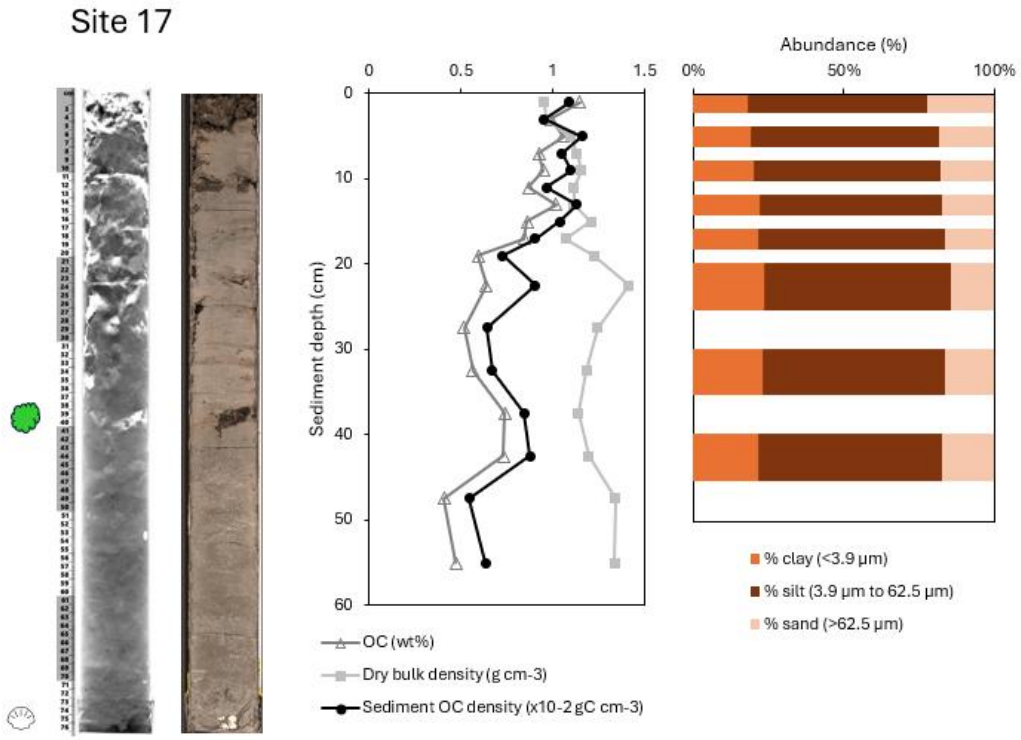

Figure A.13 Sediment depth profiles for Site 17. Left to right: X-ray radiograph; high-resolution colour image; organic carbon (OC) concentration (wt%), dry bulk density (g cm^{-3}), and sediment OC density (x10^{-2} gC cm^{-3}); and particle size distributions (% clay, % silt, % sand). Shell symbol (left) indicated the depth where whole shells or shell fragments were found (73–75 cm). Green symbol (left) indicates the depth where gelatinous green material and tube-like sediment microstructures were found (35–40 cm).

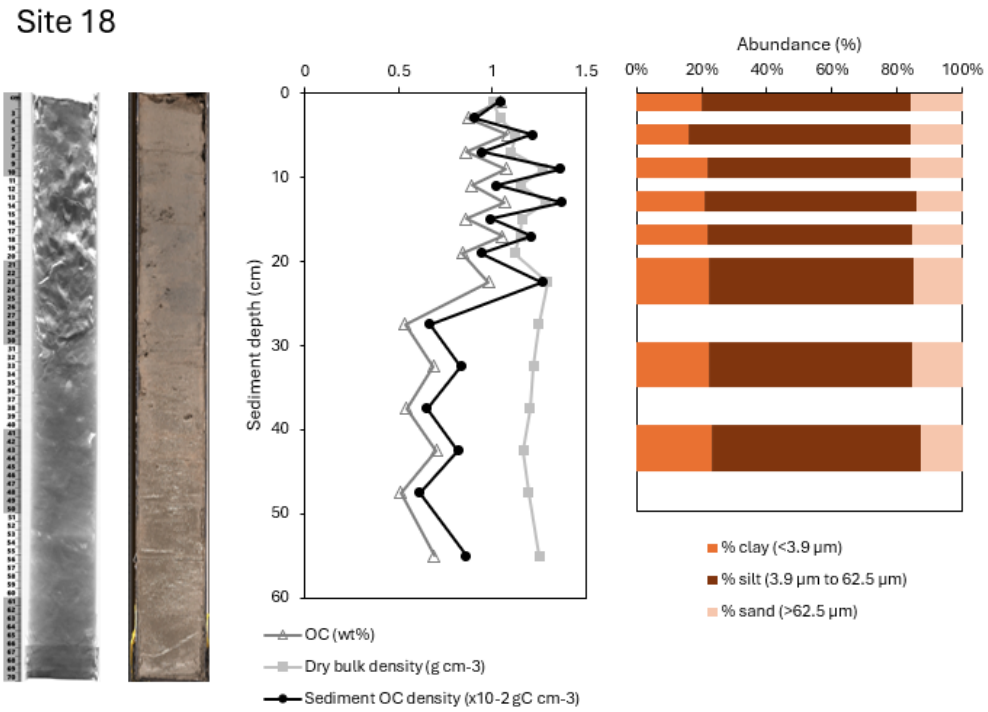

Figure A.14 Sediment depth profiles for Site 18. Left to right: X-ray radiograph; high-resolution colour image; organic carbon (OC) concentration (wt%), dry bulk density (g cm^{-3}), and sediment OC density (x10^{-2} gC cm^{-3}); and particle size distributions (% clay, % silt, % sand).

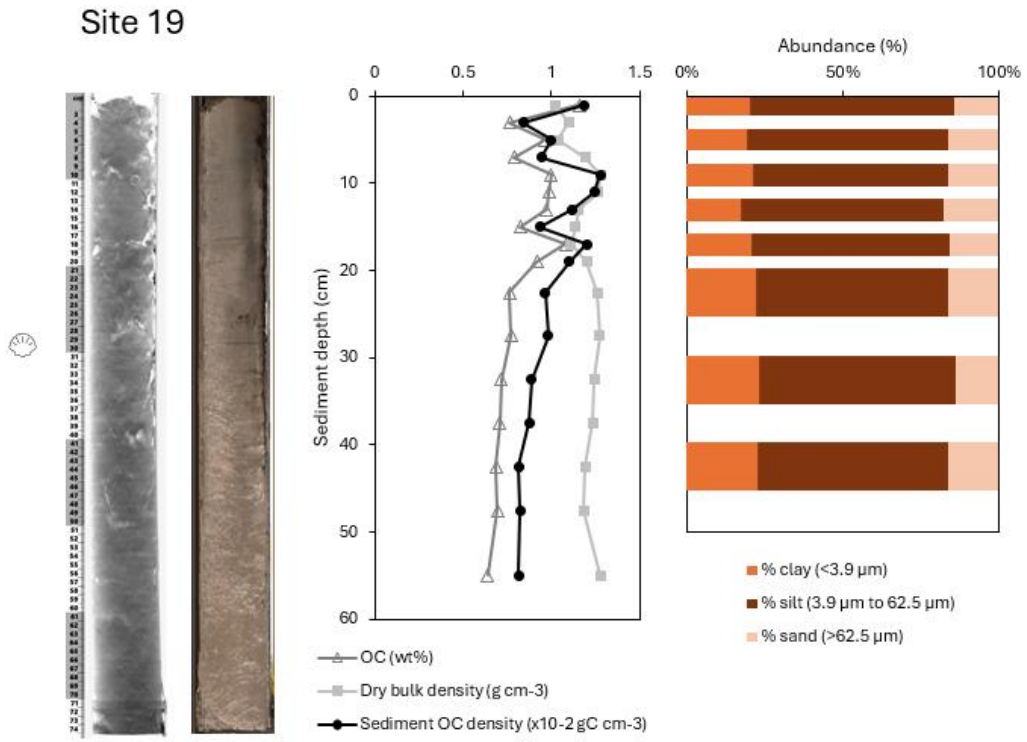

Figure A.15 Sediment depth profiles for Site 19. Left to right: X-ray radiograph; high-resolution colour image; organic carbon (OC) concentration (wt%), dry bulk density (g cm^{-3}), and sediment OC density (x10^{-2} gC cm^{-3}); and particle size distributions (% clay, % silt, % sand). Shell symbol (left) indicates the depth where whole shells or shell fragments were found (26–28 cm).

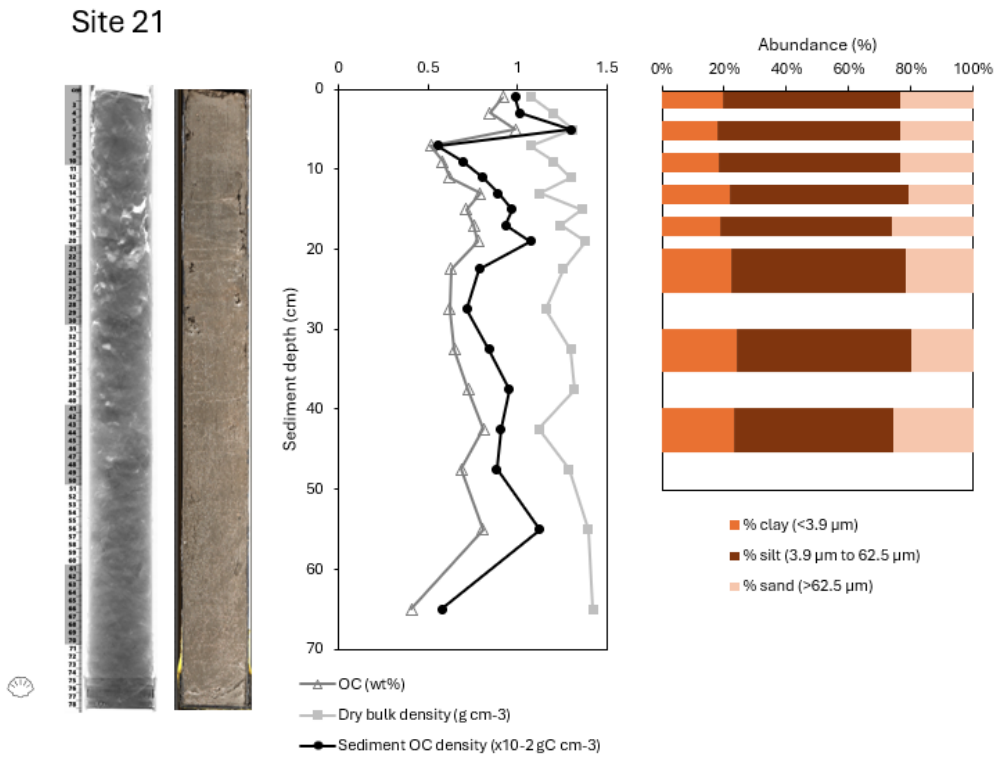

Figure A.16 Sediment depth profiles for Site 21. Left to right: X-ray radiograph; high-resolution colour image; organic carbon (OC) concentration (wt%), dry bulk density (g cm^{-3}), and sediment OC density (x10^{-2} gC cm^{-3}); and particle size distributions (% clay, % silt, % sand). Shell symbol (left) indicates depth where whole shells or shell fragments were found (75–77 cm). Shell fragments were found throughout core, but other depths were not noted.

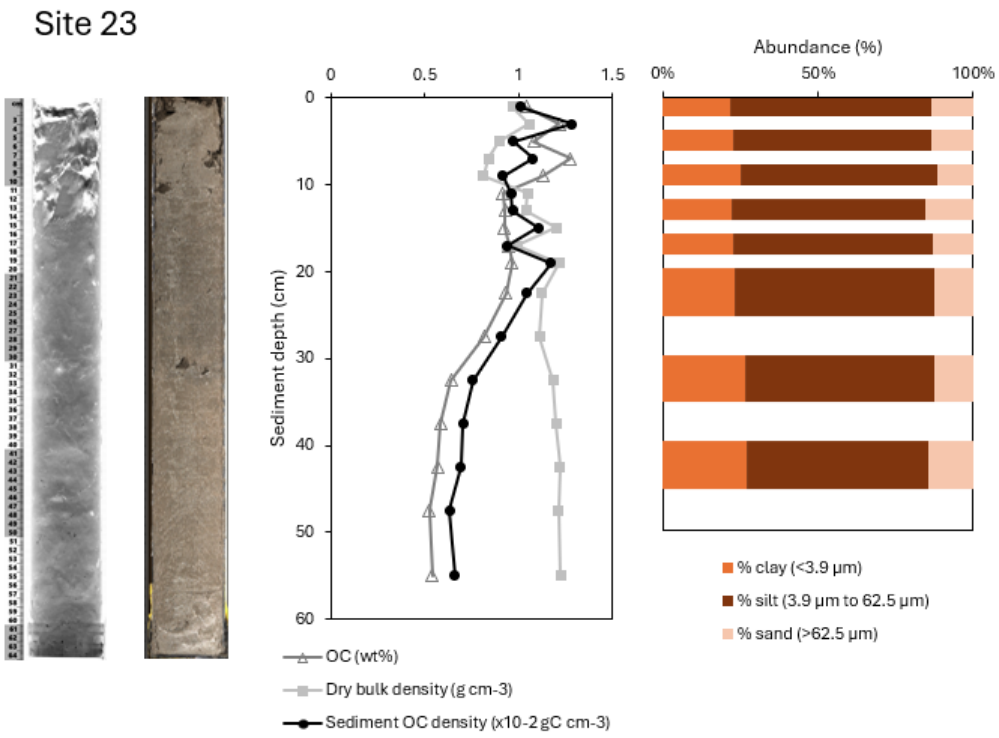

Figure A.17 Sediment depth profiles for Site 23. Left to right: X-ray radiograph; high-resolution colour image; organic carbon (OC) concentration (wt%), dry bulk density (g cm^{-3}), and sediment OC density (x10^{-2} gC cm^{-3}); and particle size distributions (% clay, % silt, % sand).

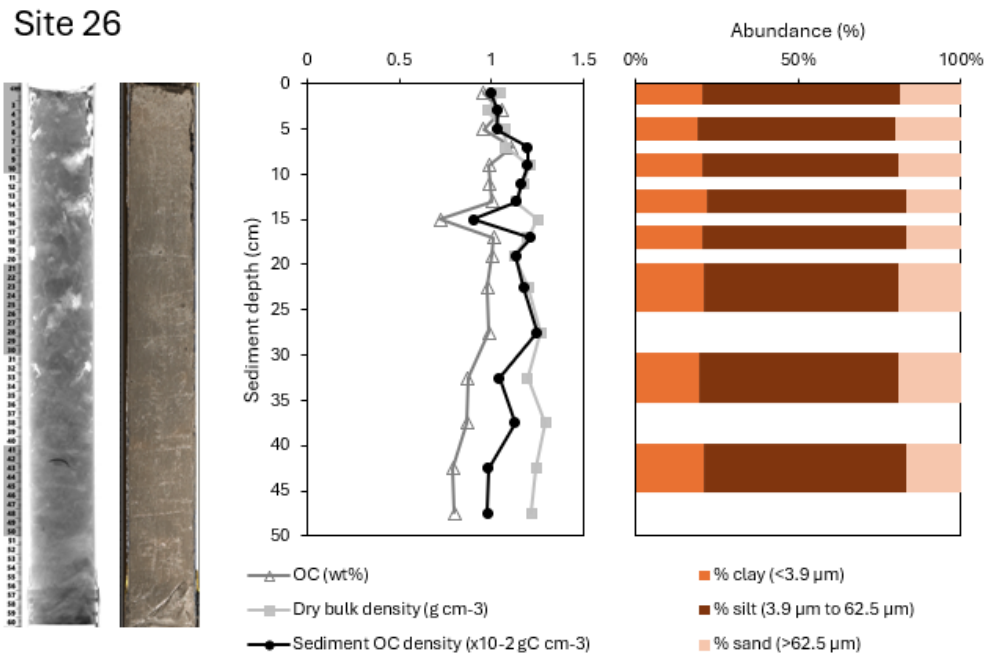

Figure A.18 Sediment depth profiles for Site 26. Left to right: X-ray radiograph; high-resolution colour image; organic carbon (OC) concentration (wt%), dry bulk density (g cm^{-3}), and sediment OC density (x10^{-2} gC cm^{-3}); and particle size distributions (% clay, % silt, % sand).

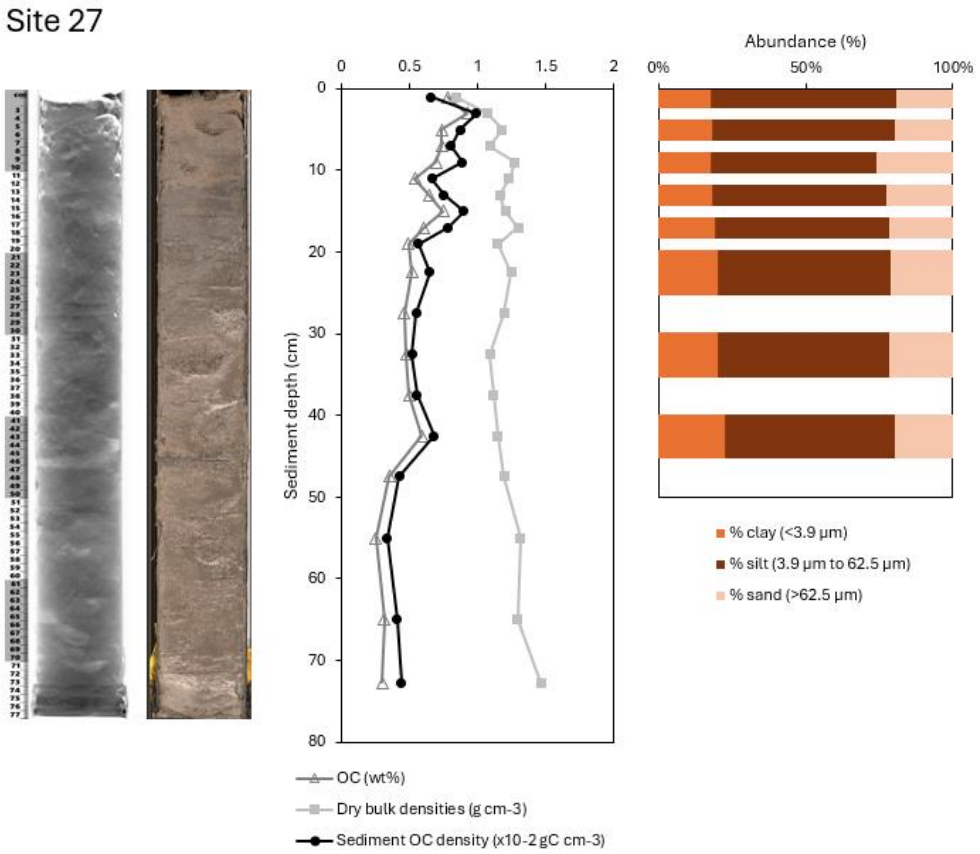

Figure A.19 Sediment depth profiles for Site 27. Left to right: X-ray radiograph; high-resolution colour image; organic carbon (OC) concentration (wt%), dry bulk density (g cm^{-3}), and sediment OC density (x10^{-2} gC cm^{-3}); and particle size distributions (% clay, % silt, % sand).

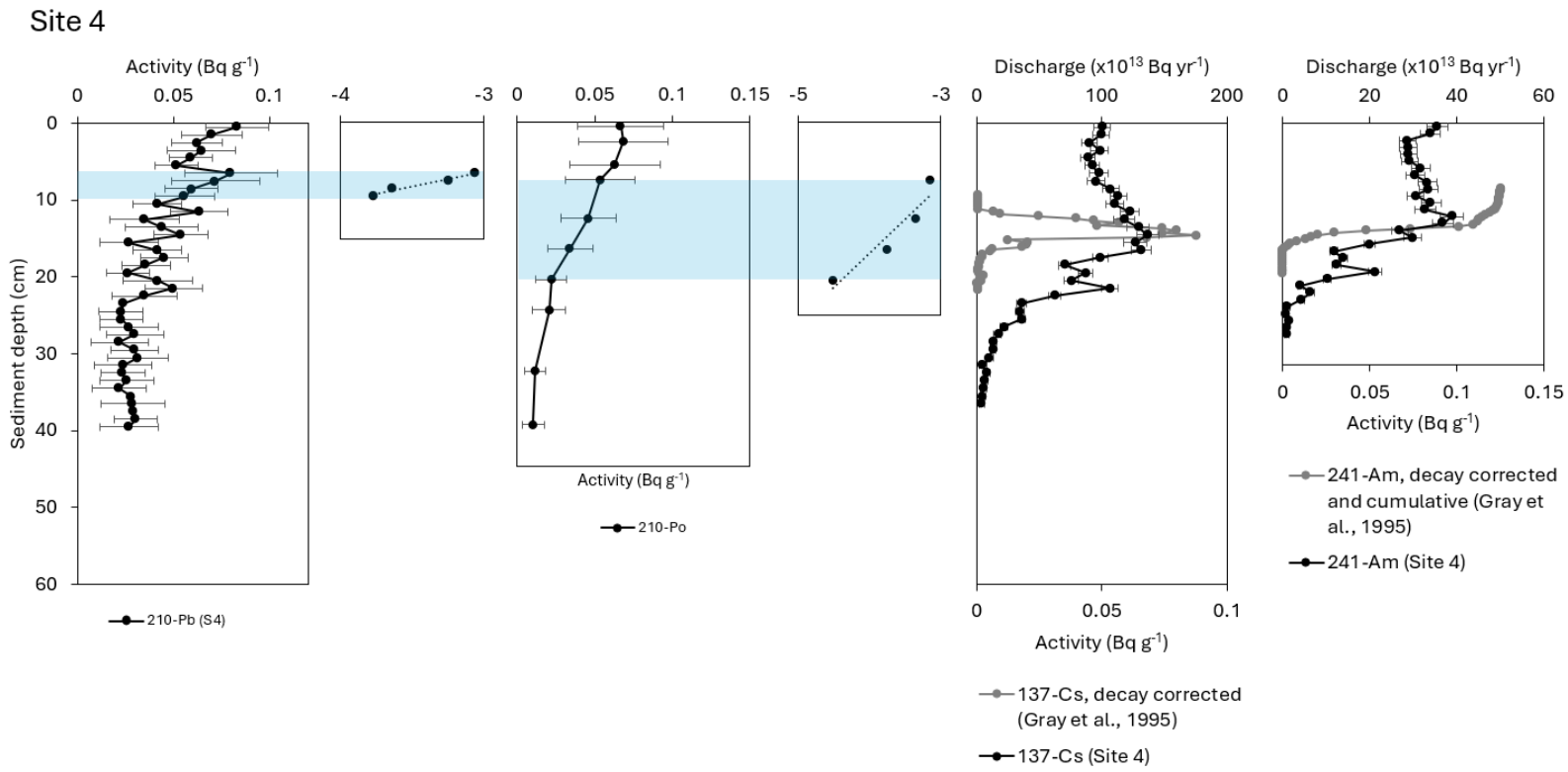

Figure A.20 Radionuclide profiles for Site 4. Left to right: ^{210}Pb activities; natural logarithm of excess ^{210}Pb activities; ^{210}Po activities; natural logarithm of excess ^{210}Po activities; ^{137}Cs activities (black, lower axis) and ^{137}Cs discharge profile from Sellafield nuclear facility (grey, upper axis) with 0.31 cm yr^{-1} sedimentation rate applied; ^{241}Am activities (black, lower axis) and cumulative ^{241}Am discharge profile from Sellafield nuclear facility (grey, upper axis) with 0.31 cm yr^{-1} sedimentation rate applied. Blue bands indicate the regions of data used for estimating sedimentation rates for ^{210}Po and ^{210}Pb.

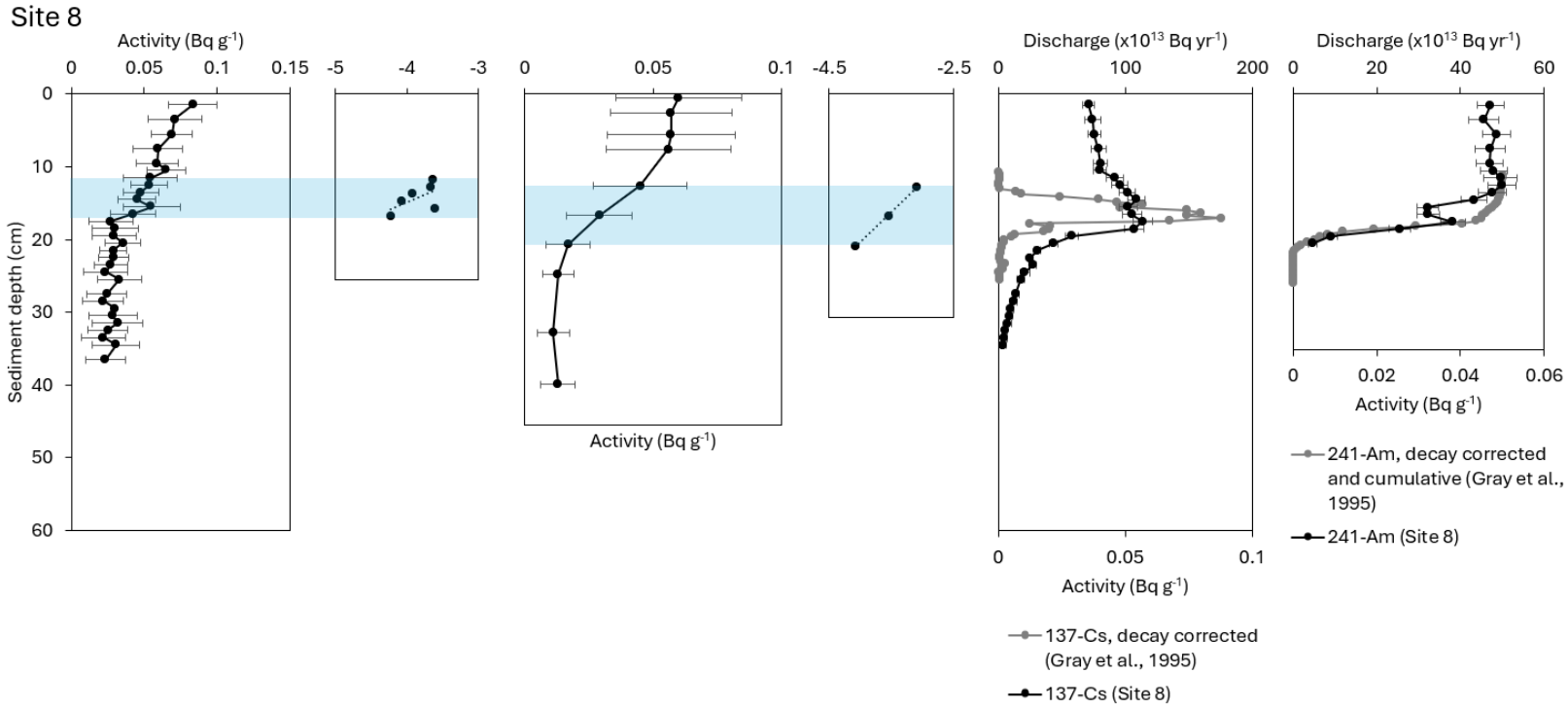

Figure A.21 Radionuclide profiles for Site 8. Left to right: ^{210}Pb activities; natural logarithm of excess ^{210}Pb activities; ^{210}Po activities; natural logarithm of excess ^{210}Po activities; ^{137}Cs activities (black, lower axis) and ^{137}Cs discharge profile from Sellafield nuclear facility (grey, upper axis) with 0.37 cm yr^{-1} sedimentation rate applied; ^{241}Am activities (black, lower axis) and cumulative ^{241}Am discharge profile from Sellafield nuclear facility (grey, upper axis) with 0.37 cm yr^{-1} sedimentation rate applied. Blue bands indicate the regions of data used for estimating sedimentation rates for ^{210}Po and ^{210}Pb.

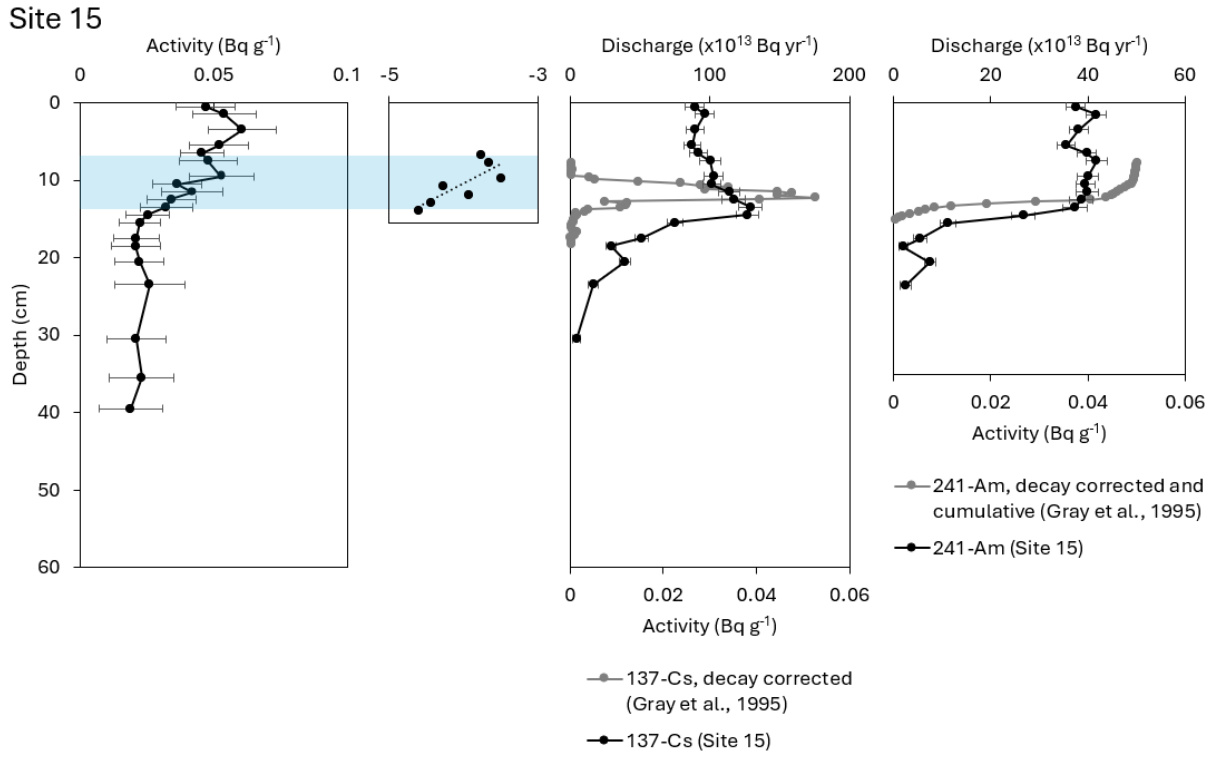

Figure A.22 Radionuclide profiles for Site 15. Left to right: ^{210}Pb activities; natural logarithm of excess ^{210}Pb activities; ^{137}Cs activities (black, lower axis) and ^{137}Cs discharge profile from Sellafield nuclear facility (grey, upper axis) with 0.26 cm yr^{-1} sedimentation rate applied; ^{241}Am activities (black, lower axis) and cumulative ^{241}Am discharge profile from Sellafield nuclear facility (grey, upper axis) with 0.26 cm yr^{-1} sedimentation rate applied. The blue band indicates the regions of data used for estimating sedimentation rates for ^{210}Po and ^{210}Pb.

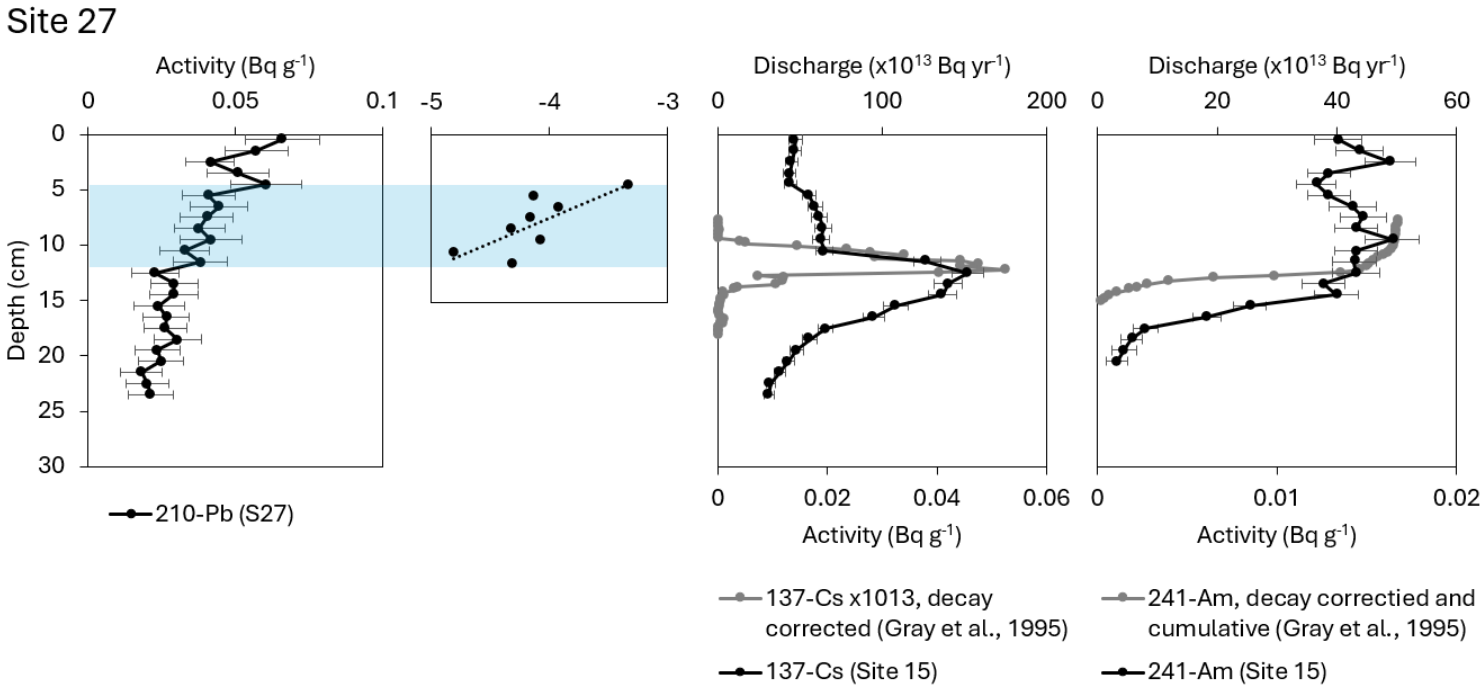

Figure A.23 Radionuclide profiles for Site 27. Left to right: ^{210}Pb activities; natural logarithm of excess ^{210}Pb activities; ^{137}Cs activities (black, lower axis) and ^{137}Cs discharge profile from Sellafield nuclear facility (grey, upper axis) with 0.26 cm yr^{-1} sedimentation rate applied; ^{241}Am activities (black, lower axis) and cumulative ^{241}Am discharge profile from Sellafield nuclear facility (grey, upper axis) with 0.26 cm yr^{-1} sedimentation rate applied. The blue band indicates the regions of data used for estimating sedimentation rates for ^{210}Po and ^{210}Pb.

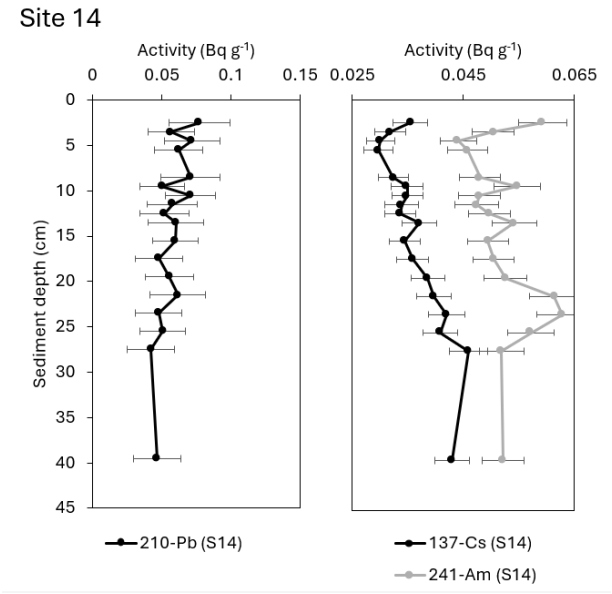

Figure A.24 Radionuclide profiles for Site 14. Left to right: ^{210}Pb activities; ^{137}Cs activities (black) and ^{241}Am activities (grey).

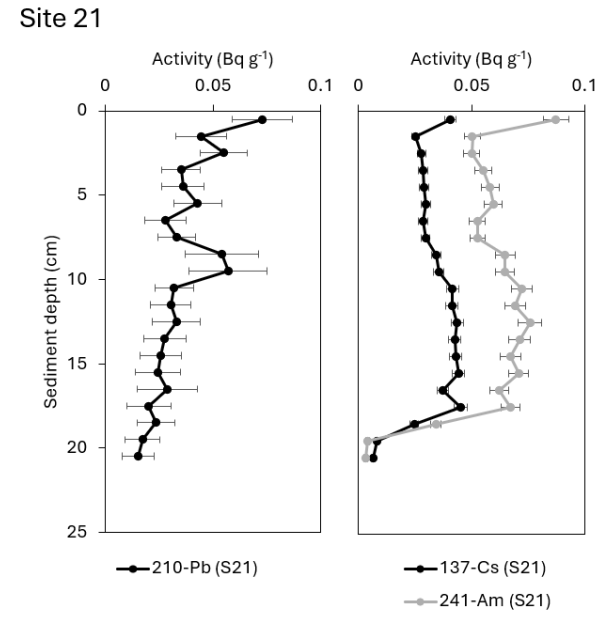

Figure A.25 Radionuclide profiles for Site 21. Left to right: ^{210}Pb activities; ^{137}Cs activities (black) and ^{241}Am activities (grey).

Table A.1 The average proportion (%) of clay (<3.9 μm), silt (3.9 μm to 62.5 μm), mud (clay + silt, <3.9 μm to 62.5 μm), and sand (62.5 μm to 2000 μm) for 0–10 cm and 0–50 cm for each sampling location (Site ID) in the Western Irish Sea Mud Belt study region, based on Udden (1914) and Wentworth (1922). Sediment classifications are based on the Folk (1954) classification scheme. Site 6b was unclassified, as it had a high fraction of particles >1000 μm after sieving, which could be attributed to sand or gravel (unresolved).

Site ID	Sediment depth (cm)	Clay (%)	Silt (%)	Mud (%)	Sand (%)	Folk class
Site 8	0-10	27.12	67.49	94.61	5.39	Mud
	0-50	26.39	67.06	93.45	6.55	Mud
Site 14	0-10	24.08	66.72	90.8	9.19	Mud
	0-50	23.89	67.26	91.15	8.85	Mud
Site 5	0-10	29.12	66.81	95.93	4.07	Mud
	0-50	31.02	65.11	96.13	3.87	Mud
Site 3	0-10	29.18	66.1	95.28	4.72	Mud
	0-50	29.6	65.79	95.39	4.62	Mud
Site 27	0-10	17.76	60.57	78.33	21.67	Sandy mud
	0-50	19.21	59.29	78.5	21.5	Sandy mud
Site 20	0-10	20.45	62.51	82.97	17.03	Sandy mud
	0-50	21.03	62.4	83.43	16.57	Sandy mud
Site 21	0-10	18.46	58.18	76.63	23.37	Sandy mud
	0-50	20.65	56.3	76.95	23.05	Sandy mud
Site 10	0-10	19.38	66.92	86.3	13.7	Sandy mud
	0-50	21.99	66.53	88.53	11.48	Sandy mud
Site 18	0-10	19.26	64.77	84.03	15.97	Sandy mud
	0-50	21	63.95	84.95	15.05	Sandy mud
Site 12b	0-10	22.87	61.65	84.52	15.48	Sandy mud
	0-50	24.6	60.96	85.56	14.44	Sandy mud

Site 17	0-10	19	61.37	80.37	19.62	Sandy mud
	0-50	21.15	61.3	82.45	17.55	Sandy mud
Site 16	0-10	20.01	59.26	79.27	20.73	Sandy mud
	0-50	22.33	59.55	81.88	18.12	Sandy mud
Site 23	0-10	23.06	63.98	87.04	12.96	Sandy mud
	0-50	23.86	62.85	86.71	13.29	Sandy mud
Site 15	0-10	23.07	62.63	85.7	14.3	Sandy mud
	0-50	24.07	62.72	86.79	13.2	Sandy mud
Site 4	0-10	30.36	65.21	95.57	4.43	Mud
	0-50	31.41	64.38	95.79	4.21	Mud
Site 19	0-10	20.23	64.21	84.44	15.56	Sandy mud
	0-50	20.83	63.39	84.22	15.79	Sandy mud
Site 26	0-10	20.05	60.7	80.75	19.25	Sandy mud
	0-50	20.42	61.29	81.71	18.29	Sandy mud
Site 13	0-10	26	66.44	92.44	7.56	Mud
	0-50	27.39	66.02	93.41	6.59	Mud
Site 2c	0-10	18.5	49.62	68.12	31.74	Sandy mud
	0-50	21.53	50.24	71.77	27.95	Sandy mud
Site 6b	0-10	32.2	49.17	81.37	13.33	Unclassified
	0-50	24.89	43.66	68.55	20.61	Unclassified

Table A.2 Mean sedimentation rates and their range (2 sigma) estimated from ^{210}Pb, ^{210}Po, and ^{137}Cs radioisotope data. *The range (1 sigma) is given for Site 8 ^{210}Pb radioisotope data, as the 2 sigma error calculation wasn't possible due to poor fit.

Site	Mean rate (Range), ^{210}Pb (cm yr^{-1})	Mean rate (Range), ^{210}Po (cm yr^{-1})	Mean rate, ^{137}Cs (cm yr^{-1})
4	0.12 (0.07–0.28)	0.32 (0.22–0.61)	0.31
8	0.37 (0.21–1.55)*	0.26 (0.15–0.89)	0.37
15	0.23 (0.13–2.08)	-	0.29
20	0.35 (0.20–1.44)	0.23 (0.14–0.61)	0.29
27	0.24 (0.13–1.53)	-	0.29

Appendix B

Stratigraphic Evidence of Organic Carbon Depletion in an Intensely Trawled Muddy Seabed

Table B.1 Gear codes and type, their benthic footprint (yes or no), and their inclusion/exclusion from the dataset used to generate fishing pressure maps.

Gear code	Full gear type (métier)	Benthic footprint	Included
DRB	Boat dredge	Yes	Yes
FPO	Pots and traps	Yes	No
GND	Driftnet	No	No
GNS	Set gillnet	No	No
HMD	Mechanised/suction dredge	Yes	No
LHP	Hand and pole lines (hand-operated)	No	No
LL	Drifting longlines	No	No
LLS	Set longlines	No	No
NOT KNOWN	Not known	No	No
OTB	Bottom otter trawl	Yes	Yes
OTM	Midwater otter trawl	No	No
OTT	Multi-rig otter trawl	Yes	Yes
PS	Purse seine	No	No
PTB	Bottom pair trawl	Yes	Yes
PTM	Pelagic pair trawl	No	No
SPR	Pair seine	No	No
SSC	Scottish seine (fly dragging)	Yes	No
TB	Beam trawl	Yes	Yes
TBB	Beam trawl	Yes	Yes
TBN	Beam trawl	Yes	Yes

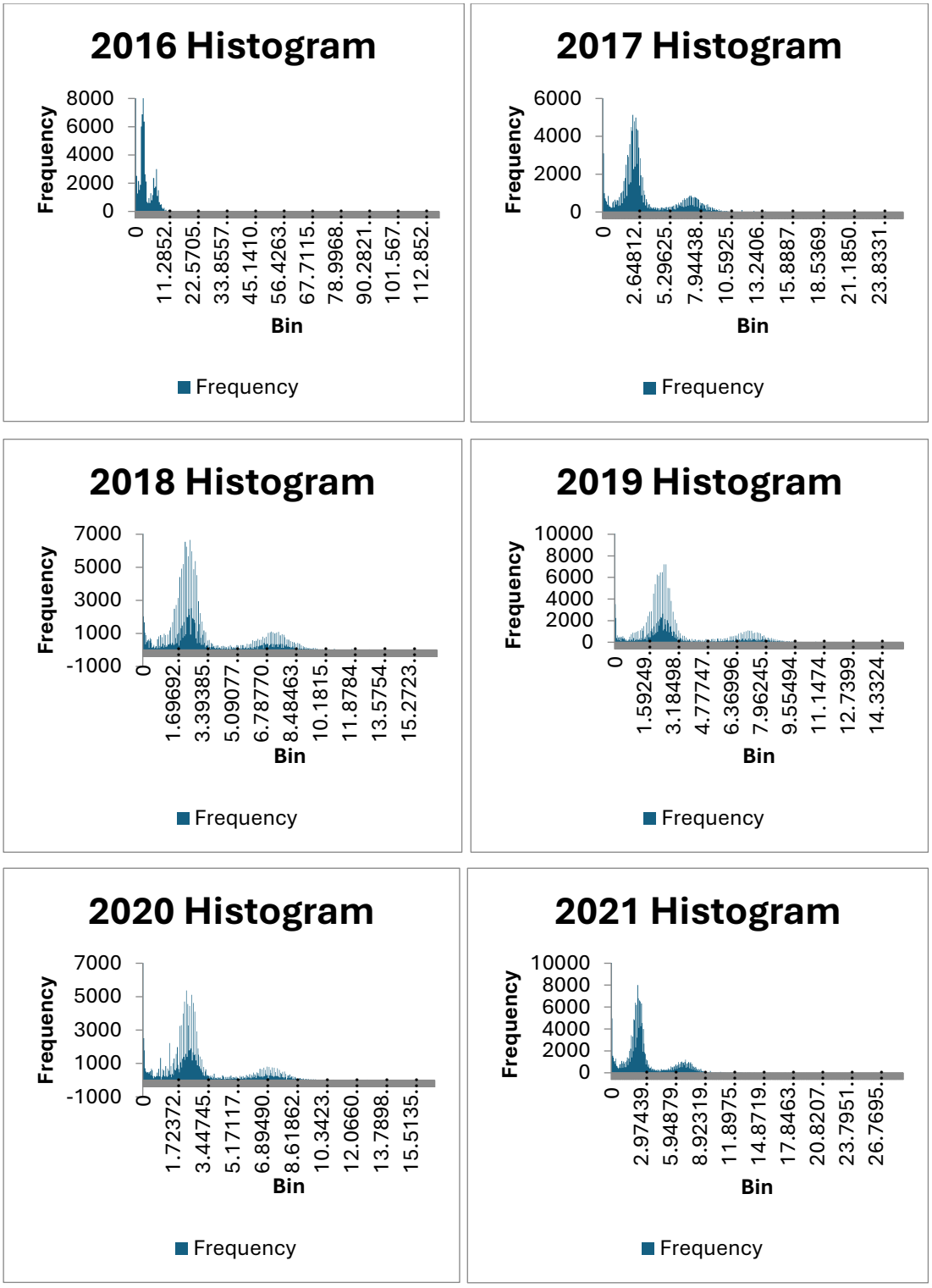

Figure B.1 Histograms of vessel speeds (kt) on the x-axis ('Bin') for the years 2016–2021.

Table B.2 Comparison between seabed surface and subsurface abrasion estimated for different gears, as advised by the Joint Nature Conservation Committee (JNCC) (Church et al., 2016).

	Surface			**Subsurface**			**Surface - Subsurface**
	Minimum	Maximum	Proposed	Minimum	Maximum	Proposed	Change (Proposed)
	Width (m)	**Width (m)**	**Width (m)**	**Width (m)**	**Width (m)**	**Width (m)**	**Width (m)**
Dredge	6.8	23.8	12	6.8	23.8	12	0
***Nephrops* trawl**	50	100	60	0.5	4	2	-58
Otter trawl	50	100	60	0.5	4	2	-58
Otter trawl twin	60	200	100	1	5	3	-97
Demersal	50	100	60	0.5	4	2	-58
Pair trawl and Seine	200	300	250	N/A	N/A	N/A	N/A
Beam	8	24	18	8	24	18	0

Table B.3 Data for sediment depths 0–10 cm, 10–20 cm, 20–30 cm, 30–40 cm, and 40–50 cm: Sampling Site ID; Sediment dry bulk density (DBD, g cm^{-3}); Organic carbon concentration (OC, %); Sediment carbon density (SCD, gC cm^{-3}); Average proportion (%) of mud (clay + silt, <3.9 μm to 62.5 μm), clay (<3.9 μm), silt (3.9 μm to 62.5 μm), and sand (62.5 μm to 2000 μm).

Site ID	Depth (cm)	DBD (g cm^{-3})	OC (%)	SCD (gC cm^{-3})	Mud (%)	Clay (%)	Silt (%)	Sand (%)
3	0–10	0.88	1.43	0.01	95.28	29.18	66.10	4.72
	10–20	0.87	1.31	0.01	94.24	28.20	66.05	5.76
	20–30	0.91	1.12	0.01	95.81	28.29	67.52	4.18
	30–40	0.85	0.96	0.01	96.59	31.81	64.78	3.41
	40–50	1.03	0.92	0.01	96.36	32.76	63.60	3.64
4	0–10	0.86	1.41	0.01	95.57	30.36	65.21	4.43
	10–20	0.85	1.32	0.01	95.92	31.34	64.58	4.09
	20–30	0.79	1.14	0.01	96.11	30.61	65.50	3.88
	30–40	0.92	0.93	0.01	95.90	32.37	63.53	4.10
	40–50	0.96	0.86	0.01	87.92	26.21	61.71	12.08
5	0–10	0.78	1.48	0.01	95.93	29.12	66.81	4.07
	10–20	0.85	1.31	0.01	96.10	30.04	66.06	3.91
	20–30	0.93	1.11	0.01	95.76	34.37	61.39	4.24
	30–40	0.91	1.04	0.01	96.40	32.77	63.63	3.61
	40–50	0.91	1.01	0.01	96.91	33.59	63.32	3.09
8	0–10	0.87	1.59	0.01	94.61	27.12	67.49	5.39
	10–20	0.88	1.35	0.01	88.48	21.30	67.18	11.53
	20–30	0.83	1.11	0.01	93.60	26.32	67.28	6.40
	30–40	0.85	1.01	0.01	97.93	34.29	63.64	2.07
	40–50	0.92	0.99	0.01	95.31	26.55	68.76	4.69
10	0–10	1.05	1.00	0.01	86.30	19.38	66.92	13.70
	10–20	1.19	0.86	0.01	88.71	19.91	68.80	11.30
	20–30	1.18	0.67	0.01	91.70	24.15	67.55	8.30
	30–40	1.13	0.69	0.01	90.41	26.27	64.14	9.60

	40–50	1.23	0.72	0.01	89.76	27.55	62.21	10.24
13	0–10	0.80	1.29	0.01	92.44	26.00	66.44	7.56
	10–20	0.60	1.18	0.01	93.11	27.01	66.11	6.89
	20–30	0.55	1.24	0.01	94.17	26.80	67.37	5.83
	30–40	1.02	0.86	0.01	94.27	29.14	65.13	5.73
	40–50	1.02	0.99	0.01	95.28	31.17	64.11	4.73
14	0–10	0.80	1.32	0.01	90.80	24.08	66.72	9.19
	10–20	0.86	1.36	0.01	89.09	21.74	67.35	10.91
	20–30	0.89	1.38	0.01	92.79	27.45	65.34	7.20
	30–40	0.89	1.32	0.01	92.92	22.84	70.08	7.08
	40–50	1.05	1.22	0.01	92.90	25.14	67.76	7.10
15	0–10	1.00	0.89	0.01	85.70	23.07	62.63	14.30
	10–20	1.10	0.75	0.01	85.91	21.70	64.22	14.09
	20–30	1.04	0.74	0.01	87.99	25.71	62.28	12.00
	30–40	1.09	0.53	0.01	89.51	28.03	61.48	10.48
	40–50	1.08	0.50	0.01	95.74	34.55	61.19	4.26
16	0–10	1.10	0.84	0.01	79.27	20.01	59.26	20.73
	10–20	0.90	0.82	0.01	86.36	23.39	62.98	13.64
	20–30	1.26	0.48	0.01	83.03	24.10	58.93	16.97
	30–40	1.25	0.41	0.01	79.10	22.32	56.78	20.91
	40–50	1.26	0.45	0.01	82.35	25.42	56.93	17.65
17	0–10	1.06	1.01	0.01	80.37	19.00	61.37	19.62
	10–20	1.15	0.84	0.01	83.29	21.95	61.34	16.71
	20–30	1.33	0.58	0.01	85.66	23.44	62.22	14.34
	30–40	1.16	0.65	0.01	83.57	23.18	60.39	16.43
	40–50	1.27	0.57	0.01	82.64	21.68	60.96	17.36
18	0–10	1.11	0.98	0.01	84.03	19.26	64.77	15.97
	10–20	1.17	0.94	0.01	85.33	21.35	63.98	14.68
	20–30	1.27	0.76	0.01	85.08	22.38	62.70	14.92
	30–40	1.21	0.61	0.01	84.71	22.04	62.67	15.29

	40–50	1.18	0.61	0.01	87.06	23.08	63.98	12.95
19	0–10	1.13	0.94	0.01	84.44	20.23	64.21	15.56
	10–20	1.17	0.96	0.01	83.49	18.88	64.61	16.51
	20–30	1.27	0.77	0.01	83.74	22.25	61.49	16.27
	30–40	1.24	0.71	0.01	86.04	23.20	62.84	13.97
	40–50	1.19	0.69	0.01	83.66	22.73	60.93	16.34
20	0–10	1.08	0.92	0.01	82.97	20.45	62.51	17.03
	10–20	1.23	0.83	0.01	85.13	20.12	65.01	14.87
	20–30	1.25	0.70	0.01	84.65	22.23	62.42	15.34
	30–40	1.24	0.48	0.01	82.55	22.23	60.32	17.45
	40–50	1.25	0.49	0.01	81.08	22.17	58.91	18.92
21	0–10	1.17	0.77	0.01	76.63	18.46	58.18	23.37
	10–20	1.28	0.73	0.01	76.48	20.27	56.21	23.53
	20–30	1.21	0.62	0.01	78.26	22.13	56.13	21.73
	30–40	1.31	0.69	0.01	80.19	23.85	56.34	19.81
	40–50	1.20	0.75	0.01	74.31	23.32	50.99	25.69
23	0–10	0.92	1.15	0.01	87.04	23.06	63.98	12.96
	10–20	1.10	0.94	0.01	86.06	22.47	63.59	13.94
	20–30	1.12	0.87	0.01	87.50	23.06	64.44	12.50
	30–40	1.19	0.61	0.01	87.40	26.71	60.69	12.60
	40–50	1.22	0.55	0.01	85.56	27.02	58.54	14.44
26	0–10	1.08	1.01	0.01	80.75	20.05	60.70	19.25
	10–20	1.18	0.95	0.01	83.15	21.06	62.09	16.85
	20–30	1.23	0.98	0.01	81.00	20.76	60.24	19.00
	30–40	1.25	0.87	0.01	80.68	19.30	61.38	19.32
	40–50	1.23	0.80	0.01	83.46	21.05	62.41	16.54
27	0–10	1.09	0.78	0.01	78.33	17.76	60.57	21.67
	10–20	1.21	0.60	0.01	77.81	18.79	59.02	22.20
	20–30	1.22	0.49	0.01	78.88	20.29	58.59	21.12
	30–40	1.10	0.49	0.01	78.48	20.10	58.38	21.51

	40–50	1.17	0.47	0.01	80.05	22.46	57.59	19.95
12b	0–10	0.96	1.06	0.01	84.52	22.87	61.65	15.48
	10–20	1.08	0.75	0.01	87.81	25.89	61.92	12.19
	20–30	1.18	0.62	0.01	86.74	26.04	60.70	13.27
	30–40	1.17	0.65	0.01	84.58	25.70	58.88	15.42
	40–50	1.22	0.51	0.01	84.00	24.68	59.32	16.00
2c	0–10	1.08	0.62	0.01	68.12	18.50	49.62	31.74
	10–20	1.30	0.63	0.01	79.35	24.74	54.61	20.59
	20–30	1.36	0.48	0.01	75.01	23.19	51.81	24.33
	30–40	1.39	0.47	0.01	67.76	21.46	46.30	31.77
	40–50	1.52	0.48	0.01	68.35	22.60	45.75	31.12
6b	0–10	1.22	0.23	0.00	81.37	32.20	49.17	13.33
	10–20	0.76	0.21	0.00	44.48	16.22	28.26	28.98
	20–30	1.30	0.22	0.00	59.82	20.95	38.87	26.56
	30–40	1.25	0.36	0.00	76.31	25.07	51.24	20.20
	40–50	1.20	0.57	0.01	79.22	24.04	55.18	20.16

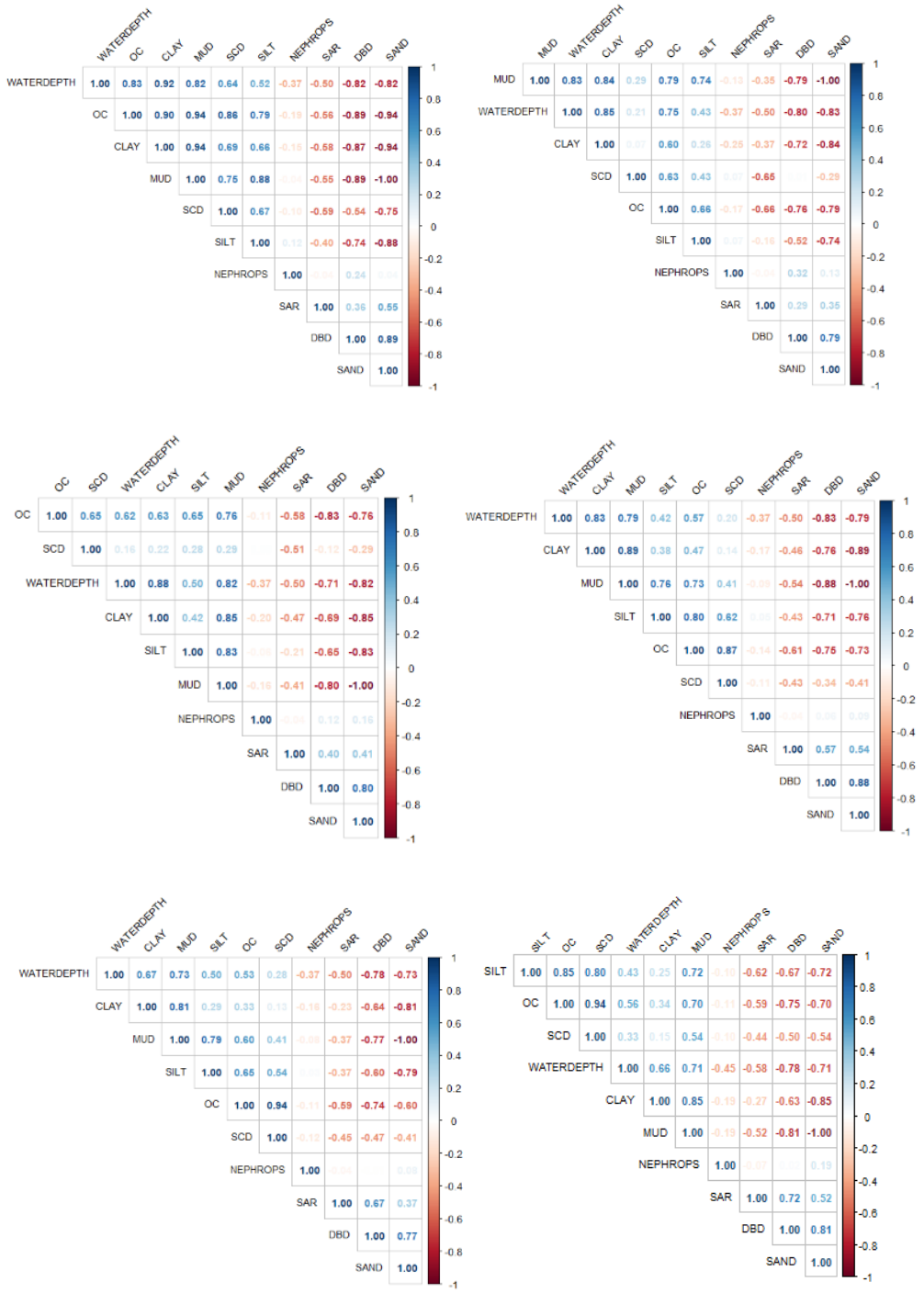

Figure B.2 Correlograms of Pearson's correlations coefficients (blue = positive, red = negative) at 95% significance for 0–10 cm, 10–20 cm, 20–30 cm, 30–40 cm, and 40–50 cm sediment depths. OC = organic carbon content (%); SCD = sediment organic carbon density (gC cm^{-3}); WATERDEPTH = water depth (m); NEPHROPS = Nephrops norvegicus burrow densities (m^{-2}); SAR = swept area ratio (yr^{-1}); DBD = sediment dry bulk density (g cm^{-3}); CLAY = clay (%); SILT = silt (%); and SAND = sand (%).

General Linear Model Validation (methods)

Model validation was performed to check that the assumptions of the selected model were met. A frequency distribution histogram and a Q-Q (quantile-quantile) plot of the of the sresids were plotted to check the sresids were normally distributed. A Shapiro-Wilk test for normality was also used to check the sresids were normally distributed. A graph of sresids versus the fitted values was plotted to check for homoscedasticity of the standardised residuals, i.e. that the variances of the sresids were homogenous across the range of fitted values of the dependent variable. A Breusch–Pagan test was run to validate these results for homoscedasticity.

General Linear Model Validation (results)

The assumption of normality was met for models at all sediment depths, whereby sresids were normally distributed at all sediment depths (Appendix Figure B.3), which was corroborated by plots of the residuals versus fitted values and quantile–quantile (Q–Q) plots of the theoretical quantiles versus sresids (Appendix Figure B.4–B.9). Shapiro–Wilk tests confirmed deviations from normality, which were observed as slight left (negative) skewed and right (positive) skewed tails, were insignificant ($p > 0.05$) (Appendix Table B.5). A Breusch–Pagan test for homoscedasticity confirmed that the assumption of homoscedasticity was met for models for all sediment depths ($p > 0.05$) (Appendix Table B.6), despite a degree of non-linearity and heteroscedasticity in some models (Appendix Figure B.4–B.9). There were no extreme, highly influential values in the regression models down to 40; however, observation 7 (Site 21) was highly influential at 40–50 cm, due to its relatively low silt content (50.99%), representing a rare but valid condition in the dataset (average silt content = 61.29% ± 4.06%; Appendix Figure B.8). Therefore, data for Site 21 was removed from the dataset for sediment depth 40–50 cm, acknowledging its role in contributing to heteroscedasticity in the model reflecting real-world variability in silt content at the edge of the WISMB.

Table B.4 Variance Inflation Factors (VIFs) for the models.

	Variance Inflation Factors			
Sediment depth (cm)	***Nephrops norvegicus***	**SAR**	**Clay**	**Silt**
0–10	1.147443	1.542155	2.513934	1.930121
10–20	1.110017	1.191555	1.345088	1.095214
20–30	1.072765	1.318400	1.590770	1.215956
30–40	1.060958	1.427065	1.411639	1.305461
40–50	1.035309	1.183166	1.152591	1.225897
40–50 (outlier removed)	1.088991	1.729810	1.135170	1.688084

Table B.5 Results of the Shapiro-Wilk test for normality for the models. Significance at p-value < 0.05 (non-normal distribution).

Sediment depth (cm)	**Shapiro-Wilk statistics**
0–10	W = 0.94615, p-value = 0.3679
10–20	W = 0.97252, p-value = 0.8436
20–30	W = 0.90717, p-value = 0.0767
30–40	W = 0.97643, p-value = 0.9059
40–50	W = 0.94533, p-value = 0.3565
40–50 (outlier removed)	W = 0.91782, p-value = 0.1357

Table B.6 Breusch-Pagan test for homoscedasticity. Significance at p < 0.05 indicates heteroscedasticity in the model.

Sediment depth (cm)	**Breusch-Pagan values**
0–10	BP = 1.2865, df = 4, p-value = 0.8637
10–20	BP = 0.71106, df = 4, p-value = 0.95
20–30	BP = 1.483, df = 4, p-value = 0.8297
30–40	BP = 3.9099, df = 4, p-value = 0.4183
40–50	BP = 1.8587, df = 4, p-value = 0.7617
40–50 (outlier removed)	BP = 3.7466, df = 4, p-value = 0.4414

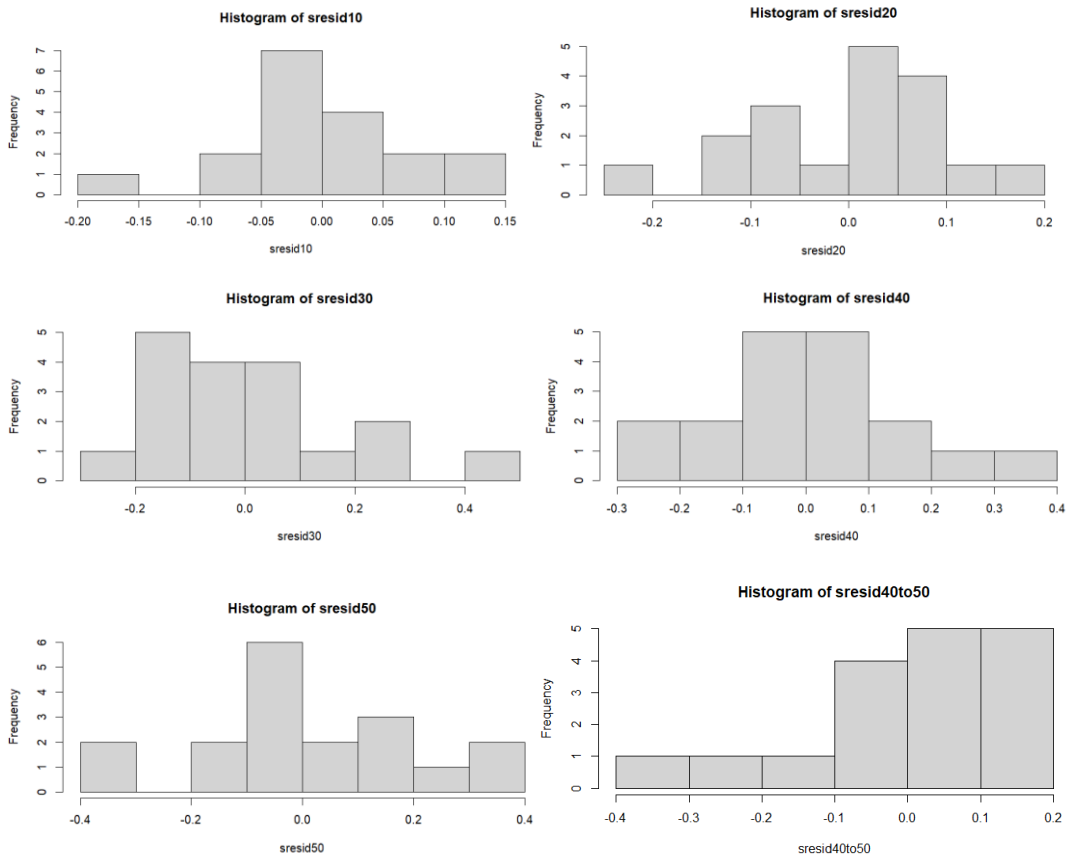

Figure B.3 Frequency distribution histograms for the standardised residuals (sresids) for the models with dependent variable as log-transformed organic carbon (OC) concentration (%) and independent variables swept area ratio (SAR, yr^{-1}), *Nephrops norvegicus* burrow densities (m^{-2}), silt content (%), and clay content (%), for sediment depths 0–10 cm, 10–20 cm, 20–30 cm, 30–40 cm, 40–50 cm, and 40–50 cm (outlier removed).

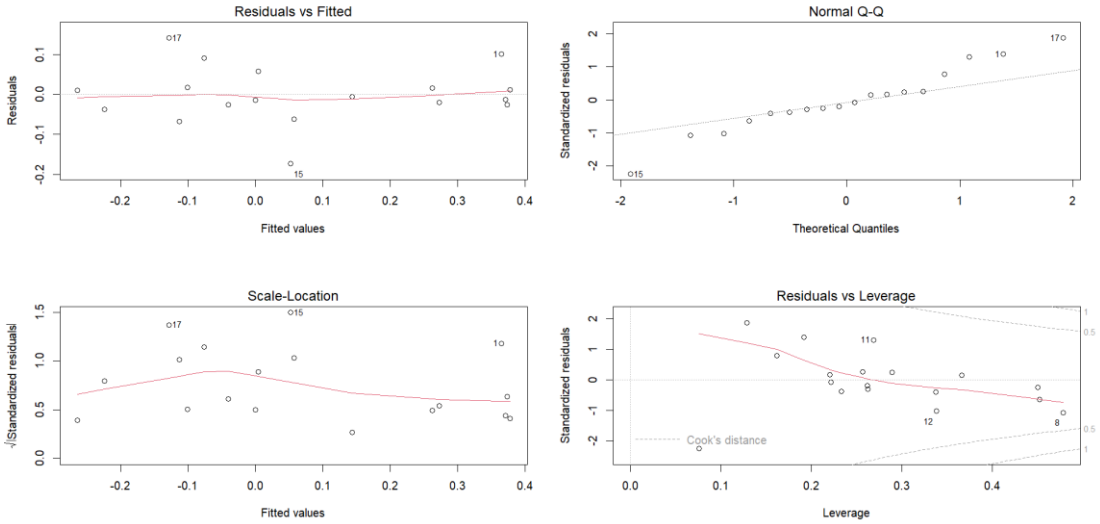

Figure B.4 Model validation plots for the 0–10 cm sediment depth. A plot of the residuals versus fitted values (top left), a Q-Q (quantile-quantile) plot of the theoretical quantiles versus standardised residuals (sresids) (top right), scale-location plot of the fitted values of the regression model versus square root of the sresids (bottom left), and a plot of the leverage versus sresids with Cook's distance boundaries (bottom right).

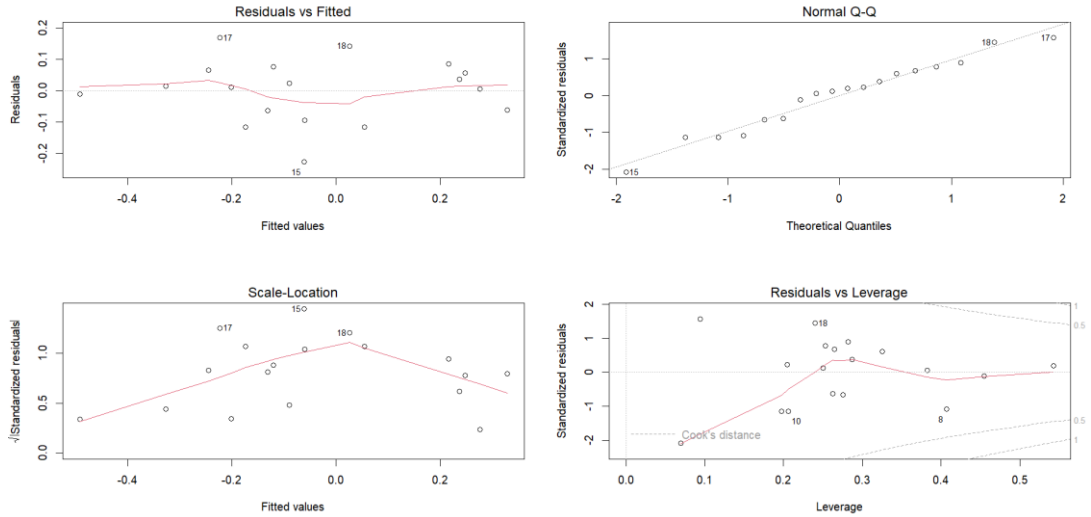

Figure B.5 Model validation plots for 10–20 cm sediment depth. A plot of the residuals versus fitted values (top left), a Q-Q (quantile-quantile) plot of the theoretical quantiles versus standardised residuals (sresids) (top right), scale-location plot of the fitted values of the regression model versus square root of the sresids (bottom left), and a plot of the leverage versus sresids with Cook's distance boundaries (bottom right).

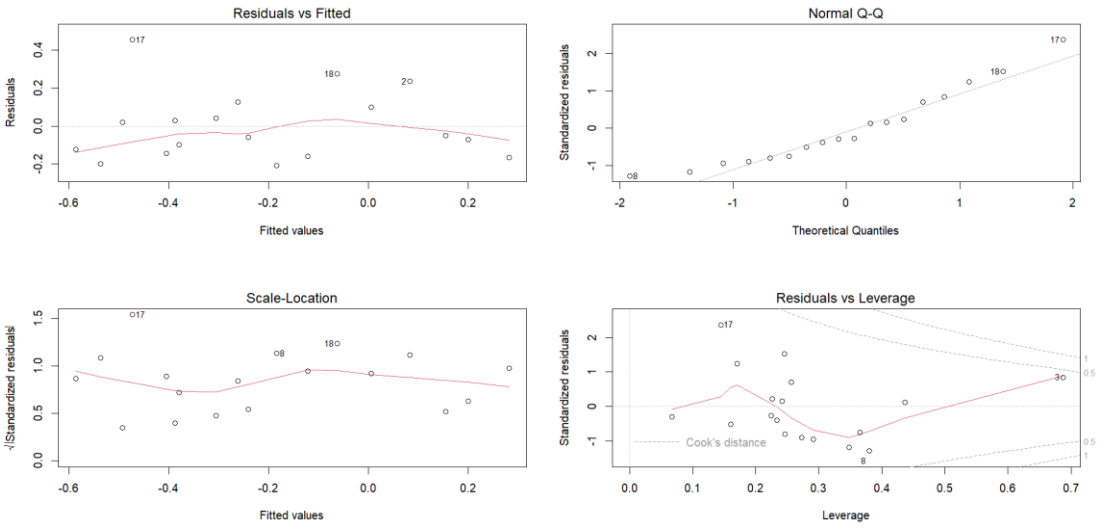

Figure B.6 Model validation plots for 20–30 cm sediment depth. A plot of the residuals versus fitted values (top left), a Q-Q (quantile-quantile) plot of the theoretical quantiles versus standardised residuals (sresids) (top right), scale-location plot of the fitted values of the regression model versus square root of the sresids (bottom left), and a plot of the leverage versus sresids with Cook's distance boundaries (bottom right).

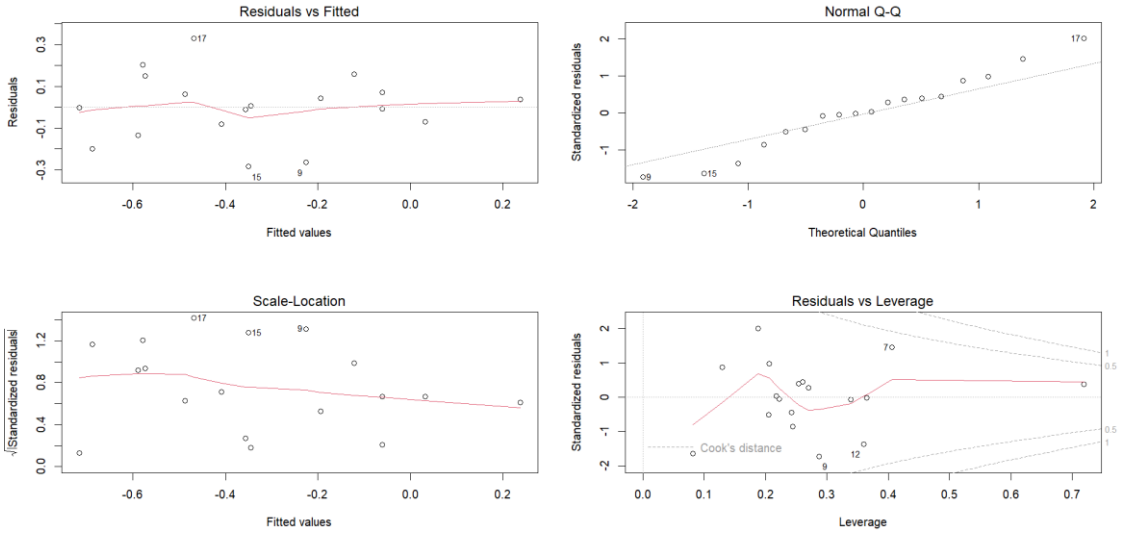

Figure B.7 Model validation plots for 30–40 cm sediment depth. A plot of the residuals versus fitted values (top left), a Q-Q (quantile-quantile) plot of the theoretical quantiles versus standardised residuals (sresids) (top right), scale-location plot of the fitted values of the regression model versus square root of the sresids (bottom left), and a plot of the leverage versus sresids with Cook's distance boundaries (bottom right).

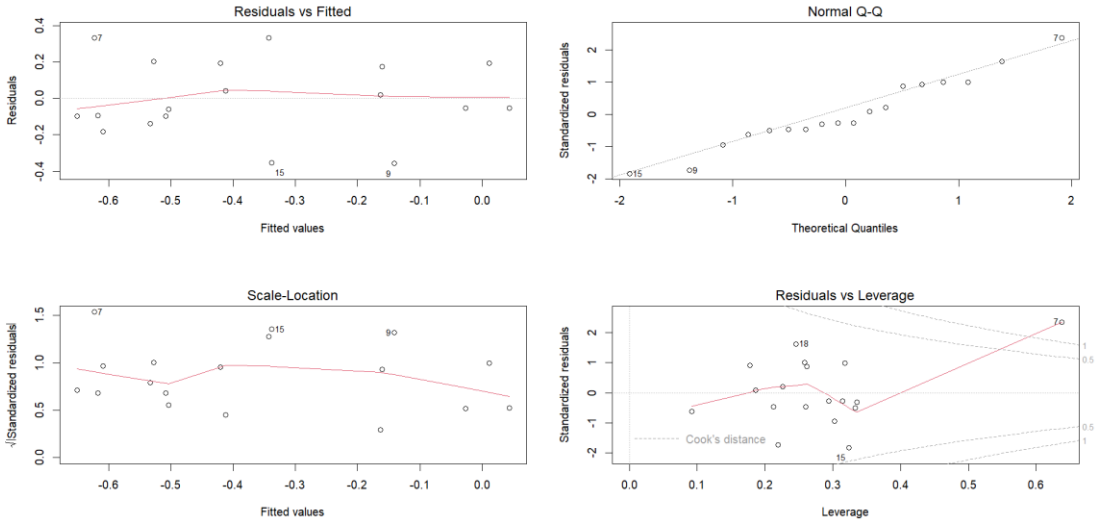

Figure B.8 Model validation plots for 40–50 cm sediment depth. A plot of the residuals versus fitted values (top left), a Q-Q (quantile-quantile) plot of the theoretical quantiles versus standardised residuals (sresids) (top right), scale-location plot of the fitted values of the regression model versus square root of the sresids (bottom left), and a plot of the leverage versus sresids with Cook's distance boundaries (bottom right).

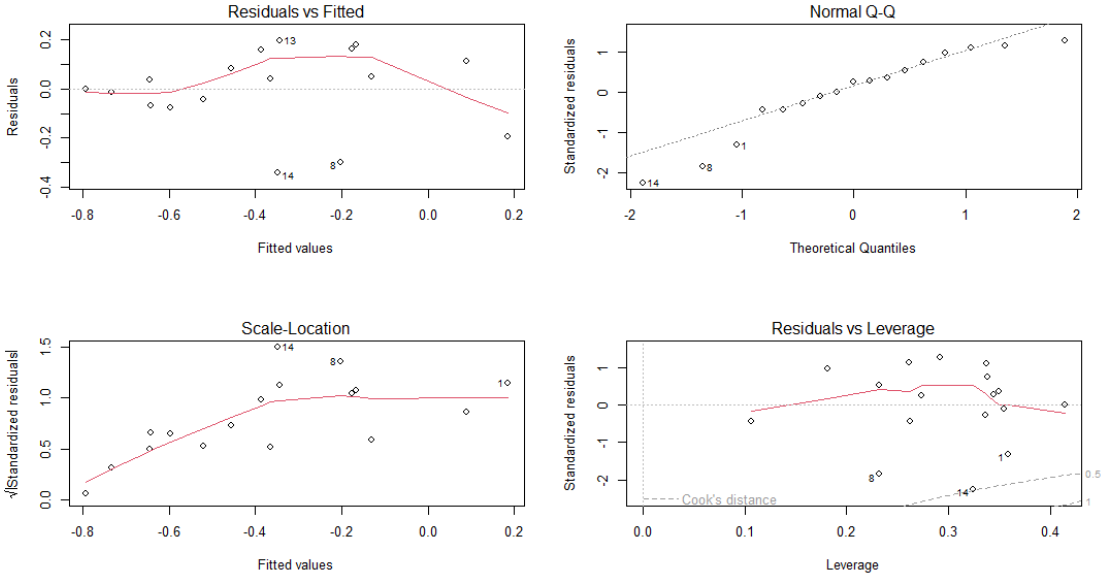

Figure B.9 Model validation plots for 40–50 cm sediment depth, with outlier removed. A plot of the residuals versus fitted values (top left), a Q-Q (quantile-quantile) plot of the theoretical quantiles versus standardised residuals (sresids) (top right), scale-location plot of the fitted values of the regression model versus square root of the sresids (bottom left), and a plot of the leverage versus sresids with Cook's distance boundaries (bottom right).

Appendix C

Organic Carbon Storage and Accumulation in Saltmarshes and Seagrass Meadows along an Exposed Temperate Coastline

Seagrass Meadows: Ecosystem Extent Estimates

Side Scan Sonar (SSS) Images

Seagrass presence was identified from reflectance patterns as areas with high reflectivity and undefined edges (darker areas on SSS images), based on previous studies (Fournier et al., 2010; Greene et al., 2018; Strong et al., 2023). Seagrass has a stronger return signal than background sediment due to air in the seagrass blades forming a strong reflector for acoustic energy (Wilson and Dunton, 2009). Point datasets obtained by TUV surveys, DD video surveys, and diver surveys were used to validate these interpretations. Confidence levels are provided for each SSS map.

Thiessen Polygons

Thiessen polygons were generated for Ramsey Bay and Bulgham Bay using presence and absence data provided by diver surveys (Manx Wildlife Trust), a towed underwater video (TUV) survey (Barrule), and drop-down (DD) video survey (Manx Blue Carbon Project). Data were constrained within a shallow water limit (absence data) by adding data points separated by 5 meters along lines plotted on the hard substrate shoreline based on an aerial image of the rocky coastline (Isle of Man Government). Data were constrained within shallow and deep-water limits using a bathymetry raster (Edina), which was converted to points and selected by attribute for depths where seagrass had not been identified in the region, to generate an absence dataset for inshore and deeper water. In Bulgham Bay, additional presence and absence data points were generated along the diver transects and TUV surveys,

according to observations, and additional absence points were generated along the outer edge of the diver survey that outlined the periphery of the seagrass meadow in the southwest of the bay. Data on seagrass meadow density were omitted from the dataset; therefore, seagrass presence denotes anything from low density (a few plants) to abundant (100% canopy cover) seagrass density.

Ramsey Bay

Seagrass meadows were mapped and their extents estimated in ArcGIS Pro software from SSS surveys and seagrass presence and absence datasets obtained by TUV camera surveys (Barrule, 2021), DD video camera (Manx Blue Carbon Project, 2023), and diver surveys (Manx Wildlife Trust, 2021 and 2024) (Appendix Figure C.1). Polygons were corroborated with Thiessen polygons (methods above). Confidence is highest in the centre of the meadow to the west of the headland Gob ny Rona, where point datasets from TUV surveys, DD video surveys, and diver surveys are abundant along the length of the meadow. Confidence is lower on the east of the headland and along the periphery of the meadow, where presence data are sparser. The Thiessen polygons have good overlap with both the medium and low confidence polygon. The seagrass meadow density varied from low to high, but these data were omitted from the datasets for simplicity. DD video and diver surveys found that seagrass cover was patchy on muddy sand with occasional seaweed.

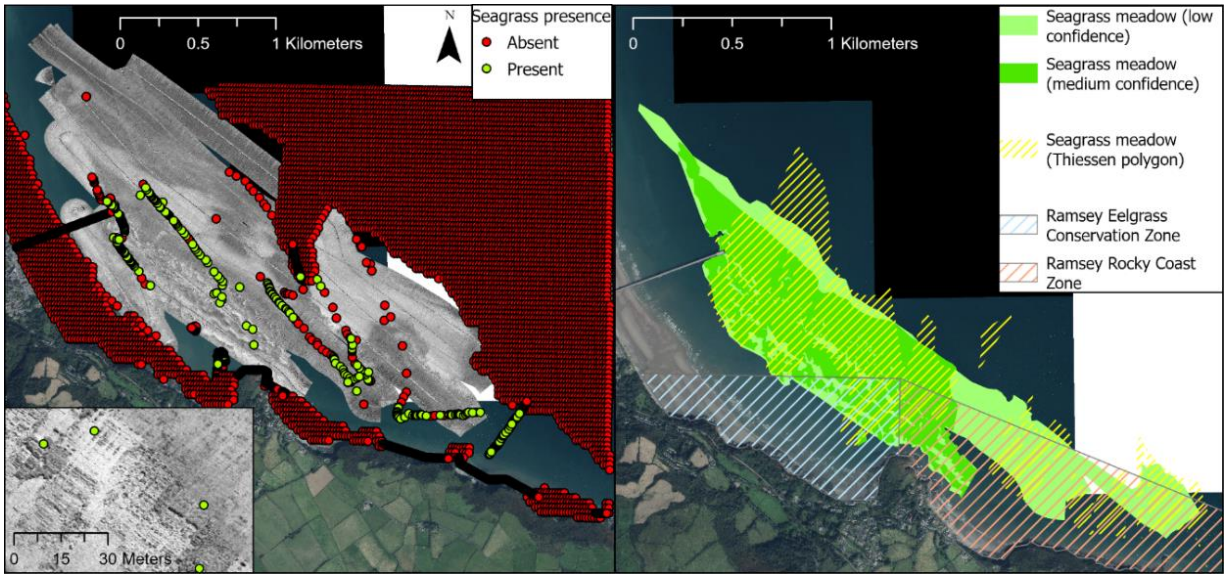

Figure C.1 Ramsey Bay seagrass maps showing raw datasets (left) and polygon products (right). Left: Side scan sonar composite image overlain onto an aerial image of the coastline with point datasets showing seagrass presence (green) and absence (red). Inset map shows seagrass reflectance pattern, where dark areas show seagrass presence. Right: Polygons showing the outer perimeter of seagrass meadows deduced from side scan sonar and presence/absence point datasets, with the densest seagrass meadow assigned medium confidence (dark green) and the mixed or sparsest seagrass meadow assigned low confidence (pale green). A Thiessen polygon (hatched yellow) indicates the modelled extent of the seagrass meadow based on presence/absence point datasets, showing close alignment with the low and medium confidence polygons. Ramsey Eelgrass Conservation Zone (hatched blue) and Rocky Coast Zone (hatched red) shows overlap with seagrass meadow. Low confidence (largest) polygon area equates to 125.27 ha; Medium confidence (smallest) polygon area equates to 65.28 ha; Thiessen polygon area equates to 103.06 ha.

Laxey Bay

Seagrass meadows were mapped and their extents estimated in ArcGIS Pro software, based on SSS surveys (2023) and seagrass presence and absence datasets obtained by TUV camera surveys (Barrule, 2022) and DD video camera (Manx Blue Carbon Project, 2023) (Appendix Figure C.2). Confidence in identifying seagrass presence based on SSS images is highest in the centre of Laxey Bay, where there is overlap with TUV surveys and DD survey points. Confidence is lower in regions where the reflectance pattern on the SSS images is comparable with seagrass but where these have not been mapped using TUV or DD surveys. The seagrass meadow density varied, but these data were omitted from the datasets for simplicity. DD video survey in Laxey Bay found that seagrass cover was patchy and sparse to medium on sandy mud to muddy sand, with occasional seaweed present.

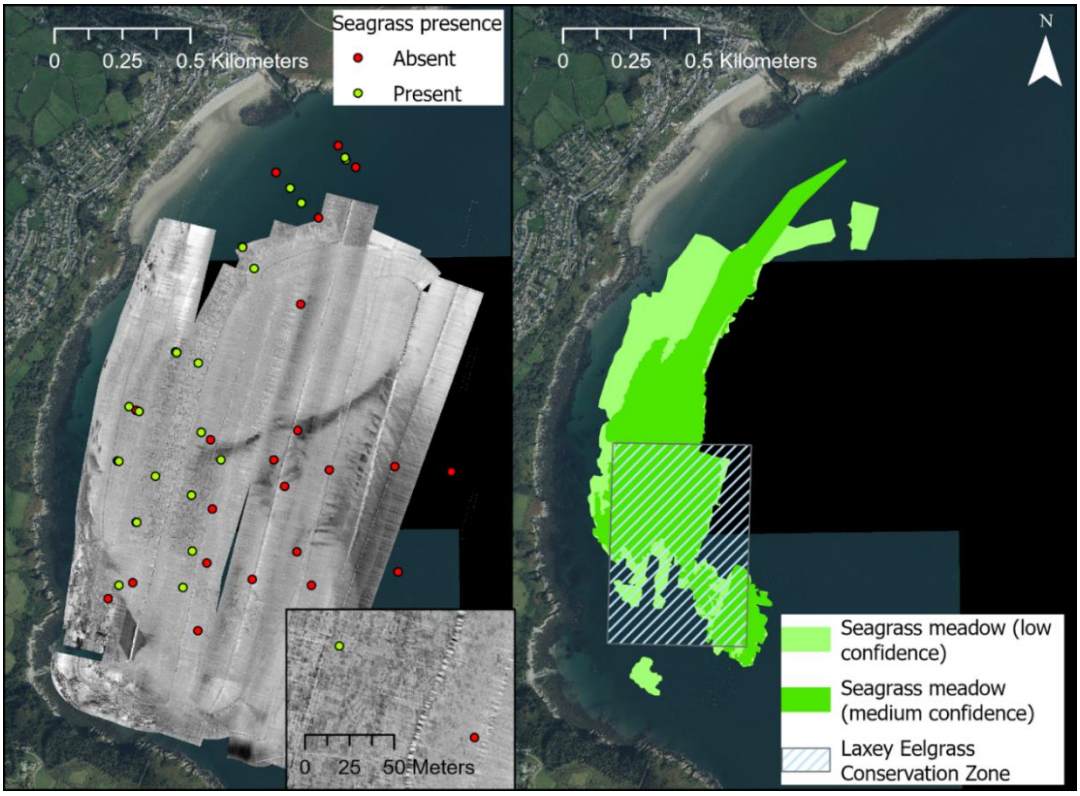

Figure C.2 Laxey Bay seagrass maps showing raw datasets (left) and polygon products (right). Left: Side scan sonar composite image overlain onto an aerial image of the coastline with point datasets showing seagrass presence (green) and absence (red). Inset map shows seagrass reflectance pattern, where dark areas show seagrass presence. Right: Polygons showing the outer perimeter of seagrass meadows deduced from side scan sonar and presence/absence point datasets, with the densest seagrass meadow assigned medium confidence (dark green) and the mixed or sparsest seagrass meadow assigned low confidence (pale green). Laxey Eelgrass Conservation Zone (hatched blue) shows overlap with the seagrass meadow. Low confidence (largest) polygon area equates to 60.63 ha; Medium confidence (smallest) polygon area equates to 38.94 ha.

Bulgham Bay

Seagrass meadows were mapped and their extents estimated in ArcGIS Pro software using Thiessen polygons (methods above), based on seagrass presence and absence datasets obtained by TUV camera surveys (Barrule, 2021), DD video camera (Manx Blue Carbon Project, 2023), and diver surveys (Manx Wildlife Trust, 2021 and 2024)

(Appendix Figure C.3). Confidence in identifying seagrass presence based on Thiessen polygons is highest in the south of Bulgham Bay, as a diver survey (2024) mapped the outer extent of a seagrass meadow, which was corroborated by diver transects (2021). Confidence is medium in the north of Bulgham Bay, where a diver survey (2024) corroborated the results of a TUV survey (2021). Confidence is low elsewhere in Bulgham Bay, where absence data were generated based on water depth only. The seagrass meadow density varied from low to medium, but these data were omitted from the datasets for simplicity. DD video and diver surveys in Bulgham Bay found that seagrass cover was patchy and varied between sparse and dense on sandy substrate with rocky outcrops.

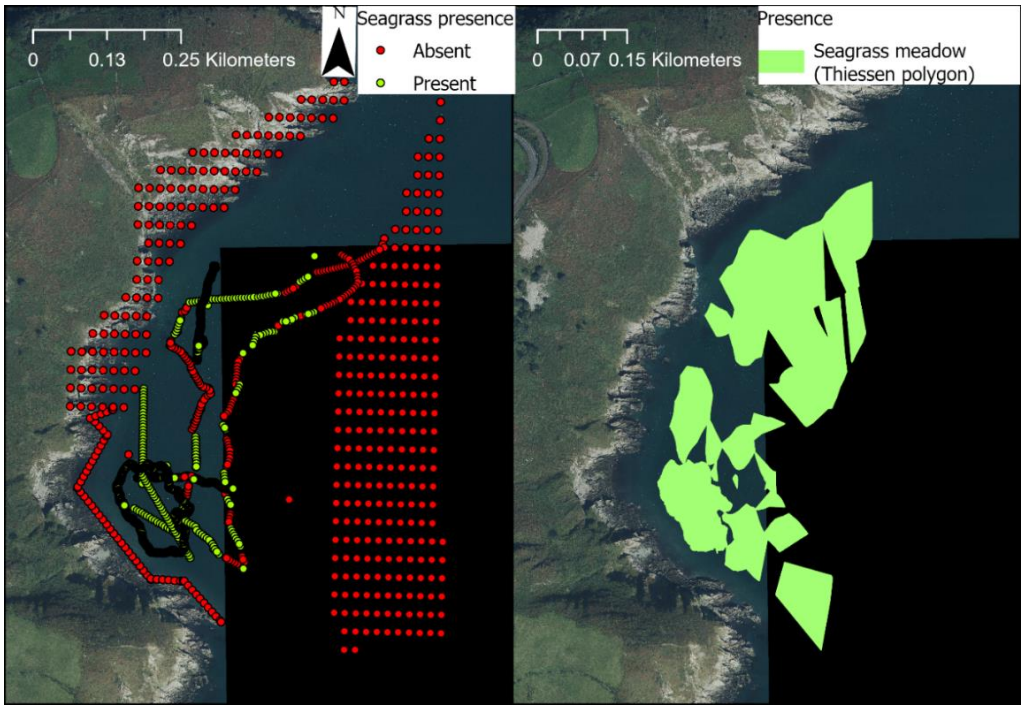

Figure C.3 Bulgham Bay seagrass maps showing raw datasets (left) and polygon products (right). Left: Aerial image of the coastline with point datasets showing seagrass presence (green) and absence (red). Right: Polygons showing the outer perimeter of seagrass meadows deduced from a Thiessen polygon (pale green) indicating the modelled extent of the seagrass meadow based on presence/absence point datasets.

Derbyhaven and Langness

Seagrass meadows were mapped by Manx Wildlife Trust and Seasearch diver surveys (2022) and their extents estimated in ArcGIS Pro software (Appendix Figure C.4). Confidence is high based on these diver surveys which provided high-resolution estimates of seagrass meadow peripheries. Dive records also recorded 2–3 smaller patches of approx. 10 m^2 north of the Fort Island jetty, and a small patch at the end of the jetty of approx. 0.6 m^2, but these were not included in the extent estimates due to insufficient data. The seagrass meadows were recorded as having dense and sparse regions interspersed with boulders on mixed ground (cobbles, pebbles, sand and gravel) in Fort Island Gully.

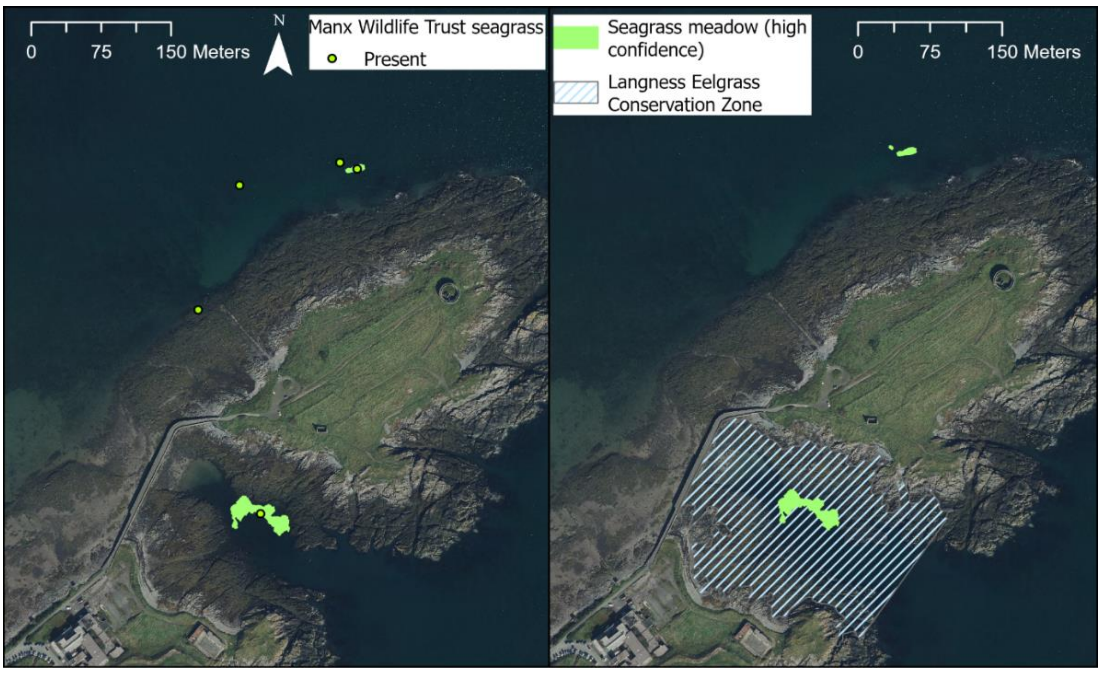

Figure C.4 Derbyhaven and Langness (Fort Island Gully) seagrass maps showing raw datasets (left) and polygon products (right). Left: Aerial image of the coastline with point datasets showing seagrass presence (green) and polygons showing the outer perimeter of seagrass meadows (high confidence) based on dive surveys. There were no absence data points. Right: High-confidence seagrass extents (green) and Langness Eelgrass Conservation Zone (hatched blue).

Baie Ny Carrickey

Seagrass meadows were mapped by Manx Wildlife Trust diver surveys (2024) and their extents estimated in ArcGIS Pro software (Appendix Figure C.5). Confidence is high based on the diver surveys which provided high-resolution estimates of seagrass meadow periphery. Other seagrass meadow areas have been recorded historically within the Eelgrass Conservation Zone, but could not be located during a diver survey in 2024, therefore overall confidence in seagrass meadow extent at Baie Ny Carrickey is uncertain/low. The seagrass meadows had sparse patches interspersed by kelp on mixed ground (cobbles, pebbles, sand and gravel).

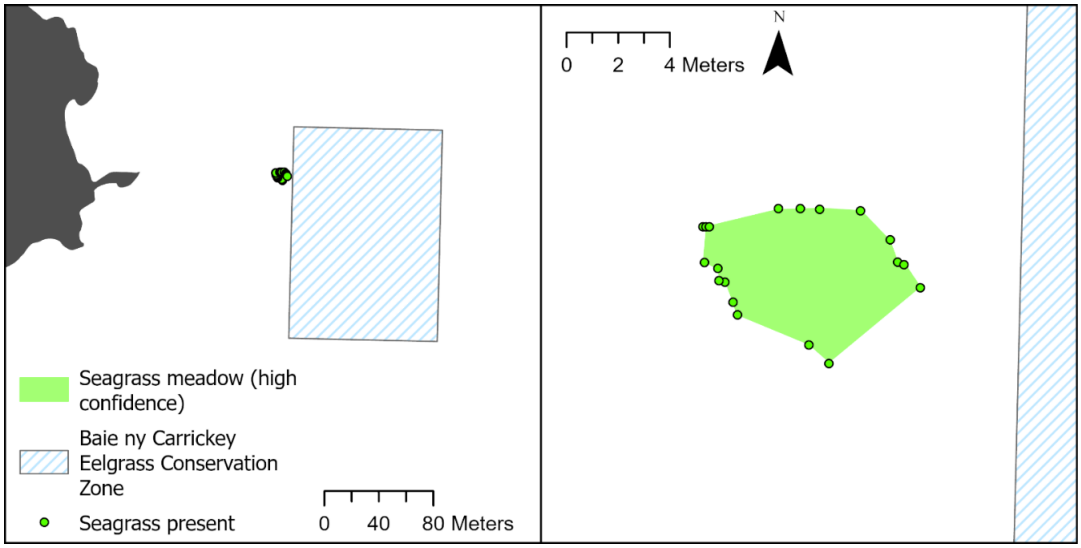

Figure C.5 Baie Ny Carrickey seagrass maps showing the broad location (left) and raw data with polygon products (right). Left: Map of Baie Ny Carrickey (grey) with point datasets showing seagrass presence (green) and Baie ny Carrickey Eelgrass Conservation Zone (hatched blue). Right: Seagrass presence (green) and polygon showing the outer perimeter of the seagrass meadow (high confidence) based on dive surveys. There were no absence data points.

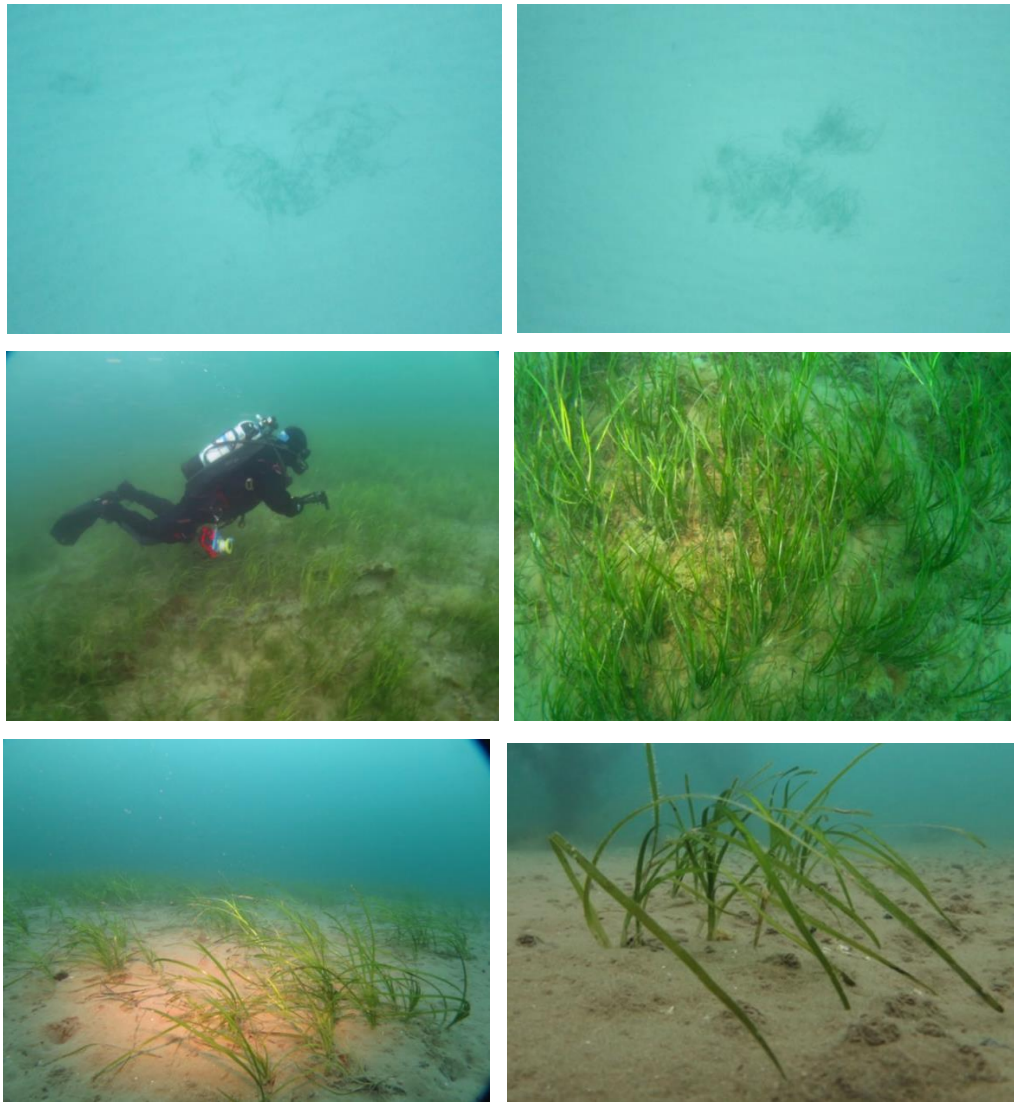

Figure C.6 Ramsey Bay seagrass meadow: The inshore extent observed during diver surveys in December 2023 (top two photographs) (Photo credit: Lara Howe, Manx Wildlife Trust (2023)). At Ramsey Pier and the Dolphin recorded during dive surveys on 1st November 2022 (bottom four photographs) (Photo credit: Leigh Morris, Manx Wildlife Trust (2022)).

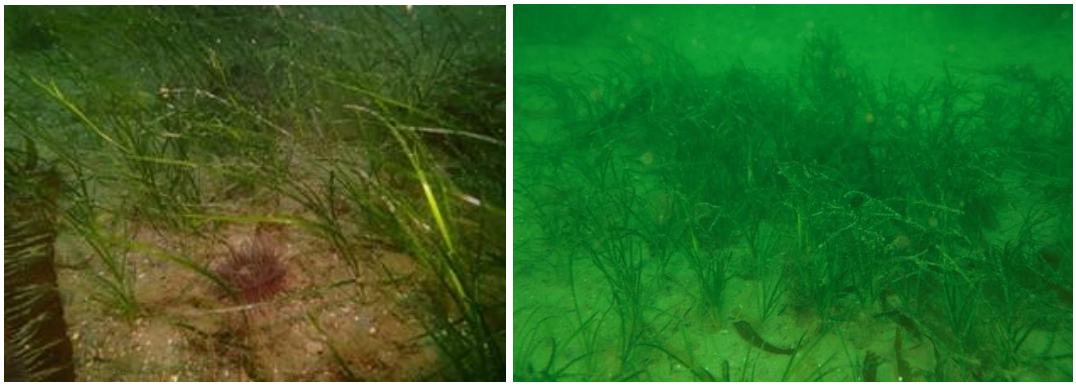

Figure C.7 Zostera marina seagrass meadow at Bulgham Bay during a diver survey in June 2021. Photo credit: Lara Howe, Manx Wildlife Trust (2021).

Figure C.8 Langness (Fort Island Gully) seagrass meadow recorded during a diver survey in June 2022 (top two and bottom left photographs) (Photo credit: Lara Howe, Manx Wildlife Trust (2022)). Zostera marina plant from the seagrass bed, during a seagrass restoration trial (bottom right photograph) (Photo credit: Leigh Morris, Manx Wildlife Trust (2022)).

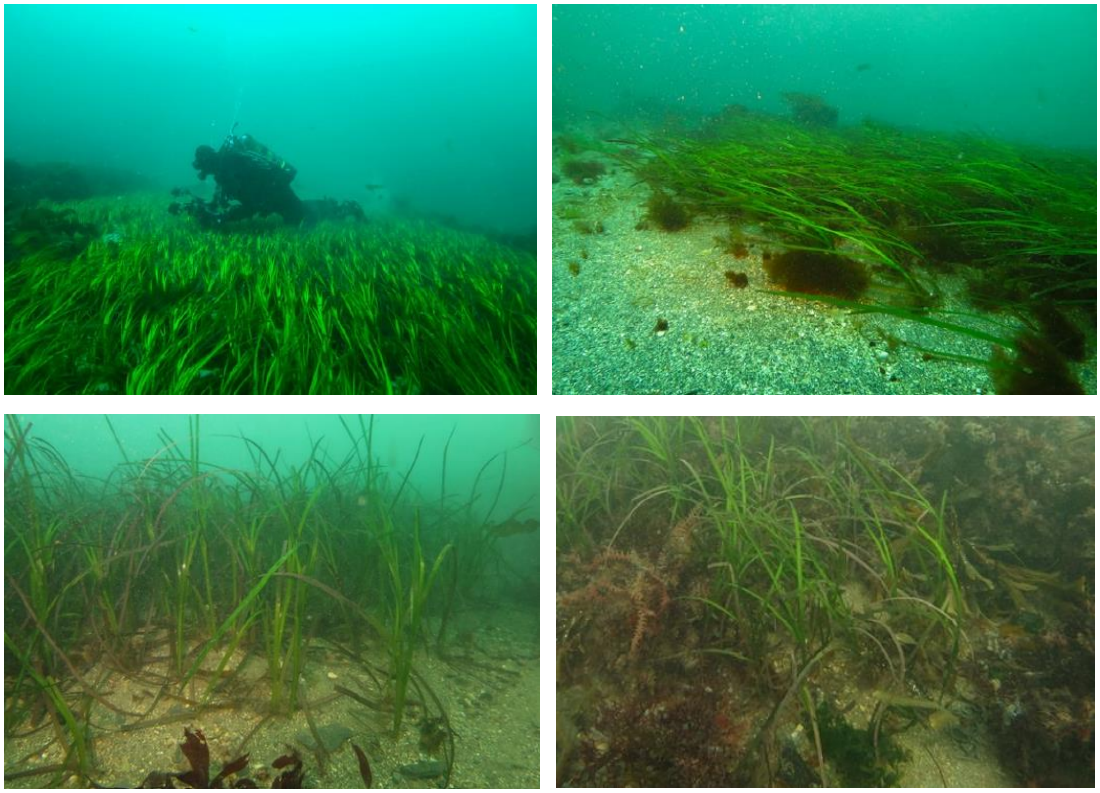

Figure C.9 Derbyhaven seagrass meadow showing the largest mapped seagrass bed (top two photographs) during a dive survey on 1st May 2022. Derbyhaven seagrass meadow showing the smallest mapped seagrass bed (bottom left photograph) and the mixed seagrass bed (unmapped) at the end of the jetty in Derbyhaven Bay (bottom right photograph) during a dive survey on 6th November 2022 (Photo credit: Leigh Morris, Manx Wildlife Trust (2022)).

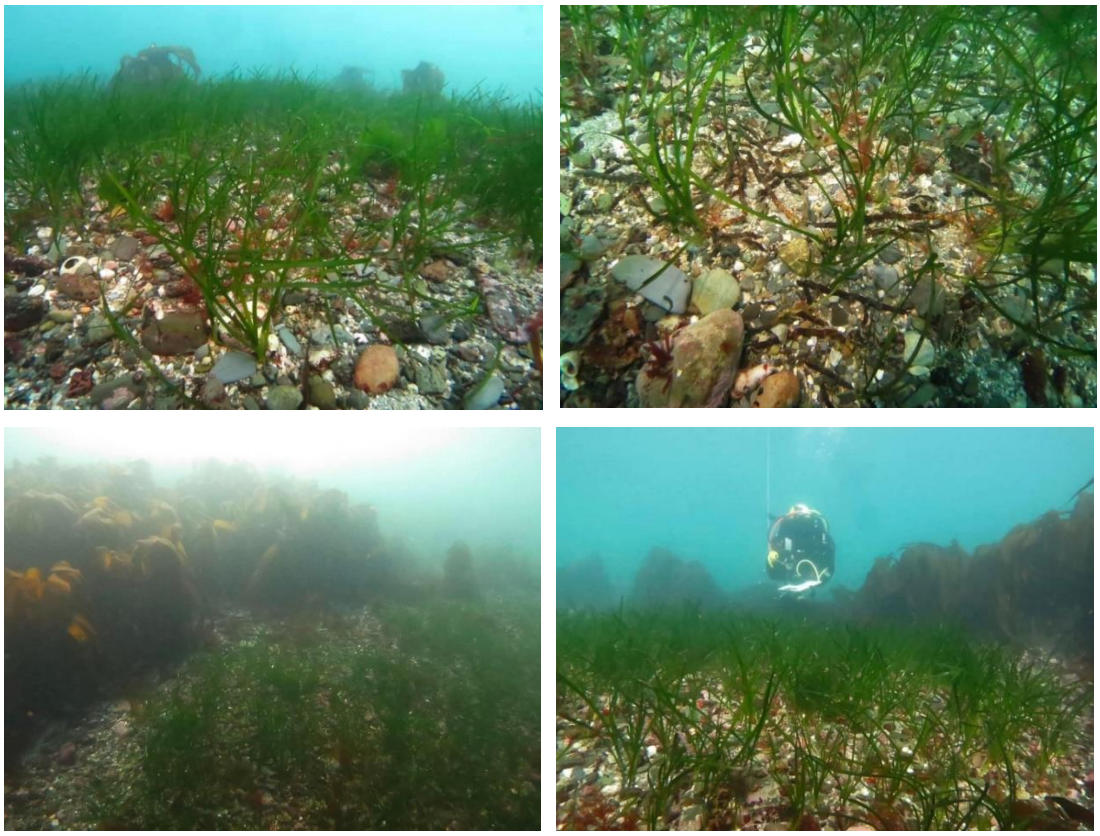

Figure C.10 Baie Ny Carrickey seagrass meadow recorded in March 2024, showing coarse substrate, mixed kelp habitat (top left photograph), rhizomes at the sediment surface (top right photograph), and the edge of a kelp forest (bottom two photographs) (Photo credit: Leigh Morris, Manx Wildlife Trust (2024)).

Table C.1 Isle of Man seagrass meadow descriptions of surface sediments, seagrass canopy (cover and leaf length), biodiversity, and description, based on diver surveys by Manx Wildlife Trust (MWT) and Seasearch (unpublished) and drop-down (DD) video surveys (this study).

Site	Location	Surface sediment	Seagrass canopy	Biodiversity	Description	Source
Ramsey Bay	Whole meadow	Muddy sand with occasional worm casts	<5% to 75%, 20 cm to 30 cm	Occasional bryazoans	Occasional detached *Saccharina latissima* and kelp, brown leaf marks	This study (DD, 2023)
	East (low confidence zone)	Sand and gravel	<5% to 100%, a few cm	Plumose and snakelocks anemones, occasional kelp, red seaweeds, and shells (full species list in report)	N/A	MWT divers (unpublished, 2024)
	West/inshore (medium confidence zone)	Sand, clean with ripples	N/A, 10 cm to 20 cm	*Fucus serratus, Fucus vesiculous, Saccharina latissima, Laminaria digitata, Halidrys siliquosa, Pagurus bernhardus, Astropecten irregularis, Enis spp* (dead)	N/A	MWT divers (unpublished, 2023)
	Ramsey Pier	N/A	N/A, 25 cm	Wireweed (*Sargassum*)	Seeds on leaves (rare), drift/unattached red algae	MWT/Seasearch divers (unpublished, 2022)
	Ramsey Pier	N/A	N/A, 45 cm to 60 cm	N/A	Seeds on leaves (common on smaller plants)	MWT/Seasearch divers

						(unpublished, 2022)
Laxey Bay	South/East to West	Muddy sand and sandy mud, with occasional worm casts	<5% to 25%, N/A	Occasional red seaweed	Dead shells	This study (DD, 2023)
Bulgham Bay	South	Muddy sand	10% to 50%, N/A	Occasional chorda filum	N/A	This study (DD, 2023)
	South	Sand	"sparse" to "dense", ~30 cm	Hermit crabs, fish fry, netted dogwhelk egg cases, small spider crabs, snakelocks anemones, John Dory (full species list in report)	Occasional rocky outcrop and gravel patches, developing seeds on some leaves	MWT divers (unpublished, 2021)
	North and South	N/A	<5% to <50%, N/A	Moon snail, hermit crab	N/A	MWT divers (unpublished, 2024)
Langness	Fort Island Gully	N/A	N/A, 35 cm to 40 cm	Snakelocks anemones (rare), occasional grooved topshell, mermaid tresses (*Chorda filum*), and wireweed (*Sargassum muticum*)	N/A	MWT/Seasearch divers (unpublished, 2022)
	Fort Island Gully	Mixed (sand and gravel with pebbles)	N/A	Snakelocks anemones, juvenile fish, daisy anemone, *Jujubirus striatus* (full species list in report)	Occasional boulder with mixed seaweeds (incl. harpoon weed) and sea lace	MWT/Seasearch divers (unpublished, 2022)

Derbyhaven	Whole meadow	Sand and gravel	N/A	Daisy anemone, encrusting pink algae, mixed seaweeds (full species list in report)	Rocky reef nearby	MWT/Seasearch divers (4x unpublished, 2022)
	Whole meadow	N/A	N/A, >50 cm	*Jujubinus striatus* (common), Cat shark, *Aplysia punctata*, Daisy anemone, Spider crab	N/A	MWT/Seasearch divers (2x unpublished, 2022)
	Whole meadow	Occasional worm casts	N/A, >60 cm	Occasional *Jujubinus striatus* (grooved topshell), algae (red, brown, green, all common), grey encrusting sea squirt, branched fine red algae	Calcium deposit on older leaves, dead shells	MWT/Seasearch divers (unpublished, 2022)
Baie Ny Carrickey	Whole meadow	Sandy, gravelly, pebblly	“patchy and sparse”, <14 cm to 20 cm	Occasional cobbles with typical kelp and understory species present, common grooved topshell, algae/plants, cnidarians, polychaetes, crustaceans, molluscs, and ascidians (full species list in report)	Short and thin seagrass blades, clean, “little signs of blackening leaves”, raised sediment under meadows, bedrock and kelp habitat on seaward site, exposed rhizomes	MWT divers (unpublished, 2024)

Figure C.11 Port Cornaa saltmarsh photoquadrat (0.25 m^2) of Site S2C5, sampled in April 2022. Saltmarsh species identified as *Juncetum (Juncus) maritimus* (SM16) by Spencer (2005).

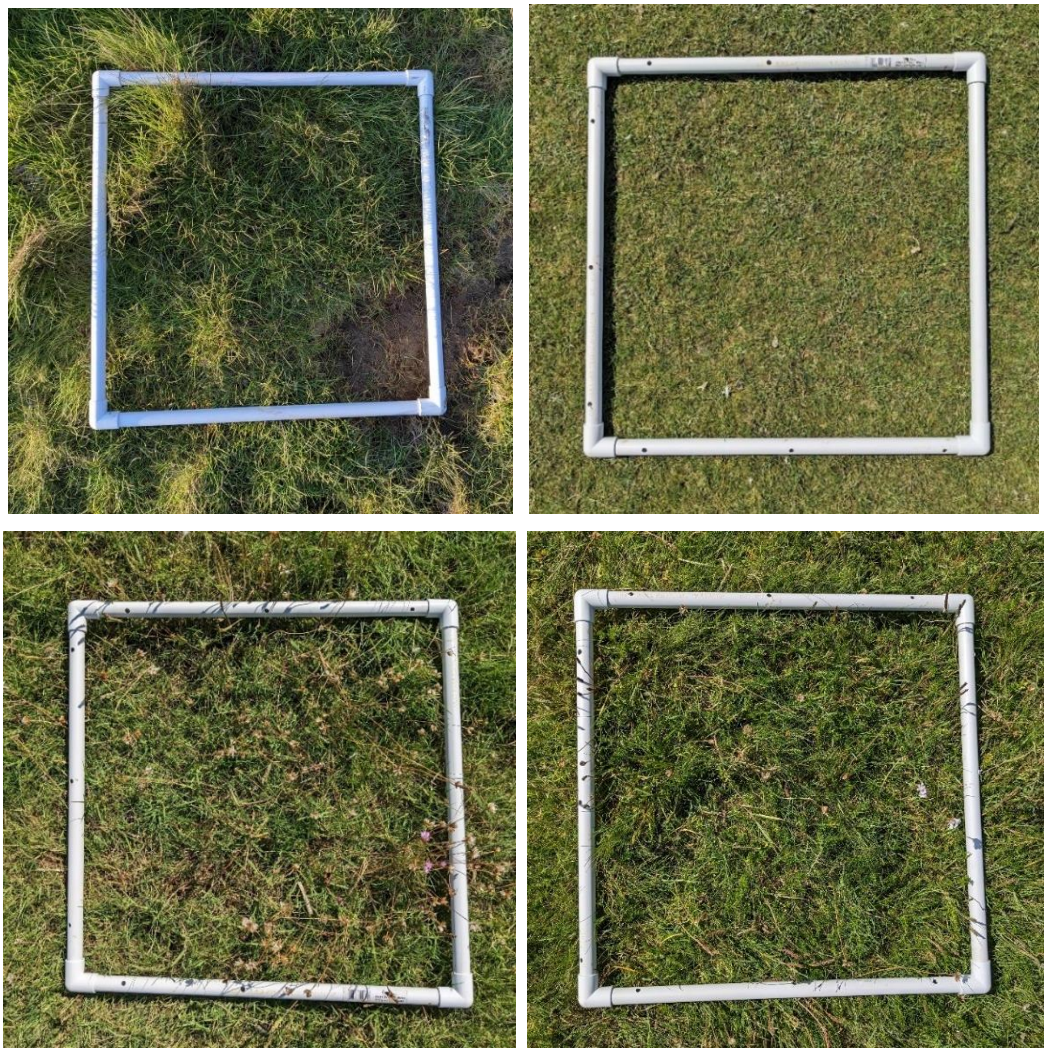

Figure C.12 Poyll Dooey saltmarsh photoquadrat (0.25 m^2) of Site S7C1 (*Puccinellia maritima* (SM13)), sampled in April 2022 (top left), and of Site SM8 (*Salicornia europea* (SM8)) (top right), Site SM13 (*Puccinellia maratima* (SM13)) (bottom left), and Site SM16 (*Junecitum (Juncus) maritimusi* (SM16)) (bottom right), all sampled in August 2023. Saltmarsh vegetation communities were classified by Spencer (2005).

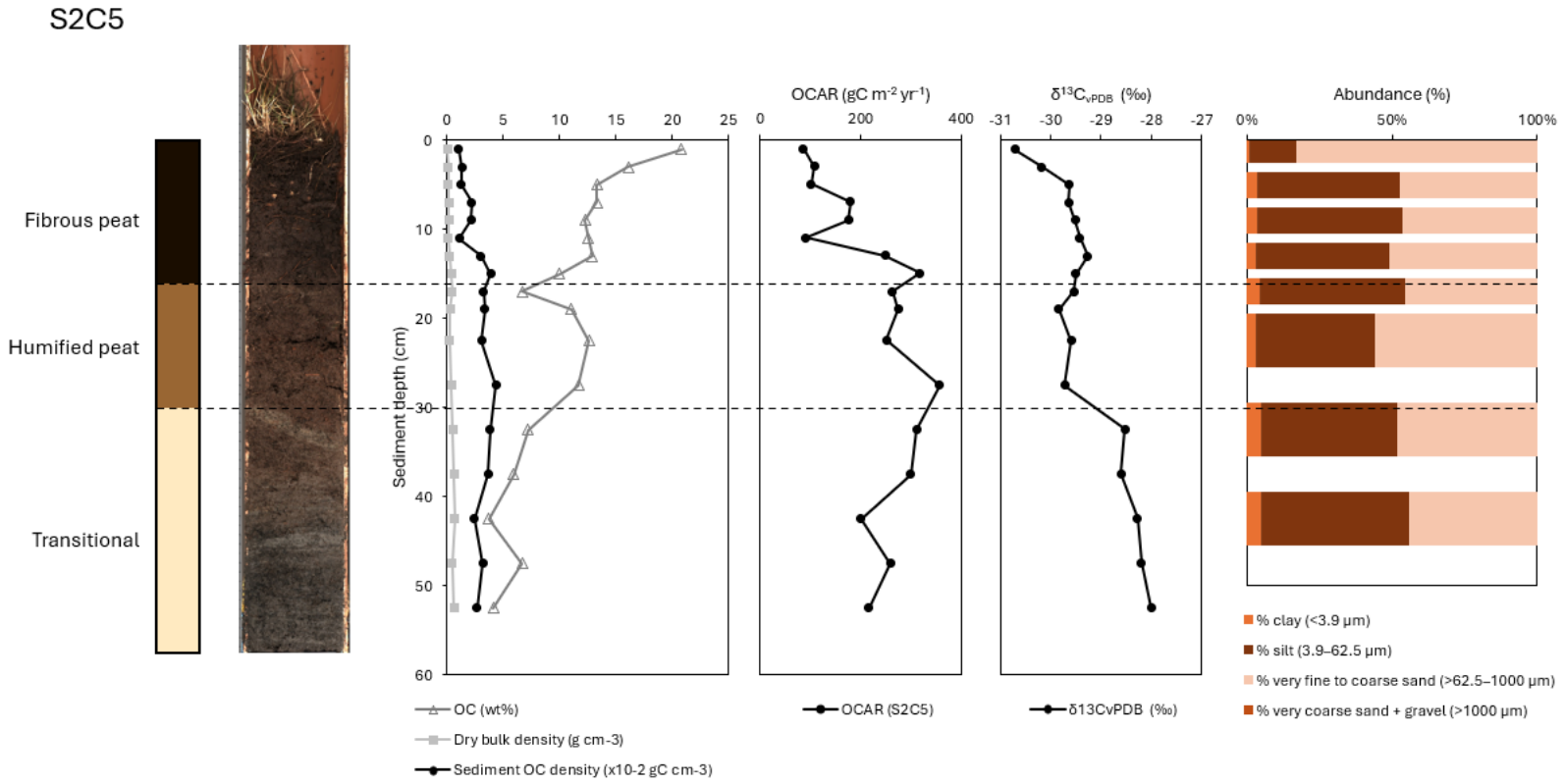

Figure C.13 Sediment core depth profiles for saltmarsh Site S2C5. Left to right: Sediment layer graphic based on data, high-resolution surface image, organic carbon (OC) concentration (%), sediment dry bulk density (DBD, g cm^{-3}), sediment organic carbon density (SCD, gC cm^{-3}), OC accumulation rate (OCAR, gC m^{-2} yr^{-1}), $\delta^{13}C_{vPDB}$ (‰), and sediment grain size fractions. Roots were observed at all depths.

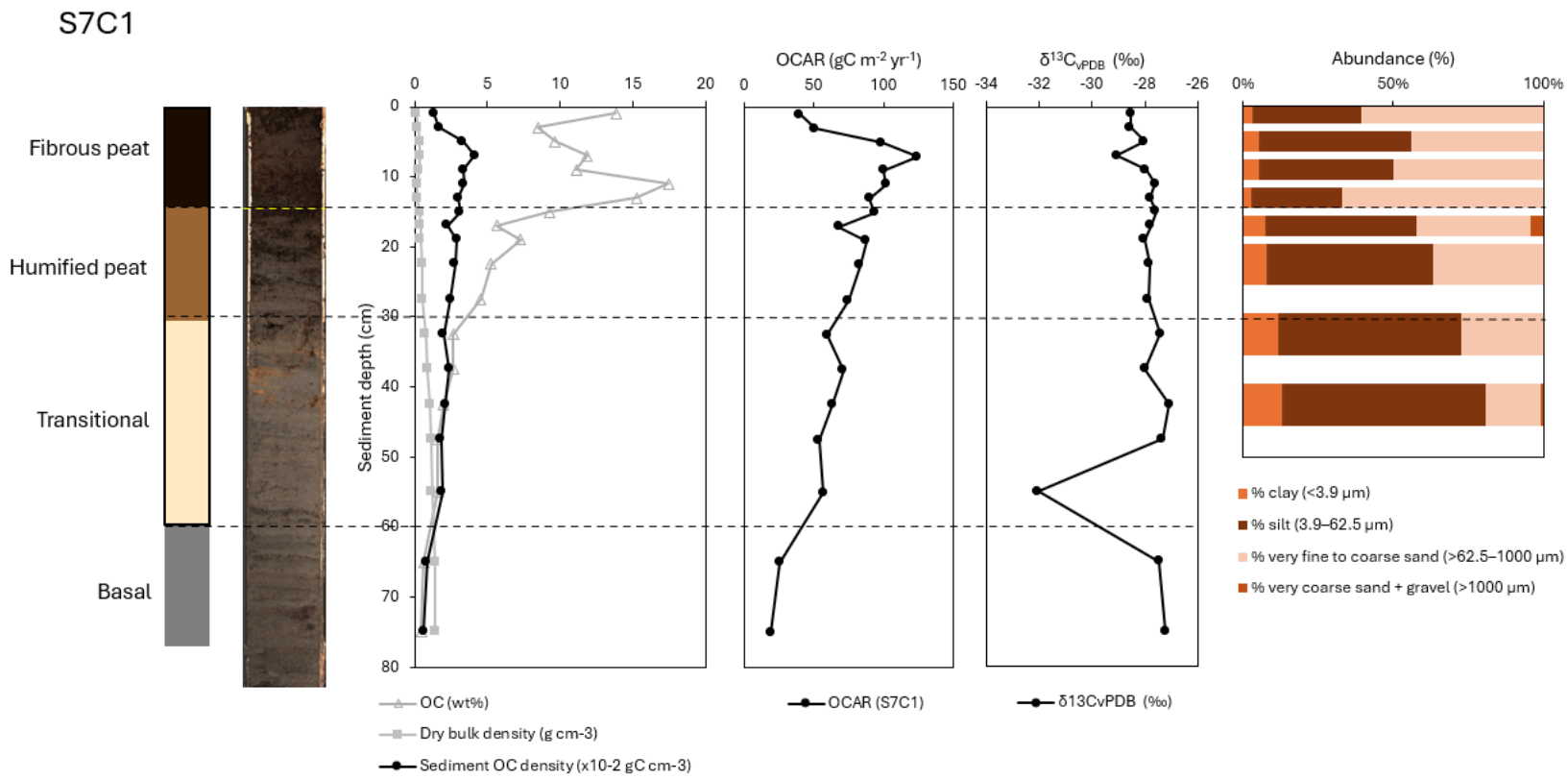

Figure C.14 Sediment core depth profiles for saltmarsh Site S7C1. Left to right: Sediment layer graphic based on data, high-resolution surface image, organic carbon (OC) concentration (%), sediment dry bulk density (DBD, g cm^{-3}), sediment organic carbon density (SCD, gC cm^{-3}), OC accumulation rate (OCAR, gC m^{-2} yr^{-1}), $\delta^{13}C_{vPDB}$ (‰), and sediment grain size fractions. The yellow dashed line at 14 cm indicates where the sediment cores split during sampling and was re-combined for analysis. Roots were observed at all depths.

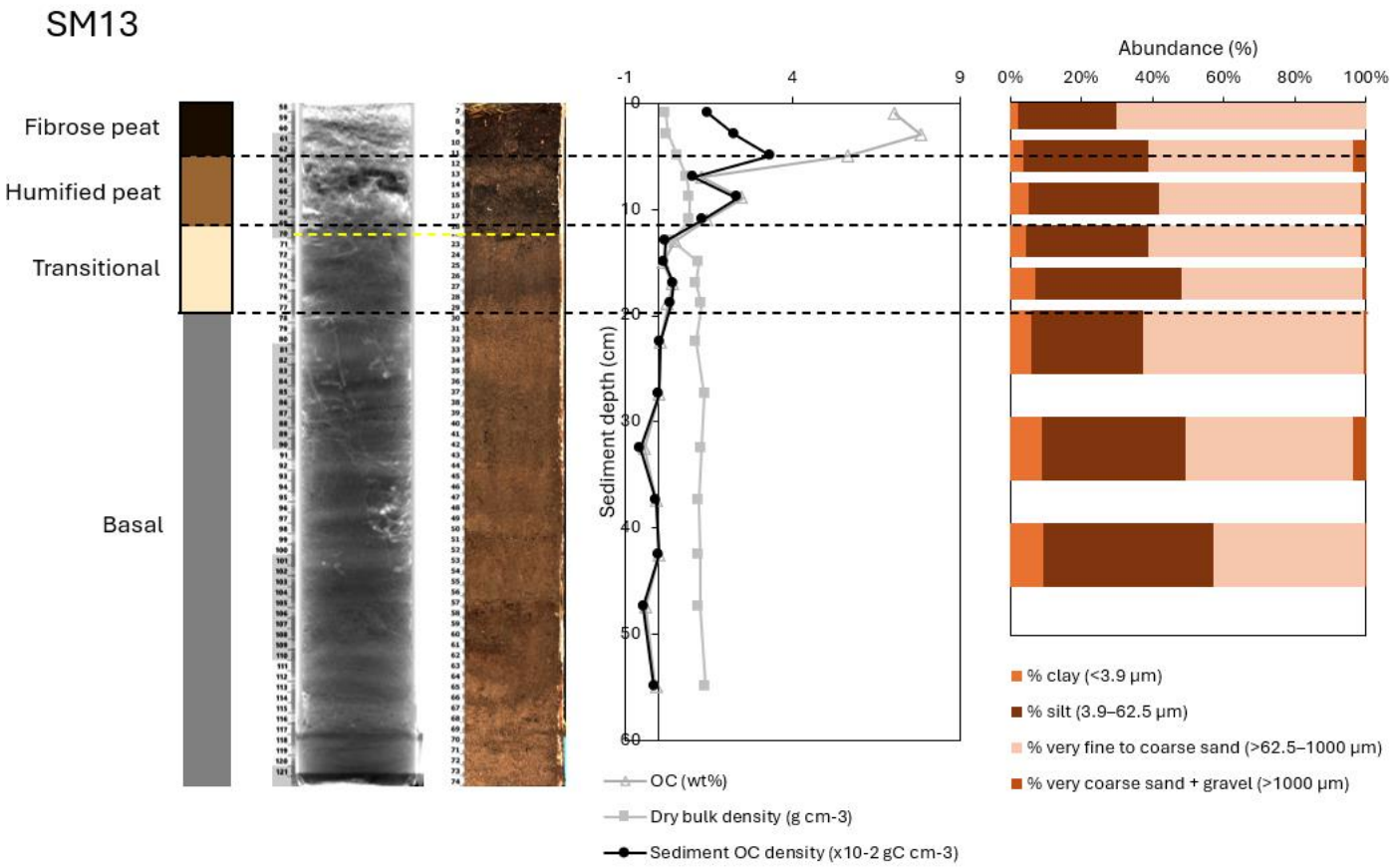

Figure C.15 Sediment core depth profiles for saltmarsh Site SM13. Left to right: Sediment layer graphic based on data, X-ray radiograph image, high-resolution surface image, organic carbon (OC) concentration (%), sediment dry bulk density (DBD, g cm^{-3}), sediment organic carbon density (SCD, gC cm^{-3}), and sediment grain size fractions. The yellow dashed line at 12 cm indicates where the sediment core split during sampling and was re-combined for analysis. Root penetration depth was not recorded.

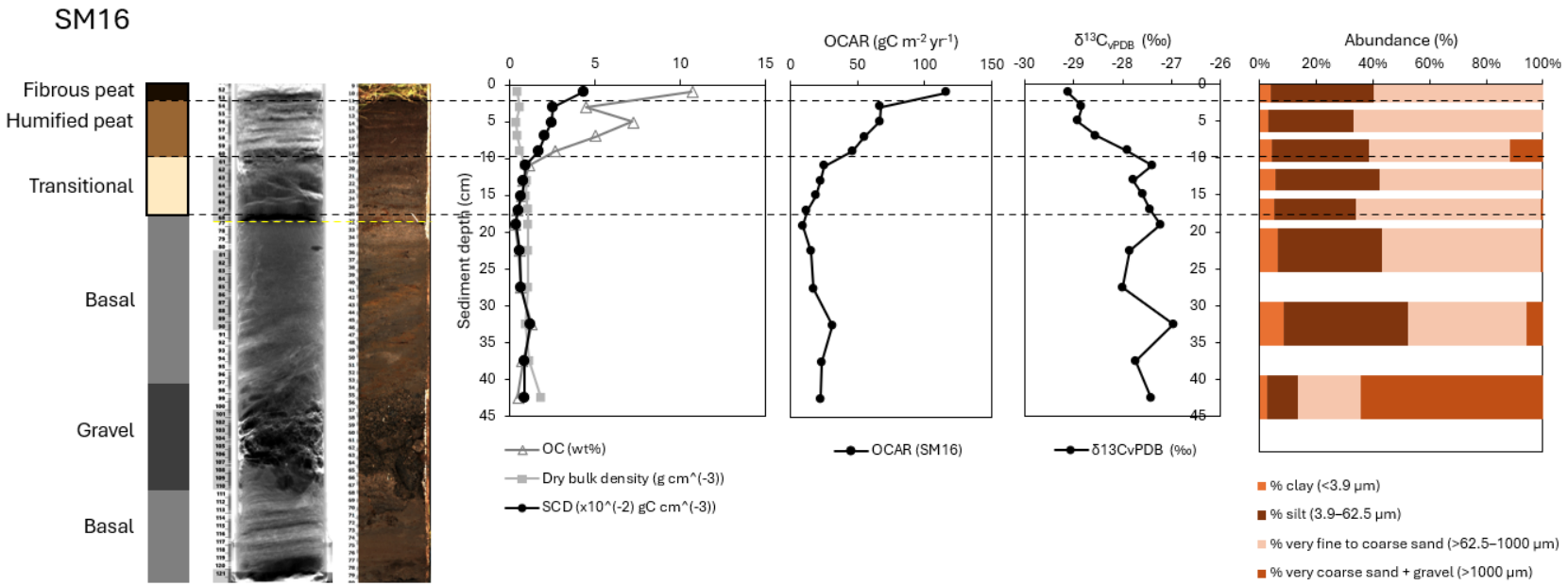

Figure C.16 Sediment core depth profiles for saltmarsh Site SM16. Left to right: Sediment layer graphic based on data, X-ray radiograph image, high-resolution surface image, organic carbon (OC) concentration (%), sediment dry bulk density (DBD, g cm^{-3}), sediment organic carbon density (SCD, gC cm^{-3}), OC accumulation rate (OCAR, gC m^{-2} yr^{-1}), $\delta^{13}C_{vPDB}$ (‰), and sediment grain size fractions. The yellow dashed line at 18 cm indicates where the sediment core split during sampling and was re-combined for analysis. Root penetration depth was not recorded.

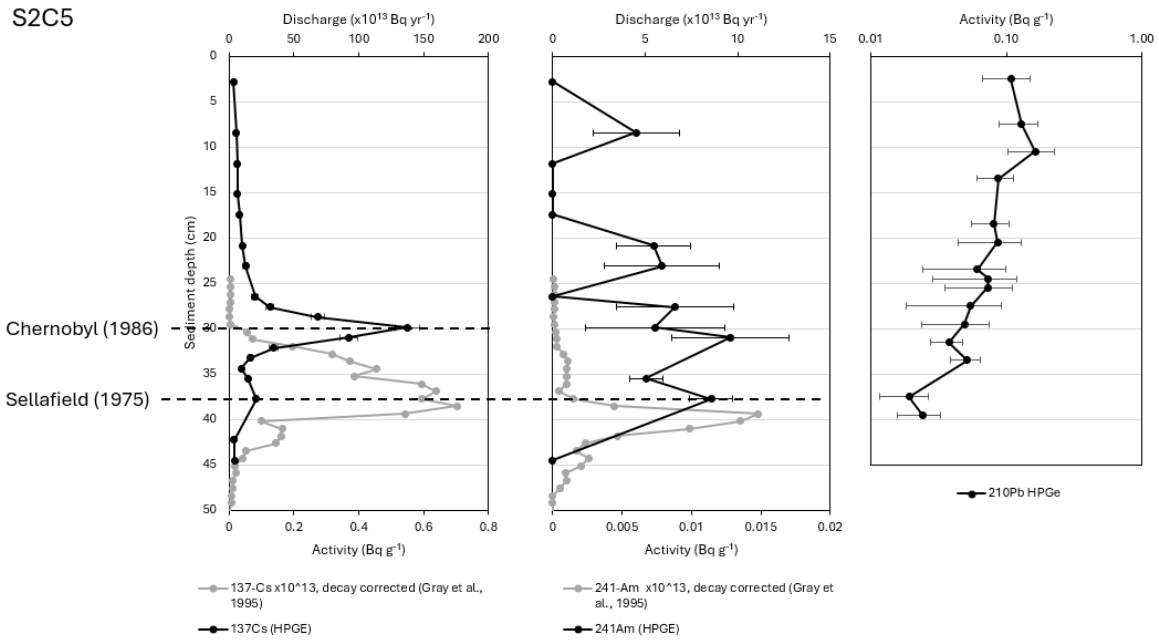

Figure C.17 Radionuclide profiles for saltmarsh Site S2C5. Left to right: ^{137}Cs activities (black, lower axis) and ^{137}Cs discharge profile from Sellafield nuclear facility (grey, upper axis) with the average sedimentation rate applied; ^{241}Am activities (black, lower axis) and ^{241}Am discharge profile from Sellafield nuclear facility (grey, upper axis) with the average sedimentation rate applied; ^{210}Pb activities.

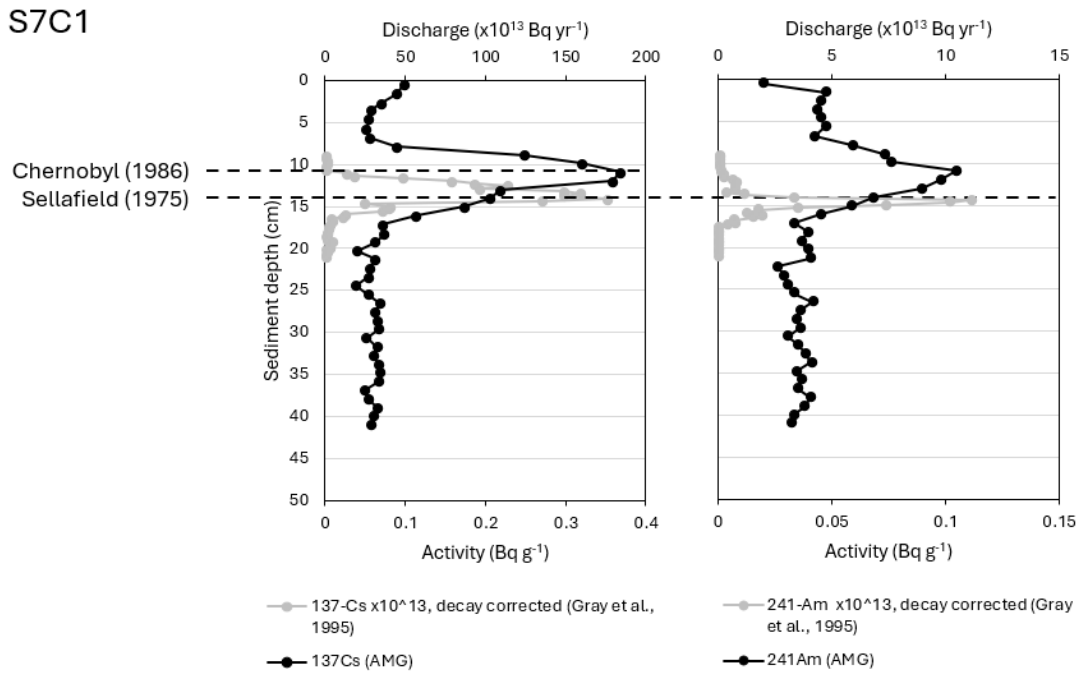

Figure C.18 Radionuclide profiles for saltmarsh Site S7C1. Left to right: ^{137}Cs activities (black, lower axis) and ^{137}Cs discharge profile from Sellafield nuclear facility (grey, upper axis) with the average sedimentation rate applied; ^{241}Am activities (black, lower axis) and ^{241}Am discharge profile from Sellafield nuclear facility (grey, upper axis) with the average sedimentation rate applied.

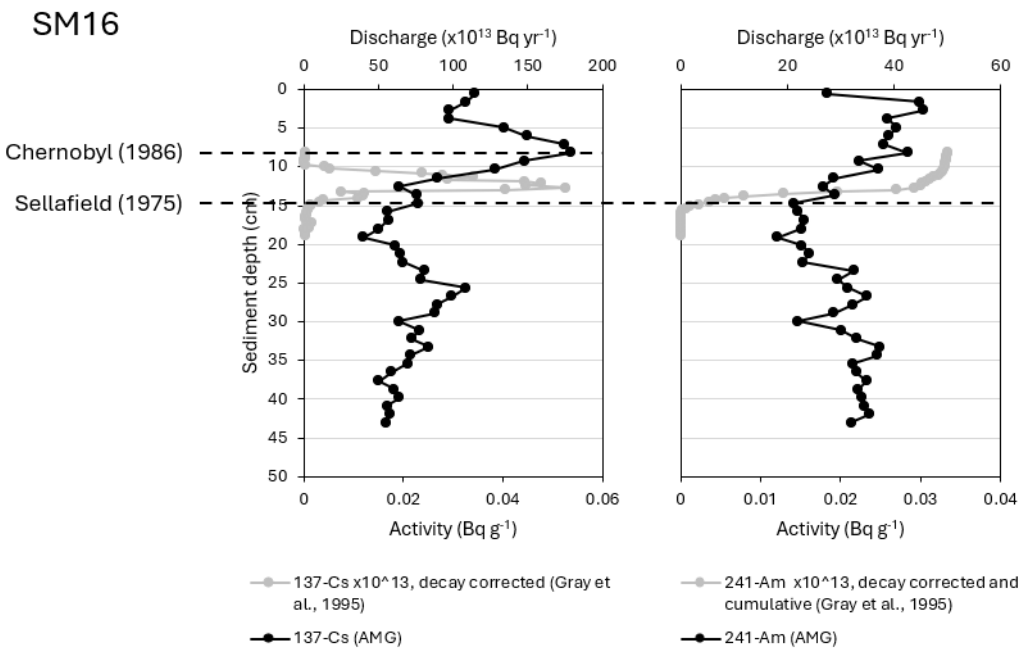

Figure C.19 Radionuclide profiles for saltmarsh Site SM16. Left to right: ^{137}Cs activities (black, lower axis) and ^{137}Cs discharge profile from Sellafield nuclear facility (grey, upper axis) with the average sedimentation rate applied; ^{241}Am activities (black, lower axis) and ^{241}Am discharge profile from Sellafield nuclear facility (grey, upper axis) with the average sedimentation rate applied.

Table C.2 Saltmarsh sediment classification for Isle of Man saltmarsh layers. Average proportion (%) of clay (<3.9 µm), silt (3.9 µm to 62.5 µm), mud (<62.5 µm), very fine to coarse sand (62.5–1000 µm) and sand and gravel (>62.5 µm), based on Udden (1914) and Wentworth (1922). Proportion of particles <1000 µm (analysed by laser diffraction) and >1000 µm (sieved and weighed). Sediment classifications are based on the Folk (1954) classification scheme for sediment depths having >99% of sediment <1000 µm (i.e. trace gravel and/or very coarse sand).

Site ID	Sediment layer	Depth (cm)	Clay (%)	Silt (%)	Mud (%)	Sand (%)	Sand-and-gravel (%)	<1000 µm (%)	>1000 µm (%)	Folk class
S2C5	Peat (fibrous)	1	0.84	16.15	16.99	83.01	83.01	100.00	0.00	Muddy sand (silty sand)
	Peat (fibrous)	5	3.39	49.44	52.83	47.18	47.17	100.01	-0.01	Sandy mud (sandy silt)
	Peat (fibrous)	9	3.62	50.05	53.67	46.34	46.33	100.01	-0.01	Sandy mud (sandy silt)
	Peat (fibrous)	13	3.17	45.85	49.02	50.98	50.98	100.00	0.00	Muddy sand (silty sand)
	Peat (humified)	17	4.20	50.40	54.60	45.40	45.40	100.00	0.00	Sandy mud (sandy silt)
	Peat (humified)	22.5	3.06	41.24	44.30	55.70	55.70	100.00	0.00	Muddy sand (silty sand)
	Transitional	32.5	4.76	46.85	51.61	48.39	48.39	100.00	0.00	Sandy mud (sandy silt)

	Transitional	42.5	4.86	50.83	55.69	44.31	44.31	100.00	0.00	Sandy mud (sandy silt)
S7C1	Peat (fibrous)	1	3.25	36.23	39.48	60.52	60.52	100.00	0.00	Muddy sand (silty sand)
	Peat (fibrous)	5	5.34	50.81	56.15	43.85	43.85	100.00	0.00	Sandy mud (sandy silt)
	Peat (fibrous)	9	5.14	45.09	50.23	49.77	49.77	100.00	0.00	Sandy mud (sandy silt)
	Peat (fibrous)	13	2.83	30.18	33.01	66.99	66.99	100.00	0.00	Muddy sand (silty sand)
	Peat (humified)	17	7.24	50.29	57.54	38.28	42.46	95.81	4.19	N/A
	Peat (humified)	22.5	7.94	55.15	63.09	36.91	36.91	100.00	0.00	Sandy mud (sandy silt)
	Transitional	32.5	11.41	61.22	72.63	27.37	27.37	100.00	0.00	Sandy mud (sandy silt)
	Transitional	42.5	12.96	67.75	80.71	18.42	19.29	99.12	0.88	Sandy mud (sandy silt)
SM8	Peat (fibrous)	1	4.83	42.06	46.89	53.11	53.11	100.00	0.00	Muddy sand (silty sand)
	Peat (fibrous)	5	3.63	35.00	38.63	61.37	61.37	100.00	0.00	Muddy sand (silty sand)

	Peat (fibrous)	9	6.04	52.63	58.67	41.33	41.33	100.00	0.00	Sandy mud (sandy silt)
	Peat (humified)	13	6.37	48.89	55.26	44.73	44.74	99.99	0.01	Sandy mud (sandy silt)
	Peat (humified)	17	6.17	53.02	59.19	40.81	40.81	100.00	0.00	Sandy mud (sandy silt)
	Peat (humified)	22.5	9.22	67.56	76.78	23.22	23.22	100.00	0.00	Sandy mud (sandy silt)
	Transitional	32.5	8.38	61.53	69.91	28.72	30.09	98.63	1.37	Sandy mud (sandy silt)
	Transitional	42.5	10.13	53.56	63.69	33.13	36.31	96.82	3.18	N/A
SM13	Peat (fibrous)	1	2.32	27.30	29.62	70.38	70.38	100.00	0.00	Muddy sand (silty sand)
	Peat (fibrous)	5	3.61	34.97	38.58	57.81	61.42	96.38	3.62	N/A
	Peat (humified)	9	5.00	36.65	41.65	56.88	58.35	98.53	1.47	Muddy sand (silty sand)
	Transitional	13	4.51	34.21	38.72	59.86	61.28	98.58	1.42	Muddy sand (silty sand)
	Transitional	17	7.14	40.99	48.13	50.92	51.87	99.06	0.94	Muddy sand (silty sand)

	Basal	22.5	5.80	31.35	37.16	62.19	62.84	99.35	0.65	Muddy sand (silty sand)
	Basal	32.5	8.99	40.13	49.12	47.07	50.88	96.20	3.80	N/A
	Basal	42.5	9.36	47.87	57.23	42.44	42.77	99.66	0.34	Sandy mud (sandy silt)
SM16	Peat (fibrous)	1	4.02	36.06	40.08	59.92	59.92	100.00	0.00	Muddy sand (silty sand)
	Peat (humified)	5	2.96	29.99	32.95	67.05	67.05	100.00	0.00	Muddy sand (silty sand)
	Peat (humified)	9	4.08	34.64	38.72	49.48	61.28	88.20	11.80	N/A
	Transitional	13	5.55	36.67	42.22	57.26	57.78	99.48	0.52	Muddy sand (silty sand)
	Transitional	17	5.23	28.92	34.15	64.90	65.85	99.05	0.95	Muddy sand (silty sand)
	Basal	22.5	6.29	37.03	43.31	55.98	56.69	99.29	0.71	Muddy sand (silty sand)
	Basal	32.5	8.46	43.91	52.37	41.72	47.63	94.09	5.91	N/A
	Basal	42.5	2.71	10.85	13.56	22.22	86.44	35.78	64.22	N/A

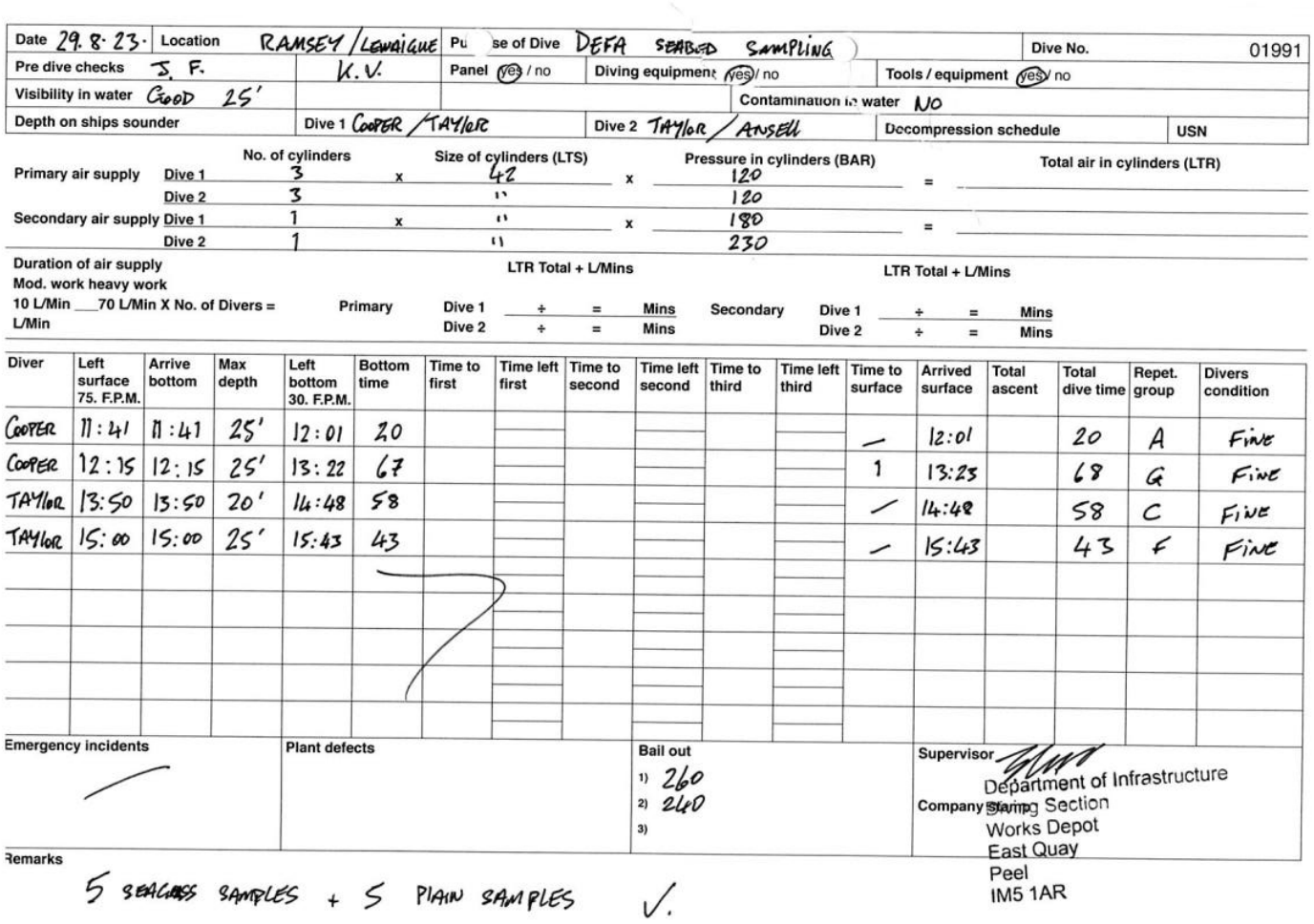

Date 29.8.23 · Location RAMSEY / LEWAIGUE · Purpose of Dive DEFRA SEABED SAMPLING · Dive No. 01991

Pre dive checks J. F. K.V. · Panel (yes) / no · Diving equipment (yes) / no · Tools / equipment (yes) / no

Visibility in water GOOD 25' · Contamination in water NO

Depth on ships sounder · Dive 1 COOPER / TAYLOR · Dive 2 TAYLOR / ANSELL · Decompression schedule · USN

		No. of cylinders		Size of cylinders (LTS)		Pressure in cylinders (BAR)		Total air in cylinders (LTR)
Primary air supply	Dive 1	3	x	42	x	120	=	
	Dive 2	3		〃		120		
Secondary air supply	Dive 1	1	x	〃	x	180	=	
	Dive 2	1		〃		230		

Duration of air supply
Mod. work heavy work
10 L/Min ___70 L/Min X No. of Divers = L/Min

LTR Total + L/Mins

Primary Dive 1 ÷ = Mins
Dive 2 ÷ = Mins

LTR Total + L/Mins

Secondary Dive 1 ÷ = Mins
Dive 2 ÷ = Mins

Diver	Left surface 75. F.P.M.	Arrive bottom	Max depth	Left bottom 30. F.P.M.	Bottom time	Time to first	Time left first	Time to second	Time left second	Time to third	Time left third	Time to surface	Arrived surface	Total ascent	Total dive time	Repet. group	Divers condition
COOPER	11:41	11:41	25'	12:01	20							—	12:01		20	A	FINE
COOPER	12:15	12:15	25'	13:22	67							1	13:23		68	G	FINE
TAYLOR	13:50	13:50	20'	14:48	58							—	14:48		58	C	FINE
TAYLOR	15:00	15:00	25'	15:43	43							—	15:43		43	F	FINE

Emergency incidents: —

Plant defects:

Bail out
1) 260
2) 240
3)

Supervisor

Company Stamp: Department of Infrastructure
Ports Section
Works Depot
East Quay
Peel
IM5 1AR

Remarks: 5 SEAGRASS SAMPLES + 5 PLAIN SAMPLES ✓

Figure C.20 Ramsey Bay seagrass sediment coring dive log.

Table C.3 Ramsey Bay seagrass meadow sediment classifications. Average proportion (%) of clay (<3.9 µm), silt (3.9 µm to 62.5 µm), mud (<62.5 µm), very fine to coarse sand (62.5–1000 µm) and sand and gravel (>62.5 µm), based on Udden (1914) and Wentworth (1922). Proportion of particles <1000 µm (analysed by laser diffraction) and >1000 µm (sieved and weighed). Sediment classifications are based on the Folk (1954) classification scheme for sediment depths having >99% of sediment <1000 µm (i.e. trace gravel and/or very coarse sand).

Site	Depth	Clay (%)	Silt (%)	Mud (%)	Sand (%)	Sand-and-gravel (%)	<1000 µm (%)	>1000 µm (%)	Folk class
V2	1	1.40	3.75	5.15	94.49	94.85	99.64%	0.36%	Sand
V2	5	1.08	2.57	3.65	96.12	96.35	99.78%	0.22%	Sand
V2	9	1.09	2.17	3.25	96.56	96.75	99.82%	0.18%	Sand
V2	13	0.72	1.54	2.26	97.39	97.74	99.65%	0.35%	Sand
V2	17	0.13	0.97	1.10	98.63	98.90	99.73%	0.27%	Sand
V2	22.5	0.41	0.93	1.34	98.66	98.66	100.00%	0.00%	Sand
V2	32.5	0.91	1.34	2.25	79.74	97.75	82.00%	18.00%	N/A
V3	1	0.76	1.70	2.46	96.85	97.54	99.31%	0.69%	Sand
V3	5	0.95	2.03	2.97	96.51	97.03	99.49%	0.51%	Sand
V3	9	0.91	1.92	2.83	95.96	97.17	98.79%	1.21%	Sand
V3	13	0.61	1.12	1.73	96.44	98.27	98.17%	1.83%	N/A
V3	17	0.00	0.58	0.58	98.26	99.42	98.85%	1.15%	Sand
V3	22.5	0.39	0.59	0.98	98.97	99.02	99.95%	0.05%	Sand
V3	32.5	0.82	1.04	1.86	94.68	98.14	96.53%	3.47%	N/A
V4	1	0.00	0.05	0.05	93.96	99.95	94.01%	5.99%	N/A
V4	5	0.64	1.45	2.09	96.52	97.91	98.61%	1.39%	Sand
V4	9	0.00	0.69	0.69	83.06	99.31	83.75%	16.25%	N/A
V4	13	0.85	1.10	1.95	97.55	98.05	99.49%	0.51%	Sand
V4	17	0.93	1.36	2.29	96.93	97.71	99.22%	0.78%	Sand

V4	22.5	0.82	1.06	1.87	90.80	98.13	92.68%	7.32%	N/A
V4	32.5	0.76	0.89	1.65	97.73	98.35	99.37%	0.63%	Sand
V5	1	0.50	1.39	1.89	97.65	98.11	99.53%	0.47%	Sand
V5	5	1.37	3.21	4.58	94.50	95.42	99.08%	0.92%	Sand
V5	9	1.03	1.86	2.89	91.62	97.11	94.51%	5.49%	N/A
V5	13	0.95	1.53	2.48	97.13	97.52	99.61%	0.39%	Sand
V5	17	1.10	1.52	2.62	96.27	97.38	98.89%	1.11%	Sand
V5	22.5	1.15	1.82	2.97	96.61	97.03	99.58%	0.42%	Sand
V5	32.5	0.99	1.44	2.43	97.48	97.57	99.91%	0.09%	Sand
V5	42.5	0.77	0.95	1.72	98.11	98.28	99.81%	0.19%	Sand
V6	1	0.49	1.04	1.53	98.21	98.47	99.74%	0.26%	Sand
V6	5	0.86	2.04	2.90	96.64	97.10	99.52%	0.48%	Sand
V6	9	0.51	1.34	1.85	97.89	98.15	99.74%	0.26%	Sand
V6	13	0.63	1.11	1.74	98.02	98.26	99.75%	0.25%	Sand
V6	17	0.32	0.58	0.90	52.96	99.10	53.86%	46.14%	N/A
V6	22.5	1.07	1.44	2.51	97.07	97.49	99.59%	0.41%	Sand
V6	32.5	1.33	1.97	3.29	96.50	96.71	99.79%	0.21%	Sand
V6	42.5	0.96	1.05	2.00	97.70	98.00	99.70%	0.30%	Sand

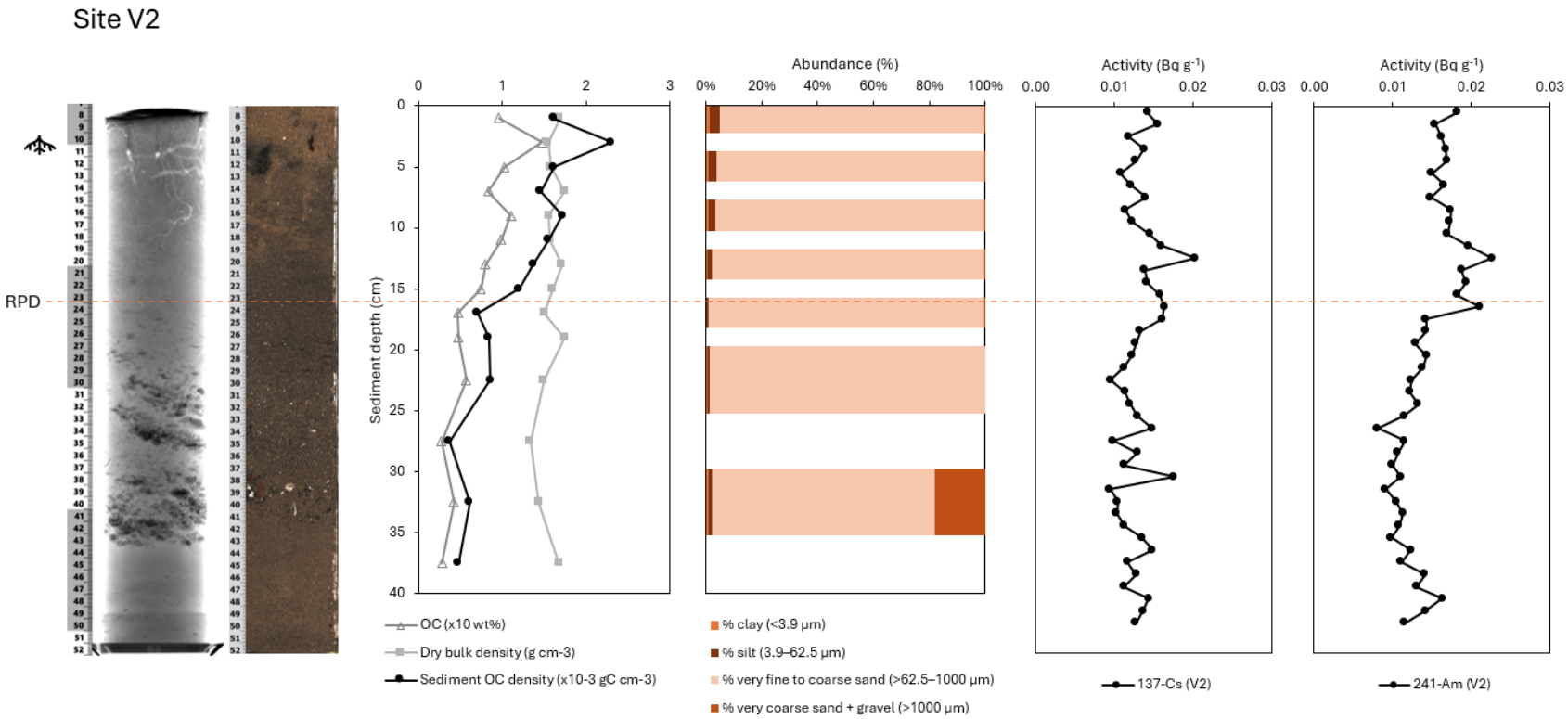

Figure C.21 Sediment core depth profiles for seagrass meadow sediments from Site V2. Left to right: X-ray radiograph image, high-resolution surface image, root penetration depth (RPD, dashed orange line), organic carbon (OC) concentration (%), sediment dry bulk density (DBD, g cm^{-3}), sediment organic carbon density (SCD, gC cm^{-3}), sediment grain size fractions, and radionuclide profiles for ^{137}Cs and ^{241}Am. Root icon indicates where rhizome were present.

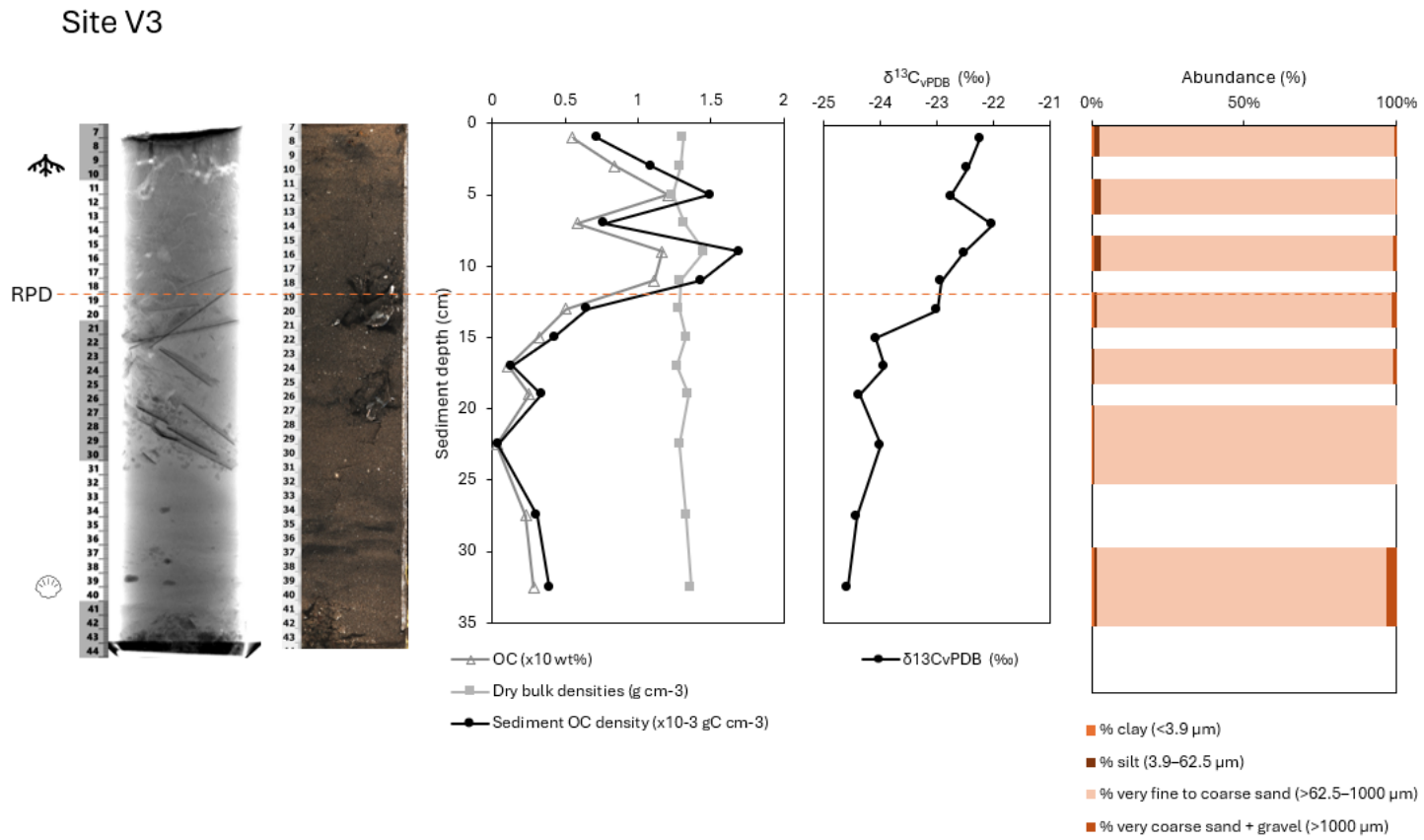

Figure C.22 Sediment core depth profiles for seagrass meadow sediments from Site V3. Left to right: X-ray radiograph image, high-resolution surface image, root penetration depth (RPD, dashed orange line), organic carbon (OC) concentration (%), sediment dry bulk density (DBD, g cm^{-3}), sediment organic carbon density (SCD, gC cm^{-3}), $\delta^{13}C_{vPDB}$ (‰), and sediment grain size fractions. Root icon indicates where rhizomes were present, while shell icon indicates where whole shell or shell fragments were present.

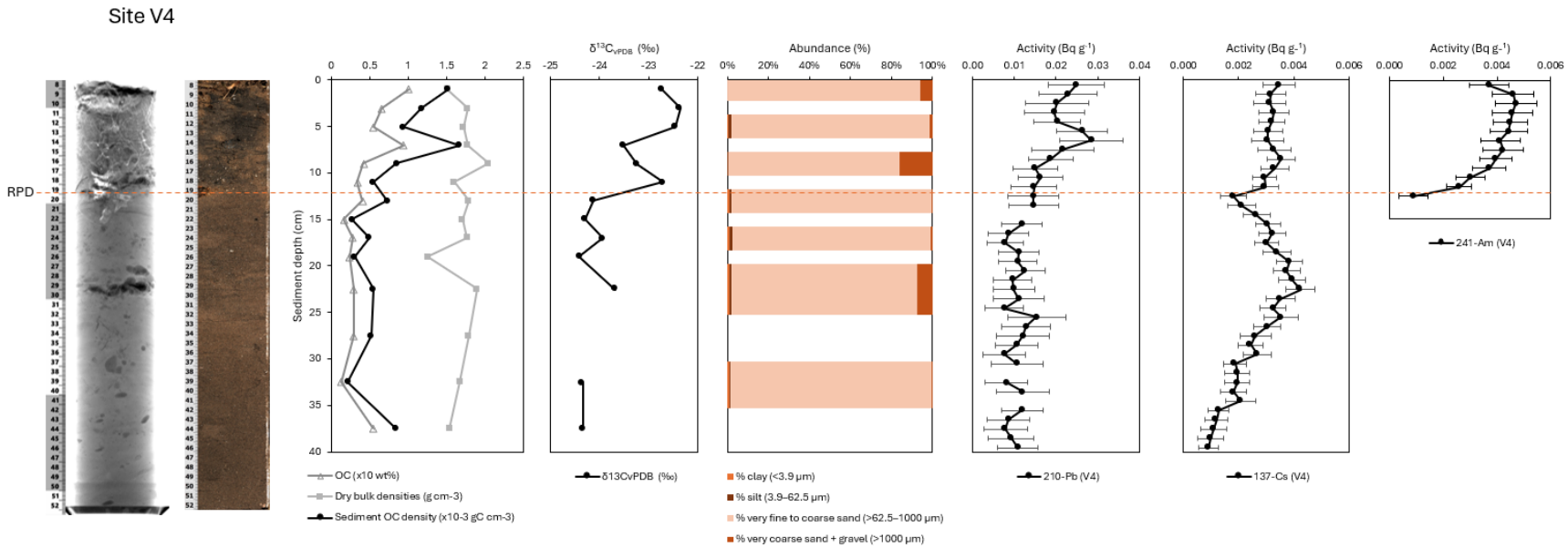

Figure C.23 Sediment core depth profiles for seagrass meadow sediments from Site V4. Left to right: X-ray radiograph image, high-resolution surface image, root penetration depth (RPD, dashed orange line), organic carbon (OC) concentration (%), sediment dry bulk density (DBD, g cm^{-3}), sediment organic carbon density (SCD, gC cm^{-3}), $\delta^{13}C_{vPDB}$ (‰), sediment grain size fractions, and radionuclide profiles for ^{210}Pb, ^{137}Cs, and ^{241}Am.

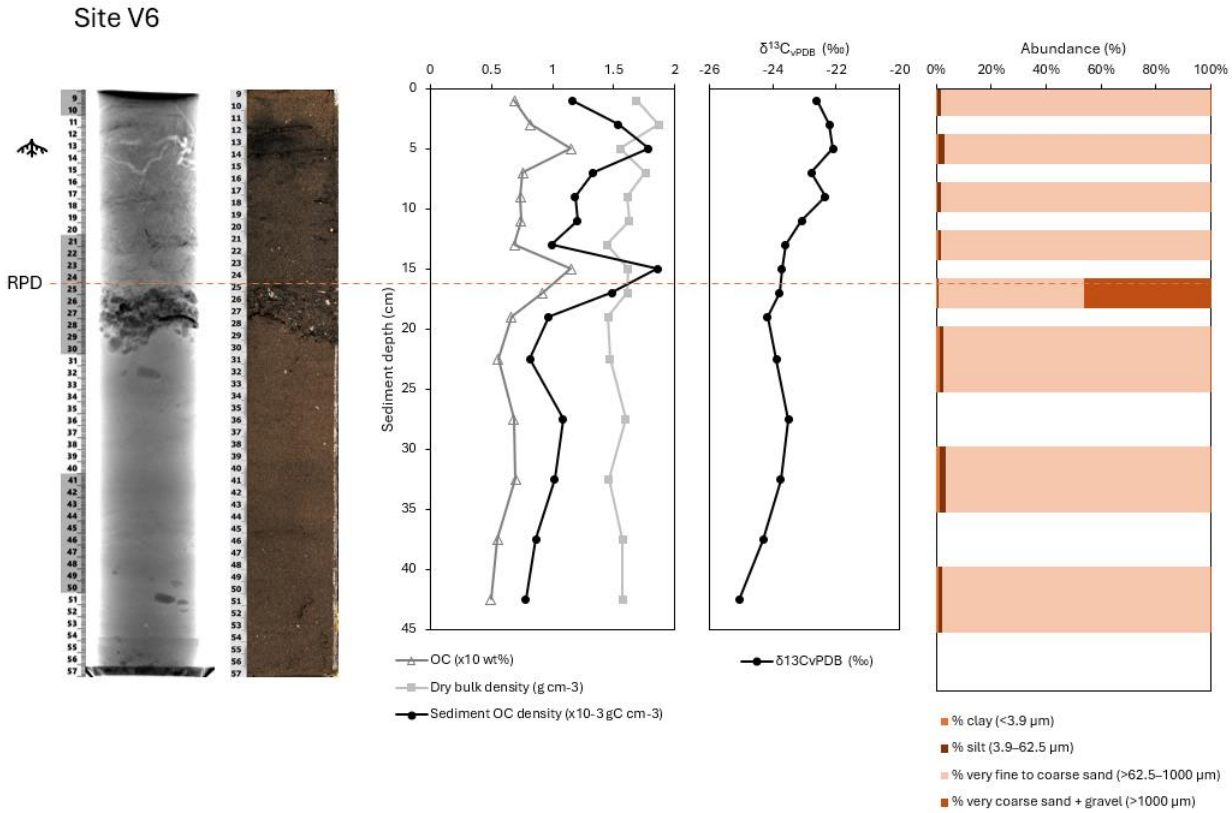

Figure C.24 Sediment core depth profiles for seagrass meadow sediments from Site V6. Left to right: X-ray radiograph image, high-resolution surface image, root penetration depth (RPD, dashed orange line), organic carbon (OC) concentration (%), sediment dry bulk density (DBD, g cm^{-3}), sediment organic carbon density (SCD, gC cm^{-3}), $\delta^{13}C_{vPDB}$ (‰), and sediment grain size fractions. Root icon indicates where rhizomes were present.

Table C.4 Sediment classification for Ramsey Bay unvegetated sediment adjacent to the seagrass meadow. Average proportion (%) of clay (<3.9 μm), silt (3.9 μm to 62.5 μm), mud (<62.5 μm), very fine to coarse sand (62.5–1000 μm) and sand and gravel (>62.5 μm), based on Udden (1914) and Wentworth (1922). Proportion of particles <1000 μm (analysed by laser diffraction) and >1000 μm (sieved and weighed). Sediment classifications are based on the Folk (1954) classification scheme for sediment depths having >99% of sediment <1000 μm (i.e. trace gravel and/or very coarse sand).

Site ID	Depth (cm)	Clay (%)	Silt (%)	Mud (%)	Sand (%)	Sand-and-gravel (%)	<1000 μm (%)	>1000 μm (%)	Folk class
UV1	1	1.06	3.57	4.63	89.33	95.37	93.96	6.04	N/A
	5	1.54	4.89	6.43	88.01	93.57	94.44	5.56	N/A
	9	0.81	2.38	3.19	58.48	96.81	61.67	38.33	N/A
UV2	1	0.85	2.00	2.85	94.36	97.15	97.21	2.79	N/A
	5	1.54	4.21	5.75	91.66	94.25	97.41	2.59	N/A
	9	1.99	5.37	7.36	90.15	92.64	97.52	2.48	N/A
	13	1.32	3.41	4.73	62.10	95.27	66.83	33.17	N/A
	17	0.14	0.54	0.68	36.48	99.32	37.16	62.84	N/A
	22.5	18.73	23.11	41.84	43.56	58.16	85.40	14.60	N/A
UV3	1	0.35	2.18	2.53	94.36	97.47	96.89	3.11	N/A
	5	1.28	4.09	5.37	92.46	94.63	97.83	2.17	N/A
	9	0.42	1.49	1.91	26.93	98.09	28.84	71.16	N/A
	13	27.27	34.97	62.24	26.99	37.76	89.24	10.76	N/A
	17	12.46	19.09	31.55	27.34	68.45	58.89	41.11	N/A
	22.5	24.70	30.56	55.26	22.97	44.74	78.23	21.77	N/A
UV4	1	0.75	3.47	4.22	94.04	95.78	98.25	1.75	N/A
	5	1.41	5.08	6.49	92.11	93.51	98.60	1.40	Sand

UV5	1	1.26	3.59	4.85	92.83	95.15	97.68	2.32	N/A
	5	1.60	5.13	6.72	91.87	93.28	98.59	1.41	Sand
	9	1.95	5.81	7.76	91.26	92.24	99.03	0.97	Sand
	13	8.44	17.64	26.08	72.40	73.92	98.48	1.52	Muddy sand (silty sand)

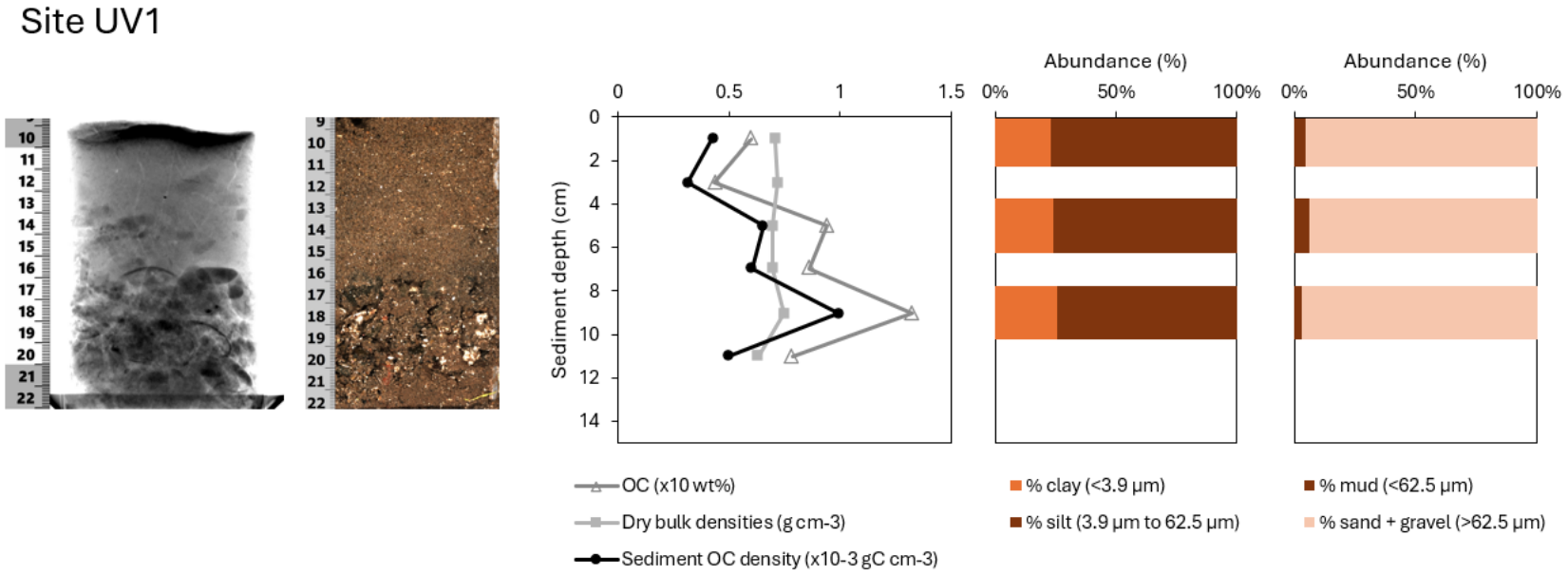

Figure C.25 Sediment core depth profiles for unvegetated sediments adjacent to the seagrass meadow from Site UV1. Left to right: X-ray radiograph image, high-resolution surface image, organic carbon (OC) concentration (%), sediment dry bulk density (DBD, g cm^{-3}), sediment organic carbon density (SCD, gC cm^{-3}), and sediment grain size fractions.

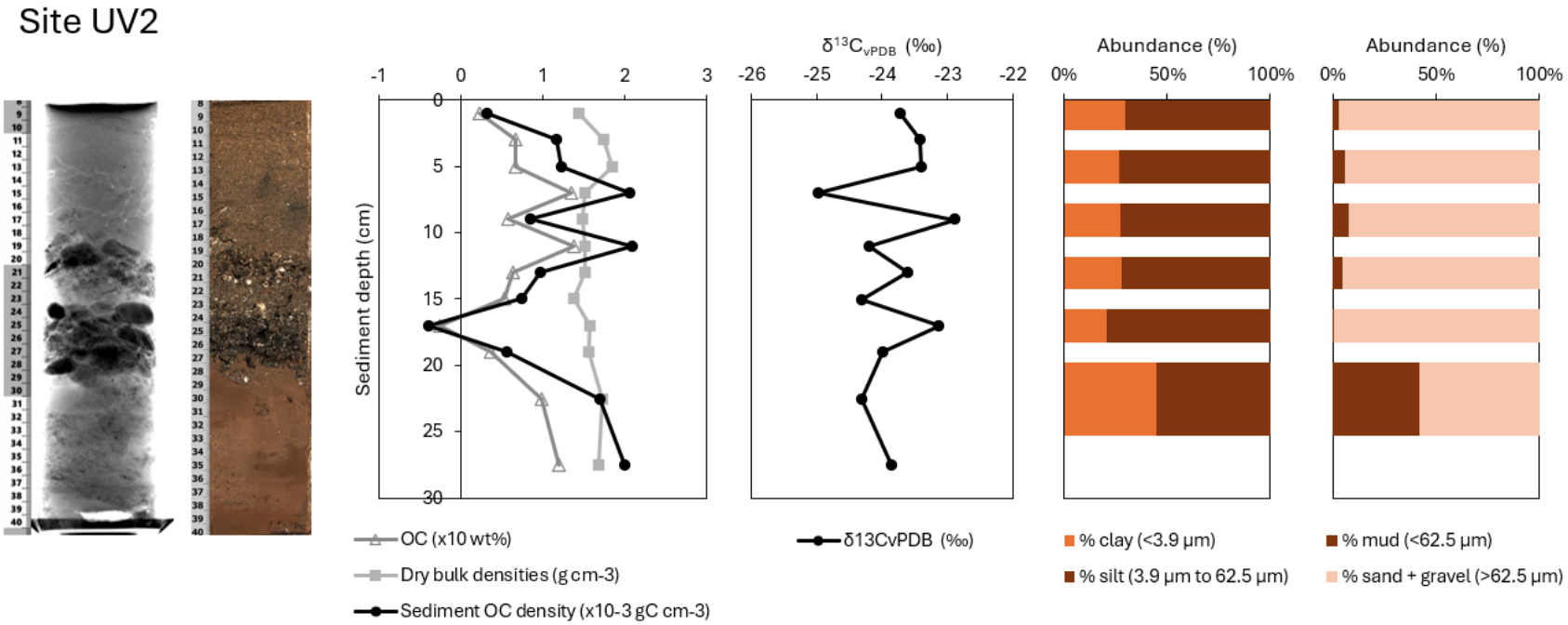

Figure C.26 Sediment core depth profiles for unvegetated sediments adjacent to the seagrass meadow from Site UV2. Left to right: X-ray radiograph image, high-resolution surface image, organic carbon (OC) concentration (%), sediment dry bulk density (DBD, g cm^{-3}), sediment organic carbon density (SCD, gC cm^{-3}), $\delta^{13}C_{vPDB}$ (‰), and sediment grain size fractions.

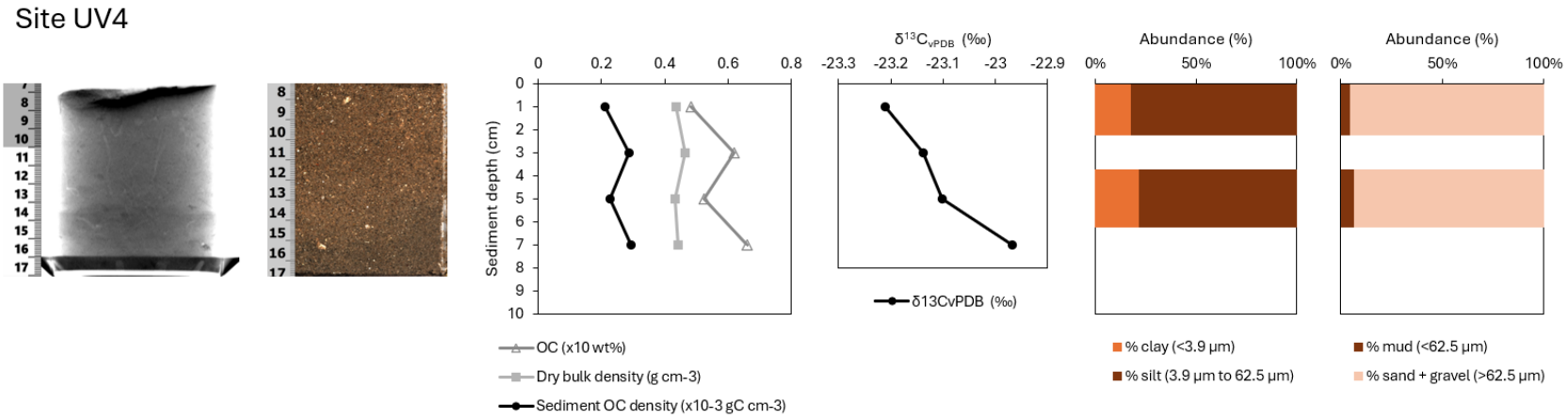

Figure C.27 Sediment core depth profiles for unvegetated sediments adjacent to the seagrass meadow from Site UV4. Left to right: X-ray radiograph image, high-resolution surface image, organic carbon (OC) concentration (%), sediment dry bulk density (DBD, g cm^{-3}), sediment organic carbon density (SCD, gC cm^{-3}), $\delta^{13}C_{vPDB}$ (‰), and sediment grain size fractions.

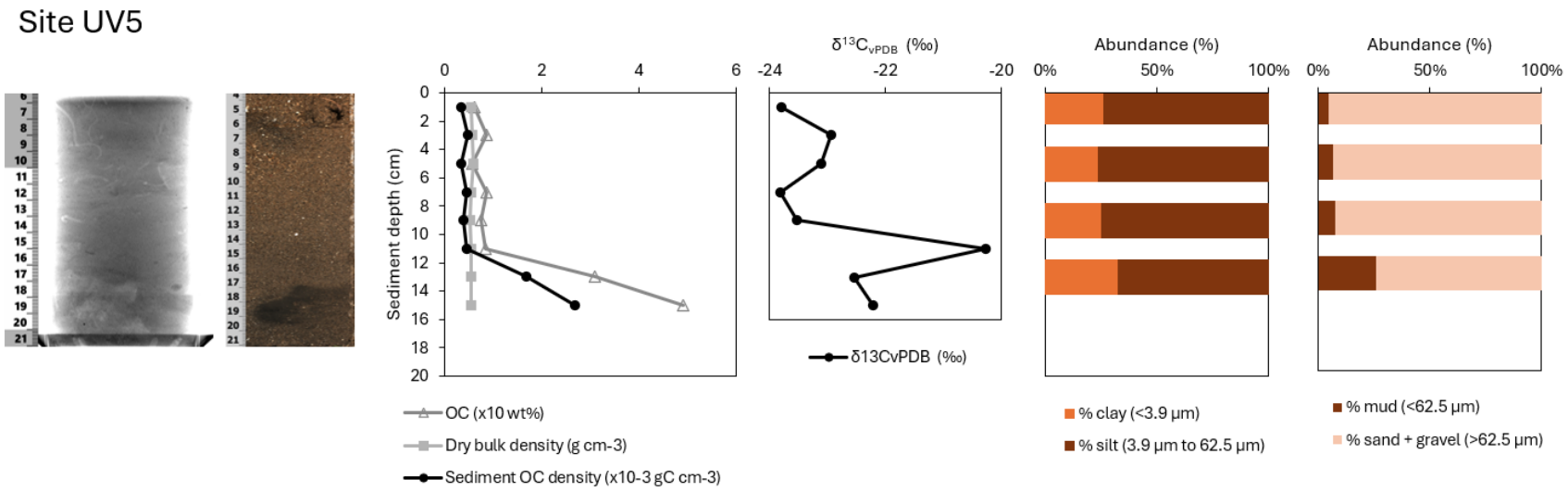

Figure C.28 Sediment core depth profiles for unvegetated sediments adjacent to the seagrass meadow from Site UV5. Left to right: X-ray radiograph image, high-resolution surface image, organic carbon (OC) concentration (%), sediment dry bulk density (DBD, g cm^{-3}), sediment organic carbon density (SCD, gC cm^{-3}), $\delta^{13}C_{vPDB}$ (‰), and sediment grain size fractions.

References

Agri-Food and Biosciences Institute (2023). Nephrops norvegicus kriged density estimates, Northeast Western Irish Sea Mud Belt (2013–2022) [unpublished raw data]. Agri-Food and Biosciences Institute (AFBI), Northern Ireland.

Amoroso, R. O., Pitcher, C. R., Rijnsdorp, A. D., McConnaughey, R. A., Parma, A. M., Suuronen, P., et al. (2018). Bottom trawl fishing footprints on the world's continental shelves. *Proceedings of the National Academy of Sciences of the United States of America*, *115(43), E10275-E10282*. https://doi.org/10.1073/pnas.1802379115.

Appleby, P. G. & Oldfield, F. (1978). The calculation of lead-210 dates assuming a constant rate of supply of unsupported 210Pb to the sediment. *CATENA, 5(1), 1–8.* https://doi.org/10.1016/S0341-8162(78)80002-2.

Arias-Ortiz, A., Masqué, P., Garcia-Orellana, J., Serrano, O., Mazarrasa, I., Marbà, N., et al. (2018). Reviews and syntheses: 210Pb-derived sediment and carbon accumulation rates in vegetated coastal ecosystems – setting the record straight. *Biogeosciences, 15, 6791–6818*. https://doi.org/10.5194/bg-15-6791-2018.

Arndt, S., Jørgensen, B. B., LaRowe, D. E., Middelburg, J. J., Pancost, R. D. & Regnier, P. (2013). Quantifying the degradation of organic matter in marine sediments: A review and synthesis. *Earth-Science Reviews, 123, 53–86*. https://doi.org/10.1016/j.earscirev.2013.02.008.

Atwood, T. B., Sala, E., Mayorga, J., Bradley, D., Cabral, R. B., Auber, A., et al. (2023). Reply to: Quantifying the carbon benefits of ending bottom trawling. *Nature 617, E3–E5*. https://doi.org/10.1038/s41586-023-06015-6.

Atwood, T. B., Witt, A., Mayorga, J., Hammill, E., & Sala, E. (2020). Global Patterns in Marine Sediment Carbon Stocks. *Frontiers in Marine Science, 7:165, 1–9.* https://doi.org/10.3389/fmars.2020.00165.

Bakker, J. F. & Helder, W.(1993). Skagerrak (northeastern North Sea) oxygen microprofiles and porewater chemistry in sediments. *Marine Geology, 111(3–4), 299–321*. https://doi.org/10.1016/00253227(93)90137-K.

Barsanti, M., Garcia-Tenorio, R., Schirone, A., Rozmaric, M., Ruiz-Fernández, A. C., Sanchez-Cabeza, J. A., et al. (2020). Challenges and limitations of the 210Pb sediment dating method: Results from an IAEA modelling interlaboratory comparison exercise. *Quaternary Geochronology, 59, 101093.* https://doi.org/10.1016/j.quageo.2020.101093.

Bauer, J., Cai, W. J., Raymond, P., Bianchi, T. S., Hopkinson, C. S. & Regnier, P. A. G. (2013). The changing carbon cycle of the coastal ocean. *Nature, 504, 61–70*. https://doi.org/10.1038/nature12857.

Belderson, R. H. (1964). Holocene sedimentation in the western half of the Irish Sea. *Marine Geology, 2(1), 147–163.* https://doi.org/10.1016/0025-3227(64)90032-5.

Bertram, C., Quaas, M., Reusch, T. B. H., Vafeidis, A. T., Wolff, C. & Rickels, W. (2021). The blue carbon wealth of nations. *Nature Climate Change, 11, 704–709*. https://doi.org/10.1038/s41558-021-01089-4

Black, K. E., Smeaton, C., Turrell, W. R., & Austin, W. E. N. (2022). Assessing the potential vulnerability of sedimentary carbon stores to bottom trawling disturbance within the UK EEZ. *Frontiers in Marine Science, 9, 892892*. https://doi.org/10.3389/fmars.2022.892892.

Bowers, D. G., Roberts, E. M., White, M., & Moate, B. D. (2013). Water masses, mixing, and the flow of dissolved organic carbon through the Irish Sea. *Continental Shelf Research, 58(5), 12-20*. https://doi.org/10.1016/j.csr.2013.02.007.

Bradley, J. A., Hülse, D., LaRowe, D. E. & Arndt, S. (2022). Transfer efficiency of organic carbon in marine sediments. *Nature Communications, 13, 7297.* https://doi.org/10.1038/s41467-022-35112-9.

British Geological Survey (2024). Seabed sediments 250K [Dataset]. Available at: https://www.bgs.ac.uk/datasets/marine-sediments-250k/ (Accessed: 10 March, 2025).

Burden, A. & Clilverd, H. (2021). Moving towards Inclusion of Coastal Wetlands in the UK LULUCF Inventory - Rapid Assessment of Activity Data Availability. UK Centre for Ecology & Hydrology, Bangor. Report to the Department for Business, Energy & Industrial Strategy (BEIS), pp 61. Available at: https://nora.nerc.ac.uk/id/eprint/533055/ (Accessed: 3 April, 2025).

Burdige, D. J. (2007). Preservation of Organic Matter in Marine Sediments: Controls, Mechanisms, and an Imbalance in Sediment Organic Carbon Budgets?. *Chemical Reviews, 107(2), 467–485.* https://doi.org/10.1021/cr050347q.

Burrows, M. T., Smeaton, C., Tillin, H., Grundy, S., Sugden, H., Moore, P., et al. (2024). The United Kingdom's Blue Carbon Inventory: Assessment of Marine Carbon Storage and Sequestration Potential in the Irish Sea and Welsh Coast Region (Including Within Marine Protected Areas). Scottish Association for Marine Science. Oban, Scotland. Available at: https://www.wildlifetrusts.org/sites/default/files/2024-09/Irish%20Sea%20%26%20Welsh%20Coast%20-%20scientific%20report.pdf (Accessed: 2 April, 2025).

Campbell, A. D., Fatoyinbo, L., Goldberg, L. & Lagomasino, D. (2022). Global hotspots of salt marsh change and carbon emissions. *Nature, 612, 701–706*. https://doi.org/10.1038/s41586-022-05355-z.

Chen, Z., Nie, T., Zhao, X., Li, J., Yang, B., Cui, D., et al. (2022). Organic carbon remineralization rate in global marine sediments: A review. *Regional Studies in Marine Science, 49, 102112.* https://doi.org/10.1016/j.rsma.2021.102112.

Church, N. J., Carter, A. J., Tobin, D., Edwards, D., Eassom, A., Cameron, A., et al. (2016). JNCC Pressure Mapping Methodology. Physical Damage (Reversible Change) - Penetration and/or disturbance of the substrate below the surface of the seabed, including abrasion. JNCC Report No. 515. JNCC, Peterborough. Available at: https://hub.jncc.gov.uk/assets/5874e65d-324b-4f6b-bce2-bfc7aab5ba7f (Accessed: 2 April, 2025).

Cornacchia, L., van de Vijsel, R.C., van der Wal, D., Ysebaert, T. Sun, J., van Prooijen, B., et al. (2024). Vegetation traits and biogeomorphic complexity shape the resilience of salt marshes to sea-level rise. *Communications Earth & Environment, 5, 658*. https://doi.org/10.1038/s43247-024-01829-2.

Coughlan, M., Guerrini, M., Creane, S., O'Shea, M., Ward, S. L., Van Landeghem, K. J. J., et al. (2021). A new seabed mobility index for the Irish Sea: Modelling seabed shear stress and classifying sediment mobilisation to help predict erosion, deposition, and sediment distribution. *Continental Shelf Research,* 229, 104574. https://doi.org/10.1016/j.csr.2021.104574.

Coughlan, M., Wheeler, A. J., Dorschel, B., Lordan, C., Boer, W., van Gaever, P., et al. (2015). Record of anthropogenic impact on the Western Irish Sea mud belt. *Anthropocene, 9, 56–69*. https://doi.org/10.1016/j.ancene.2015.06.001.

Crooks, S., Windham--Myers, L., & Troxler, T. G. (2018). Defining blue carbon: The emergence of a climate context for coastal carbon dynamics. In L. Windham-Myers, S. Crooks, & T. G. Troxler (Eds.), A blue carbon primer (pp. 1–8). CRC Press. https://doi.org/10.1201/9780429435362.

Croudace, I. W., Teasdale, P. A., & Cundy, A. B. (2019). 200-year industrial archaeological record preserved in an Isle of Man saltmarsh sediment sequence: Geochemical and radiochronological evidence. *Quaternary International, 514, 195–203.* https://doi.org/10.1016/j.quaint.2018.09.045.

Curran, J. C. (2019). Isle of Man Programme for Achievement of Climate Targets (IMPACT) Report, Appendix 10c. Isle of Man: Isle of Man Government. Available at: https://www.gov.im/media/1368097/gd20190102_james-curran-report.pdf (Accessed: 2 April, 2025)

Dahl, M., Asplund, M. E., Bergman, S., Björk, M., Braun, S., Löfgren, E. et al. (2023). First assessment of seagrass carbon accumulation rates in Sweden: A field study from a fjord system at the Skagerrak coast. *PLOS Climate, 2(1), e0000099*. https://doi.org/10.1371/journal.pclm.0000099.

Dahl, M., Asplund, M. E., Björk, M., Deyanova, D., Infantes, E., Isaeus, M., et al. (2020a). The influence of hydrodynamic exposure on carbon storage and nutrient retention in eelgrass (Zostera marina L.) meadows on the Swedish Skagerrak coast. *Scientific Reports, 10(1), 13666*. https://doi.org/10.1038/s41598-020-70403-5.

Dahl, M., Asplund, M. E., Deyanova, D., Franco, J. N., Koliji, A., Infantes, E., et al. (2020b). High Seasonal Variability in Sediment Carbon Stocks of Cold-Temperate Seagrass Meadows. *Journal of Geophysical Research: Biogeosciences, 125(1), e2019JG005430.* https://doi.org/10.1029/2019JG005430.

Dahl, M., Deyanova, D., Gütschow, S., Asplund, M. E., Lyimo, L. D., Karamfilov, V. et al. (2016). Sediment Properties as Important Predictors of Carbon Storage in *Zostera marina* Meadows: A Comparison of Four European Areas. *PLOS ONE, 11(12), e0167493*. https://doi.org/10.1371/journal.pone.0167493

Davidson, K. E., Fowler, M. S., Skov, M. W., Doerr, S. H., Beaumont, N. & Griffin, J. N. (2017). Livestock grazing alters multiple ecosystem properties and services in salt marshes: a meta-analysis. *Journal of Applied Ecology, 54, 1395-1405*. https://doi.org/10.1111/1365-2664.12892

Davie, S. & Lordan, C. (2011). Definition, dynamics and stability of métiers in the Irish otter trawl fleet. *Fisheries Research, 111(3), 145–158*. https://doi.org/10.1016/j.fishres.2011.07.005.

Davis, B. W., Groom, R. A., Carle, C. J., Hutley, L. B., Lovelock, C., & Perry, J. (2023) Investigating the potential for a blue carbon economy on Australia's northern coastline. *The APPEA Journal, 63, S367-S370*. https://doi.org/10.1071/AJ22021.

de Haas, H., van Weering, T. C. E., & de Stigter, H. (2002). Organic carbon in shelf seas: sinks or sources, processes and products. *Continental Shelf Research, 22(5), 691–717.* https://doi.org/10.1016/S0278-4343(01)00093-0.

Diesing, M., Stephens, D. & Aldridge, J. (2013). A proposed method for assessing the extent of the seabed significantly affected by demersal fishing in the Greater North Sea. *ICES Journal of Marine Science, 70(6), Pp. 1085-1096.* https://doi.org/10.1093/icesjms/fst066.

Diesing, M., Thorsnes, T., & Bjarnadóttir, L. R. (2021). Organic carbon densities and accumulation rates in surface sediments of the North Sea and Skagerrak. *Biogeosciences, 18(6), 2139–2160*. https://doi.org/10.5194/bg-18-2139-2021.

Dobby, H., Doyle, J., Jonasson, J., Jonsson, P., Leocadio, A., Lordan, C., et al. (2021). ICES Survey Protocols – Manual for Nephrops Underwater TV Surveys, coordinated under ICES Working Group on Nephrops Surveys (WGNEPS). ICES Techniques in Marine Environmental Science (TIMES). Report. https://doi.org/10.17895/ices.pub.8014.

Duarte, C. M. (2017). Reviews and syntheses: Hidden forests, the role of vegetated coastal habitats in the ocean carbon budget. *Biogeosciences, 14, 301–310.* https://doi.org/10.5194/bg-14-301-2017m.

Duarte, C. M. & Kirkman, H. (2001). Chapter 7 - Methods for the measurement of seagrass abundance and depth distribution, Global Seagrass Research Methods.

Amsterdam: Elsevier Science. *141–153*. https://doi.org/10.1016/B978-044450891-1/50008-6 (Accessed: 20 December 2023).

Duarte, C. M., Middelburg, J. J., & Caraco, N. (2005). Major role of marine vegetation on the oceanic carbon cycle. *Biogeosciences. 2(1), 1–8*. https://doi.org/10.5194/bg-2-1-2005.

Dubosq, N., Schmidt, S., Walsh, J. P., Grémare, A., Gillet, H., Lebleu, P., et al. (2021). A first assessment of organic carbon burial in the West Gironde Mud Patch (Bay of Biscay). *Continental Shelf Research*, 221, 104419. https://doi.org/10.1016/j.csr.2021.104419.

Dunic, J. C., Brown, C. J., Connolly, R. M., Turschwell, M. P. & Côté, I. M. (2021). Long-term declines and recovery of meadow area across the world's seagrass bioregions. *Global Change Biology, 27, 4096-4109*. https://doi.org/10.1111/gcb.15684

Eigaard, O. R., Bastardie, F., Breen, M., Dinesen, G. E., Hintzen, N. T., Laffargue, P., et al. (2016). Estimating seabed pressure from demersal trawls, seines, and dredges based on gear design and dimensions. *ICES Journal of Marine Science, 73(1), i27–i43.* https://doi.org/10.1093/icesjms/fsv099.

Eigaard, O. R., Bastardie, F., Hintzen, N. T., Buhl-Mortensen, L., Buhl-Mortensen, P., Catarino, R., et al. (2017). The footprint of bottom trawling in European waters: distribution, intensity, and seabed integrity. *ICES Journal of Marine Science, 74(3), 847–865.* https://doi.org/10.1093/icesjms/fsw194.

Epstein, G., Middelburg, J. J., Hawkins, J. P., Norris, C. R., & Roberts, C. M. (2021). The impact of mobile demersal fishing on carbon storage in seabed sediments. *Global Change Biology, 28(9), 2875–2894.* https://doi.org/10.1111/gcb.16105.

Epstein, G. & Roberts, C. M. (2022). Identifying priority areas to manage mobile bottom fishing on seabed carbon in the UK. *PLOS Climate, 1(9), e0000059*. https://doi.org/10.1371/journal. pclm.0000059.

Folk, R. L. (1954). The Distinction between Grain Size and Mineral Composition in Sedimentary-Rock Nomenclature. *The Journal of Geology, 62(4), 344-359*. Available at: http://www.jstor.org/stable/30065016 (Accessed: 10 March, 2025).

Ford, H., Garbutt, A., Duggan-Edwards, M., Pagès, J. F., Harvey, R., Ladd, C., et al. (2019). Large-scale predictions of salt-marsh carbon stock based on simple observations of plant community and soil type. *Biogeosciences, 16, 425–436.* https://doi.org/10.5194/bg-16-425-2019.

Fourqurean, J., Duarte, C., Kennedy, H., Marbà, N., Holmer, M., & Mateo, M. A., *et al.* (2012). Seagrass ecosystems as a globally significant carbon stock. *Nature Geoscience, 5, 505–509*. https://doi.org/10.1038/ngeo1477.

GEBCO Compilation Group (2024). GEBCO 2024 Grid. https://10.5285/1c44ce99-0a0d-5f4f-e063-7086abc0ea0f.

Gerritsen, H. D. (2023). Methods to get more information from sparse vessel monitoring systems data. *Frontiers in Marine Science, 10:1223134*. https://doi.org/10.3389/fmars.2023.1223134.

Giritharan, A. (2024). Carbon Dioxide Removal through Coastal Blue Carbon: A Review of Commitments in Nationally Determined Contributions (NDCs). Sabin Center for Climate Change Law, New York. Available at: https://cdrlaw.org/resources/carbon-dioxide-removal-through-coastal-blue-carbon-a-review-of-commitments-in-nationally-determined-contributions-ndcs/ (Accessed: 19 March, 2025).

Goldberg, L., Lagomasino, D., Thomas, N., & Fatoyinbo, T. (2020). Global declines in human-driven mangrove loss. *Global Change Biology, 26, 5844–5855*. https://doi.org/10.1111/gcb.15275.

Gore, C., Gehrels, W. R., Smeaton, C., Andrews, L., McMahon, L., Hibbert, F., et al. (2024). Saltmarsh blue carbon accumulation rates and their relationship with sea-level rise on a multi-decadal timescale in northern England. *Estuarine, Coastal and Shelf Science, 299, 108665*. https://doi.org/10.1016/j.ecss.2024.108665.

Graves, C. A., Benson, L., Aldridge, J., Austin, W. E. N., Dal Molin, F., Fonseca, V. G., et al. (2022). Sedimentary carbon on the continental shelf: Emerging capabilities and research priorities for Blue Carbon. *Frontiers in Marine Science, 9:926215*. https://doi.org/10.3389/fmars.2022.926215.

Gray, J., Jones, S. R., & Smith, A. D. (1995). Discharges to the environment from the Sellafield site, 1951-1992. *Journal of Radiological Protection, 15(2), 99*. https://dx.doi.org/10.1088/0952-4746/15/2/001.

Grech, A., Chartrand-Miller, K., Erftemeijer, P., Fonseca, M., McKenzie, L., Rasheed, M., et al. (2012). A comparison of threats, vulnerabilities and management approaches in global seagrass bioregions. *Environmental Research Letters, 7(2), 024006.* https://dx.doi.org/10.1088/1748-9326/7/2/024006.

Greene, A., Rahman, A. F. Kline, R., & Rahman, M. S. (2018). Side scan sonar: A cost-efficient alternative method for measuring seagrass cover in shallow environments. *Estuarine, Coastal and Shelf Science, 207, 250-258*. https://doi.org/10.1016/j.ecss.2018.04.017.

Greiner, J. T., Wilkinson, G. M., McGlathery, K. J., & Emery, K. A. (2016) Sources of sediment carbon sequestered in restored seagrass meadows. *Marine Ecology Progress Series, 551, 95-105*. https://doi.org/10.3354/meps11722.

Griscom, B. W., Adams, J., Ellis, P. W., Houghton, R. A., Lomax, G., Miteva, D. A., et al. (2017). Natural climate solutions. *Proceedings of the National Academy of Sciences of the United States of America, 114(44), 11645-11650*. https://doi.org/10.1073/pnas.1710465114.

Hamilton, J., Kasprzyk, K., Cifuentes-Jara, M., Granziera, B., Gil, L., Wolf, S., et al. (2023). Blue Carbon and Nationally Determined Contributions, Second Edition. The Blue Carbon Initiative. Available at: https://static1.squarespace.com/static/5c7463aaa9ab95163e8c3c2e/t/64c0aa024433a35afa467b6b/1690348039325/Blue-Carbon-NDC-Guidelines-Second-Edition-2023_singles.pdf (Accessed: 2 April, 2025).

Hansen, V. D. & Reiss, K. C. (2015). Chapter 16 - Threats to Marsh Resources and Mitigation In: Coastal and Marine Hazards, Risks, and Disasters (Eds: Shroder, J. F., Ellis, J. T. and Sherman, D. J.). Elsevier. https://doi.org/10.1016/B978-0-12-396483-0.00016-9.

Harris, P. T., Macmillan-Lawler, M., Rupp, J. & Baker, E. K. (2014). Geomorphology of the oceans. *Marine Geology, 352, 4-24*. https://doi.org/10.1016/j.margeo.2014.01.011.

Hartnett, H. E., Keil, R. G., Hedges, J. I., & Devol, A. H. (1998). Influence of oxygen exposure time on organic carbon preservation in continental margin sediments. *Nature, 391, 572*. https://doi.org/10.1038/35351.

Hiddink, J. G., Jennings, S., Sciberras, M., Szostek, C. L., Hughes, K. M., Ellis, N., et al. (2017). Global analysis of depletion and recovery of seabed biota after bottom trawling disturbance. *Proceedings of the National Academy of Sciences of the United States of America,114(31), 8301-8306*. https://doi.org/10.1073/pnas.1618858114.

Hiddink, J. G., van de Velde, S. J., McConnaughey, R. A., De Borger, E., Tiano, J., Kaiser, M. J. et al. (2023). Quantifying the carbon benefits of ending bottom trawling. *Nature, 617(7960), E1–E2*. https://doi.org/10.1038/s41586-023-06014-7.

Hill, J. M. (2007). Structure and flow of carbon and nitrogen to the western Irish Sea Nephrops norvegicus fishery: a stable isotope approach. Thesis, Doctor of Philosophy. University of London. Available at: https://qmro.qmul.ac.uk/jspui/handle/123456789/1483 (Accessed: 3 April, 2025).

Hill, A. E., Brown, J., & Fernand, L. (1997). The summer gyre in the Western Irish Sea: Shelf sea paradigms and management implications, *Estuarine, Coastal and Shelf Science. 44, 83-95*. https://doi.org/10.1016/S0272-7714(97)80010-8.

Howard, S. H. J., Isensee, K., Pidgeon, E., & Telszewski, M. (2014). Coastal Blue Carbon: Methods for assessing carbon stocks and emissions factors in mangroves, tidal salt marshes, and seagrass meadows. Arlington, VA: Conservation International, Intergovernmental Oceanographic Commission of UNESCO, International Union for Conservation of Nature. Available at: https://www.cifor-icraf.org/publications/pdf_files/Books/BMurdiyarso1401.pdf (Accessed: 2 April, 2025).

Howard, J., Sutton-Grier, A. E., Smart, L. S., Lopes, C. C., Hamilton, J., Kleypas, J. et al. (2023). Blue carbon pathways for climate mitigation: Known, emerging and unlikely. *Marine Policy, 156, 105788*. https://doi.org/10.1016/j.marpol.2023.105788.

Howe, L. (2018). Subtidal Ecology. In: Manx Marine Environmental Assessment (2nd Ed). Isle of Man Government. Available at: https://www.gov.im/media/1363398/ch-33-subtidal-ecology.pdf (Accessed: 2 April, 2025).

Hu, L., Shi, X., Bai, Y., Qiao, S., Li, L., & Yu, Y. (2016). Recent organic carbon sequestration in the shelf sediments of the Bohai Sea and Yellow Sea, China. *Journal of Marine Systems, 155, 50–58*. https://doi.org/10.1016/j.jmarsys.2015.10.018

Hughes, D. J., Ansell, A. D., & Atkinson, R. J. A. (1996). Sediment bioturbation by the echiuran worm Maxmuelleria lankesteri (Herdman) and its consequences for radionuclide dispersal in Irish Sea sediments. *Journal of Experimental Marine Biology and Ecology, 195, 203– 220.* https://doi.org/10.1016/0022-0981(95)00098-4.

ICES (2020). Report of the Working Group for the Celtic Seas Ecoregion (WGCSE), Eds: Lundy, M. & Nimmegeers, S., ICES Scientific Reports. Copenhagen, Denmark. *2(4), 1461*. http://doi.org/10.17895/ices.pub.5978.

Intergovernmental Panel on Climate Change (2023). Glossary. In Climate Change 2022 – Impacts, Adaptation and Vulnerability: Working Group II Contribution to the Sixth Assessment Report of the Intergovernmental Panel on Climate Change (pp. 2897–2930). Cambridge: Cambridge University Press. https://doi.org/10.1017/9781009325844.029.

Isle of Man Government (2018). Manx Marine Nature Reserves Byelaws 2018 (SD2018/0186). Available at: https://www.gov.im/media/1385167/manx-marine-nature-reserves-byelaws-2018-sd0186_compressed.pdf (Accessed: 3 April, 2025).

Isle of Man Government (2021). Climate Change Act 2021. Available at: https://legislation.gov.im/cms/images/LEGISLATION/PRINCIPAL/2021/2021-0020/2021-0020_2.pdf (Accessed: 3 April, 2025).

Isle of Man Government (2022a). Isle of Man Greenhouse Gas Inventory. Available at: https://www.netzero.im/resources/isle-of-man-data/ (Accessed: 13 November, 2024).

Isle of Man Government (2022b). Understanding our emissions. Available at: https://www.netzero.im/resources/understanding-emissions/ (Accessed: 13 November, 2024).

Isle of Man Government (2025). Isle of Man Blue Carbon Strategy (In preparation).

James, K., Macreadie, P. I., Burdett, H. L., Davies, I., & Kamenos, N. A. (2024). It's time to broaden what we consider a ‘blue carbon ecosystem’. *Global Change Biology, 30, e17261*. https://doi.org/10.1111/gcb.17261.

Jankowska, E., Pelc, R., Alvarez, J., Mehra, M. & Frischmann, C. J. (2022). Climate benefits from establishing marine protected areas targeted at blue carbon solutions. *Proceedings of the National Academy of Sciences of the United States of America, 119 (23), e2121705119*. https://doi.org/10.1073/pnas.2121705119.

Jones, B. L. & Unsworth, R. K. F. (2016). The perilous state of seagrass in the British Isles. Royal Society Open Science, 3(1), 150596. https://doi.org/10.1098/rsos.150596.

Kelleway, J. J., Saintilan, N., Macreadie, P. I. & Ralph, P. J. (2016). Sedimentary Factors are Key Predictors of Carbon Storage in SE Australian Saltmarshes. *Ecosystems, 19, 865–880*. https://doi.org/10.1007/s10021-016-9972-3.

Kershaw, P. J. (1986). Radiocarbon dating of Irish Sea sediments. *Estuarine, Coastal and Shelf Science, 23(3), 295–303*. https://doi.org/10.1016/0272-7714(86)90029-6.

Kock, N. & Lynn, G. S. (2012). Lateral Collinearity and Misleading Results in Variance-Based SEM: An Illustration and Recommendations. *Journal of the Association for Information Systems, 13(7).* https://doi.org/10.17705/1jais.00302.

Ladd, C. J. T., Duggan-Edwards, M. F., Bouma, T. J., Pagès, J. F. & Skov, M. W. (2019). Sediment supply explains long-term and large-scale patterns in salt marsh lateral expansion and erosion. *Geophysical Research Letters*, *46, 11178–11187*. https://doi.org/10.1029/2019GL083315.

Ladd, C. J. T., Smeaton, C., Skov, M. W. & Austin, W. E. N. (2022). Best practice for upscaling soil organic carbon stocks in salt marshes. *Geoderma. 428, 116188*. https://doi.org/10.1016/j.geoderma.2022.116188.

LaRowe, D. E., Arndt, S., Bradley, J. A., Estes, E. R., Hoarfrost, A., Lang, S. Q., et al. (2020). The fate of organic carbon in marine sediments - New insights from recent data and analysis. *Earth-Science Reviews*, *103146*. https://doi.org/10.1016/j.earscirev.2020.103146.

Lee, J., South, A. B., & Jennings, S. (2010). Developing reliable, repeatable, and accessible methods to provide high-resolution estimates of fishing-effort distributions from vessel monitoring system (VMS) data. *ICES Journal of Marine Science, 67, 1260–1271.* https://doi.org/10.1093/icesjms/fsq010.

Lefebvre, A., Thompson, C. E. L., Collins, K. J. & Amos, C. L. (2009). Use of a high-resolution profiling sonar and a towed video camera to map a Zostera marina bed, Solent, UK. *Estuarine, Coastal and Shelf Science, 82(2), 323-334*. https://doi.org/10.1016/j.ecss.2009.01.027.

Legge, O. Johnson, M., Hicks, N., Jickells, T., Diesing, M., Aldridge, J., et al. (2020). Carbon on the Northwest European Shelf: Contemporary Budget and Future Influences. *Frontiers in Marine Science, 7(143), 1-23*. https://www.frontiersin.org/articles/10.3389/fmars.2020.00143.

Leiva-Dueñas, C., Graversen, A. E. L., Banta, G. T., Hansen, J. N., Schrøter, M. L. K., Masqué, P., et al. (2024). Region-specific drivers cause low organic carbon stocks and sequestration rates in the saltmarsh soils of southern Scandinavia. *Limnology and Oceanography, 69, 290-308*. https://doi.org/10.1002/lno.12480.

Lindeboom, H. J. & de Groot, S. (1998). The effects of different types of fisheries on the north sea and Irish sea benthic ecosystems. *IMACT-II. (RAPPORT; No. C003/98)*. Available at: https://edepot.wur.nl/340566 (Accessed: 2 April, 2025).

Lovelock, C. E., & Duarte, C. M. (2019). Dimensions of Blue Carbon and emerging perspectives. *Biology Letters, 15, 20180781*. http://dx.doi.org/10.1098/rsbl.2018.0781.

Lundy, M., McCorriston, P., McCausland, I., Erskine, K., Lilley, K., Heaney, G., et al. (2019). Western Irish Sea Nephrops Grounds (FU15) 2019 UWTV Survey Report and catch options for 2020. AFBI and Marine Institute UWTV Survey report. Available at: https://oar.marine.ie/handle/10793/1451 (Accessed: 10 March, 2025).

Macreadie, P. I., Anton, A., Raven, J. A., Beaumont, N., Connolly, R. M., Friess, D. A., et al. (2019). The future of Blue Carbon science, *Nature Communications, 10, 3998*. https://doi.org/10.1038/s41467-019-11693-w.

Macreadie, P. I., Costa, M. D. P., Atwood, T. B., Friess, D. A., Kelleway, J. J., Kennedy, H., et al. (2021). Blue carbon as a natural climate solution. *Nature Reviews Earth & Environment, 2, 826–839*. https://doi.org/10.1038/s43017-021-00224-1.

Maderich, V., Kim, K. O., Bezhenar, R., Jung, K. T., Martazinova, V., & Brovchenko, I. (2021). Transport and Fate of 137Cs Released From Multiple Sources in the North Atlantic and Arctic Oceans. *Frontiers in Marine Science, 8, 806450*. https://www.frontiersin.org/articles/10.3389/fmars.2021.806450.

Marouli, M., Pommé, S., Jobbágy, V., Stroh, H., Van Ammel, R., Fankhauser, A., et al. (2020). Absolute and relative measurement of the 243Am half-life. *Journal of Radioanalytical and Nuclear Chemistry, 326, 1785–1793*. https://doi.org/10.1007/s10967-020-07450-9.

Martín, J., Puig, P., Masqué, P., Palanques, A. & Sánchez-Gómez, A. (2014a). Impact of Bottom Trawling on Deep-Sea Sediment Properties along the Flanks of a Submarine Canyon. *PLOS ONE, 9(8), e104536*. https://doi.org/10.1371/journal.pone.0104536.

Martín, J., Puig, P., Palanques, A. & Giamportone, A. (2014b). Commercial bottom trawling as a driver of sediment dynamics and deep seascape evolution in the Anthropocene. *Anthropocene, 7, 1-15*. https://doi.org/10.1016/j.ancene.2015.01.002.

Martín, J., Puig, P., Palanques, A. & Ribó, M. (2014c). Trawling-induced daily sediment resuspension in the flank of a Mediterranean submarine canyon. *Deep Sea Research Part II: Topical Studies in Oceanography, 104, 174-183.* https://doi.org/10.1016/j.dsr2.2013.05.036.

Mason, C. (2022). NMBAQC's Best Practice Guidance Particle Size Analysis (PSA) for Supporting Biological Analysis, CEFAS. Available at: https://www.nmbaqcs.org/media/qiybf5sd/best-practice-guidance.pdf (Accessed: 2 April, 2025).

Mathis, M., Lacroix, F., Hagemann, S., Nielsen, D. M., Ilyina, T. & Schrum, C. (2024). Enhanced CO_2 uptake of the coastal ocean is dominated by biological carbon fixation. *Nature Climate Change, 14, 373–379.* https://doi.org/10.1038/s41558-024-01956-w.

Maxwell, T. L., Rovai, A. S., Adame, M. F., Adams, J. B., Álvarez-Rogel, J., Austin, W. E. N., et al. (2023). Global dataset of soil organic carbon in tidal marshes. *Scientific Data, 10, 797*. https://doi.org/10.1038/s41597-023-02633-x.

McKenzie, L. J., Nordlund, L. M., Jones, B. L., Cullen-Unsworth, L. C., Roelfsema, C. & Unsworth, R. K. F. (2020). The global distribution of seagrass meadows. *Environmental Research Letters, 15(7), 074041*. https://dx.doi.org/10.1088/1748-9326/ab7d06.

Mcleod, E., Chmura, G.L., Bouillon, S., Salm, R., Björk, M., Duarte, C.M., et al. (2011). A blueprint for blue carbon: toward an improved understanding of the role of vegetated coastal habitats in sequestering CO_2. *Frontiers in Ecology and the Environment, 9, 552-560*. https://doi.org/10.1890/110004.

McMahon, L., Ladd, C. J. T., Burden, A., Garrett, E., Redeker, K. R., Lawrence, P., et al. (2023). Maximizing blue carbon stocks through saltmarsh restoration. *Frontiers in Marine Science, 10, 1106607*. https://doi.org/10. 10.3389/fmars.2023.1106607.

Middelburg, J. J. (2019). Carbon Processing at the Seafloor. In: Marine Carbon Biogeochemistry. Springer Briefs in Earth System Sciences. Springer, Cham. https://doi.org/10.1007/978-3-030-10822-9_4.

Miller, L. C., Smeaton, C., Yang. H., & Austin, W. E. N. (2023). Carbon accumulation and storage across contrasting saltmarshes of Scotland. *Estuarine, Coastal and Shelf Science, 282, 108223*. https://doi.org/10.1016/j.ecss.2023.108223.

Mueller, P., Ladiges, N., Jack, A., Schmiedl, G., Kutzbach, L., Jensen, K. & Nolte, S. (2019). Assessing the long-term carbon-sequestration potential of the semi-natural salt marshes in the European Wadden Sea. *Ecosphere, 10(1), e02556*. https://doi.org/10.1002/ecs2.2556.

Muir, H., Reading, D. G., Warwick, P. E., Strong, J. A., Peel, K., Henthorn, R., et al. (2025). Organic Carbon Burial Rates in Muddy Temperate Shelf Sea Sediments [Preprint]. *ESS Open Archive*. https://doi.org/10.22541/essoar.174293123.38519064/v1.

Needelman, B. A., Emmer, I. M., Emmett-Mattox, S., Crooks, S., Megonigal, J. P., Myers, D., et al. (2018). The science and policy of the verified carbon standard

methodology for tidal wetland and seagrass restoration. *Estuaries and Coasts, 41(8), 2159–2171*. https://doi.org/10.1007/s12237-018-0429-0.

Nellemann, C. (2009). Blue carbon: the role of healthy oceans in binding carbon. Available at: https://wedocs.unep.org/20.500.11822/7772 (Accessed: 10 March 2025).

O'Neill, L., Walter, B., & Unsworth, R. K. F. (2024). Seagrass-Associated Biodiversity Influences Organic Carbon in a Temperate Meadow. *Oceans*, *5(4), 874-888*. https://doi.org/10.3390/oceans5040050.

O'Reilly, S. S., Szpak, M. T., Flanagan, P. V., Monteys, X., Murphy, B. T., Jordan, S. F., et al. (2014). Biomarkers reveal the effects of hydrography on the sources and fate of marine and terrestrial organic matter in the western Irish Sea. *Estuarine, Coastal and Shelf Science, 136, 157-171*. https://doi.org/10.1016/j.ecss.2013.11.002.

Oreska, M. P. J., McGlathery, K. J., & Porter, J. H. (2017). Seagrass blue carbon spatial patterns at the meadow-scale. *PLOS ONE, 12(4), e0176630*. https://doi.org/10.1371/journal.pone.0176630.

Palanques, A., Puig, P., Guillén, J., Demestre, M., & Martín, J. (2014). Effects of bottom trawling on the Ebro continental shelf sedimentary system (NW Mediterranean). *Continental Shelf Research, 72, 83-98*. https://doi.org/10.1016/j.csr.2013.10.008.

Paradis, S., Goñi, M., Masqué, P., Durán, R., Arjona-Camas, M., Palanques, A. et al. (2021). Persistence of Biogeochemical Alterations of Deep-Sea Sediments by Bottom Trawling. *Geophysical Research Letters, 48(2), e2020GL091279*. https://doi.org/10.1029/2020GL091279.

Paradis, S. Pusceddu, A., Masqué, P., Puig, P., Moccia, D., Russo, T., et al. (2019). Organic matter contents and degradation in a highly trawled area during fresh particle inputs (Gulf of Castellammare, southwestern Mediterranean). *Biogeosciences, 16(21), 4307–4320.* https://doi.org/10.5194/bg-16-4307-2019.

Penk, M. R. & Perrin, P. M. (2022). Variability of Plant and Surface Soil Carbon Concentration Among Saltmarsh Habitats in Ireland. *Estuaries and Coasts, 45, 1631–1645*. https://doi.org/10.1007/s12237-021-01042-w.

Pigott, C. D., Ratcliffe, D. A., Malloch, A. J. C., Birks, H. J. B., & Proctor, M. C. F. (2000). *British Plant Communities*. (Rodwell, J. S., Ed.). Cambridge: Cambridge University Press.

Potouroglou, M., Bull, J. C., Krauss, K. W., Kennedy, H. A., Fusi, M., Daffonchio, D. et al. (2017). Measuring the role of seagrasses in regulating sediment surface elevation. *Scientific Reports, 7, 11917*. https://doi.org/10.1038/s41598-017-12354-y.

Potouroglou, M., Whitlock, D., Milatovic, L., MacKinnon, G., Kennedy, H., Diele, K., et al. (2021). The sediment carbon stocks of intertidal seagrass meadows in Scotland. *Estuarine, Coastal and Shelf Science, 258, 107442*. https://doi.org/10.1016/j.ecss.2021.107442.

Povinec, P. P., Bailly du Bois, P., Kershaw, P. J., Nies, H., & Scotto, P. (2003). Temporal and spatial trends in the distribution of 137Cs in surface waters of Northern European Seas—a record of 40 years of investigations. *Deep Sea Research Part II: Topical Studies in Oceanography, 50(17), 2785–2801.* https://doi.org/10.1016/S0967-0645(03)00148-6.

Prentice, C., Poppe, K. L., Lutz, M., Murray, E., Stephens, T. A., Spooner, A. et al. (2020). A Synthesis of Blue Carbon Stocks, Sources, and Accumulation Rates in Eelgrass (Zostera marina) Meadows in the Northeast Pacific. *Global Biogeochemical Cycles, 34(2), e2019GB006345*. https://doi.org/10.1029/2019GB006345.

Puppin, A., Tognin, D., Ghinassi, M., Franceschinis, E., Realdon, N., Marani, M. et al. (2024). Spatial patterns of organic matter content in the surface soil of the salt marshes of the Venice Lagoon (Italy). *Biogeosciences, 21(12), 2937-2954*. https://doi.org/10.5194/bg-21-2937-2024.

Pusceddu, A., Grémare, A., Escoubeyrou, K., Amouroux, J. M., Fiordelmondo, C. & Danovaro, R. (2005). Impact of natural (storm) and anthropogenic (trawling) sediment resuspension on particulate organic matter in coastal environments. *Continental Shelf Research, 25(19), 2506-2520*. https://doi.org/10.1016/j.csr.2005.08.012.

Queirós, A. M., Hiddink, J. G., Kaiser, M. J. & Hinz, H. (2006). Effects of chronic bottom trawling disturbance on benthic biomass, production and size spectra in

different habitats. *Journal of Experimental Marine Biology and Ecology, 335, 91–103*. https://doi.org/10.1016/j.jembe.2006.03.001.

Rahayu, Y. P., Kendrick, G. A., Fraser, M. W. & Vanderklift, M. A. (2023). Little change in surface sediment carbon stock following seagrass restoration in Shark Bay, Western Australia. Estuarine, Coastal and Shelf Science, 294, 108535. https://doi.org/10.1016/j.ecss.2023.108535.

Ramster, J. W. & Hill, H. W. (1969). Current System in the Northern Irish Sea. *Nature, 224(5214), 59-61*. https://doi.org/10.1038/224059a0.

Ray, D., Leary, P., Livens, F., Gray, N., Morris, K., Law, K. A., et al. (2020). Controls on anthropogenic radionuclide distribution in the Sellafield-impacted Eastern Irish Sea. *Science of The Total Environment, 743, 140765.* https://doi.org/10.1016/j.scitotenv.2020.140765.

Reading, D. G. et al. (2025). Assessment of an automated NaI gamma spectrometer for the measurement of Sellafield derived ^{137}Cs and ^{241}Am to support marine sediment dating (In preparation).

Rice, A. L. & Chapman, C. J. (1971). Observations on the burrows and burrowing behaviour of two mud-dwelling decapod crustaceans, Nephrops norvegicus and Goneplax rhomboides. *Marine Biology, 195(2), 330–342*. https://doi.org/10.1007/BF00368093.

Röhr, M. E., Holmer, M., Baum, J. K., Björk, M., Boyer, K., Chin, D., et al. (2018). Blue Carbon Storage Capacity of Temperate Eelgrass (Zostera marina) Meadows. *Global Biogeochemical Cycles, 32(10), 1457–1475*. https://doi.org/10.1029/2018gb005941.

Sala, E., Mayorga, J., Bradley, D., Cabral, R. B., Atwood, T. B., Auber, A., Cheung, W., Costelo, C., et al. (2021). Protecting the global ocean for biodiversity, food and climate. *Nature, 592, 397–-402.* https://doi.org/10.1038/s41586-021-03371-z.

Sanders, C. J., Smoak, J. M., Naidu, A. S., Sanders, L. M., & Patchineelam S. R. (2010). Organic carbon burial in a mangrove forest, margin and intertidal mud flat Estuarine. *Coastal and Shelf Science, 90(3), 168–172.* https://doi.org/10.1016/j.ecss.2010.08.013.

Sayle, T., Lamb J., Colvin A., & Harris B. (1995). Isle of Man Ecological Habitat Survey Phase 1 Report 1991-1994 DEFA Isle of Man Government (Unpublished report).

Schober, P., Boer, C., & Schwarte, L. A. (2018). Correlation Coefficients: Appropriate Use and Interpretation. *Anesthesia & Analgesia, 126(5), 1763-1768*. https://doi.org/10.1213/ANE.0000000000002864.

Sciberras, M., Parker, R., Powell, C., Robertson, C., Kröger, S., Bolam, S. et al. (2016). Impacts of bottom fishing on the sediment infaunal community and biogeochemistry of cohesive and non-cohesive sediments. *Limnology and Oceanography, 61(6), 2076-2089*. https://doi.org/10.1002/lno.10354.

Seddon, N., Smith, A., Smith, P., Key, I., Chausson, A., Girardin, C., et al. (2021). Getting the message right on nature-based solutions to climate change. *Global Change Biology, 27(8), 1518-1546*. https://doi.org/10.1111/gcb.15513.

Smeaton, C., & Austin, W. E. N. (2022). Quality not quantity: Prioritizing the management of sedimentary organic matter across continental shelf seas. *Geophysical Research Letters. 49, e2021GL097481*. https://doi.org/10.1029/2021GL097481.

Smeaton, C., Barlow, N. L. M. & Austin, W. E. N. (2020). Coring and compaction: Best practice in blue carbon stock and burial estimations. *Geoderma, 364, 114180*. https://doi.org/10.1016/j.geoderma.2020.114180.

Smeaton, C., Garrett, E., Koot, M. B., Ladd, C. J. T., Miller, L. C., McMahon, L., et al. (2024). Organic carbon accumulation in British saltmarshes. *Science of the Total Environment, 926, 172104*. https://doi.org/10.1016/j.scitotenv.2024.172104.

Smeaton, C., Hunt, C. A., Turrell, W. R., & Austin, W. E. N. (2021a). Marine Sedimentary Carbon Stocks of the United Kingdom's Exclusive Economic Zone. *Frontiers in Earth Science, 9:593324*. https://doi.org/10.3389/feart.2021.593324.

Smeaton, C., Ladd, C. J. T., Miller, L. C., McMahon, L., Garrett, E., Barlow, N. L. M., et al. (2023). Organic carbon stocks of Great British saltmarshes. *Frontiers in Marine Science, 10, 1229486*. https://doi.org/10.3389/fmars.2023.1229486.

Smeaton, C., Yang, H. & Austin, W. E. N. (2021b). Carbon burial in the mid-latitude fjords of Scotland. *Marine Geology, 106618*. https://doi.org/10.1016/j.margeo.2021.106618.

Smith, P., Davis, S., Creutzig, F., Fuss, S., Minx, J., Gabrielle, B. et al. (2016). Biophysical and economic limits to negative CO_2 emissions. *Nature Climate Change, 6, 42–50*. https://doi.org/10.1038/nclimate2870.

Song, S., Santos, I.R., Yu, H., Wang, F., Burnett, W. C., Bianchi, T. S., et al. (2022). A global assessment of the mixed layer in coastal sediments and implications for carbon storage. *Nature Communications, 13, 4903*. https://doi.org/10.1038/s41467-022-32650-0.

Spencer, E. L. (2005). Saltmarshes of the Isle of Man. PhD Thesis. University of Liverpool (Unpublished).

Strachan, L. L., Lilley, R. J. & Hennige, S. J. (2022). A regional and international framework for evaluating seagrass management and conservation. *Marine Policy, 146, 105306*. https://doi.org/10.1016/j.marpol.2022.105306.

Strong, J. A., Wardell, C., Haïssoune, A., Jones, A. L. & Coals, L. (2023). Marine habitat mapping to support the use of conservation and anti-trawl structures in Kep Province, Cambodia. *ICES Journal of Marine Science, 80(8), 2197-2209*. https://doi.org/10.1093/icesjms/fsac001.

Sun, Y., Zhang, H., Lin, Q., Zhang, C., He, C. & Zheng, H. (2024). Exploring the international research landscape of blue carbon: Based on scientometrics analysis. *Ocean & Coastal Management, 252, 107106*. https://doi.org/10.1016/j.ocecoaman.2024.107106.

Sutton-Grier, A. E. & Moore, A. (2016). Leveraging carbon services of coastal ecosystems for habitat protection and restoration. *Coastal Management, 44(3), 259–277*. https://doi.org/10.1080/08920753.2016.1160206.

Tiano, J. C., Witbaard, R., Bergman, M. J. N., van Rijswijk, P., Tramper, A., van Oevelen, D. et al. (2019). Acute impacts of bottom trawl gears on benthic metabolism and nutrient cycling. *ICES Journal of Marine Science, 76(6), 1917-1930*. https://doi.org/10.1093/icesjms/fsz060.

Thompson, C. E. L., Silburn, B., Williams, M. E., Hull, T., Sivyer, D., Amoudry, L. O., Widdicombe, S., Ingels, J., et al. (2017). An approach for the identification of exemplar sites for scaling up targeted field observations of benthic biogeochemistry in heterogeneous environments. *Biogeochemistry, 135, 1–34*. https://doi.org/10.1007/s10533-017-0366-1.

Thomson, A. C. G., Trevathan-Tackett, S. M., Maher, D. T., Ralph, P.J. & Macreadie, P. I. (2019). Bioturbator-stimulated loss of seagrass sediment carbon stocks. *Limnology & Oceanography, 64, 342-356*. https://doi.org/10.1002/lno.11044.

Tmmink, A. J. (1994). Ecology of eelgrass beds in the Isle of Man. BSc Thesis, Port Erin Marine Laboratory, Liverpool University (Unpublished).

Towle, R. (2018). Maximising the Blue Carbon potential of Isle of Man waters through the management, conservation and restoration of blue carbon ecosystems. University of York, Master of Science in Marine Environmental Management (Unpublished).

Troels-Smith, J. (1955). Characterization of Unconsolidated Sediments. Reitzels Forlag.

Udden, J. A. (1914). Mechanical composition of clastic sediments. *Geological Society of America Bulletin, 655–754*. http://dx.doi.org/10.1130/GSAB-25-655.

UK Climate Change Committee (2022). Briefing: Blue Carbon, Climate Change Committee. Available at: https://www.theccc.org.uk/publication/briefing-blue-carbon/ (Accessed: 3 April, 2025).

United Nations (2015). Paris Agreement. Available at: https://unfccc.int/sites/default/files/english_paris_agreement.pdf (Accessed: 11 February, 2025).

Unsworth, R. K. F., McKenzie, L. J., Collier, C. J., Cullen–Unsworth, L. C., Duarte, C. M., Jarvis, J. C., et al. (2019). Global challenges for seagrass conservation. *Ambio, 48, 801–815*. https://doi.org/10.1007/s13280-018-1115-y.

van de Velde, S., Van Lancker, V., Hidalgo-Martinez, S., Berelson, W. M., & Meysman, F. J. R. (2018). Anthropogenic disturbance keeps the coastal seafloor

biogeochemistry in a transient state. *Scientific Reports, 8(1), 5582*. https://doi.org/10.1038/s41598-018-23925-y.

Watling, L., Findlay, R. H., Mayer, L. M. & Schick, D. F. (2001). Impact of scallop drag on the sediment chemistry, microbiota and faunal assemblages of shallow subtidal marine benthic community. *Journal of Sea Research, 46, 309–324*. https://doi.org/10.1016/S1385-1101(01)00083-1.

Waycott, M., Duarte, C.M., Carruthers, T. J. B., Orth, R. J., Dennison, W. C., Olyarnik, S., et al. (2009). Accelerating loss of seagrasses across the globe threatens coastal ecosystems. *Proceedings of the National Academy of Sciences of the United States of America, 106 (30), 12377-12381*. https://doi.org/10.1073/pnas.0905620106.

Wentworth, C. K. (1922). A scale of grade and class terms for clastic sediments. Journal of Geology, 30(5), 377–392. Available at: https://www.jstor.org/stable/30063207 (Accessed: 10 March, 2025).

Wilkinson, G. M., Besterman, A., Buelo, C., Gephart, J. & Pace, M. L. (2018). A synthesis of modern organic carbon accumulation rates in coastal and aquatic inland ecosystems. *Scientific Reports, 8(1), 15736*. https://doi.org/10.1038/s41598-018-34126-y.

Williams, M. E., Amoudry, L. O., Brown, J. M. & Thompson, C. E. L. (2019). Fine particle retention and deposition in regions of cyclonic tidal current rotation. *Marine Geology, 410, 122–134*. https://doi.org/10.1016/j.margeo.2019.01.006

Williamson, P. & Gattuso, J.-P. (2022). Carbon Removal Using Coastal Blue Carbon Ecosystems Is Uncertain and Unreliable, With Questionable Climatic Cost-Effectiveness. *Frontiers in Climate, 4, 853666*. https://doi.org/10.3389/fclim.2022.853666.

Winogradow, A. & Pempkowiak, J. (2014). Organic carbon burial rates in the Baltic Sea sediments. *Estuarine, Coastal and Shelf Science, 138(1), 27–36*. https://doi.org/10.1016/j.ecss.2013.12.001.

Worthington, T. A., Spalding, M., Landis, E., Maxwell, T. L., Navarro, A., Smart, L. S., et al. (2024). The distribution of global tidal marshes from Earth observation data. *Global Ecology and Biogeography*, *33, e13852*. https://doi.org/10.1111/geb.13852.